DEPARTMENT OF CELL DEATH AND PROLIFERATION, IIBB-CSIC
UNIVERSITAT DE BARCELONA

ROLE OF ACID SPHINGOMYELINASE IN STEATOHEPATITIS

Raquel Fucho Salvador

2013

DOCTORAL PROGRAM IN BIOMEDICINE

ROLE OF ACID SPHINGOMYELINASE IN STEATOHEPATITIS

A dissertation submitted to the Medical School of the University of Barcelona in partial fulfillment of the requirements for the degree of Doctor of Philosophy in Biology.

By

Raquel Fucho Salvador

This thesis has been conducted under the supervision of Dra. Mª del Carmen García-Ruiz and Dr. José Carlos Fernández-Checa Torres at the Department of Cell Death and Proliferation of the Institute of Biomedical Research of Barcelona (IIBB), Spanish National Research Council (CSIC).

Als meus pares,
al Trepi i al Quim.

"Never, never, never give up"
Winston Churchill

ACKNOWLEDGMENTS

Sembla mentida que la tesi ja sigui una realitat. L'altre dia fent neteja a la meva antiga habitació de casa els pares vaig trobar el llibre de COU de Biologia i en obrir-lo, just vaig anar a petar a una pàgina que parlava dels esfingolípids! Això ve de lluny! No vaig poder evitar pensar en el llarg camí que m'ha dut a defensar la tesi. Ha estat un camí ple d'aventures, reptes i vivències compartides amb gent que m'estimo i que m'ha ajudat a créixer com a científic i sobretot, com a persona. És per això que abans de posar-me a parlar de lípids de noms impronunciables, voldria donar les gràcies a totes aquelles persones que m'han ajudat a arribar fins aquí.

El camí de la meva tesi és una mica atípic i comença molt abans d'arribar al laboratori on sóc avui. Tornant al 2003, voldria agrair a tota la gent del Departament de Biologia Cel·lular de la Facultat de Medicina, grans i petits, per ser el meu primer contacte amb la investigació científica i donar-me una base sòlida com a investigadora que em va permetre accedir a la gran aventura que va ser Boston. En aquesta segona etapa, lluny de casa, és inevitable mencionar a en Gökhan. *Gökhan, thanks for giving me a unic chance to live, breath and soak in your very special way of science making. Thanks for believing in this crazy Catalan girl! Katy and Masato San...there's a special thanks for you since my everyday in the lab is scented with your great scientific manners. Cem, your are an endless source of animal wisdom and always ready to share. MegGus... what can I say, I miss you! Specially our talks in the coffe room. Thanks to all G.S.H. lab for an amazing adventure and making me an appealing candidate for my PhD hunt!*

I ara sí, Checa lab! Voldria agrair als meus directors de tesi, la Carmen i en Carlos, per donar-me l'oportunitat d'entrar a formar part del seu gran laboratori. Per entendre la meva carrera atípica i donar-me llibertat suficient per créixer. A nivell personal m'heu donat suport sempre que l'he necessitat. Carmen, tothom sap que estàs feta un belluguet però ets una marassa i sé que si mai em passa res en podem parlar tot fent un cafetó. Gràcies també per donar-me una visió més amplia del que representa ser mare investigadora... A l'Albert, l'Anna i la Montse per mostrar-me la diversitat del grup i atendre les meves consultes. Als Post Docs del lab, començant per la Clàudia, em va ajudar molt parlar amb tu al principi del doctorat. A la Conde, pel seu "desparpajo" explicant les coses del dia a dia. I al Vicent, per escoltar-me, discutir sobre ciència i ajudar-me en aquesta última etapa sempre aportant bon humor. "Serà, s-QUIM milk"?

Als nou vinguts, Álvaro, Guille i Sandra. Molta sort en el vostre doctorat. No us adormiu però sobretot gaudiu d'aquests anys que passen molt ràpid! Dels principis del doctorat, a Laura Llacuna per fer-me riure fins a no poder més. A l'Anna Moles per ajudar-me, estar sempre a punt per ensenyar noves tècniques i portar-me a fer danses! A la Cris i a la Milica, ànims en la recta final. Milica, glamour girl... trobaré a faltar les nostres converses de "treinta-añeras" que dius tu. A la Bet, pel seu entusiasme en vers la ciència. A la Laura Martínez, la "Profeeeeeessional"... què vols que et digui "equipo ceramidas"... t'he de donar les gràcies per saltar en aquesta última etapa i estirar juntes del carro. "Señorita! Puedo subir al estrado? tararriiii-rora!" Admiro la teva voluntat i decisió a l'hora de fer les coses que de ben segur et portarà lluny. Molta sort en la recta final i salutacions al Summers, que mai se sap ;).

A la Ferni, perquè és tota una institució! I de ben segur tothom sabrà qui ets en les futures generacions Checa lab! Merci per cuidar-me amb pometes àcides i orxates de lo tió Che en plena etapa "antojil". A la Mati, perquè sense saber quina cara feia, ja m'ajudava des de Boston per poder-me matricular del màster. I com que no en vas tenir prou, em vas seguir aguantant durant tot el doctorat. Ai... Mati-Mati... merci per ensenyar-me a domar el confocal i agafar perspectiva quan les coses sembla que no van ben encarrilades. Crec que això és el que més li agrada al Quim de tu... que li dones molta pau :) Estic super contenta de veure't tan feliç amb el nou rumb que has triat tot i que perdem una gran científica. A la Natalia, que tot i venir uns mesos d'estada des de Mèxic, es va fer un lloc només arribar. *A ver cuando vienes de visita y nos cocinas unas tingas y compramos unas camisetas que no se enchuequen!* A la Bau... per ser la barreja perfecta de passió, coneixement i aptitud experimental i portar-ho amb elegància i humilitat. Merci per ajudar amb les meves <<Preguntes de Biòloga a Química Orgànica>>. Per les converses d'ascensor, per estar sempre a punt per escoltar, ajudar i ser tan detallista. Així un si que se sent estimat! A la meva Nunu... Nuns... la persona més resolutiva i amb més capacitat de treball del món. *Nuns, give me a 3!* Des del primer dia de doctorat hem estat juntes. I quan més liada he estat, has aparegut no res i t'has quedat amb mi fins les tantes acabant coses. Quan passen aquestes coses te n'adones de la gent que de veritat compta. Si fins i tot m'has fet de revisora! Sense demanar res sempre m'ho has donat tot. Tinc molta sort d'haver-te conegut i de comptar amb la teva amistat. Dra. Tarrats, que no se't quedin aquests anglesos que et volem de tornada! Suuuuuuuuuu... Suuuu... Suuuu! *A que*

te gasto el nombre! Un trosset d'aquesta tesi és teu. Com totes les tesis que es fan al laboratori. El més important que he après de tu és... que els hepatòcits de ratolí surten millor si t'has pres un cafè abans. Això no surt als protocols! No aconsegueixo visualitzar aquest lab sense tu. A nivell organitzatiu i experimental. No hi ha tècnica del lab que no hagis fet i puguis ensenyar, i si se n'han de posar noves a punt, ets a la primera voluntària. D'aquella gent que deia que realment compta... dels que no et fallen mai... doncs la peti-Su. I fora del lab... no conec dona més forta i noble. Que vals un imperi i és un honor tenir-te com a amiga. I la Ireneeee guapa! Guapa! Guapa! Una menció especial a totes les tietes científiques del Quim, perquè ell també té molta sort de tenir unes tietes que se l'estimen tant! Nenes, sóc molt afortunada d'haver-vos conegut i us trobaré molt a faltar, sobretot els nostres esmorzars en família, però això només és una etapa que tanquem per començar-ne una altre on seguirem trobant-nos i compartint noves vivències tot i que estiguem dispersades pel món ara mateix. Us estimo molt!

Als amics que tot i no entendre massa el que vol dir treballar tantes hores, anar a veure ratolins en cap de setmana i tot per amor a l'art... sempre sou aquí per animar i distreure, que la vida és molt més que el lab! A les noies de danses amb les que cada dimarts desconnecto de tot. A la Cheles, que des de Bio Cel·lular no hem perdut el contacte i sempre ets a prop per xerrar del que sigui tot fent una coke. A la Julie i el Galleguiño, la meva família Bostoniana. *Galleguiño, Fuxiña vai ser Doutora! Jules, thanks for always caring and helping with silly English questions. I miss you guys and love you tons!* A les Fenícies que tot i veure'ns poc, les nostres trobades són explosives com si no hagués passat el temps. Al Ten, la Marina, en Ruls, l'Olga, la Xaiet i en Katur pels "fungols" i les cases rurals compartides. A Sa Doctora pel Guyton. Al meu germanet postís, en Joan, per preguntar sempre com va tot i interessar-se genuïnament. A la Telli, per ser una marona i no abandonar-me quan he estat més immersa en la tesi. Merci per mantenir-me connectada! A la Carol i la Cris, pel seu suport incondicional i per uns esmorzars que han fet història. M'encanta saber que en 30 anys probablement farem el mateix però serem unes velletes!

A la meva família, per saber qui sóc, estimar-me i valorar-me. Al Tòfol i a la Montse, pel seu suport i pels cangurs durant aquests últims mesos de tesi. Als millors avis del món, el Ramon, la Maria, el Nicanor i la Rosita... en breu tindreu el primer Doctor de la família. Al Dani, per mostrar-me la importància de ser meticulós i per seguir els "ups and downs"

de la tesi. Al Ramon i la Maria Rosa, per estimar-me i fer-me sentir estimada. Per donar-me la possibilitat de dedicar-me estudiar i mostrar-me sempre el seu suport incondicional. Us estimo!

Finalment, a les dues persones que més han viscut aquesta tesi. Els dos homes de la meva vida que em donen noves forces cada dia per enfrontar-me al que sigui. Quim, sens dubte el millor resultat de tota la tesi. Gràcies per esborrar amb somriure qualsevol cabòria i fer-me veure la vida amb uns altres ulls. La teva arribada ha estat el millor regal que he tingut mai. T'estimo boleta... Finalment, al Trepi, per donar-me fortalesa i tendresa. Per creure en mi. Per no deixar-me conformar amb el que és suficient i fer-me buscar l'excel·lència en el que faig. Gràcies per aguantar els moments més durs de la tesi i celebrar els més emocionants. Ets el millor company per a qualsevol viatge. T'estimo.

Barcelona, Febrer 2013.

INDEX

INDEX

ABBREVIATIONS

3KSn- 3-keto-sphinganine

ABCA1- ATP-binding cassette transporter

ACC- acetyl-CoA carboxylase

ADH- alcohol dehydrogenase

AIF- apoptosis inducing factor

ALD- alcoholic liver disease

ALDH- acetaldehyde dehydrogenase

ALT- alanine transaminase

AMP-adenosyl monophosphate

AMPK- AMP-activated protein kinase

ApoB- apolipoprotein B

ASH- alcoholic steatohepatitis

ASMase- acid sphingomyelinase

ASMase$^{-/-}$- acid sphingomyelinase knockout mice

ATF- activating transcription factor

ATG- autophagy-related gene

ATM- adipose tissue resident macrophages

ATP- adenosyl triphosphate

Bcl-2- B-cell lymphoma 2

BHMT- betaine-homocysteine methyltransferase

BMI- body mass index

BSA- bovine serum albumin

C1P- ceramide-1-phosphate

CBS- cystathionine-β-synthase

CDases- ceramidases

CerS- ceramide synthase

CHOP- C/EBP (CCAAT/enhancer binding protein) homologous protein

CHQ- chloroquine

ChREBP- carbohydrate-responsive element binding protein

CK- ceramide kinase

CLS- crown-like structures

CMA- chaperone-mediated autophagy

Con A- concanavalin A

CPT1- carnitine palmitoyl transferase 1

Ct- cycle threshold

CTRL- control

CVD- cardiovascular disease

CYP2E1- cytochrome P450 enzymes 2E1

DALY- disability-adjusted life years

db/db- leptin receptor deficient mice

DGAT- diacylglycerol acyltransferase

DIO- diet-induced obesity

DNL- *de novo* lipogenesis

DR5- TRAIL receptor 5

EDEM- endoplasmatic reticulum degradation enhancer, monnosidase alpha-like 1

eIF2α- eukariotic translation factor 2 alpha

ER- endoplasmatic reticulum

ERAD- endoplasmatic reticulum associated degradation

EtOH- ethanol-containing Lieber-DeCarli diet

EWAT- epididymal white adipose tissue

FA(s)- fatty acid(s)

FABP- fatty acid binding protein

FAS- fatty acid synthase

FAT/CD36- FA translocase

FATP- fatty acid transporter protein

FBS- fetal bovine serum

FC- free cholesterol

FFA(s)- free fatty acid(s)

FXR- farnesoid X receptor

GADD34- DNA damage-inducible protein 34

GCS- galactosyl ceramide synthases

GR- GSH reductase

GRP78- glucose-regulated protein 78

GSH- glutathione

GSLs- glycosphingolipids

GSSG- oxidized GSH

GTT- glucose tolerance test

HCC- hepatocellular carcinoma

HCD- hypercholesterolemic diet

HDL- high-density lipoprotein

HFD- high fat diet

HHCy- hyperhomocysteinemia

HPLC- high performance liquid chromatography

HRP- horseradish peroxidase

HSC- hepatic stellate cells

IKK- IκB kinase

IL-6- interleukin 6

iNOS- nitric oxide synthase

i.p.- intraperitoneal injection

IR- insulin receptor

I/R- ischemia/reperfusion

IRE1α- inositol-requiring enzyme 1 alpha

IRS- insulin receptor substrate

ITT- insulin tolerance test

i.v.- intravenous injection

JNK- c-jun N-terminal kinase

KC- Kupffer cells

LC3- microtubule-associated protein1 light chain 3

ABBREVIATIONS

LCFA- long-chain fatty acids

LDL- Low-density lipoprotein

LDLR- LDL receptor

LPS- lipopolysaccharide

LXR- liver X receptor

M6P- mannose 6 phosphate

MAM- mitochondria associated membrane

MAT- methionine adenosyltransferase

MCD- methionine and choline deficient diet

MCP-1- monocyte chemoattractant protein 1

MDC- monodansylcadaverine

MEOS- microsomal ethanol-oxidizing system

mGSH- mitochondrial glutathione

MS- methionine synthase

MSDH- O-methyl-serine dodecylamide hydrochloride

mtGPAT- mitochondrial glycerol- 3-phosphate-acyltransferase

MTP- microsomal triglyceride transfer protein

MTT- 3-(4,5-Dimethylthiazol-2-yl)-2,5-diphenyltetrazolium bromide

NAD^+- oxidized nicotinamide adenine dinucleotide

NADH- reduced nicotinamide adenine dinucleotide

NAFLD- non-alcoholic fatty liver disease

NASH- non-alcoholic steatohepatitis

NF-κB- nuclear factor kappa B

NO- nitric oxide

NPC- Niemann-Pick type C disease

NPD- Niemann-Pick disease

NSMase- neutral sphingomyelinase

ob/ob- leptin deficient mice

PAS- phagophore assembly site

PBS- phosphate buffered saline

PCNA- proliferating cell nuclear antigen

PDI- protein disulfide isomerase

PE- phosphatidylethanolamine

PERK- protein kinase double-stranded RNA-dependent-like ER kinase

PFA- paraformaldehyde

PH- partial hepatectomy

PI3P- phosphatidylinositol 3-phosphate

PPAR-α or γ- peroxisome proliferator-activating receptor alpha or gamma

RAR- retinoic acid receptor

RD- regular diet

RIP- regulated intermembrane proteolysis

ROS- reactive oxygen species

RT-PCR- real time PCR

S1P- sphingosine-1-phosphate

sASMase- secreted ASMase

SAH- S-adenosylhomocysteine

SAM- S-adenosylmethionine

SAMe- S-adenosyl-L-methionine

SCAP- SREBP-cleavage activating protein

SCD1- stearoyl-CoA desaturase 1

SCWAT- subcutaneous white adipose tissue

SEC- sinusoidal endothelial cells

SERCA- sarco/endoplasmic reticulum calcium ATPase

SH- steatohepatitis

SLs- sphingolipids

SM- sphingomyelin

SMase- sphingomyelinase

SMS- sphingomyelin synthase

SOD- superoxid dismutase

SPH- sphingosine

SPT- serine palmitoyltransferase

SREBP- strerol-regulatory element binding protein

SubAB- AB5 subtilase cytotoxin

T2DM- type 2 diabetes mellitus

TBST- tris-buffered saline with tween

TCA- tricarbocylic acid cycle

TFAM- transcription factor A, mitochondrial

Tg- thapsigargin

TG(s)-triglyceride(s)

TGF-β- transforming growth factor β

TLC- thin layer chromatography

TLR- toll-like receptors

Tm- tunicamycin

TNFR- tumor necrosis factor receptor

TNF-α- tumor necrosis factor alpha

TRAF2- tumor necrosis factor receptor-associated factor 2

TRB3- tribbles homolog 3

TUDCA- tauroursodeoxycholic acid

TZD- thiazolidinediones

UCP- uncoupling protein

UPR- unfolded protein response

VLDL- very-low-density lipoprotein

VPS- vacuolar protein sorting

WHO- World Health Organization

WT- wild type

XPB1- X-box binding protein 1

INTRODUCTION

1. THE LIVER.

The liver is the largest organ in the body, contributing about 2% of the total body weight, equivalent to 1.5 kg in the average adult human. The liver appears wedge shaped, with its base to the right and its apex projecting to the left as it extends between the right and left upper quadrants. At its upper pole, the liver makes direct contact with the diaphragm and at its lower pole, the liver lies on the stomach and intestine (Figure I-1. A).

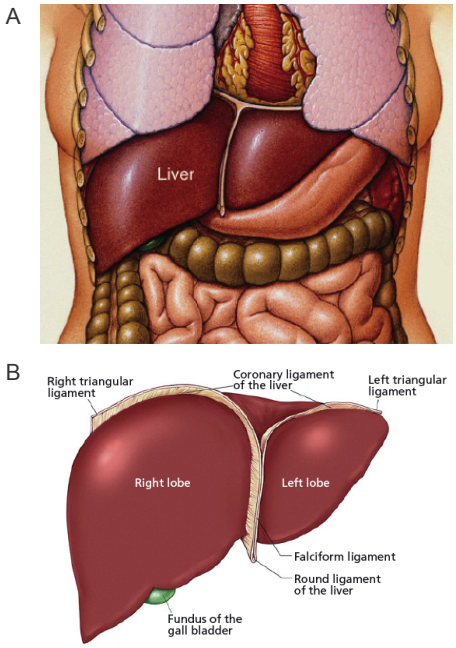

Figure I-1. A. Anterior view of liver in abdominal cavity.
B. Liver lobes and ligaments (Talley, Lindor et al. 2010).

The liver is divided into two principal lobes a large right lobe and a smaller left lobe by the falciform ligament, a fold of the mesentery (Figure I-1. B). Although the right lobe is considered by many anatomists to include an inferior quadrate lobe and a posterior caudate lobe, based on internal morphology (primarily the distribution of blood vessels), the quadrate and caudate lobes more appropriately belong to the left lobe.

1.1. Microscopic organization of the liver:

Structurally, the liver is composed of the following:

- **Parenchyma:** consists of organized plates of hepatocytes or **hepatic laminae**, normally 1-2 cells thick (Figure I-2). These are specialized epithelial cells that make up about 80% of the volume of the liver and carry out most of the liver

functions. The hepatic laminae are bordered on either side by the endothelial-lined vascular spaces called hepatic sinusoids.

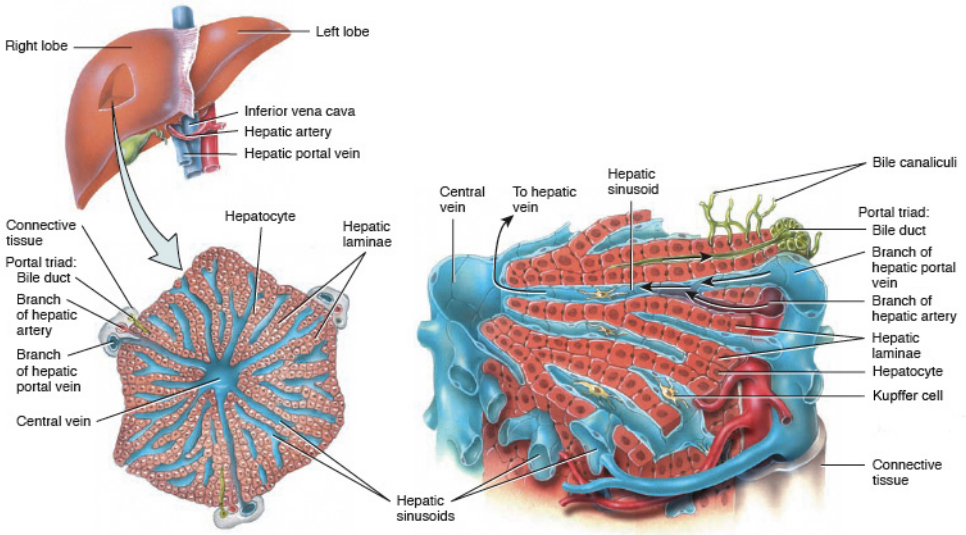

Figure I-2. Details of the histological components of the liver (J. Tortora and H. Derrickson 2009).

- **Connective tissue stroma:**

  Contains blood vessels, nerves, lymphatic vessels, and bile canaliculi.

  - **Bile canaliculi** are small ducts between hepatocytes that collect bile produced by the hepatocytes (Figure I-2). From bile canaliculi, bile will pass into different ducts until it enters the small intestine to participate in digestion.
  - **The fibrous capsule of Glisson** is a collagenous capsule that covers the external surface of the liver.

- **Sinusoidal capillaries or hepatic sinusoids:** these are highly permeable blood capillaries characterized by the absence of tight junctions located between the hepatic laminae. The hepatic sinusoids receive oxygenated blood from branches of the hepatic artery and nutrient-rich deoxygenated blood from branches of the hepatic portal vein, which brings venous blood from the gastrointestinal organs and spleen into the liver. Hepatic sinusoids converge and deliver blood into a central vein (Figure I-3). From central veins the blood flows into the hepatic veins, which drain into the inferior vena cava. Also present in the hepatic sinusoids we can find the macrophages known as Kupffer cells.

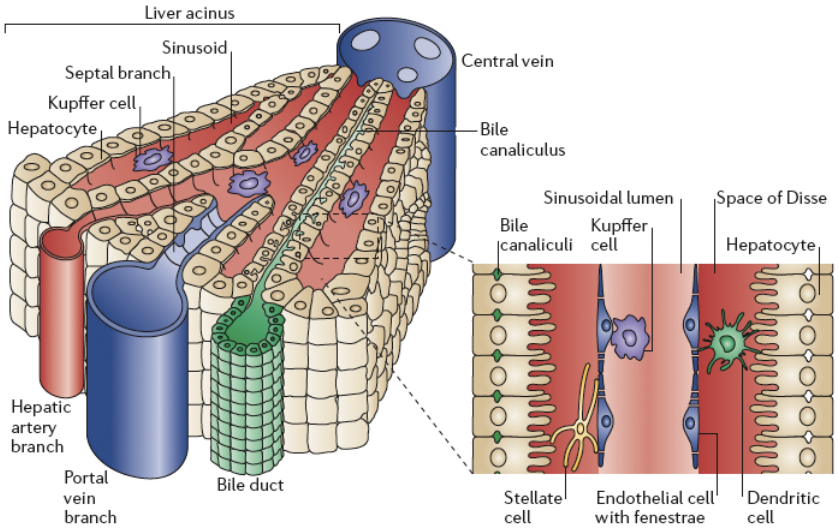

Figure I-3. Three-dimensional structure of a liver lobule (Adams and Eksteen 2006).

- **Perisinusoidal spaces or spaces of Disse:** located between the sinusoidal endothelium and hepatocytes (Figure I-3). The Disse space is the site of exchange of materials between blood and liver cells. It lies between the basal surfaces of hepatocytes and the basal surfaces of endothelial cells and Kupffer cells that line the sinusoids. Proteins and lipoproteins synthesized by hepatocytes are transferred to the blood in the perisinusoidal space; this pathway is for liver secretions other than bile. In the Disse space we can find the hepatic stellate cells.

The basic functional unit of the liver is the liver lobule, which is shaped like a hexagon. The liver lobule is constructed around a central vein that empties into the hepatic veins and then into the vena cava. The lobule itself is composed principally of many hepatic laminae that radiate from the central vein surrounded by hepatic sinusoids. In the middle of hepatic laminae, between the adjacent cells, lie small bile canaliculi that empty into bile ducts. Located at three corners of the hexagon we can find a portal triad containing a bile duct, a portal vein branch and a hepatic arterial branch (Figure I-3).

1.2. Liver cell types

The liver is organized in different cell types: parenchymal cells or hepatocytes, and nonparenchymal cells, comprising sinusoidal endothelial cells (SEC), Kupffer cells (KC), and hepatic stellate cells (HSC). While hepatocytes occupy almost 80% of the total liver volume and perform the majority of numerous liver functions, nonparenchymal liver cells

are localized in the hepatic sinusoids and space of Disse and contribute only 6.5% to the liver volume, but 40% to the total number of liver cells. It has been increasingly recognized that both under normal and pathological conditions, substances released from neighboring nonparenchymal cells regulate many hepatocyte functions (Kmieć 2001).

- **Hepatocytes** are the major functional cells of the liver and perform a wide array of metabolic, secretory, and endocrine functions. These large, polygonal and specialized epithelial cells represent most of the volume of the liver (Figure I-4). Their nuclei are large, spherical, and located in the center of the cell. In the adult liver, many cells are binucleate (this is particular so in mice hepatocytes). Cytoplasm is generally acidophilic. Hepatocytes are exceptionally active in synthesis of protein and lipids for export and as a consequence, ultrastructural examination of hepatocytes reveals large quantities of both rough and smooth endoplasmic reticulum. Hepatocytes typically contain many stacks of Golgi membranes. Golgi vesicles are particularly numerous nearby the bile canaliculi, reflecting transport of bile constituents into those channels. Numerous mitochondria can be observed (typically 1000/hepatocyte) and depending on the metabolic state of the cell large accumulations of glycogen and lipid droplets can be found as well (Kmieć 2001).
- **Sinusoidal endothelial cells (SEC)** constitute the wall of the hepatic sinusoid (Figure I-4). Their key functional role relates to filtration due to the presence of small fenestrations that allow free diffusion of many substances and particles of sizes smaller than chylomicrons, between the blood and the hepatocyte surface. SEC exhibit a large endocytic capacity for many ligands including glycoproteins, components of the extracellular matrix, immune complexes, transferrin and ceruloplasmin. SEC may function as antigen-presenting cells. They are also active in the secretion of cytokines, eicosanoids, endothelin-1, nitric oxide, and some extracellular matrix components (Kmieć 2001).
- **Kupffer cells (KC)** are tissue resident macrophages located in the hepatic sinusoids, especially in the periportal areas (Figure I-4). They have a pronounced endocytic and phagocytic capacity. KC are in constant contact with gut-derived particulate materials and soluble bacterial products. KC secrete potent mediators of the inflammatory response, and thus control the early phase of liver

inflammation, playing an important part in innate immune defense. High exposure of KC to bacterial products, especially endotoxin (lipopolysaccharide, LPS), can lead to the intensive production of inflammatory mediators, and ultimately to liver injury. KC also play an important role in the clearance of senescent and damaged erythrocytes. Moreover, during liver injury and inflammation, KC secrete enzymes and cytokines that may damage hepatocytes, and are active in the remodeling of extracellular matrix (Kmieć 2001).

- **Hepatic stellate cells (HSC)** formerly known as fat-storing cells, Ito cells, lipocytes, perisinusoidal cells, or vitamin A-rich cells are located in the space of Disse (Figure I-4). They are characterized by abundance of intracytoplasmic fat droplets. In a normal liver HSC store vitamin A, control turnover of extracellular matrix, and regulate the contractility of sinusoids. Acute damage to hepatocytes promotes the transformation of quiescent stellate cells into myofibroblast-like cells with pro-fibrogenic functions that play a key role in the development of inflammatory fibrotic response (Kmieć 2001).

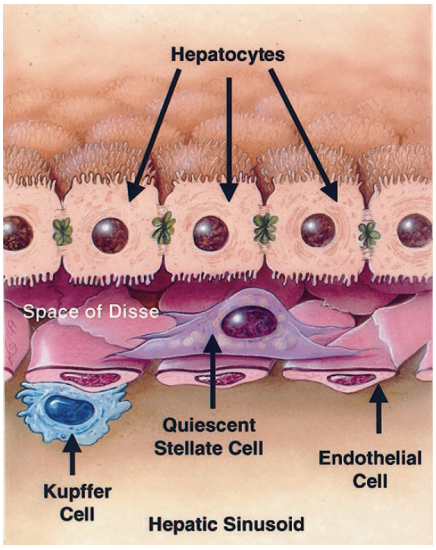

Figure I-4. Hepatic major cell types: hepatocytes, HSC in the Space of Disse, SEC forming the lining of the sinusoids and the hepatic macrophages, the KC situated in the sinusoids (Friedman 2000).

1.3. Liver functions

The liver performs a vast number of functions, some of them essential for life, meaning that their impairment can lead to death in a few days. Following there is a summary of the most important liver functions:

- **Carbohydrate metabolism:** The liver is especially important for maintaining normal blood glucose levels.
    - Glycogen storage: **Glycogenesis** and storage of glycogen allows the liver to remove excess glucose from the blood and store it as glycogen. However, if glucose blood levels fall low hepatic stored glycogen is degraded (**Glycogenolysis**) and poured into blood. This is called the *glucose buffer function* of the liver. In a person with poor liver function, blood glucose concentration after a meal rich in carbohydrates may rise two to three times above physiological levels (C. Guyton and E. Hall 2000).
    - Conversion of galactose and fructose into glucose.
    - **Gluconeogenesis:** is also important in maintaining normal blood glucose concentration when blood glucose concentration falls below normal levels. When this happens, large amounts of amino acids and glycerol from triglycerides (TGs) are converted into glucose, thereby helping to maintain a relatively normal blood glucose concentration (C. Guyton and E. Hall 2000).
- **Fat metabolism:**
    - **Fatty acid (FA) oxidation:** this function allows supplying energy for other body functions. To derive energy from neutral fats, fat is first split into glycerol and FAs; FAs are metabolized via β-oxidation primarily in mitochondria and its product can enter then the tricarboxylic acid (TCA) cycle producing a great amount of energy. β-oxidation can take place in all cells of the body, especially in the hepatic cells. If the liver cannot use all the acetyl-coA generated from the β-oxidation, it generates acetoacetic acid from the condensation of two acetyl-CoA molecules, which circulates in the blood to other tissues and serves as substrate for energy supply (C. Guyton and E. Hall 2000).
    - **Synthesis of cholesterol, phospholipids and lipoproteins:** 80% of the cholesterol synthesized in the liver is converted into bile salts, which are secreted into the bile; the rest is transported elsewhere in the form of lipoproteins. Phospholipids are likewise synthesized in the liver and transported principally in the lipoproteins. Both cholesterol and

phospholipids are key components of membrane bilayers and intracellular structures, and intermediates of important metabolic pathways (C. Guyton and E. Hall 2000).

- ***de novo* lipogenesis:** it the synthesis of fat from proteins and carbohydrates. Almost all the fat synthesis in the body from carbohydrates and proteins occurs in the liver. After fat is synthesized in the liver, it is transported in the very-low-density-lipoproteins (VLDL) to the adipose tissue to be stored (C. Guyton and E. Hall 2000).

- **Protein metabolism:**
  - **Deamination of amino acids:** Deamination of amino acids is required before they can be used for energy or converted into carbohydrates or fats.
  - **Formation of urea:** this is an essential function to remove ammonia from the blood. The deamination process forms large amounts of ammonia, and additional amounts are continually formed in the gut by bacteria and then absorbed into the blood. Therefore, if the liver fails to generate urea, the plasma ammonia concentration rises rapidly resulting in encephalopathy and death (C. Guyton and E. Hall 2000).
  - **Synthesis of plasma proteins:** 90% of all the plasma proteins are formed in the liver. The remaining gamma globulins are the antibodies formed mainly by plasma cells in the lymph tissue of the body. The liver can form plasma proteins at a maximum rate of 15 to 50 g/day. Plasma protein depletion causes rapid mitosis of the hepatic cells and growth of the liver to a larger size (hepatomegaly); these effects are coupled with rapid output of plasma proteins until the plasma concentration returns to normal. With chronic liver disease, plasma proteins, such as albumin, may fall to very low levels (C. Guyton and E. Hall 2000).
- **Synthesis and secretion of bile:** The liver synthesizes and secretes bile at a rate of 600 and 1000 ml/day. Bile serves two important functions: 1) fat digestion and absorption because it helps to emulsify large fat particles into many minute particles so lipase enzymes can attack their surface and 2) bile serves as a means for excretion of several important waste products from the blood including bilirubin, and also cholesterol excess (C. Guyton and E. Hall 2000).

- **Synthesis of coagulation factors:** the liver synthesizes coagulation factors including fibrinogen, prothrombin, accelerator globulin, Factor VII among others. Vitamin K is required for liver metabolism and formation of coagulation factors. In the absence of vitamin K, the concentrations of these factors decrease markedly, and this can impair blood coagulation (C. Guyton and E. Hall 2000).
- **Vitamins reservoir:** The vitamin stored in greatest quantity in the liver is vitamin A, but large quantities of vitamin D and vitamin B12 are normally stored as well. It also stores vitamin E and K. All these vitamins are released from the liver when needed elsewhere in the body (C. Guyton and E. Hall 2000).
- **Iron reservoir:** Except for hemoglobin of the blood, the greatest proportion of iron in the body is stored in the liver in the form of ferritin. Hepatic cells contain large amounts of apoferritin, which binds to iron reversibly. Therefore, when iron is available in body fluids in extra quantities, it combines with apoferritin to form ferritin and is stored in this form in hepatocytes until needed elsewhere. When iron in the circulating body fluids reaches a low level, ferritin releases the iron (C. Guyton and E. Hall 2000).
- **Blood reservoir:** the liver is an expandable venous organ and large quantities of blood can be stored in its blood vessels. Its normal blood volume is about 450 ml, almost 10% of the body's total blood volume. The liver acts as a blood reservoir when blood volume is high and it is capable of supplying extra blood in times of diminished blood volume (C. Guyton and E. Hall 2000).
- **Blood cleansing:** As blood flows through the intestinal capillaries it becomes enriched in bacteria derived from the gut. KC efficiently cleanse blood as it passes through the sinusoids. It has been estimated that less than 1% of the bacteria entering the portal blood from the gut succeed in passing through the liver into the systemic circulation (C. Guyton and E. Hall 2000).
- **Detoxification:** the liver is able to detoxify and excrete many drugs and metabolites (i.e. alcohol, antibodies, etc) into the bile. In a similar manner, several of the hormones secreted by the endocrine glands are either chemically altered or excreted by the liver, including all the steroid hormones. Bilirrubin derived from the heme group of aged red blood cells is absorbed by the liver, secreted into the bile, metabolized in the small intestine and eliminated in the feces (C. Guyton and E. Hall 2000).

- **Regulation of liver mass:** Unlike other organs, the liver has the ability to regenerate itself and restore its original mass after significant hepatic tissue loss from either partial hepatectomy or acute liver injury. Partial hepatectomy, in which up to 70% of the liver is removed, causes the remaining lobes to enlarge and restore the liver to its original size. This regeneration is remarkably rapid and requires only 5 to 7 days in rats. During liver regeneration, hepatocytes are estimated to replicate once or twice, and after the original size and volume of the liver are achieved, the hepatocytes revert to their usual quiescent state (C. Guyton and E. Hall 2000).

2. FROM OBESITY TO NON-ALCOHOLIC FATTY LIVER DISEASE.

2.1. Obesity:

Obesity is characterized by excessive fat accumulation in adipose tissue and other organs. Obesity reflects the imbalance between energy intake and energy expenditure. Due to the global epidemic of overweight and obesity, which is currently a major public health problem in many parts of the world, the World Health Organization (WHO) renamed it "globesity".

The body mass index or BMI is a measurement of body fat used in clinical and epidemiologic studies to assess obesity in human adults. BMI is calculated as weight (kg) divided by height squared (m^2). The WHO defines overweight as a BMI equal to or greater than 25 kg/m^2 and obese as a BMI equal to or greater than 30 kg/m^2 (Ahima 2011).

The WHO estimated that in 2008, 1.5 billion adults were overweight and over 200 million men and 300 million women, approximately 10% of adults were obese (Ahima 2011) (Figure I-5). There are three major causes that account for the increasing prevalence of obesity:

1. Calorie intake: there has been a drastic increase in total calorie intake over the past two decades. In most developed countries, the total calorie intake levels are above the recommended 2000 Kcal/day and getting close to the 3000 Kcal/day.
2. Calorie quality: there has been a switch from diets rich in vegetables, fruit and fish to more fatty (specially saturated fats) and high sugar diets. Chronic intake of fatty diets and fructose and frequent consumption of processed food increases the risk of obesity.
3. Lack of exercise: sedentary lifestyle is also a major contributor to weight gain. Low levels of physical activity are closely related to body weight gain.

Unfortunately, obesity is no longer a problem of high-income developed countries alone as it affects third world countries as well. Indeed, the largest increases in obesity since 1980 have occurred in low and middle-income countries, particularly in urban settings in Oceania, Latin America, and North Africa (Ahima 2011) (Figure I-5).

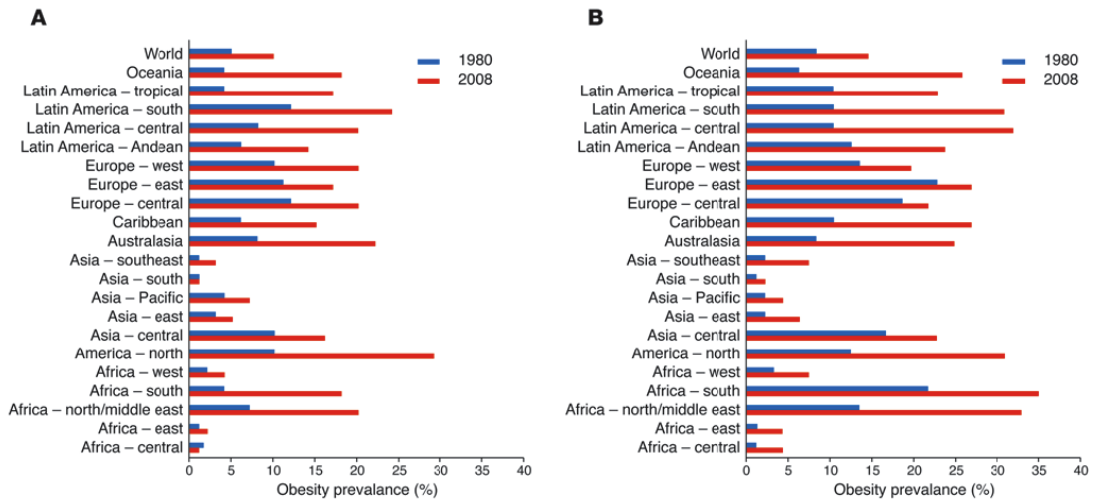

Figure I-5. Worldwide change in prevalence of obesity in men (A) and women (B) between 1980 and 2008 (Ahima 2011).

Obesity is a risk factor for other pathological conditions such as insulin resistance and type 2 diabetes mellitus (T2DM) (Kahn, Hull et al. 2006) as well as non-alcoholic fatty liver disease (NAFLD) (Fabbrini, Sullivan et al. 2010; Cusi 2012), cardiovascular disease (CVD) (Van Gaal, Mertens et al. 2006) and cancer (Sun and Karin 2012).

Diet, exercise, and other lifestyle modifications are the first line of protection against obesity. However, compliance with these measures is difficult to maintain for long periods of time. Anti-obesity drugs are largely ineffective, and even bariatric surgery provides and efficient and rapid reduction in weight followed by weight regain over time. Thus, there is a need for understanding the regulation of energy homeostasis and the mechanisms whereby obesity causes diabetes and other complications like fatty liver disease.

2.2. Adipose tissue during obesity:

Adipose tissue can respond rapidly and dynamically to alterations in nutrient availability, contributing to the maintenance of body energy homeostasis. Adipose tissue remodeling is an active process that is pathologically accelerated in the obese state (Sun, Kusminski et al. 2011).

2.2.1. Adipose tissue plasticity:

The first adaptation in adults to avoid systemic lipotoxicity from chronic overfeeding is enlargement of adipocytes (hypertrophy), followed by a longer-term

compensatory mechanism involving fat cell replication (hyperplasia) (Cusi 2012). Adipocyte hypertrophy prevails in obesity. Healthy adipose tissue expansion consists in effective recruitment of adipogenic precursor cells to the adipogenic program, along with an adequate angiogenic response and appropriate remodeling of the extracellular matrix. In contrast, pathological adipose tissue expansion consists of massive enlargement of existing adipocytes, limited angiogenesis, and ensuing hypoxia (Sun, Kusminski et al. 2011) (Figure I-6).

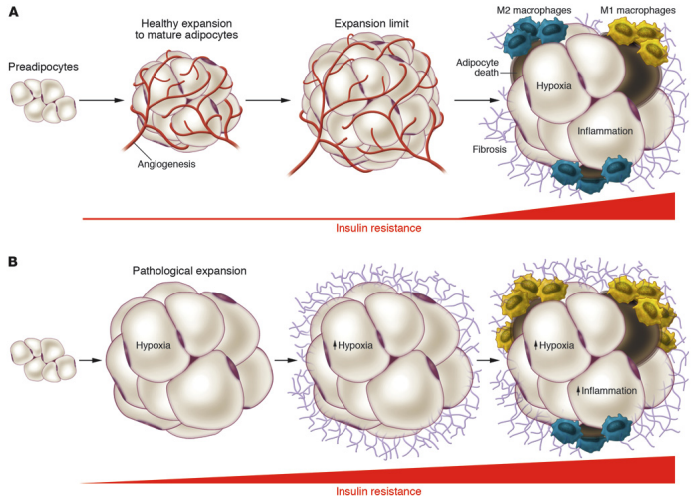

Figure I-6. (A) Healthy adipose tissue expansion (B) Pathological adipose tissue expansion (Sun, Kusminski et al. 2011).

2.2.2. Adipose tissue dysfunction:

Protection from chronic energy supply and excess TG accumulation in tissues such as liver, muscle, and pancreatic beta cells requires an extraordinary adaptation by adipocytes that involves activation of several inflammatory pathways and inflammatory cells but at the cost of adipose tissue function (Cusi 2012).

2.2.2.1. Inflammation:

Obesity is associated with a chronic low-grade systemic inflammation, particularly in white adipose tissue, which is believed to contribute to metabolic disorders, and progression from hepatic steatosis to non-alcoholic steatohepatitis (NASH), fibrosis, cirrhosis and eventually hepatocellular carcinoma (HCC) (Cusi 2012). Hypertrophic adipocytes actively produce

and secrete cytokines that contribute to the local and systemic inflammation. Among others, Tumor Necrosis Factor α (TNF-α), Interleukin 6 (IL-6) and Monocyte chemoattractant protein 1 (MCP-1) are hallmarks of obese adipose tissue (Wellen and Hotamisligil 2005) (Figure I-7).

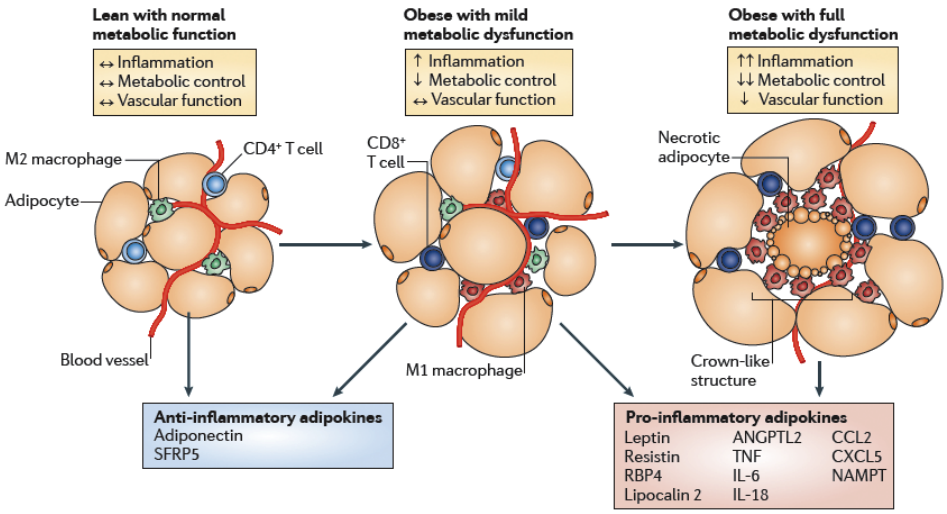

Figure I-7. Adipose tissue evolution from lean to obese: inflammation, vascular function and metabolic control (Ouchi, Parker et al. 2011).

Inflammatory pathways can be initiated by extracellular mediators such as cytokines and lipids or by intracellular stresses induced by obesity like Endoplasmatic Reticulum stress (ER stress) (Ozcan, Cao et al. 2004) or Reactive Oxygen Species (ROS) production by mitochondria due to an increased glucose metabolism. Signals from all of these mediators converge on inflammatory signaling pathways, including the kinases c-jun N-terminal kinase (JNK) and IκB Kinase (IKK), inducer of Nuclear Factor Kappa B (NF-κB) pathway. These pathways not only induce the production of additional inflammatory mediators at the transcriptional level, but also directly inhibit insulin signaling pathway, thus establishing a feed forward cycle between inflammation and insulin resistance (Wellen and Hotamisligil 2005) (Figure I-8).

2.2.2.2. Macrophage infiltration:

As discussed before, adipose tissue expansion can lead to hypoxia, adipocyte cell death, enhanced chemokine secretion, and deregulation of FA fluxes.

This requires macrophages to create a permissive environment for the remodeling process. The adipose tissue has a pool of adipose tissue resident macrophages (ATM) that during obesity are activated by various stimuli:

- Adipocyte cell death: Macrophages aggregate, forming crown-like structures (CLSs) surrounding necrotic adipocytes in advanced obesity (Figure I-7).
- Chemotactic regulation. There is an increased expression of chemokines by the adipose tissue during obesity that promotes macrophage mobilization from bone marrow into tissues.
- Hypoxia.
- FA flux.

2.2.2.3. Insulin resistance:

As previously stated, adipocyte adaptation has its costs. The activation of inflammatory pathways described above is known to block the insulin-signaling pathway leading to insulin resistance in the adipose tissue (Figure I-8). At this point, the adipose tissue becomes blind to insulin signals driving adipose tissue to a catabolic state. The adipose tissue behaves as if the body were in a fasting state where enhanced lipolysis increases free FA (FFA) release to the circulation and energy storing capacity is inhibited.

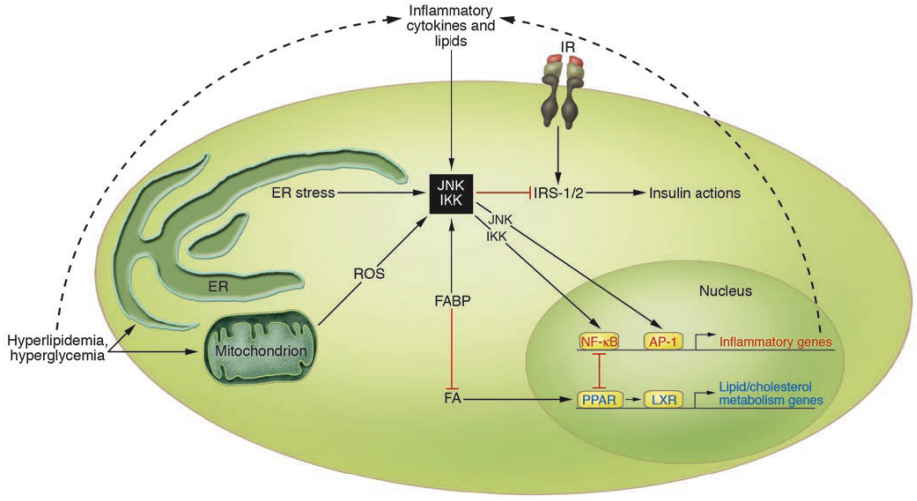

Figure I-8. Model of overlapping metabolic and inflammatory signaling in adipocytes (Wellen and Hotamisligil 2005).

2.3. Systemic implications of adipose tissue dysfunction:

The increased secretion of cytokines and FFAs to the circulation derived from adipose tissue linked to its inability to properly store nutrients coming from the diet increases systemic inflammation and promotes ectopic lipid accumulation (Figure I-9).

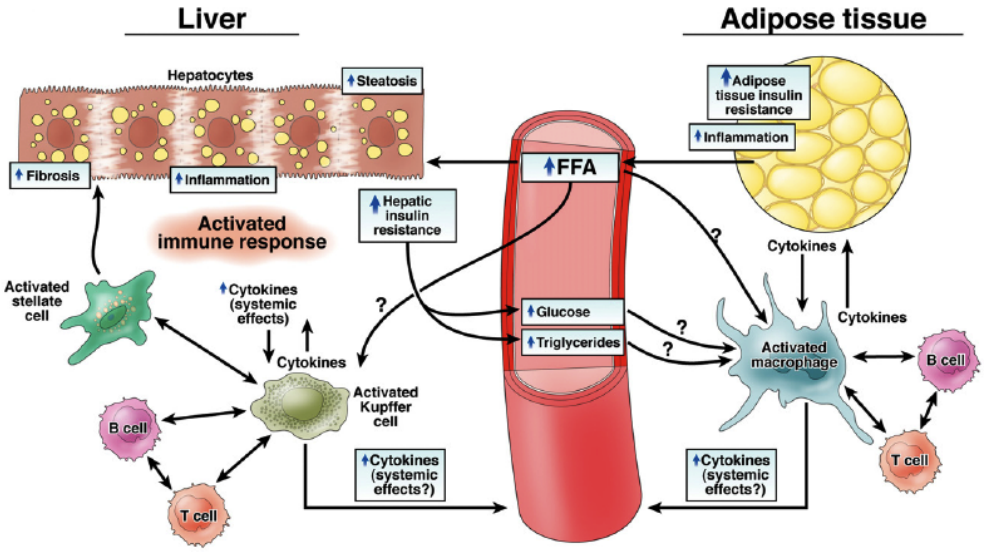

Figure I-9. Systemic effects of adipose tissue dysfunction during obesity (Cusi 2012).

Tissues like liver or muscle take over the physiological function of adipose tissue of storing fat. However, since these organs are not prepared for such function, they undergo cellular stress and tissue inflammation, leading eventually to tissue dysfunction and insulin resistance. The stress caused by the ectopic fat accumulation, specially saturated FFAs, is known as lipotoxicity. Some of the mechanisms of action underlying FA-induced lipotoxicity will be discussed in Section 2.5.

2.4. Non-Alcoholic Fatty Liver Disease:

The rapid increase in obesity worldwide is associated with an increase in prevalence of non-alcoholic fatty liver disease. NAFLD is the most common form of chronic liver disease in the Western countries and it is considered the hepatic manifestation of metabolic syndrome (Bechmann, Hannivoort et al. 2012).

2.4.1. Natural history of NAFLD:

Historically, NAFLD refers to TG accumulation in the liver in the absence of excessive alcohol consumption. NAFLD encompasses a spectrum of liver disorders

ranging from simple steatosis progressing through NASH and fibrosis to cirrhosis and end-stage liver failure. Simple steatosis is defined histologically as >5% hepatic steatosis in the absence of inflammation or hepatocellular damage, whereas NASH is characterized by inflammation and hepatocellular damage with variable degrees of fibrosis. Simple steatosis rarely progresses to advanced liver disease, whereas NASH has the potential to progress to cirrhosis, end-stage liver failure and HCC (Cusi 2012) (Figure I-10).

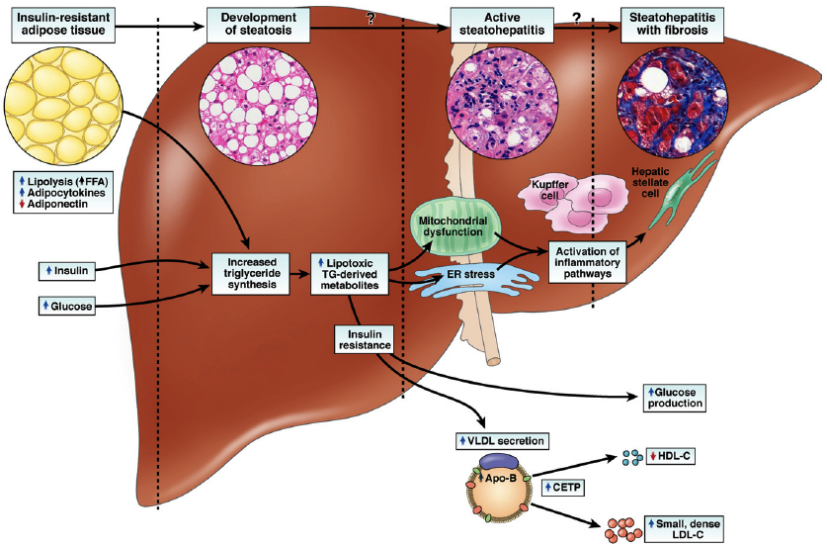

Figure I-10. Schematic representation of the pathophysiology of NASH (Cusi 2012).

The pathogenesis of NAFLD has classically been thought of as a "two hit" process; the first resulting in hepatic TG accumulation and the second being responsible for hepatocyte death and scar formation. As the understanding of the pathogenesis of NAFLD evolves, alternative hypotheses are gaining favor, switching from a two hit hypothesis to a "multi parallel hits" hypothesis. Some of these multi parallel hits will be further discussed in section 2.5.

2.4.2. Epidemiology of NAFLD:

NAFLD is the most common cause of liver test abnormalities; NAFLD accounts for 70% of all cases of asymptomatic elevated transaminase enzyme levels in US adults. Population based studies of Western countries such as the US, Italy and Israel have demonstrated a prevalence of NAFLD between 20-30%, whereas the prevalence in Eastern countries such as China has been documented to be 13-

17%. Among the US population, there are significant differences in NAFLD prevalence according to ethnicity, affecting 45% of Hispanics, 33% of Caucasians and 24% of blacks (Smith and Adams 2011).

The presence of NAFLD is closely associated with metabolic syndrome. The prevalence of NAFLD is increased in the presence of obesity, impaired glucose tolerance or T2DM, dyslipidemia with hypertriglyceridema and low high-density lipoprotein (HDL) cholesterol levels and hypertension (Figure I-11). 85% of patients with NAFLD have at least one metabolic risk factor with one-third of individuals having the metabolic syndrome itself. The prevalence of obesity in patients with NAFLD is reported to range between 61% and 100% and the prevalence of dyslipidemia between 27% and 67%. Among morbidly obese patients who undergo bariatric surgery, 90% have NAFLD (Smith and Adams 2011).

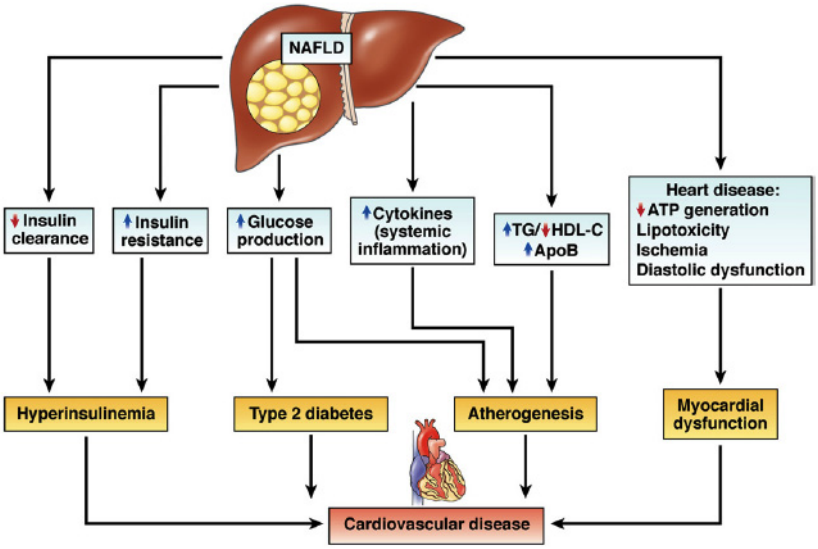

Figure I-11. Risk factors that coexist in patients with NAFLD (Cusi 2012).

Subjects with NAFLD are at increased risk of death compared to the general population, NAFLD subjects have a 34% increase in hazard ratio for overall mortality. In large cohorts, death related to liver disease is the third most common cause of death, suggesting it is partly responsible for the increase in overall mortality. Risk factors for mortality in subjects with simple steatosis include the presence of cirrhosis, impaired fasting glycemia or diabetes. In contrast, NASH is more frequently progressive and may lead to cirrhosis with

complications of HCC, liver failure and liver related death or requirement for liver transplantation. In addition to liver related morbidity and mortality, subjects with NASH are at increased risk of cardiac morbidity and mortality (Smith and Adams 2011).

2.4.3. Hepatic lipid metabolism in NAFLD:

There is a close relationship between adipose tissue and liver because adipocytes supply more than two-thirds of FAs used for hepatic TG synthesis (Barrows and Parks 2006). A lesser but important fraction of hepatic FAs are synthesized *de novo* by the transcriptional up-regulation of enzymes involved in FA synthesis. Hepatic lipid accumulation results from an imbalance between lipid availability (from circulating lipid uptake or *de novo* lipogenesis) and lipid disposal (via FFA oxidation or TG-rich lipoprotein secretion). Each of these steps is altered in NAFLD. Regulation of these pathways is complex and involves nuclear receptors, membrane transport proteins and cellular enzymes (Musso, Gambino et al. 2009).

The sources of FA contributing to fatty liver include:

- Plasma FFA pool from the adipose tissue: Insulin resistance is associated with dysregulation of adipose-derived FFA flux in a fed state, and strong evidence exists demonstrating that in NAFLD patients, insulin fails to suppress adipose tissue lipolysis. The plasma FFA pool contributes the majority of FFAs flowing to the liver in the fasted state and thus provides the bulk of the FFAs secreted by the liver in VLDL particles.
- *de novo* lipogenesis (DNL): FAs newly made in the liver through DNL. During obesity, DNL regulation is lost and constitutively active due to activation of transcription factors that regulate key enzymes of DNL.
- Dietary FAs: which can enter the liver through spillover into the plasma FFA pool and through the uptake of intestinally derived chylomicron remnants.

Contribution of FA sources to hepatic TG content in obese subjects:

- 59% of hepatic TG arose from circulating FFA pool
- 26% of hepatic TG arose from DNL

- 15% of hepatic TG arose from the diet

These metabolic data indicate that both elevated peripheral FFA flux and DNL are major contributors to hepatic steatosis in NAFLD.

2.4.3.1. FA uptake:

Circulating FFAs deriving from adipose tissue lipolysis provide most of the hepatic lipid content in NAFLD, thus mechanisms of hepatic FA uptake are important to understand the disease. FFAs are highly insoluble in aqueous media and are kept in circulation by binding to albumin. It was previously thought that FFAs entered the cell by passive diffusion through the bilayer lipid membrane. However, many studies proved that uptake of FAs is far more complex and involves several steps: dissociation from albumin, transport across the membrane, binding to intracellular proteins and esterification to acyl-CoA.

The main plasma membrane protein transporters involved in FA transmembrane translocation are: caveolins, FA transport proteins (FATPs), FA translocase (FAT/CD36) and FA binding proteins (FABPs) (Figure I-12).

Caveolins can be found in the lipid rafts of the plasma membrane (Figure I-12). These structures are important for cell signaling and protein trafficking processes and are essential for lipid droplet formation. Caveolin-1 deficient mice exhibit defective lipid droplet formation and are unable to regenerate the liver (Pol, Martin et al. 2004).

FATPs are a family of six members. FATP2 and FATP5 are mainly expressed in liver. Their expression is regulated by insulin, inflammatory mediators and by activators of peroxisome proliferator activated receptor PPAR-α and PPAR-γ. FATP5 deficiency decreases by 50% FA uptake in primary mouse hepatocytes and whole body deficiency protects mice from diet-induced obesity, insulin resistance and hepatosteatosis (Doege, Baillie et al. 2006; Musso, Gambino et al. 2009).

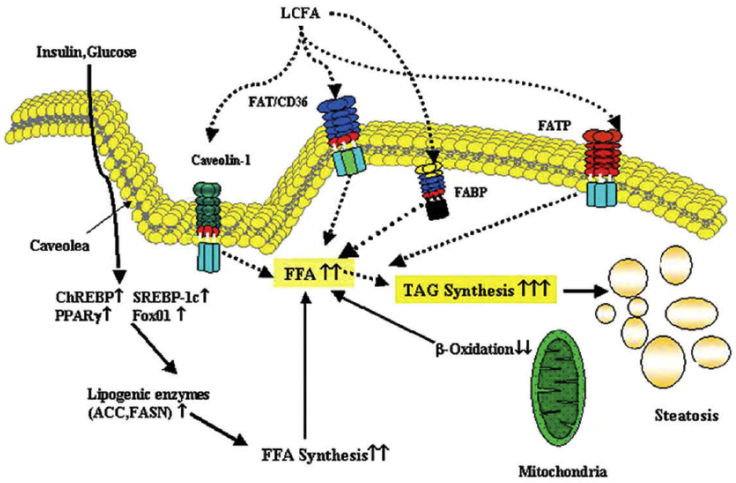

Figure I-12. Hepatic lipid metabolism and hepatic steatosis. Increased hepatic TG comes from FAs that are formed by up-regulated de novo lipogenesis (DNL) and from plasma long chain fatty acids (LCFA) that are taken up by the liver; reduced mitochondrial FA oxidation also favors TG accumulation (Musso, Gambino et al. 2009).

CD36 is a multifunctional protein since it enhances FA uptake and it is a receptor for different ligands including VLDLs and oxidized low-density lipoproteins (LDLs) (Figure I-12). Its expression can be induced by PPAR-α and PPAR-γ and liver X receptor (LXR). It is expressed in many cell types and tissues but its presence is low in hepatocytes. Although, it has been reported that its expression is increased in patients with NAFLD. In mouse models of diet-induced obesity, increased levels of hepatic TG correlated with increased levels of CD36 expression and specific induction of CD36 in liver leads to hepatomegaly and fatty liver (Musso, Gambino et al. 2009).

FABPs are small, highly expressed proteins that reversibly bind FAs, eicosanoids, and other lipids. These lipid chaperones facilitate the transport of FAs and other lipid mediators across cellular membranes. FABPs are also located in the cytosol, where they mediate intracellular transport of FAs throughout the cytosol to their nuclear receptors, including PPARs, retinoic acid receptor (RAR), LXRα and NF-kB, thus controlling the availability of ligands to regulate transcription of genes involved in important metabolic and inflammatory processes (Figure I-12). FABPs are a family of 9 members. FABP-1 is abundant in liver cytoplasm. The role of FABP- deficiency in diet-induced hepatic steatosis is controversial. In this regard, one study demonstrated that its deficiency protected mice from high saturated fat diet-

induced liver steatosis and weight gain but it didn't have any impact on insulin resistance (Furuhashi and Hotamisligil 2008).

2.4.3.2. *de novo* hepatic lipogenesis:

Physiologically DNL occurs postprandially in healthy subjects. In NAFLD, however, there is a paradoxical sustained elevation of DNL in fasting conditions that lacks further postprandial elevation. The regulation of hepatic lipogenesis involves a complex network of nuclear receptors, coordinately regulating enzymes involved in different steps of hepatic lipid metabolism, from DNL to FA oxidation and uptake onto TG secretion (Musso, Gambino et al. 2009).

Hepatic lipogenesis includes *de novo* synthesis of FAs from acetyl-CoA or malonyl-CoA and further processing to TGs. In mammals, FA synthesis is catalyzed by acetyl-CoA carboxylase (ACC) and fatty acid synthase (FAS), an enzyme that exhibits a complex regulation by nuclear receptors (PPARα, PPARγ and the bile acid receptor/farnesoid X receptor [FXR]). DNL is extremely sensitive to insulin since it activates the expression of FAS, thus hyperinsulinemia states such as obesity may activate DNL. At the transcriptional level, sterol-regulatory element binding protein 1c (SREBP1c) and carbohydrate-responsive element binding protein (ChREBP), a glucose dependent transcription factor, synergistically induce expression of FAS and ACC.

As FAs and their metabolites are the major cause for lipotoxicity and promote ROS formation, FAs are stored for future use as TGs, which are relatively inert and consist of three FAs esterified to a glycerol backbone. TGs are then either stored in lipid droplets within hepatocytes or processed to VLDL. TG synthesis is catalyzed by the enzymes mitochondrial glycerol- 3-phosphate-acyltransferase (mtGPAT) and diacylglycerolacyltransferase (DGAT). TGs are then packaged into VLDL particles by conjugation to apoB-100 in a 5:1 TG/cholesterol ratio. These processes are controlled by SREBP1c, the LXR,

FXR and ChREBP, which link glucose and lipid metabolism (Bechmann, Hannivoort et al. 2012).

2.4.3.3. FA oxidation:

Oxidation of FAs facilitates degradation of activated FAs to acetyl-CoA. It is a rapid and effective way of energy allocation since, the oxidation of one molecule of palmitate produces up to 129 ATP equivalents.

FAs are activated by acyl-CoA-synthetase to acyl-CoA in the cytosol. This process is indispensable for enabling FAs to cross membranes and enter organelles. While short and medium-chain FAs pass the mitochondrial membrane without activation, activated LCFAs are shuttled across the membrane via carnitine palmitoyltransferase-1 (CPT1). Malonyl-CoA, an early intermediate of DNL that accumulates upon insulin receptor activation, is an allosteric inhibitor of CPT1. Thus, in the fed state, FA oxidation is inhibited promoting DNL, which results in fat storage and distribution of lipids.

Different hepatic FA oxidative pathways are involved in the pathogenesis of NAFLD. Most FAs are metabolized through β-oxidation, which occurs mainly in mitochondria, and to a lesser extent in peroxisomes. A third FA metabolizing pathway is ω-oxidation by members of the cytochrome P450 in the ER (Figure I-13). The extramitochondrial FA oxidative pathways become more important in conditions of increased FA availability in the liver like NAFLD. Key enzymes of FA oxidation are regulated by PPARα (Musso, Gambino et al. 2009).

In general, short-, medium- and LCFAs are oxidized within mitochondria, while toxic, LCFAs are oxidized within peroxisomes. During the process of β-oxidation, electrons are indirectly donated to the electron transport chain to drive ATP synthesis. Acetyl-CoA can be further processed via the TCA cycle or, in the case of FA abundance, be converted into ketone bodies. As the oxidative capacity of the mitochondria becomes impaired, like in cases of

diabetes or FA overload, cytosolic FAs accumulate. Alternative pathways in the peroxisomes (β-oxidation) and in microsomes (ω-oxidation) are activated, resulting in the formation of additional ROS (Figure I-13). Microsomal ω-oxidation of FAs is catalyzed primarily by cytochrome P450 enzymes 2E1, 4A10, and 4A14, generating ROS. Additionally, dicarboxylic acids, another product of microsomal FA ω-oxidation, impair mitochondrial function by uncoupling oxidative phosphorylation. Protonated dicarboxylic acids shuttling from the inner to the outer mitochondrial membrane dissipate the mitochondrial proton gradient without concomitant ATP production (Musso, Gambino et al. 2009) (Figure I-13).

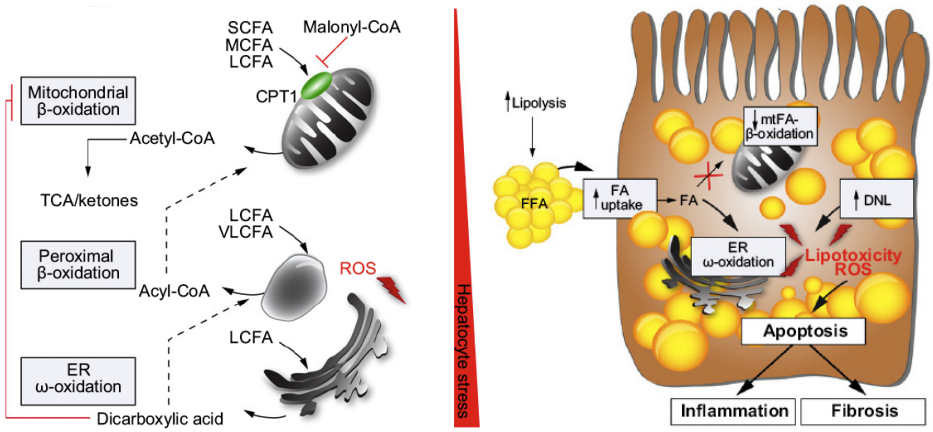

Figure I-13. Fatty acid oxidation under physiologic conditions and NASH (Bechmann, Hannivoort et al. 2012).

Increased availability of intracellular FAs, as well as PPARα activation, induce microsomal CYP2E1 and CYP4A1 activity, leading to generation of ROS and dicarboxylic acids. CYP2E1 is overexpressed in both experimental and human NAFLD and in vivo measured CYP2E1 activation correlates with the severity of liver necroinflammation, suggesting that this mechanism may contribute substantially to ROS-induced hepatic injury (Musso, Gambino et al. 2009). The cumulative effect of extramitochondrial FA oxidation is a further increase in oxidative stress and mitochondrial impairment.

2.5. Hepatic lipotoxicity:

By definition, lipotoxicity reflects the toxic effects due to the accumulation of lipids. In the context of NAFLD, there is a wide array of lipids known to accumulate including

diacylglycerol, ceramide, FC, cholesterol esters and FFAs. Among them, FFAs are considered of relevance, particularly saturated FFAs, which impair insulin signaling, activate stress pathways and induce cell death, thereby resulting in lipoapoptosis. Hepatic lipotoxicity due to FFAs accumulation occurs when the hepatic capacity to oxidize, store and export FFAs as TG is overwhelmed by FFA flux from the periphery or hepatic *de novo* lipogenesis (Trauner, Arrese et al. 2010) (Figure I-14).

In contrast to saturated FFAs, unsaturated FFAs are nontoxic and are stored as TG. The mechanisms that discriminate toxic versus nontoxic effects of saturated and unsaturated FFAs are poorly understood. Thus, experimental studies suggest that lipid compartmentalization in hepatocytes and in particular the type or "quality" as opposed to the "quantity" of lipids accumulating may play a central role in the risk for progressive disease (Alkhouri, Dixon et al. 2009). Key examples of this emerging concept in NAFLD include the dissociation between hepatic steatosis and insulin resistance in mice overexpressing DGAT2, and the role of FC in the sensitization of fatty liver to inflammatory cytokines (Marí, Caballero et al. 2006; Monetti, Levin et al. 2007)

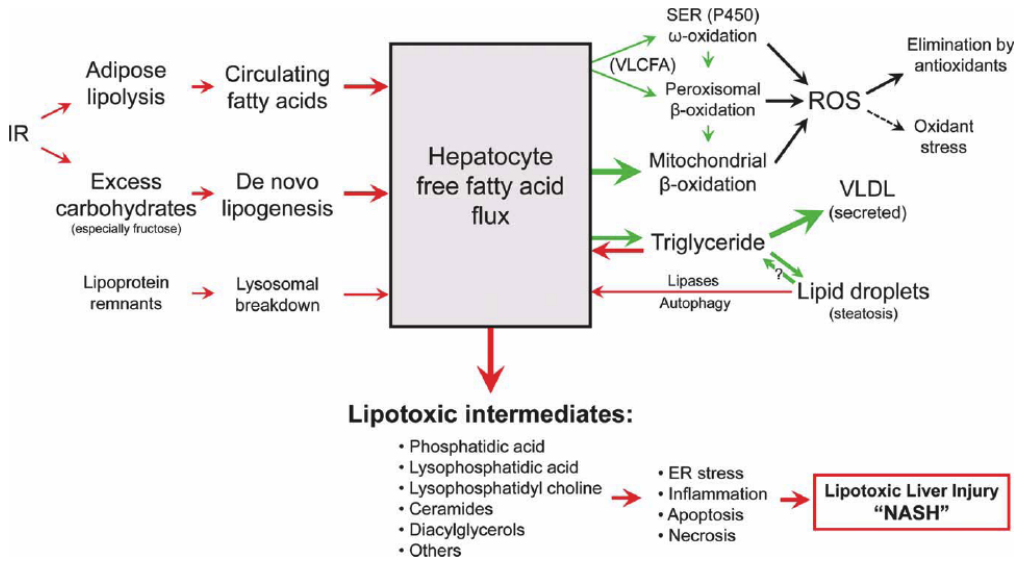

Figure I-14. Causes and mechanisms of hepatic lipotoxicity in NAFLD (Neuschwander-Tetri 2010).

TG accumulation in the liver in response to lipid overloading has been historically considered the "first hit" in NAFLD development and it was associated with features of insulin resistance. However, hepatocellular TG storage *per se* does not appear to be directly hepatotoxic but rather may be a marker of hepatocyte exposure to potentially

toxic FAs. Therefore, the ability to synthesize TG may, in fact, be protective against lipotoxicity of FAs in liver (Trauner, Arrese et al. 2010).

2.5.1. FFAs:

FFAs are highly noxious to biological systems. There is a great amount of evidence linking FFAs to hepatic lipotoxicity. Some of the mechanisms described are listed below (Figure I-15):

- Nature of FFAs: Saturated FFAs are more hepatotoxic than unsaturated FFAs. The toxic effects of saturated FFAs are believed to be due to their inability, relative to unsaturated FFAs, to be esterified and incorporated into TG. Saturated FFAs need additional esterification by Stearoyl-CoA desaturase-1 (SCD-1) enzyme in order to be incorporated into TG (Ibrahim, Kohli et al. 2011).

- Ligands of Toll-like receptors (TLRs): TLRs are a family of pattern-recognition receptors that play a critical role in the innate immune system by activating proinflammatory-signaling pathways in response to microbial pathogens. Saturated FFAs, like palmitate, can serve as activating ligands for TLR-4, leading to a cascade of inflammatory events precipitating apoptosis (Alkhouri, Dixon et al. 2009) (Figure I-15).

- Transcriptional regulation of death receptors: FFA can also induce up-regulation of death receptors such as Fas and TRAIL receptor 5 (DR5) sensitizing liver cells to apoptotic cell death. Both Fas and DR5 expression is increased in liver of patients with NASH (Alkhouri, Dixon et al. 2009) (Figure I-15).

- Lysosomal pathway: FFAs are capable of directly destabilizing lysosomal membranes, leading to inappropriate release of cathepsin B and causing activation of apoptotic pathways (Li, Berk et al. 2008; Neuschwander-Tetri 2010). FFA-induced lysosome permeabilization and release of cathepsin B to the cytosol is an early event that occurs prior to mitochondrial depolarization

and cytochrome c redistribution to the cytosol. More importantly, cathepsin B silencing by siRNA, or chemical inhibition significantly prevented FFA-induced mitochondrial dysfunction, highlighting the relevance of cathepsin B in FFA-induced mitochondrial dysfunction (Alkhouri, Dixon et al. 2009). In human liver specimens, release of cathepsin B into the cytoplasm is observed in NAFLD patients and it correlates with disease severity (Ibrahim, Kohli et al. 2011) (Figure I-15).

- Mitochondrial pathway: Mitochondria are involved in many processes essential for liver cell survival, including energy production, redox control, calcium homeostasis, and certain metabolic and biosynthetic pathways. In addition, mitochondria often play an essential role in cell death mechanisms (Tait and Green 2010). Mitochondrial function is impaired in NAFLD and this is believed to play an important role in the progression of the disease. Patients with NASH display ultrastructural mitochondrial abnormalities, decreased mitochondrial DNA and protein expression. However, recent findings in mouse genetic models of mitochondrial dysfunction due to ablation of Apoptosis inducing factor (AIF) or the mitochondrial transcription factor (TFAM) in liver or adipose tissue, dispute this association, as these mice are protected against diet-induced obesity and insulin resistance (Pospisilik, Knauf et al. 2007; Vernochet, Mourier et al. 2012). Nevertheless, FFAs can affect mitochondrial function at different levels, some of which are listed below:
    - Mitochondrial membrane permeabilization: FFAs are capable of inducing mitochondrial membrane permeabilization and increase ROS production. This oxidative stress can damage DNA, proteins and lipids. Specifically, lipid peroxidation has been linked to mitochondrial dysfunction. They are capable of altering mitochondrial DNA and proteins decreasing respiratory chain protein expression and activity (Musso, Gambino et al. 2009).
    - Proton leak: FFAs can directly act on the mitochondrial respiratory chain and induce an increase in the proton leak. In addition, saturated FFAs, through PPARγ activation, can induce the expression

of uncoupling protein family members (UCPs). UCPs are proteins associated to the mitochondrial inner membrane, where they mediate proton leak to uncouple substrate oxidation from ATP synthesis. This leads to increasing ROS that may cause cell damage at different levels (Musso, Gambino et al. 2009; Gambino, Musso et al. 2011).

• Intrinsic apoptotic pathways: saturated FFAs induce JNK-dependent hepatocyte lipoapoptosis by activating the pro-apoptotic proteins Bim and Bax (Alkhouri, Dixon et al. 2009). Furthermore, saturated FFAs induce rapid degradation of antiapoptotic proteins of Bcl-2 family in hepatocytes (Ibrahim, Kohli et al. 2011). These saturated FFA-induced effects can trigger intrinsic mitochondrial apoptotic pathways.

• ER stress: excessive saturated FFAs may induce ER stress and subsequent activation of the unfolded protein response (UPR). In principle, UPR is a compensatory and protective mechanism aimed to establish ER homeostasis. However if stress persists, UPR activates apoptotic pathways to eliminate damaged cells. ER stress is a mechanism that links saturated FFAs to lipotoxicity in NAFLD (Gentile, Frye et al. 2011) (Figure I-15). This mechanism will be further discussed in section 4.

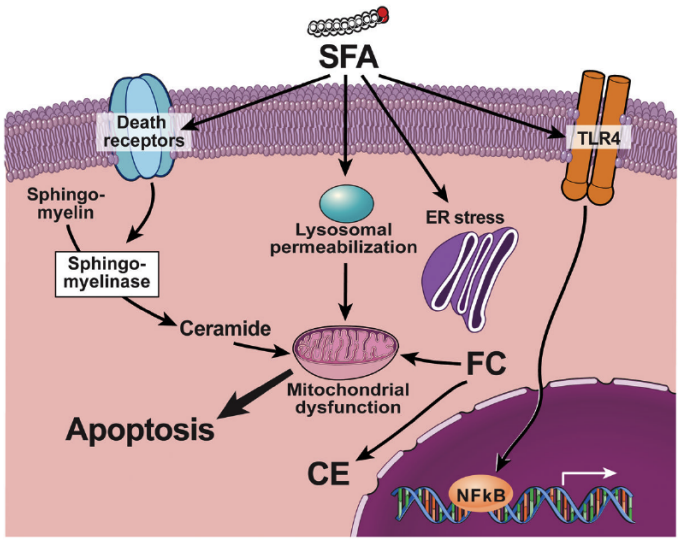

Figure I-15. Mechanisms of FA-induced lipoapoptosis (Alkhouri, Dixon et al. 2009).

2.5.2. Ceramide:

Ceramide is the prototype sphingolipid that has been intensively studied in the last two decades due to its emerging role in regulation of cell functions. Indeed, although sphingolipids have been considered mere structural components of biological membranes, it has been established that ceramide has a dynamic role in cell signaling, cell stress and death ligand-induced death (Marí and Fernández-Checa 2007; Morales, Lee et al. 2007). It has also been recognized as an important mediator of insulin resistance and obesity (Holland, Brozinick et al. 2007). The role of ceramide role in NAFLD and metabolic syndrome will be discussed in section 6.

Cells generate ceramide by two different pathways. Its *de novo* synthesis occurs in the ER with the condensation of serine and a saturated acyl-CoA, usually palmitoyl CoA, the rate-limiting step catalyzed by serine palmitoyl transferase (SPT), and the acylation of sphingosine with FFA catalyzed by ceramide synthases (CerS). Ceramide synthesis rate is dependent, among other factors, on the availability of palmitic acid and its activation to pamitoyl-CoA; therefore, obesity can be associated with excess ceramide production. In addition, ceramide can also be generated from sphingomyelin (SM) hydrolysis by sphingomyelinases. The generation of ceramide through this pathway is quick and transient and it has been involved in apoptosis induced by death ligands such as TNF-α and Fas that are also induced in obesity (Alkhouri, Dixon et al. 2009). While the impact of ceramide in obesity and NAFLD has not been well described, genetic evidence in mice deficient in dihydroceramide synthase, which exhibit 60-80% decreased ceramide content, established a role for ceramide in insulin resistance (Holland, Brozinick et al. 2007).

In vitro evidence indicated the correlation between staurated FFAs and increased ceramide accumulation. Animal studies established that feeding rats high fat diet enriched in saturated FFAs resulted in accumulation of hepatic ceramide and SM levels. In addition, obese mice with hepatic steatosis also have increased hepatic ceramide content (Pagadala, Kasumov et al. 2012). Interestingly, the type of FFAs also affects ceramide synthesis since saturated FA but not unsaturated oil infusion

results in a 60% increase in hepatic ceramide content in rats, compared to controls (Holland, Brozinick et al. 2007).

In contrast to experimental models, human data linking ceramides to the pathogenesis of NAFLD are sparse. Nevertheless, data in obese subjects showed increased hepatic ceramide and SM levels compared to subcutaneous and intra-abdominal adipose tissue (Kotronen, Seppänen-Laakso et al. 2010). Moreover, hepatic steatosis in human correlates with increased adipose tissue ceramide content (Pagadala, Kasumov et al. 2012). It has also been reported that weight loss resulted in decreased hepatic ceramide-related gene expression in obese patients with NAFLD that correlated with decreased serum ceramide levels. In addition, obese patients with T2DM, compared to lean healthy controls, had increased plasma ceramides and this observation correlated with degree of insulin resistance and plasma TNF-α (Haus, Kashyap et al. 2008). Moreover, liver samples of patients with NASH exhibit increased gene expression of key enzymes that regulate ceramide production (Moles, Tarrats et al. 2010; Promrat, Longato et al. 2011).

Ceramide has been strongly linked to induction of mitochondrial damage and apoptosis (Chavez and Summers 2010). Specific mechanisms for ceramide-induced mitochondrial damage and apoptosis are:

- Recruitment of pro-apoptotic protein Bax to mitochondrial membranes (Birbes, El Bawab et al. 2001; Birbes, Luberto et al. 2005).
- Generation of ROS through the inhibition of the electron transport chain or regulation of NADPH oxidase (García-Ruiz, Colell et al. 1997; Cacicedo, Benjachareowong et al. 2005). Interestingly, ROS in turn promote further ceramide synthesis (Summers 2006).
- Mediation of clustering of death receptors at the plasma membrane by the action of acid sphingomyelinase (ASMase) thereby triggering the extrinsic apoptotic pathway (Grassmé, Riethmüller et al. 2007).
- Direct increase of mitochondrial membrane permeability and subsequent cytochrome c release activating intrinsic apoptosis pathways (Colombini 2010).

- Activation of JNK and NFκB inflammatory pathways that are also known to inhibit insulin signaling (Summers 2006).

Thus, ceramide emerges as a key player in NASH, linking the FFA overload to inflammation and insulin resistance, which are the hallmarks of obesity and associated comorbidities (Figure I-15).

2.5.3. Free Cholesterol:

Due to its low abundance in free form, the role of cholesterol in liver diseases, and NASH in particular, has been neglected. However, recent data in both experimental models and patients have sparked the interest on the role of free cholesterol (FC) in liver pathology and NASH. Pioneering work from our laboratory showed that nutritional and genetic models of hypercholesterolemia promoted the transition from steatosis to NASH due to the specific trafficking of FC to mitochondria. The accumulation of FC in mitochondrial membranes impaired the transport of glutathione (GSH) from the cytosol to the mitochondrial matrix, thereby sensitizing hepatocytes to oxidative stress and TNF-α (Figure I-16). Repletion of mitochondrial GSH (mGSH) rescued FC-loaded livers from TNF-α-induced NASH (Marí, Caballero et al. 2006).

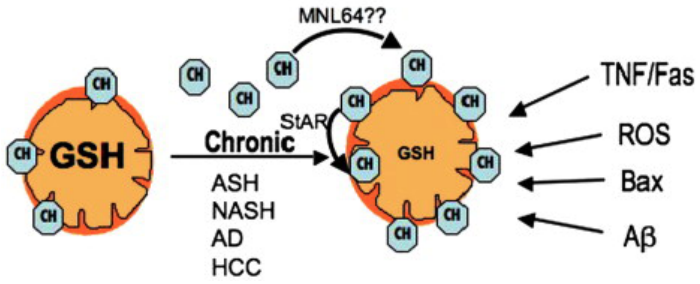

Figure 1-16. Mitochondrial FC reduces mGSH and sensitizes cells to other insults (Montero, Mari et al. 2010).

In addition, liver samples from patients with NASH exhibit increased FC compared to subjects with simple steatosis (Caballero, Fernández et al. 2009; Puri, Wiest et al. 2009). Interestingly, increased hepatic FC correlated with SREBP2 induction in the liver human samples (Caballero, Fernández et al. 2009; Min, Kapoor et al. 2012). Moreover, mitochondrial cholesterol transporter StAR overexpression in NASH suggested that mitochondrial FC might be a player in NASH (Caballero, Fernández et al. 2009).

2.6. NAFLD management:

2.6.1. Lifestyle intervention:

The most effective treatment of NAFLD is the weight loss through dietary change coupled with exercise. Dietary intervention (with or without exercise) improves hepatic steatosis and metabolic profile of patients with NAFLD. In short-term studies, a >5% weight loss appears to be the minimal threshold to decrease TG accumulation, whereas a 7% to 10% weight loss appears to be needed to reduce necroinflammation (Cusi 2012).

2.6.2. Insulin sensitizers:

Metformin is an insulin-sensitizing agent that is associated with reduced cardiovascular mortality in patients with T2DM. Improvement of insulin resistance occurs primarily in the liver. However, in patients with NAFLD, a number of small-randomized clinical trials of relatively short duration (6–12 months) have failed to demonstrate an improvement in liver steatosis, inflammation or fibrosis with metformin (Cusi 2012).

2.6.3. Antioxidants:

As discussed earlier, oxidative stress and lipid peroxidation within the liver appear to contribute to progressive liver damage in patients with NAFLD. Therefore, several trials investigated the use of antioxidant compounds, including vitamins E and C and betaine, for the treatment of NASH. Vitamin E is believed to ameliorate intracellular oxidative stress, which makes it an attractive therapeutic approach since it targets intracellular targets different from insulin sensitizers and offers an opportunity for combined therapy in NASH (Smith and Adams 2011).

Trials of antioxidants did not find any benefit on liver histology. However, a combination of pioglitazone and vitamin E were significantly better than placebo at improving hepatic steatosis and inflammation but not fibrosis in patients with NASH. Unfortunately, safety issues have been raised regarding long-term use of vitamin E, as it associates with an increased risk of cardiovascular disease and hemorrhagic stroke (Smith and Adams 2011).

Recent work from our lab in mouse models of NAFLD underscored a critical role for mGSH in the therapeutic potential of superoxide scavenging in NAFDL. These findings have potential clinical implications as they may help explain the failure of antioxidant treatment in human diseases so far. This study indicates that a better approach for NAFLD treatment is the combination of superoxide dismutase (SOD) mimetics together with mGSH restoration rather than improving SOD action only, illustrating the importance of a delicate equilibrium between these two antioxidants to ensure protection and therapeutic benefit (von Montfort, Matias et al. 2012).

2.6.4. PPAR agonists:

Thiazolidinediones (TZDs: pioglitazone and rosiglitazone) are PPARγ agonists that redistribute fat from the muscle and liver to peripheral adipose tissue and, thereby, improve insulin resistance and inflammation but stimulate weight gain. Different clinical trials of 6–24 months duration have demonstrated the efficacy of TZDs in patients with NASH. However, concerns have been raised regarding long-term safety of TZDs and heart failure, cardiovascular disease, bone loss and bladder cancer. For those reasons, pioglitazone has been discontinued in France and Germany (Smith and Adams 2011).

Taken together, there is an urgent need for new therapies to effectively treat NAFLD. An essential step towards this aim will be to better understand the mechanisms underlying NAFLD in order to define new targets and therapeutic strategies. The present thesis aims to elucidate the role of ceramide, and in particular, ASMase-mediated ceramide generation, on key aspects of NAFLD including, hepatic steatosis, liver injury and insulin resistance.

3. FROM ALCOHOLISM TO ALCOHOLIC LIVER DISEASE.

Alcohol has been used in society over centuries all over the world for its mood lifting properties and taste. Fortunately, only a small proportion of consumers develop clinically significant liver disease. It is probably, the commonest drug of abuse worldwide and unfortunately causes considerable morbidity, mortality and social disruption.

The relationship between alcohol and mankind is well documented from the earliest times. Winemaking equipment was found in the remains of an early Neolithic village in Northern Iran dated about 5.000 BC. Beer was first produced in Ancient Mesopotamia, Egypt and Greece. The Ancient Greeks worshipped the God of wine, Dionysus, and seem to have been the first to develop large-scale wine fermentation and production, with export to other countries (Figure I-17). The Romans in turn worshipped Bacchus, their God of wine, and were significant wine producers, planting vineyards across Europe.

Figure I-17. Dionysus. The Greek God of wine represents the intoxicating power of wine, its social and beneficial influences. Also known as the Liberator, freeing one from one's normal self, by madness, ecstasy, or wine.

Alcohol has long been accepted as part of human daily life, and its consumption gradually increased through centuries both in man and women. Sentiment toward moderation in drinking was documented in China in the 12th century BC. The association of alcohol with liver disease appeared to have been noticed by the ancient Egyptians, who linked the use of beer with ascites, and the ancient Greeks, who described the association with icterus and gastrointestinal bleeding. At the start of the twentieth century, concern for the effects of alcohol misuse in England induced the creation of licensing laws in Britain limiting the hours during which alcohol could be served, and these are currently still in place (Gordon 2001).

Alcohol abuse may result in a broad spectrum of medical, psychiatric and social problems, which constitutes an expensive burden to public health services and society in general. However, because alcohol is widely available and enjoyable there is a strong interest in identifying the threshold of alcohol levels associated with tissue damage and the molecular mechanisms of alcohol-induced liver injury.

3.1. Alcohol absorption, distribution and metabolism:

Blood alcohol peak occurs approximately 20 minutes after ingestion. The rate of rise and height of peak is a function of alcohol absorption and tissue distribution. It has been suggested that the peak value may also be influenced by first-pass metabolism of alcohol by alcohol dehydrogenase (ADH) activity within the gastric mucosa (Stewart and Day 2011).

3.1.1. Alcohol absorption:

Alcohol is absorbed from the gastrointestinal tract by simple diffusion. Because of slow absorption of ethanol in the stomach, 50% to 80% of absorption occurs in the duodenum and upper jejunum. The rate of absorption is delayed following a meal and increases in proportion to the alcohol concentration of the drink consumed. Because absorption is more rapid from the intestine than the stomach, any pathologic condition, drug, or surgical intervention that delays or increases gastric emptying will also affect alcohol absorption accordingly (Stewart and Day 2011).

First-pass metabolism of alcohol: the presence of ADH in gastric mucosa contributes to a first alcohol oxidation that determines both alcohol bioavailability and its toxic effects. Any given condition that influences gastric ADH activity will affect alcohol bioavailability.

3.1.2. Alcohol tissue distribution:

Following absorption, the tissue distribution of alcohol is determined principally by blood flow and water content. Thus, in organs with rich vasculature, such as brain, lungs, and liver, alcohol levels rapidly equilibrate with the blood. Alcohol is poorly soluble in lipids, which take up only 4% of the amount of ethanol that can

be dissolved in a corresponding volume of water. As a result, tissues with a high fat/water ratio attain much lower alcohol levels than organs such as the kidneys, where the high water content results in urinary alcohol levels 1.3 times higher than those in blood. The low lipid solubility of alcohol also explains why, following ingestion of the same amount of alcohol per unit weight, obese subjects attain higher levels of blood alcohol than lean subjects (Stewart and Day 2011).

3.1.3. Hepatic ethanol metabolism:

More than 90% of circulating alcohol is oxidatively metabolized, primarily in the liver, and excreted as carbon dioxide and water. The remaining is eliminated unchanged the urine (<1%) and breath (1% to 5%).

Alcohol oxidation in the liver takes place via three steps. First, alcohol is oxidized principally within the cytosol to acetaldehyde. Then acetaldehyde is further oxidized to acetate, primarily within the mitochondria, and finally, acetate is released into the blood and oxidized to carbon dioxide and water in peripheral tissues (Figure I-18).

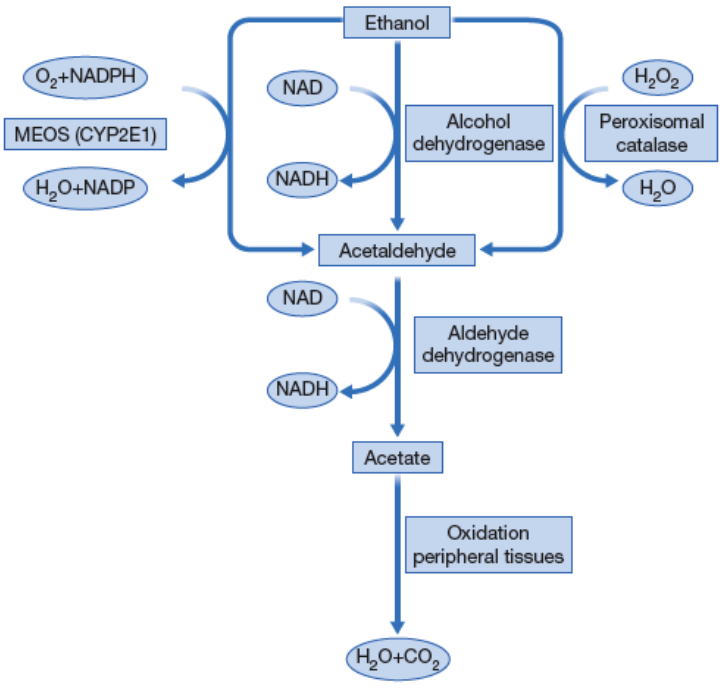

Figure I-18. The three pathways of alcohol oxidation: alcohol dehydrogenase (ADH), microsomal ethanol-oxidizing system (MEOS), and catalase (Stewart and Day 2011).

At least three enzyme systems with the capacity to oxidize alcohol to acetaldehyde have been described in the liver (Stewart and Day 2011):

- The Alcohol Dehydrogenase (ADH) pathway: ADH catalyzes the oxidation of a variety of alcohols to aldehydes and ketones. This includes catalyzing the oxidation of ethanol to acetaldehyde with the transfer of hydrogen to the cofactor nicotinamide adenine dinucleotide (NAD^+), which is converted to its reduced form, NADH (Figure I-18). The resulting increase in the ratio of NADH/NAD^+, which is further increased by acetaldehyde oxidation, is partly responsible for the metabolic imbalances that occur following alcohol ingestion and has been considered to play a major role in the initial pathogenesis of alcohol-induced fatty liver. The principal regulatory mechanism for the ADH pathway is the capacity of the mitochondria to reoxidize NADH back to NAD^+.
- The Microsomal Ethanol-Oxidizing System (MEOS) pathway: MEOS is an accessory pathway to metabolize ethanol that principally involves a specific alcohol-inducible form of cytochrome P450 designated CYP2E1. The enzyme is located on the ER and requires oxygen and NADPH (Figure I-18). CYP2E1 appears to play an important role at high blood alcohol levels or following chronic alcohol abuse, due to its up-regulation. Moreover, alcohol induction of CYP2E1, and microsomal enzyme systems in general, has also been implicated in the tolerance to various drugs commonly observed in alcoholics, and may explain their increased susceptibility to hepatotoxicity by other drugs and xenobiotics that are converted to toxic metabolites by microsomal enzyme systems.
- The Catalase pathway: This enzyme is located in the peroxisomes of most tissues and requires the presence of H_2O_2 (Figure I-18). The reaction is limited by the availability of H_2O_2, which in normal circumstances is low and suggests that the catalase pathway accounts for less than 2% of overall in vivo alcohol oxidation.

After alcohol oxidation, more than 90% of the acetaldehyde generated is further oxidized in the liver to acetate by aldehyde dehydrogenases (ALDH). ALDH, like

ADH, uses NAD^+ as a co-factor and further increases the NADH/NAD^+ ratio (Figure I-18). ALDH inhibitors such as disulfuram (Antabuse) have been used in the treatment of alcoholism to sensitize alcoholics to the unpleasant effects of alcohol intake secondary to high levels of acetaldehyde. This same principle has been described in people with mutations in ALDH, particularly prevalent among Japanese population (Stewart and Day 2011).

3.2. Natural history of Alcoholic Liver Disease:

Alcoholic liver disease (ALD) presents as a broad spectrum of disorders, ranging from simple fatty liver to more severe forms of liver injury, including alcoholic steatohepatitis (ASH), cirrhosis, and HCC. Up to 90% of patients with heavy alcohol intake have some degree of steatosis, which is usually asymptomatic and rapidly reversible with abstinence. Continued heavy alcohol consumption, however, leads to inflammation of the liver characterized by the infiltration of polymorphonuclear leukocytes and hepatocellular damage, both of which define ASH. Eventually, patients develop liver fibrosis deposition (30%) and cirrhosis (8–20%), which confers a high risk of complications (such as ascites, variceal bleeding, hepatic encephalopathy, renal failure and bacterial infections). Severe forms of ASH have a very high short-term mortality (Gao and Bataller 2011) (Figure I-19).

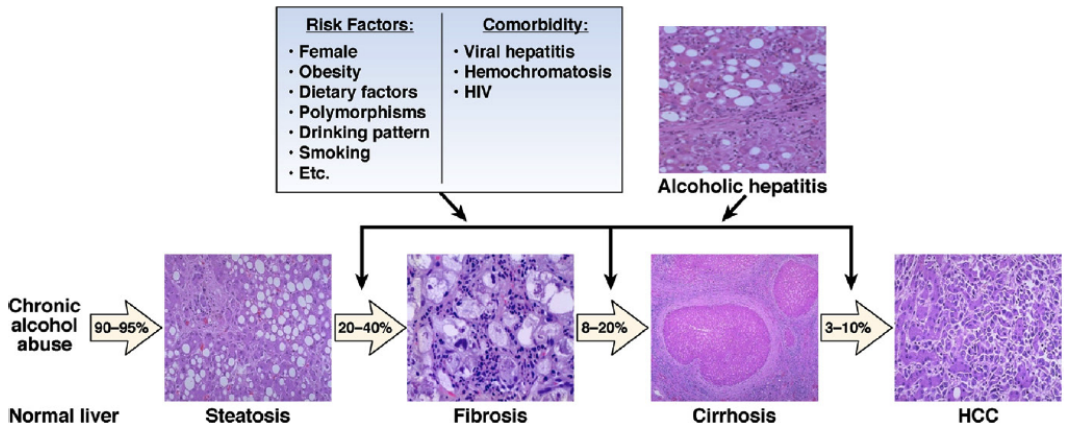

Figure I-19. Spectrum of ALD, risk factors and comorbidity (Gao and Bataller 2011).

The fact that only about 30% of heavy drinkers develop advanced ALD indicates that other factors are involved. Several risk factors for ALD have been identified. These include sex, obesity, drinking patterns, dietary factors, non–sex-linked genetic factors,

and cigarette smoking. In addition, long-term alcohol drinking has synergistic effects with hepatitis virus B or C and/or human immunodeficiency virus infection, nonalcoholic fatty liver disease, and disorders such as hemochromatosis to accelerate progression of liver diseases (Gao and Bataller 2011).

As alcohol abuse can lead to severe damage in the nervous system, heart, kidney and pancreas, patients with ALD may also develop a variety of symptoms unrelated to the liver, such as psychiatric manifestations, heart failure, renal failure and abdominal pain.

3.3. Epidemiology of ALD:

Alcohol abuse is a major cause of preventable morbidity and mortality worldwide. According to the WHO, morbidity from alcohol misuse in developed countries accounts for 10.3% of disability-adjusted life-years (DALYs—a measure of overall disease burden that reflects the years of healthy life lost owing to both premature mortality and prolonged poor health), a figure that comes second only to the morbidity associated with tobacco use in developed countries (11.7% of DALYs). Alcohol misuse also affects individuals in developing countries, where it is responsible for almost 9% of DALYs. Worldwide, ALD is responsible for about 4% of DALYs (Altamirano and Bataller 2011).

ALD is probably the main cause of death among people with severe alcohol abuse and is responsible for about 3.8% of global mortality. Remarkably, data from the European Liver Transplant Registry show that ALD was recorded as the indication for liver transplantation in almost half (41.6%) of procedures performed between 1996 and 2005. ALD is, therefore, the second most common indication for liver transplantation in Europe and North America (Altamirano and Bataller 2011).

3.4. Pathogenesis of ALD:

Mechanisms through which ethanol metabolism causes steatosis, oxidative stress and hepatotoxic effects are discussed below:

3.4.1. Steatosis:

The accumulation of TG, FFAs and cholesterol within the liver is an early and reversible effect of alcohol consumption in humans and animal models of ALD. It

is the consequence of increased substrate supply (glycerol and FFAs), increased esterification, and decreased export of TG from the liver.

3.4.1.1. Increased adipose tissue lipolysis:

Alcohol intake increases lipolysis in adipose tissue increasing FFAs in circulation that are up taken by the liver providing the substrate for TG synthesis (Stewart and Day 2011).

3.4.1.2. Altered redox state:

The ethanol-oxidizing pathways ADH and MEOS are coupled to the reduction of NAD^+ to NADH. The increased NADH/NAD^+ ratio has profound effects on the metabolism of carbohydrates and lipids. Gluconeogenesis is impaired and substrate flow through the TCA cycle is diminished, with acetyl CoA diverted toward ketogenesis and FA synthesis. In addition to increased FA synthesis, the altered redox state also directly inhibits FA β-oxidation in the mitochondria. Through these two mechanisms, the altered redox state can contribute toward increased substrate supply and FFA accumulation (Stewart and Day 2011).

3.4.1.3. PPARα inhibition:

Ethanol can also inhibit FA oxidation through inhibition of the transcription factor PPARα, a known regulator of FA oxidation in the liver. Ethanol feeding decreases transcription and DNA binding activity of PPARα, leading to the accumulation of FFAs in the liver after ethanol feeding, thus promoting TG synthesis and potentially necroinflammation and fibrosis (Stewart and Day 2011).

3.4.1.4. TG export inhibition:

Another contributor to alcohol-induced hepatic steatosis is the decrease in the export of TG from the liver. Usually fat is exported into the circulation in the form of VLDL. Chronic ethanol ingestion generates a defect in VLDL exporting mechanisms. Acetaldehyde can bind to α-tubulin and disrupt microtubule dynamics. In addition, ethanol intake down-regulates

microsomal triglyceride transfer protein (MTP), principal enzyme responsible for packing TG and apolipoprotein B (ApoB) into VLDL particles (Stewart and Day 2011). In addition, ethanol-mediated decrease in phosphatidylcholine contributes to the impairment in VLDL secretion (Ji, Shinohara et al. 2008).

3.4.2. Ethanol hepatotoxicity:

3.4.2.1. Inhibition of the methionine cycle:

Ethanol is capable of inhibiting transmethylation reactions in the liver and this is the major mechanism leading to abnormal methionine metabolism associated with ethanol consumption. Methionine adenosyltransferase (MAT) catalyzes the synthesis of S-adenosyl-L-methionine (SAMe) from methionine and ATP. After donation of a methyl group, SAMe becomes S-adenosylhomocysteine (SAH), which, through homocysteine, acts as a precursor for GSH. Methionine synthase (MS) regenerates methionine from homocysteine in a reaction that requires normal levels of folate and vitamin B12, and betaine-homocysteine methyltransferase (BHMT) regenerates methionine from homocysteine in a reaction that requires betaine (Figure I-20). The principal enzyme inhibited by ethanol is MS, causing as a result hyperhomocysteinemia (HHcy) (Stewart and Day 2011).

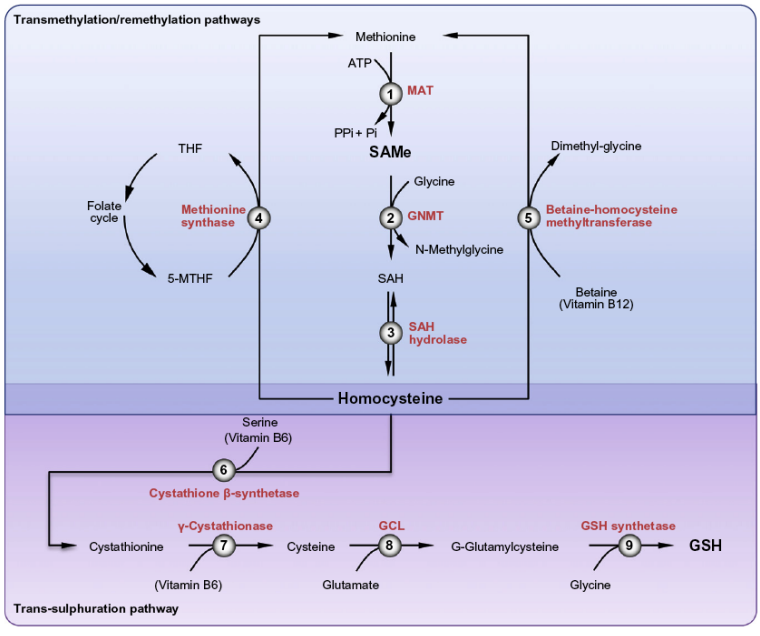

Figure I-20. Methionine metabolism (Anstee and Day 2012).

HHcy has been implicated in the pathogenesis of atherosclerosis, Alzheimer disease and ALD through activation of ER stress, which can explain many processes of homocysteine-promoted cell injury such as apoptosis, fat accumulation, and inflammation (Ji and Kaplowitz 2004). As for the fat accumulation, ER stress triggered by homocysteine increases the gene expression of SREBP1c, transcription factor that promotes FA synthesis via up-regulation of lipogenic enzymes. Studies have shown that ethanol induces SREBP1c in rat hepatoma cell lines and mouse liver with a concomitant increase in the expression of lipogenic genes, and that this induction may be related to inhibition of AMP-activated protein kinase (AMPK) (You, Fischer et al. 2002). However, SREBP1c deletion prevents alcohol-induced hepatic steatosis but it is associated with liver injury and up-regulation of SREBP2 and cholesterol synthesis (Ji, Chan et al. 2006).

Ethanol induces HHcy, triggers ER stress, and promotes the features of ALD including steatosis. Furthermore, feeding mice betaine, a methyl donor converting homocysteine to methionine via BHMT, significantly inhibits the development of steatosis, implying that it is the inhibition of methylation and resulting HHcy that is responsible for alcohol-induced steatosis (Ji and Kaplowitz 2003). It has been shown that the effect of ethanol on development of HHcy is independent of TNF-α, and that these two mechanisms induce steatosis independently and in parallel (Stewart and Day 2011).

3.4.2.2. ER stress:

The contribution of ER stress to ALD has been identified in animal models. First, in intragastric model of alcohol-fed mice, severe steatosis, scattered apoptosis and necroinflammation were observed. Microarray gene expression profiling of liver samples from the intragastric alcohol-fed versus pair-fed mice revealed altered expression of genes related to ER stress response. Moderate up-regulation of SREBP1c and SREBP2 expression and their responsive genes was detected by RT-PCR and immunoblotting (Ji 2008).

In addition to HHcy, alcohol intake induces ER stress by other mechanisms including acetaldehyde-protein adduct formation, and oxidative stress. Oxidative stress resulting mainly from alcohol-induced CYP2E1 and increased ratio of NADH/NAD^+ causes many nonspecific effects, including the ER stress response. Acetaldehyde is able to induce ER stress in cultured Hep G2 cells and activation of SREBP1c in rat hepatoma cells (Lluis, Colell et al. 2003). Homocysteine-induced ER stress in ALD has been also observed *in vivo* (Kaplowitz and Ji 2006; Ji 2008).

ER stress turns on key mechanisms which contribute not only to ALD but also to NAFLD, including:

1. Induction of steatosis through activation of SREBPs, transcription factors that will up-regulate both cholesterol and TG synthesis.
2. Induction of inflammation and death pathways if ER homeostasis cannot be re-established.

ER stress response will be further discussed in Section 4.

3.4.2.3. Acetaldehyde:

It is widely considered that acetaldehyde, the first metabolite of ethanol, has a central role in the pathogenesis of ALD. Several mechanisms of acetaldehyde toxicity have been established:

- Protein and DNA adducts: acetaldehyde can bind covalently to albumin, tubulin, hemoglobin, plasma proteins, collagen, and microsomal enzymes and results in both stable and unstable adduct formation. This binding may affect protein function, which has been implicated in the pathogenesis of ALD (Figure I-21). Defects in assembly of microtubules, protein excretion, and enzymatic activity have all been attributed to acetaldehyde; however, no clear-cut evidence exists for the contribution of these mechanisms to disease progression (Stewart and Day 2011). Along the potential disruption

of protein function, the formation of protein-acetaldehyde adducts results in the production of immunodominant antigenic determinants that activate the adaptive immune system and contribute to ALD progression.

- ER stress: related to generation of protein adducts due to its reactivity, acetaldehyde induces ER stress by a poorly understood mechanism (Lluis, Colell et al. 2003). However, it is tempting to speculate that perturbation of protein secretion and perpetuation of protein-acetaldehyde adducts in the ER may promote ER stress, which in turn may lead to disturbed protein and lipid homeostasis, such as cholesterol regulation and trafficking to mitochondria.
- Reduced mGSH pool: acetaldehyde induces a selective reduction of mGSH and increases hepatocyte sensitivity to TNF-α. The mechanism of acetaldehyde-induced mGSH depletion involves inhibition of GSH transport from cytosol into the mitochondria secondary to accumulation of cholesterol within the mitochondrial inner membrane, resulting in increased viscosity (Lluis, Colell et al. 2003).

3.4.2.4. Oxidative stress:

It has been established a role for oxidative stress and lipid peroxidation in the pathogenesis of ethanol-induced liver injury. These are some of the evidences:

- Products of lipid peroxidation can be detected in the peripheral blood of heavy drinkers and in the livers of patients with ALD, and the magnitude of lipid peroxidation correlates with the degree of liver injury (Figure I-21).
- In patients and animal models of ALD, lipid peroxidation is most prominent in the perivenular region where liver injury is typically most severe.
- A variety of sources of oxidative stress have been identified in patients with ALD and in animal models of disease.

- Ethanol consumption results in the depletion of endogenous antioxidant capabilities and patients with ALD have evidence of antioxidant deficiencies.
- In animal models of ALD, dietary and genetic manipulations that increase oxidative stress increase the severity of liver injury and reducing oxidative stress ameliorates hepatic injury (Stewart and Day 2011).

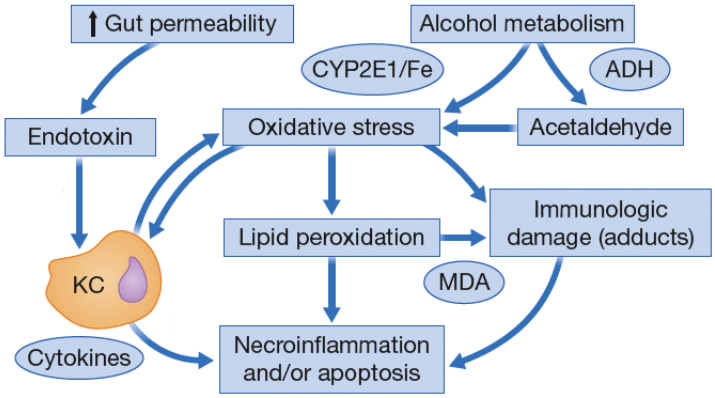

Figure I-21. Mechanisms of ethanol hepatotoxicity in ALD(Stewart and Day 2011).

In addition to oxidative stress, ethanol consumption results in a depletion of endogenous antioxidant defenses. Consumption of GSH during oxidative stress and inhibition of the synthesis of its precursor SAMe through inhibition of MS and MAT1A contribute to the decreased levels of hepatic SAMe and GSH observed in patients with ALD.

Moreover, depletion of mGSH precedes and promotes the progression of alcoholic liver injury in animal models increasing sensitivity of hepatocytes to TNF-α induced cytotoxicity (Lluis, Colell et al. 2003; Marí, Morales et al. 2012).

3.4.2.5. Mitochondrial cholesterol:

Mitochondria are cholesterol-poor organelles with estimates ranging from 0.5-3% of the content found in other cellular membranes. This cholesterol in mitochondria plays important physiological roles in specific processes including steroidogenesis and synthesis of steroid hormones in specialized

tissues, as well as bile acids in hepatocytes. As discussed in the NAFLD section 2.5.3., the over enrichment of cholesterol in mitochondria can result in mitochondrial dysfunction and impairment of specific carriers, including the mitochondrial transporters of GSH, through alterations in mitochondrial membrane order.

Alcohol feeding causes mGSH depletion due to alcohol-stimulated cholesterol *de novo* synthesis. Alcohol causes cholesterol-mediated loss of mitochondrial membranes dynamics, which then impairs mitochondrial transport of GSH from the cytosol resulting in its depletion (Lluis, Colell et al. 2003).

The mechanisms involved in the trafficking of cholesterol to this compartment involve a role of StART family of proteins in the mitochondrial delivery of cholesterol. StARD1, founding member of the growing family of proteins, plays a major role in the intramitochondrial movement of cholesterol from the mitochondrial outer membrane to the mitochondrial inner membrane. Moreover, StARD1 mRNA and protein have been detected in primary human hepatocytes and Hep G2 cells, and its overexpression in rat hepatocytes increased bile acid production (Garcia-Ruiz, Marí et al. 2011).

Another emerging player of cholesterol trafficking to the mitochondria is caveolin-1 since it has cholesterol-binding properties, which makes it a potential intracellular transporter of lipids. Work in our lab described that caveolin-1 knockout mice exhibit increased mitochondrial cholesterol causing mitochondrial dysfunction and disease susceptibility including NASH (Bosch, Marí et al. 2011).

3.4.2.6. Endotoxin activation of innate immunity:

Endotoxin, which refers collectively to the LPS components of the cell wall of all gram-negative bacteria, appears to play an important role in the development of ALD. Alcohol consumption not only causes enteric dysbiosis

and bacterial overgrowth but also increases gut permeability and translocation of bacteria-derived LPS from the gut to the liver. These changes ultimately contribute to increased levels of LPS observed in patients with ALD. In Kupffer cells, LPS interacts with TLR4 leading to production of oxidative stress and proinflammatory cytokines, including TNF-α, which causes hepatocellular damage. Alcohol consumption also activates complement C3 and C5, which subsequently activate Kupffer cells (Gao and Bataller 2011). Thus, LPS acting as a second hit in an alcohol-induced fatty liver contributes to ALD progression (Figure I-21).

3.4.2.7. TNF-ASMase-Ceramide axis in ALD:

TNF is of great relevance to liver pathology, as its expression and levels increase in many forms of liver diseases such as ALD. TNF is a proinflammatory cytokine produced mainly by activated macrophages and in smaller levels by other cell types. TNF exerts a variety of effects that are mediated by TNF receptor 1 and 2 (TNFR1 and TNFR2), with TNFR1 being mainly responsible for the apoptotic effects of TNF. *In vivo* data, have demonstrated the implication of TNF in alcohol-induced hepatocyte death. Mice lacking TNFR1 are protected against alcohol-induced liver damage. Moreover, treatment with antibodies anti-TNF attenuates hepatic necrosis and inflammation caused by chronic exposure to ethanol. Furthermore, patients with ALD exhibit increased expression of TNF and TNFR1 in plasma and liver (Fernandez-Checa, Colell et al. 2005).

Normally, hepatocytes are resistant to TNF-α as it generates both survival and death pathways. Interestingly, hepatocytes isolated from alcohol-fed rats develop an unusual sensitivity to TNF-α exposure in the absence of any other sensitizing factor (Colell, García-Ruiz et al. 1998). Acetaldehyde induces ER stress activating cholesterol synthesis, which results in FC accumulation in mitochondrial membranes. This FC impairs mGSH transport depleting GSH reserves, thus sensitizing hepatocytes to TNF-α (Lluis, Colell et al. 2003) (Figure I-22). Other models that decrease mGSH levels such as acetaminophen also sensitize hepatocytes to TNF-induced apoptosis. These

observations indicate that changes in antioxidant status resulting in altered redox environment may be key in the final outcome of hepatocytes in response to TNF-α (Fernandez-Checa, Colell et al. 2005).

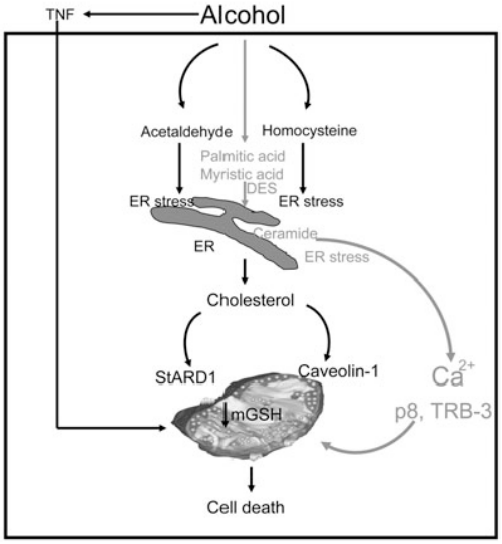

Figure I-22. Role of cholesterol and ceramide in ALD (Fernández, Colell et al. 2008).

An interesting intermediate of TNF-induced hepatocellular death is the sphingolipid ceramide, which has been implicated as effector of TNF-mediated apoptosis (Hannun and Luberto 2000). Ceramide can be generated through several mechanisms, including *de novo* synthesis in the ER and by the hydrolysis of membrane SM by the action of SMases. This pathway promotes specific macrodomain formation in the plasma membrane allowing oligomerization of cell surface proteins such as TNF receptors. In particular, ASMase has been shown to contribute to FAS and irradiation-mediated apoptosis through targeting glycosphingolipids to the mitochondria (García-Ruiz, Colell et al. 2003) and through the down-regulation of MAT1A with the subsequent SAMe depletion (Marí, Colell et al. 2004). These studies established a hierarchical ordering of intermediates in TNF-α signaling where ASMase was required for optimal caspase-8 activation. Thus, TNF-α induces apoptosis through ASMase activation and subsequent increased ceramide levels, which activate caspase-8 to start cell death programs (Fernandez-Checa, Colell et al. 2005).

In addition, chronic alcohol feeding to mice activates hepatic ASMase, and increases hepatic ceramide levels. This activation contributes to hepatic steatosis (Deaciuc, Nikolova-Karakashian et al. 2000; Setshedi, Longato et al. 2011; Liangpunsakul, Rahmini et al. 2012). Moreover, imipramine ASMase inhibition in alcohol-fed mice improves hepatic steatosis, decreases ceramide levels and stress kinases activation like JNK (Liangpunsakul, Rahmini et al. 2012). Although more mechanistic studies will be needed to completely understand the participation of ASMase in ALD, these findings point ASMase as potential new target for ALD treatment

3.5. Management of ALD:

Despite the profound economic and health impact of ALD, little progress has been made in the management of patients with this severe clinical condition and no new drugs for ALD have been successfully developed since the early 1970s, at which time the use of corticosteroids was proposed for the treatment of severe alcoholic hepatitis. The current therapeutic options for ALD include:

3.5.1. Abstinence:

Just like in NAFLD, the most successful treatment is a life style change eliminating ethanol intake. Continued alcohol ingestion is the single most important risk factor for progression of the disease. Abstinence is also critical for patients with advanced disease who could eventually require liver transplantation, because patients who actively engage in alcohol consumption are not eligible for transplantation programs. Referral to rehabilitation programs, in combination with family support, is usually necessary. Some patients require pharmacological treatment to help fighting ethanol cravings but special care must be taken because of the potential hepatotoxicity of these drugs (Gao and Bataller 2011).

3.5.2. Corticosteroids:

Of all the treatments available for patients with severe ALD, corticosteroids are the most intensively studied, and probably the most effective. Steroids are aimed at suppressing the hepatic inflammatory response seen in liver biopsies from patients with severe ALD. Despite many clinical trials, the debate over the use of

steroids in ALD continues. It appears that they are probably beneficial in patients with severe disease; however, mortality on treatment remains high. On the other hand, is relatively contraindicated in the large number of patients with concomitant infection and gastrointestinal bleeding. In addition, there are also significant numbers of patients that fail to respond to corticosteroids. It is because of these limitations that alternative therapeutic strategies have been sought (Gao and Bataller 2011; Stewart and Day 2011).

3.5.3. TNF-α blockage:

As TNF-α is an important mediator of ALD treatments targeting TNF-α action have been developed. Pentoxifylline is a phosphodiesterase inhibitor that blocks transcription of TNF-α and decreases serum levels of the gene product. Pentoxifylline has been used in patients with severe ASH who cannot be given corticosteroids. Unfortunately, pentoxifylline is not effective as a rescue therapy for patients who do not respond to corticosteroids (Gao and Bataller 2011). Another TNF-α blocking strategy was the use of monoclonal antibodies against TNF-α. Early-stage studies showed positive results in terms of survival and safety, but later-stage clinical trials showed that these drugs actually increased mortality and risk of infection among patients with ASH. These reagents are therefore not recommended for the treatment of ASH (Gao and Bataller 2011).

3.5.4. SAMe:

SAMe is a methyl donor that has been shown to protect against alcoholic liver injury via multiple mechanisms, including antioxidant functions, maintenance of mitochondrial function, and down-regulation of TNF-α. An early-stage trial showed that SAMe as a supplemental agent significantly decreased mortality and need for liver transplantation among patients with ALD and it had a favorable safety profile. However, long-term, high-quality, randomized trials are required to establish its therapeutic effects (Gao and Bataller 2011).

3.5.5. Antioxidants:

Because ALD is associated with increased levels of oxidative stress, a number of studies have investigated the benefits of antioxidants (e.g. vitamin E).

Unfortunately, in early-stage studies, survival times of patients with ASH did not increase. However, a combined therapy study with N-acetylcysteine with corticosteroids showed an increase number of patients survived a short-therm follow-up period (Gao and Bataller 2011).

3.5.6. Liver transplantation

Liver transplantation has been used to treat patients with decompensated ALD. Outcomes are equal to or better than those obtained when it is used to treat end-stage liver disease from other causes. Several liver transplantation centers have therefore proposed that this be a rescue option for patients with severe ASH who do not respond to medical therapy and are unlikely to survive the mandatory, 6-month abstinence period but who fulfill all other standard criteria for transplantation, including a thorough psychosocial evaluation (Gao and Bataller 2011).

4. ENDOPLASMATIC RETICULUM STRESS IN LIVER DISEASE.

The ER is the intracellular organelle responsible for synthesis, folding, trafficking, and maturation of proteins. In addition, the ER has other important functions such as TG, sphingolipids and cholesterol synthesis, drug metabolism, as well as storage and release of Ca^{2+}. The ER membrane is composed of very low concentrations of cholesterol and complex sphingolipids, which likely provides an adequate environment for insertion and transport of newly synthesized lipids and proteins. The requirement for such a specialized lipid environment may be relevant to diseases characterized by abnormal lipid accumulation (Zhang and Kaufman 2008).

Under normal conditions, a homeostatic equilibrium exists between influx of unfolded peptides and folding capacity of the ER. As the physiologic rate of protein synthesis changes, a signal transduction pathway between the ER and other organelles has evolved to mediate adaptation to the new folding demands to regain homeostasis and promote survival. These physiological adaptive responses are called the unfolded protein response or UPR. The UPR is of particular importance in cells rich in ER content and responsible for protein synthesis, such as hepatocytes. The insufficiency of the ER stress response to meet the increased folding needs of the cell, activates a pathologic response resulting in lipogenesis, inflammation, and activation of apoptotic pathways.

Hepatocytes, like other secretory cells, are rich in ER. Because of their high protein synthesizing capacity, it is easy to postulate that ER stress plays an important role either in preventing or mediating pathological changes in various liver diseases (Zhang and Kaufman 2008).

When protein load in the ER increases, three main branches of the UPR are activated. These homeostatic responses aim to bring the organelle and the cell into a state of equilibrium through several strategies:

- Increase chaperone capacity: producing more chaperones to increase folding capacity of the ER. Prototype: glucose-regulated protein 78 (GRP78)
- Enhancing folding capacity: through transcriptional up-regulation of enzymes participating in protein folding processes. Prototype: Protein disulfide isomerase (PDI).

- Inhibition of protein synthesis: decreasing protein entry through affecting the translation and synthesis of new polypeptides. Prototype: inhibitory phosphorylation of eukaryotic translation factor-2α (p-eIF2α), initiator of protein translation.
- Enhancing ER-associated protein degradation (ERAD) and autophagy. Prototype: ER degradation enhancer, mannosidase alpha-like 1 (EDEM).

The three branches of the UPR are:

1. Activating transcription factor-6 (ATF6)
2. Inositol-requiring enzyme-1α (IRE1α)
3. Protein kinase double-stranded RNA-dependent–like ER kinase (PERK).

All of them are transmembrane sensors embedded in the ER, which are kept inactive by binding to the intraluminal chaperone, GRP78. When the ER is stressed either by glucose deprivation, the depletion of calcium stores, oxidative stress or the accumulation of misfolded proteins, GRP78 is displaced from the stress sensors to aid in protein folding (Figure I-23). This event initiates an intricate cascade that ultimately determines the fate of the cell. These sensors are activated by self-association and autophosphorylation (IRE1α and PERK) or translocation to the Golgi (ATF6) for proteolytic release of the active transcription factor (referred to as regulated intramembrane proteolysis [RIP]) (Dara, Ji et al. 2011) (Figure I-23).

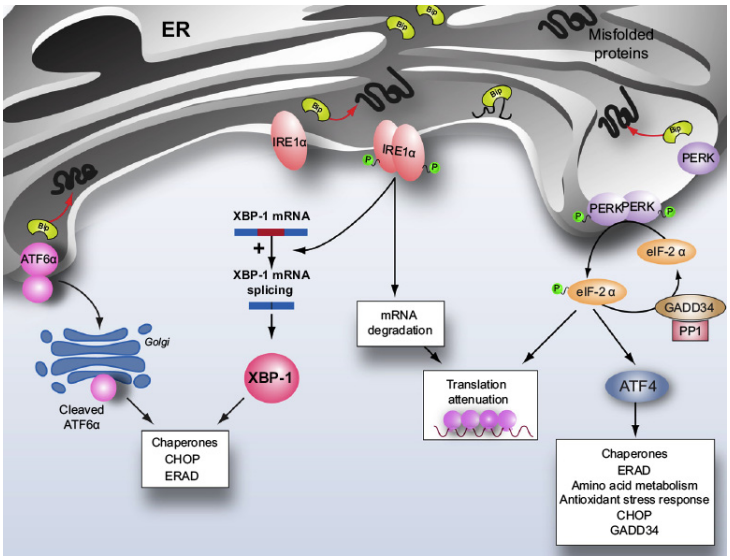

Figure I-23. The unfolded protein response (Malhi and Kaufman 2011).

PERK acts by global inhibition of protein synthesis through phosphorylation of eIF2α. PERK also regulates the transcription of ribosomal RNA via phosphorylated eIF2α and preferentially increases the translation of activating transcription factor 4 (ATF4), which in turn activates the transcription of C/EBP (CCAAT/enhancer binding protein) homologous protein (CHOP), involved in cell death pathways. IRE1α is an endoribonuclease that activates X-box binding protein 1 (XBP1) by unconventional splicing of XBP1 messenger RNA, resulting in transcription of UPR elements and ER stress response element genes that control ERAD and chaperones. IRE1α also degrades the messenger RNA of many secretory and transmembrane proteins and thus also helps in decreasing the protein load that enters the ER. Active ATF6 after RIP translocates to the nucleus, which together with ATF4 and sXBP1, activate ER stress response and UPR elements. The products of the genes regulated by these elements facilitate the folding and elimination of accumulated proteins via EDEM, a component of ERAD, as well as up-regulation of chaperones that aid in protein folding (Dara, Ji et al. 2011) (Figure I-23).

All arms of the UPR are signal transduction mechanisms that lead to the production or release of transcription factors, which regulate the UPR (sXBP, ATF4, ATF6). This mechanism is primarily a cytoprotective survival response that seeks to regulate protein folding and restore homeostatic balance. When the activation of the UPR fails to promote cell survival, a proapoptotic ER stress pathway is activated, which can ultimately lead to apoptotic cell death, inflammation, and/or fat accumulation (Zhang and Kaufman 2008).

4.1. ER stress, inflammation and cell death:

The pathologic ER stress response can be activated in a variety of ways. Some of them are summarized bellow:

- Increased CHOP expression leading to activation of the proapoptotic pathways by:
    - Promotion of oxidative stress and inflammation which down-regulates anti-apoptotic Bcl2 proteins and up-regulates transcription of pro-apoptotic protein Bim.
    - CHOP induces growth arrest and DNA damage-inducible protein 34 (GADD34), which associates with protein phosphatase- 1 and promotes

dephosphorylation of p-eIF2α resuming protein synthesis, which could be harmful if protein overload were to continue (Figure I-24).

- CHOP and ATF4 together induce tribbles homolog 3 (TRB3), which inhibits the cytoprotective, insulin-sensitizing Akt kinase.

- PERK-mediated global protein translation shutdown results in decreased IκB, which leads to inflammation through NF-κB activation (Figure I-24).
- IRE1α-mediated recruitment of proapoptotic signals such as tumor necrosis factor receptor–associated factor 2 (TRAF2) and JNK which can lead to autophagy, insulin resistance, and apoptosis. TRAF2 can recruit IKK and promote NF-κB-mediated inflammation (Figure I-24).
- Proapoptotic Bcl2 proteins regulate apoptotic cell death via altering Ca^{2+} homeostasis have been linked to the ER stress response and in particular to the IRE1α branch. When activated, Bcl2 proteins can lead to Ca^{2+} release, calpain activation causing mitochondrial depolarization, and increased ROS, as well as the activation of caspase 4, which along with JNK modulates apoptosis. Ca^{2+} release is a critical factor in affecting mitochondrial function, particularly in areas in which the ER is in close association with the mitochondria; so-called mitochondria associated membrane (MAM) (Dara, Ji et al. 2011) (Figure I-24). As mitochondria dysfunction is associated with ER stress via Ca^{2+} release from the ER, understanding of the mechanism of mitochondrial Ca^{2+} uptake, and subsequent onset of mitochondrial permeability transition may be of interest to modulate ER stress mediated cell death.

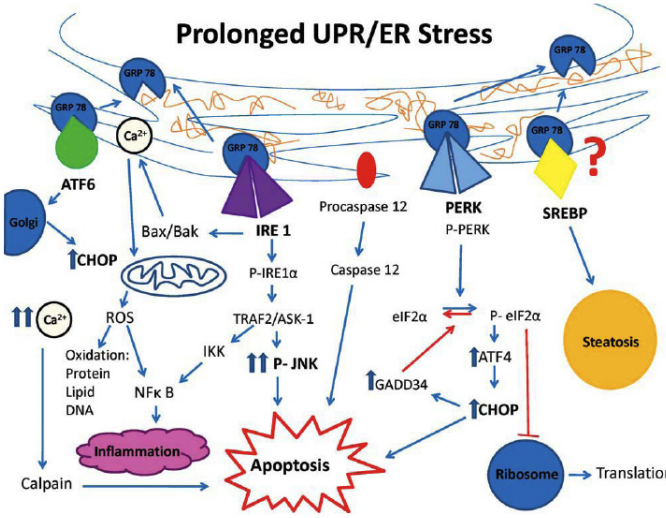

Figure I-24. Cell signaling pathways in prolonged ER stress (Dara, Ji et al. 2011).

4.2. ER stress and lipogenesis:

Prolonged ER stress response leads to steatosis: SREBPs are a family of ER resident proteins which function as transcription factors in the control of FA, TG, and cholesterol synthesis. They are synthesized as inactive precursors bound to the ER in a complex with SREBP-cleavage activating protein (SCAP). In the presence of cholesterol and oxysterols, SCAP undergoes conformational changes causing it to bind to its protein inhibitor Insig. Insig prevents translocation of the SREBP/SCAP complex to the Golgi. Protein attenuation after ER stress induction decreases Insig protein synthesis and as a result SCAP is free to escort SREBPs to the Golgi where they undergo RIP activation, translocate to the nucleus and promote lipogenesis (Basseri and Austin 2012) (Figure I-25).

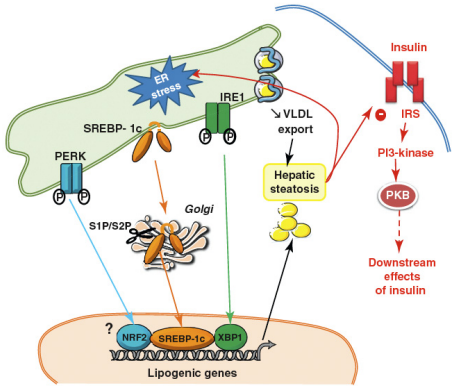

Figure I-25. ER stress-induced lipogenesis (Flamment, Hajduch et al. 2012).

In addition, ER stress activation of JNK pathway can lead to insulin resistance (Ozcan, Cao et al. 2004) and insulin resistance leads to steatosis. Moreover, PERK-induced protein synthesis attenuation decreases ApoB, a very important lipoprotein vital for VLDL assembly and secretion. Impaired VLDL secretion via decreased ApoB contributes to ER stress-induced hepatic steatosis. Furthermore, GRP78 may directly interact with SREBPs inhibiting its translocation, so displacement of GRP78 induced by increased unfolded proteins in the ER may also allow SREBPs to translocate to the Golgi and undergo RIP contributing this way to hepatic steatosis (Dara, Ji et al. 2011) (Figure I-25).

4.3. ER stress and fatty liver disease:

The relationship between ER stress and fatty liver is reciprocal. Steatosis has been shown to promote ER stress and viceversa; ER stress response leads to steatosis. Induction of

ER stress response by treatment with tunicamycin leads to alteration of SREBP expression and hepatic steatosis in Hep G2 cells (Dara, Ji et al. 2011).

On the other hand, genetically obese ob/ob mice displaying hepatic steatosis show increased markers of ER stress in liver and white adipose tissue. This observation is paired with JNK activation and linked insulin resistance through JNK-mediated inhibitory phosphorylation of insulin signaling pathway. Likewise, mice exposure to high fat diet for four months also increases ER stress markers compared to mice fed a regular diet (Ozcan, Cao et al. 2004). Moreover, treatment with chemical chaperones, which may increase ER folding capacity, has been shown to decrease ER stress, insulin resistance and resolve fatty liver in ob/ob mice (Ozcan, Yilmaz et al. 2006). In addition, selective liver deletion of XBP1 in mice results in marked hypocholesterolemia and hypotriglyceridemia. Furthermore, hepatic overexpression of protein chaperone GRP78 in ob/ob mice reduces ER stress markers and inhibits SREBPs expression and activation, resulting in decreased hepatic TG and cholesterol content and improved insulin sensitivity (Kammoun, Chabanon et al. 2009). Furthermore, it has been demonstrated that alterations in ER lipid composition in obesity disrupts Ca^{2+} homeostasis through inhibition of sarco/endoplasmic reticulum calcium ATPase (SERCA) activity causing liver ER stress. Correction of obesity-induced alteration of ER phospholipid composition improves ER stress and glucose homeostasis (Fu, Yang et al. 2011). These data demonstrates that ER stress response can promote lipogenesis and fatty liver and that its inhibition can help improve hepatic manifestations of NAFLD like steatosis, insulin resistance and inflammation.

The human relevance of these findings in mouse models was established in a study that used human liver and white adipose tissue samples from obese patients who underwent gastric bypass. Samples before the procedure showed increased ER stress markers that were markedly lowered after the surgery-induced weight loss (Gregor, Yang et al. 2009). In another study, liver samples from patients with NAFLD and NASH demonstrated increased eIF2α phosphorylation and GRP78 expression (Puri, Mirshahi et al. 2008).

Regarding ALD, hepatic ethanol-induced steatosis and apoptosis has been linked to ER stress. Mice fed alcohol intragastrically exhibit severe steatosis, apoptosis, and

necroinflammation as well as up-regulation of UPR genes and ER stress response (Ji 2008). In addition, increased expression and activation of SREBPs has been detected in alcohol-fed mice, further supporting the relation between alcohol, steatosis, and ER stress (Dara, Ji et al. 2011). Moreover, CHOP knockout mice fed ethanol show no change in ER stress markers or steatosis but they display marked inhibition of apoptosis (Ji, Mehrian-Shai et al. 2005). Furthermore, in micropigs fed alcohol, liver steatosis is accompanied by increased transcription of GRP78, SREBP, and activated caspase 12 (Dara, Ji et al. 2011). Also, cirrhotic rat livers exhibit markers of ER stress response after challenge with lipopolysaccharide, which has been implicated in alcohol-induced liver injury (Tazi, Bièche et al. 2007).

The mechanism proposed for ethanol-induced ER stress is HHcy, hallmark of alcohol intake, which is believed to interfere with protein folding, thus causing ER stress. Alcohol feeding decreases MS activity, Hcy cannot be recycled to methionine resulting in HHcy. HHCy interference with protein folding causes ER stress that activates SREBPs leading to TG and cholesterol accumulation. The later one will affect mitochondrial membrane physic properties resulting in impairment of mGSH transport. mGSH depletion sensitizes the cells to other insults (Lluis, Colell et al. 2003). On the other hand, ER stress will also activate apoptotic pathways like CHOP and lead the cell to death (Figure I-26).

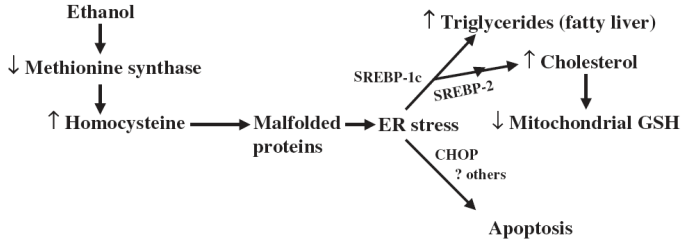

Figure I-26. Ethanol-induced ER stress model (Kaplowitz and Ji 2006).

Knowing that HHcy causes alcohol-induced ER stress, several studies aimed to decrease its levels by supplementing the alcoholic diets with betaine that will activate BHMT Hcy conversion to methionine or by directly overexpressing BHMT itself. These strategies have proven to decrease ER stress response, steatosis and inflammation both in cells and mouse models (Dara, Ji et al. 2011). These results indicate that lowering Hcy exposure to the liver is key in preventing alcohol-induced liver injury.

5. AUTOPHAGY IN LIVER DISEASE.

The word autophagy is derived from the Greek roots "auto" (self) and "phagy" (eating) and refers to cellular catabolic processes in which cellular components are transported to lysosomes for degradation.

Autophagy is a gatekeeper of cellular functions. Degradation of damaged and excess organelles as well as elimination of invading pathogens is essential to maintain cell homeostasis. Autophagy is the principal catabolic pathway allowing cells to survive the stress of intrinsic and extrinsic insults. Because of its ability to rapidly eliminate unwanted structures, this conserved eukaryotic pathway plays a central role in a multitude of physiological processes including cell death, development, cellular remodeling, differentiation and energy homeostasis (Czaja 2010). In addition, it plays a protective role against aging, tumorigenesis, neurodegeneration and infections. As a consequence of its crucial role in cell and organism physiology, impaired autophagy correlates with various severe pathologies including cardiovascular and autoimmune diseases, neuro- and myo-degenerative disorders, and liver diseases (Ravikumar, Sarkar et al. 2010; Komatsu 2012).

Three major types of autophagy have been described in eukaryotes: chaperone-mediated autophagy (CMA), microautophagy and macroautophagy. CMA involves a direct translocation of cytosolic proteins containing a pentapeptide motif across the lysosomal membrane. Microautophagy is the process by which cytoplasmic material is sequestered through a direct invagination of the lysosomes. Macroautophagy, from now on autophagy, which is highly conserved from yeast to humans, is a bulk degradation process involved in the clearance of long-lived proteins and organelles.

The autophagic process can be separated in five different stages (Figure I-27):

- Induction: in liver, several stimuli can induce autophagy. For example, intracellular pathogens, hypoxia, ROS, ER stress, starvation or amino acid deprivation, radiation, proteasome inhibition and protein aggregation. The initial event upon induction is the formation of a membranous cistern called the phagophore, or isolation membrane. This compartment appears to be generated from what has been defined in yeast as the phagophore assembly site (PAS) or

pre-autophagosomal structure, a putative early autophagosome precursor that is formed by the sequential association of at least a subset of Autophagy-related genes (Atg) proteins, which are known to be specifically involved in autophagy.

- Expansion: the phagophore expands through acquisition of additional lipids allowing the kidnapping of intracellular material targeted for degradation.
- Vesicle completion: the double-membrane vesicle is completed when the inner and outer bilayers fuse to form two distinct membranes, one inside the other. At this point of the process the vesicle is called autophagosome.
- Fusion: completed autophagosomes first fuse with endosomal structures to form amphisomes, and then with lysosomes forming the autolysosomes.
- Cargo degradation: autophagosome fusion with the lysosome allows the degradation of the inner vesicle and its cargo by acid hydrolases residing in these lytic compartments.

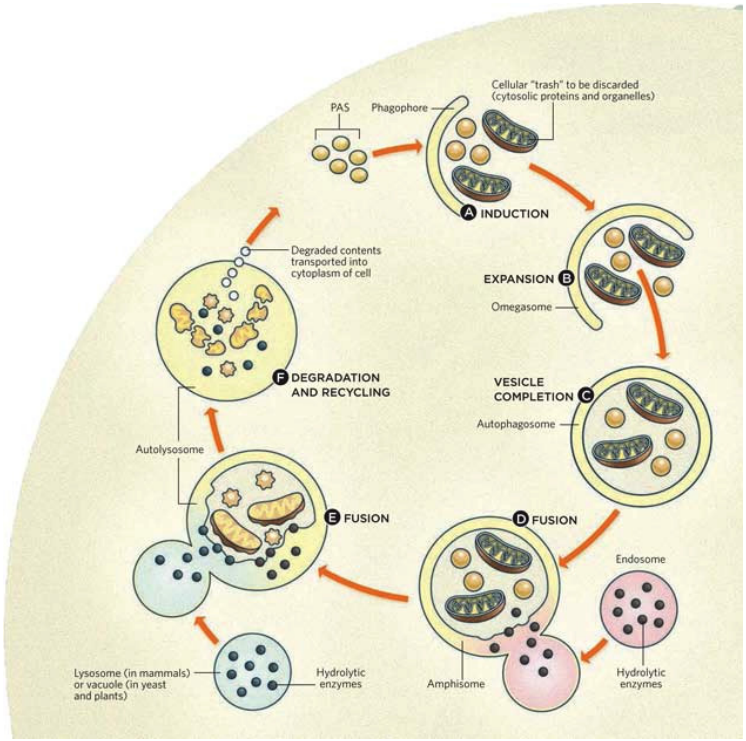

Figure I-27. Autophagic process (Mari, Tooze et al. 2011).

Lastly, the basic metabolites generated from this catabolic processing of biological macromolecules are transported into the cytoplasm, where they are reused as either a source of energy or as building blocks for new proteins and lipids (Mari, Tooze et al. 2011) (Figure I-27).

5.1. Autophagic machinery:

So far, more than 30 different Atgs have been identified in yeast and most of them have mammalian homologs that participate in autophagy or in autophagy-related processes. Several multi molecular complexes have been found to contribute to autophagosome formation (Mehrpour, Esclatine et al. 2010; Ding, Manley et al. 2011) (Figure I-28):

1. ULK1 protein-kinase complex: regulates autophagy initiation. This complex works downstream of mammalian target of rapamycin (mTOR) and serves as the cellular sensor for nutrient status to initiate autophagy by recruiting downstream autophagy proteins to the autophagosomes (Figure I-28).
2. VPS34-Beclin1 class III PI3-kinase complex: regulates autophagy initiation. VPS34 is a class III PI-3-kinase that acts as an essential regulator of autophagy by producing phosphatidylinositol-3-phosphate (PI3P). The Beclin1 complex regulates VPS34 activity. Bcl-2 and Bcl-xL interact with Beclin1 to keep autophagy in check by dissociating the interaction of Beclin 1 and VPS34 (Figure I-28).
3. Atg9-Atg2-Atg18 complex: regulates expansion of PAS by carrying lipids. Atg9 is a transmembrane protein located on the PAS. Atg9 is thought to cycle between the trans-Golgi network, late endosomes and the PAS to bring the additional membrane sources necessary for the growth of the autophagosomal membranes (Figure I-28).
4. Atg5-Atg12-Atg16 complex: it is an ubiquitin-like conjugation system that provides the necessary platform for autophagy activation (Figure I-28).
5. LC3 (microtubule-associated protein 1 light chain 3) conjugation systems: is the second ubiquitin-like conjugation system that regulates elongation of autophagosome membranes. LC3 is cleaved by Atg4 to form LC3-I. Then LC3-I is conjugated to phosphatidylethanolamine (PE) via Atg7 and Atg3. The unconjugated form LC3-I is in the cytosol, whereas the PE-conjugated form (LC3-II) targets the autophagosomal membrane following the Atg12-Atg5-Atg16 complex. This association of LC3-PE to autophagosomes is considered important for membrane extension of the autophagosome and the eventual closure of the membrane to form a complete vesicle. LC3-I/II is thus widely used as a marker for monitoring the autophagic process (Figure I-28).

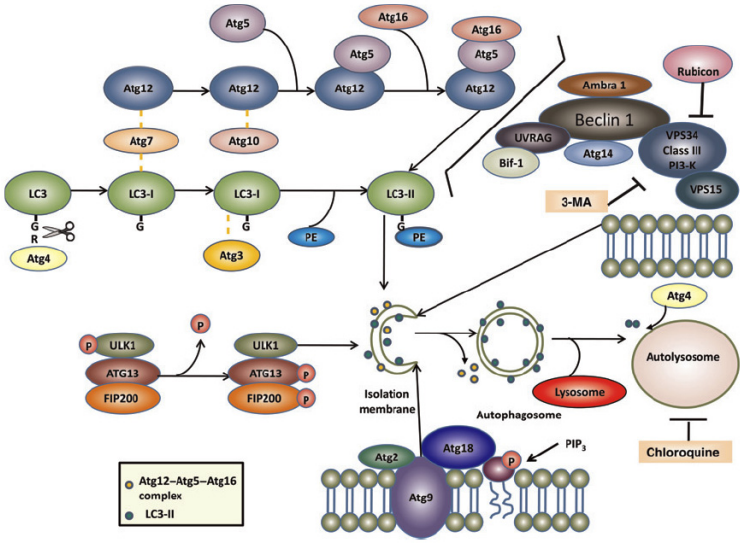

Figure I-28. Autophagic machinery (Ding, Manley et al. 2011).

Newly formed autophagosomes are randomly distributed in the cytoplasm. During their maturation, autophagosomes move along microtubules toward the microtubule-organizing center, where the lysosomes are enriched. Autophagosomes then fuse with lysosomes to form autolysosomes possibly through the small GTPase Rab7 and/or two lysosomal membrane proteins, LAMP1/2. Chemicals that disrupt microtubule structures such as vinblastine can inhibit autophagy. In addition to disruption of the fusion machinery, chemicals that increase lysosomal pH such as chloroquine and bafilomycin A 1 or lysosomal protease inhibitors such as leupeptin and pepstatin A are all potent autophagy inhibitors.

5.2. Autophagy regulation:

Several signaling pathways appear to be involved in the regulation of autophagy in mammalian cells. The most relevant are summarized below:

- Class I PI3K-Akt-mTOR: mTOR is a serine/threonine kinase involved in many aspects of cellular physiology, including transcription, translation, cell size and cytoskeletal organization. mTOR inhibition is a key signaling step in autophagy activation. The use of the mTOR inhibitor rapamycin significantly activates autophagy in rat hepatocytes (Ding, Manley et al. 2011). The activity of mTOR is regulated by the integration of various signals, including growth factors, insulin, nutrients, energy availability and cellular stressors such as hypoxia, osmotic stress, reactive ROS and viral infection. In response to growth factors, PI3K increases

PI3P that activate Akt, which in turn activates mTOR, thus inhibiting autophagy (Figure I-29).

- AMP-activated protein kinase: AMPK is another upstream regulator of mTOR. AMPK monitors cell energy status through sensing adenosine monophosphate (AMP)/ATP ratio. Low-energy status, reflected by high AMP/ATP ratio, activates AMPK. AMPK activation down-regulates mTOR activity resulting in decreased protein translation and activation of autophagy (Figure I-29).
- Bcl-2 family proteins: antiapoptotic Bcl-2 family proteins such as Bcl-2 can suppress autophagy by directly binding and inhibiting Beclin 1 complex. In contrast, proapoptotic BH3-only Bcl-2 family proteins can induce autophagy through their binding to antiapoptotic Bcl-2 proteins and subsequent displacement of the inhibitory Bcl-2 from Beclin 1 complex (Figure I-29).
- ER stress: misfolded proteins in the ER normally undergo degradation through ERAD mediated by ubiquitin proteasome system. It was found that inhibition of proteasome activity triggers ER stress and autophagy through activation of IRE1α and JNK. JNK may further phosphorylate Bcl-2 and dissociate its binding from Beclin 1 and in turn activate autophagy (Figure I-29).
- ROS: Inhibition of mitochondrial complexes as well as the use of mitochondrial uncouplers generate ROS and induce autophagy. Moreover, this induction can be suppressed by antioxidant treatment. One possible mechanism of ROS-mediated autophagy induction is the inhibition of Atg4-induced delipidation of LC3-II from the autophagosome for its recycling, thus activating autophagy (Figure I-29).

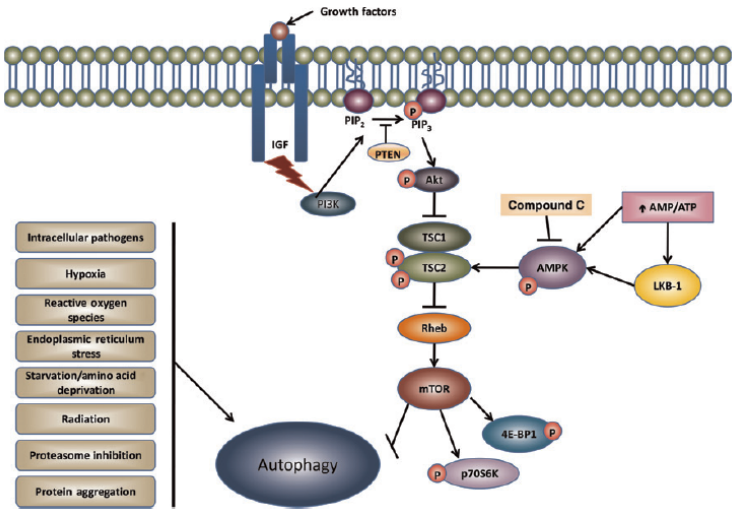

Figure I-29. Autophagy regulation (Ding, Manley et al. 2011).

5.3. Macrolipophagy and NAFLD:

It was recently established a new role of autophagy in the regulation of hepatic lipid metabolism (Singh, Kaushik et al. 2009). Besides the classical cytosolic lipases, autophagy regulates intracellular lipid stores through a process called macrolipophagy. Lipid droplets become trapped inside the double-membrane-bound autophagosome vesicles and are transported to lysosomes, where they are degraded to FAs (Figure I-30). The ability of autophagy to respond to changes in nutrient supply allows the cell to alter lipid droplet metabolism to meet energy demands. This alternative lysosomal lipid degradative pathway in hepatocytes explains their ability to rapidly mobilize large amounts of lipids despite their low levels of cytosolic lipases in comparison with adipocytes. In a physiological state, insulin inhibits both lipolysis and macrolipophagy (Rautou, Mansouri et al. 2010).

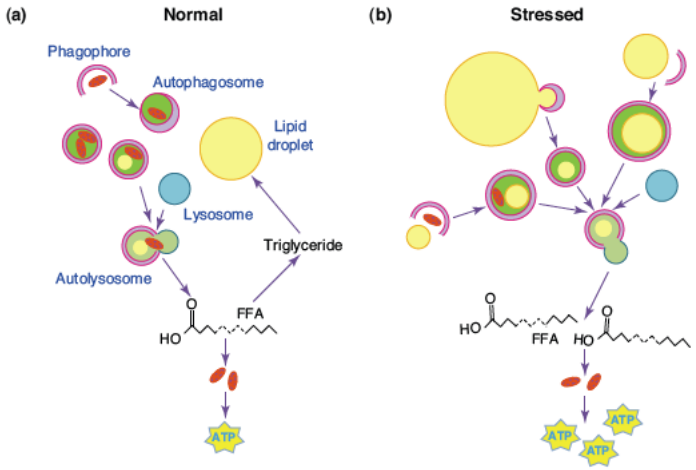

Figure I-30. Macrolipophagy. A. Normal state, the minority of autophagosomes contain lipid and usually in combination with other cytosolic components. B. Nutrient deprivation, more autophagosomes contain lipids, often in the absence of other cargo (Dong and Czaja 2011).

Pathophysiological changes in autophagy function can alter cellular lipid metabolism and promote disease states. For instance, autophagy inhibition can promote liver steatosis. Hepatocyte-specific Atg7-knockout mice have markedly increased hepatic lipid deposition (Singh, Kaushik et al. 2009). In both genetic (ob/ob mice) and dietary mouse models of chronic obesity and insulin resistance, a sustained increase in lipid availability results in markedly decreased hepatic autophagy (Liu, Han et al. 2009; Singh, Kaushik et al. 2009; Yang, Li et al. 2010). This decreased autophagy level impacts on other cellular functions and particularly on ER stress. Indeed, in liver tissue of lean mice, deficiency of

autophagy, induced by suppression of Atg7, results in ER stress (Yang, Li et al. 2010). This could be explained by the known role of autophagy in the degradation of unfolded proteins and in the removal of superfluous ER membranes: defect in autophagy may lead to the accumulation of unfolded proteins and thus to ER stress. In obesity, ER function is compromised due to nutrient and energy surplus in an inflammatory setting. Concomitantly, autophagy level is decreased, suggesting that failure to achieve autophagy may further impair ER function in the face of continuous energy and nutrient stress, contributing to organelle dysfunction and insulin resistance, a known consequence of ER stress. Interestingly, restoration of Atg7 expression results in significant reduction of obesity-induced ER stress in the liver of ob/ob mice. It rescues the defects in insulin receptor signaling, reduces serum insulin level, improves glucose tolerance and whole body insulin sensitivity through the suppression of hepatic glucose production and enhancement of insulin-stimulated glucose disposal in the periphery. It also decreases hepatic FA infiltration and liver TG accumulation (Singh, Kaushik et al. 2009; Yang, Li et al. 2010). Autophagy therefore represents a cellular target for abnormalities in lipid metabolism and accumulation.

Interestingly, it has been described an opposite role of autophagy in adipocytes: inhibition of autophagy in adipocytes, rather than its stimulation, confers them a brown-fat-cell-like phenotype that favors FA oxidation and increases insulin sensitivity (Singh, Xiang et al. 2009). In addition, adipose tissue autophagy seems to be essential for adipogenesis and its deficiency causes lipodistrophy (Zhang, Goldman et al. 2009).

5.4. Autophagy and lysosomal storage disorders:

Lysosomes are essential to fully complete autophagy; therefore, disorders that impair lysosomal fusion with autophagosomes or degradation capability will negatively impact autophagy.

Among all lysosomal storage diseases, the sphingolipidose disease Niemann-Pick type C disease (NPC) is of special interest. NPC is a genetic disease caused by mutations in *NPC1* or *NPC2* genes whose protein products are thought to act cooperatively in the efflux of cholesterol from the late endosomes and lysosomes. As a result of *NPC1* or *NCP2* deficiency, FC derived from receptor-mediated endocytosis of LDL-cholesterol

accumulates in endolysosomal compartments in neurons and hepatocytes causing progressive neurological impairment that often begins in childhood. NPC is ultimately fatal and is currently untreatable (Schuchman 2010). Moreover, many patients exhibit severe liver function deterioration leading to premature death even before neurological symptoms arise (Schuchman 2010). A broad array of sphingolipids like SM and glycosphingolipids accumulate as well. NPC deficient mice show increased accumulation of autophagosomes in the brain. This is due, in part, to the induction of autophagy through increased Beclin 1, important player of initiation of autophagosome formation and maturation (Pacheco and Lieberman 2007). In addition, treatment of wild type fibroblast with U18666A, a small molecule that induces NPC-like lipid trafficking defects, increases Beclin 1 and LC3-II levels, suggesting that FC accumulation or sphingolipids may act as a proximal trigger (Ishibashi, Yamazaki et al. 2009; Lieberman, Puertollano et al. 2012). This induction was accompanied by the accumulation of the autophagic substrate p62/Sequestosome 1 (SQSTM1) (Pacheco and Lieberman 2007). These findings suggest that NPC1 deficiency leads to both induction of the early phases of autophagy, and impairment of autophagic flux. In addition, lysosomal cholesterol accumulation associated with NPC1 deficiency protects against lysosomal permeabilization and subsequent cell death induced by lysomotropic agents (Appelqvist, Nilsson et al. 2011). Thus, given that FFA induce lysosomal permeabilization (Li, Berk et al. 2008), lysosomal cholesterol accumulation may be a protective mechanism against cell injury of potential relevance in steatohepatitis and metabolism liver disease.

NPC is a severe form of Niemann-Pick disease, while Niemann-Pick types A and B exhibit with milder symptoms. NPD type A and B are inherited disorders caused by loss of function mutations in the gene encoding ASMase. Reduced function or deficiency in ASMase leads to accumulation of sphingolipids and cholesterol as well in the cellular membranes. Till date, no experimental evidences on autophagy in these diseases or mouse models of these diseases have been published.

6. CERAMIDE & ACID SPHINGOMYELINASE IN METABOLIC DISEASES.

The concept of "bioactive lipids", defined as changes in lipid levels that result in functional consequences, has been developed over the years. In the past 2 decades, many studies focused on this concept providing evidence on the role of bioactive lipids in cell biology and regulation of many cell functions. Thus seminal findings expanded the view that lipids are more than structural components of membrane bilayers, regulating a wide array of processes, including differentiation, proliferation, senescence and cell death among others.

6.1. Sphingolipids:

A big group of bioactive lipids that centered attention in the past two decades are the sphingolipids (SLs). SLs are a major class of lipids that are ubiquitous constituents of membranes in eukaryotes. As most of the lipids, when first discovered SLs were considered to play only structural roles in membrane formation. The backbone of SLs is sphingosine (SPH). J. L. W. Thudichum named the backbone of SLs in 1884 for its enigmatic ‘‘Sphinx-like’’ nature. Over the past 20 years, much progress has been achieved on SLs knowledge and new tools have been developed to uncover their function in physiology and disease.

All SLs are defined by their 18-carbon amino-alcohol backbone or SPH, which is synthesized in the ER from an aminoacid and a FFA. Acylation of SPH by ceramide synthases (CerS) yields ceramide, the prototype SLs. Different acyl-CoAs can be used to form ceramide giving as a result a heterogeneous family of species whose function depends on the chain length of the FFA added (Hannun and Obeid 2011).

Importantly, ceramide serves as a hub in SL metabolism, acting as a precursor of many other SLs. Complex SLs may be formed by addition of head groups to ceramide:

- Sphingomyelins: SMs have a phosphocholine or phosphoethanolamine molecule with an ester linkage to the 1-hydroxy group of a ceramide.
- Glycosphingolipids (GSLs): are ceramides with one or more sugar residues attached in a β-glycosidic linkage at the 1-hydroxyl position.
    - Cerebrosides have a single glucose or galactose at the 1-hydroxy position.
        - Sulfatides are sulfated cerebrosides.

- Gangliosides have at least three sugars, one of which must be sialic acid.

Ceramide is key in SL metabolism, serving as a precursor to ceramide-1-phosphate (C1P), SM and the entire family of GSLs. Moreover, in the degradative pathway, ceramide is the precursor of SPH, which in turn can be phosphorylated to sphingosine-1-phosphate (S1P). Thus, ceramide not only stands as a key player in SL metabolism, but its functions depend on its biotransformation into other derivatives (Gault, Obeid et al. 2010).

6.2. Ceramide metabolism:

Cumulative evidence over the last few decades revealed that most stress stimuli (e.g. inflammatory mediators, heat, UV radiation, hypoxia, chemotherapeutics, and oxidative stress) increase ceramide production as part of an evolutionarily conserved cellular response. Three major pathways account for the production of ceramide within the cell:

- *De novo* ceramide synthesis: this pathway is compartmentalized in the ER and its rate-limiting step is the availability of substrates for the first reaction. *De novo* synthesis begins with the transfer of a serine residue onto an acyl-CoA, preferably a saturated one like palmitoyl-CoA, via serine SPT to form 3-keto-sphinganine (3KSn). Three subsequent enzymatic reactions, catalyzed by 3KSn reductase, CerS, and dihydroceramide desaturases, convert this transient intermediate into ceramide (Figure I-31). Originally, it was thought that this pathway was a slow and constant source of ceramide generation important for cellular membrane structure. However, recent studies showed how *de novo* synthesis enzymes are regulated under pathological scenarios where inflammation and ROS regulate their gene expression. In addition, inhibition of this pathway, correlating with decreased levels of ceramide content, improved pathological conditions such as obesity, insulin resistance, diabetes and atherosclerosis. These studies suggest that disruption of *de novo* ceramide synthesis may have a beneficial impact on metabolism (Bikman and Summers 2011).
- Sphingomyelin hydrolysis pathway: is a second ceramide-generating pathway that involves the hydrolysis of the phosphocholine head group from SM by a small family of sphingomyelinase (SMase) enzymes distinguished by their pH optima

and/or subcellular distribution (Figure I-31). Compared with the *de novo* synthesis, the generation of ceramide through SMase activation is quick and transient, and has been involved in the apoptosis induced by apoptotic stimuli, such as death ligands, chemotherapeutic agents or ionizing radiation (Morales, Lee et al. 2007). Several SMases have been characterized of which two classes are of relevance in signaling:

- The membrane-bound neutral SMases (NSMases) exhibit an optimum pH of 7.4. Three mammalian NSMases have been cloned. NSMase2 exhibits a requirement for Mg^{2+} and a pH optimum of 7.4 and it is membrane bound. However, its expression is specific to the brain. NSMase3 exhibits Mg^{2+} dependency and pH optimum of 7.4 but unlike NSMase2 is ubiquitously expressed. NSMase3 is distributed mainly in the ER and Golgi and becomes activated very quickly upon stimulation with TNF-α. NSMase1 function still needs to be characterized.
- Acidic SMases (ASMases) exhibit a pH optimum around 5. Three different pools or ASMase isoforms have been described. An acidic lysosomal/endosomal ASMase consistent with its strict acidic pH requirement, a secretory ASMase associated with inflammation and stress responses, and a receptor-activated ASMase, which undergoes a translocation to the outer cell membrane in specific microdomains, where it creates signaling platforms by the cell surface for receptors such as Fas. In addition, ceramide pool released upon ASMase activation has been shown to contribute to TNF-mediated death by downstream mechanisms that ultimately target and recruit mitochondria (Morales, Lee et al. 2007).

- Salvage pathway: ceramide can also be produced by the catabolism of other complex SLs. Through a series of events referred to as SL recycling or the salvage pathway, complex SLs (SM and GSLs) are degraded within acidic cellular compartments by resident enzymes to form ceramide, which is itself degraded into SPH and FFAs that are able to enter the cytosol. Once in the cytosol, SPH is converted back to ceramide via CerS. Though less well known, the salvage pathway may account for over half of the SL pool within the cell (Bikman and Summers 2011).

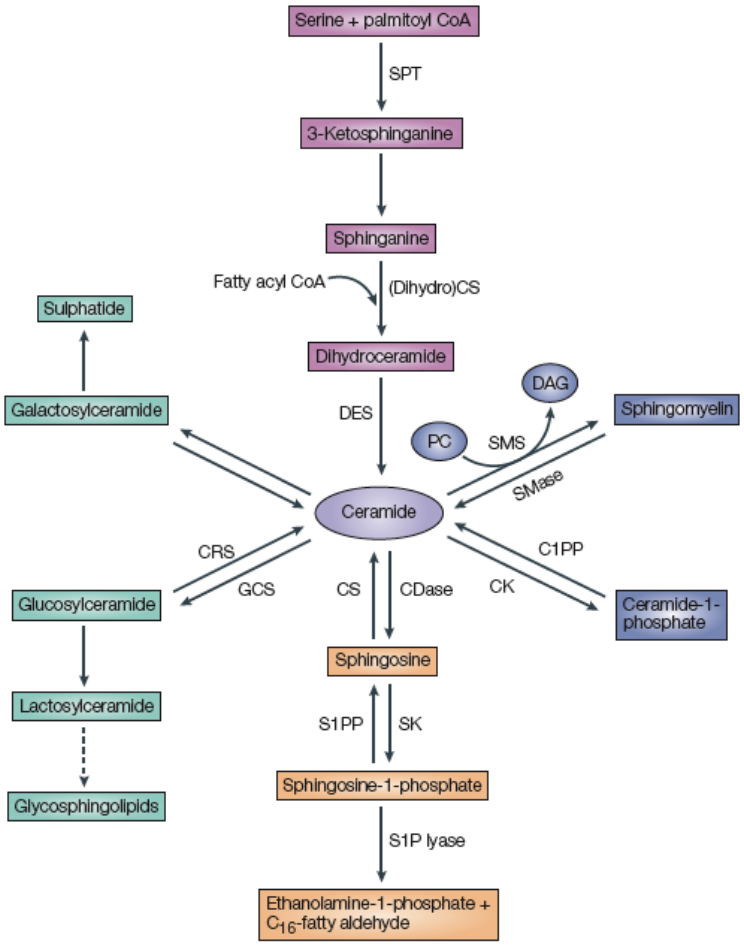

Figure I- 31. Sphingolipid metabolism (Ogretmen and Hannun 2004).

SL metabolism is very dynamic and once ceramide is formed it can either mediate its actions as a secondary messenger or it can be metabolized into other SL. Ceramide is primarily used for the synthesis of SM by transferring a phosphocholine headgroup from phosphatidylcholine through the action of SM synthases, thereby also generating diacylglycerol (Figure I-30). Ceramide can also be phosphorylated by ceramide kinase (CK) to form C1P, which in turn can be recycled by a C1P phosphatase or glycosylated by glucosyl or galactosyl ceramide synthases (GCS) (Figure I-30). Ceramide is also metabolized by ceramidases (CDases), which remove the amide-linked FA to form SPH (Figure I-30). Three types of CDases have been classified by their pH optimum and subcellular localization: acid CDase, neutral/alkaline CDase, and alkaline CDase. SPH is then available for recycling into SL pathways or for phosphorylation by one of two SPH kinases, SK1 and SK2, to form S1P (Figure I-30). In turn, S1P phosphatases dephosphorylate S1P regenerating SPH. Finally, S1P lyase can metabolize S1P to release ethanolamine phosphate and hexadecenal (Bartke and Hannun 2009) (Figure I-31).

In addition to ceramide, S1P has attracted a great deal of attention due to its role regulating cell functions. Ceramide mediates many cell-stress responses, including the regulation cell growth, differentiation, senescence necrosis and apoptosis. However, S1P has crucial roles in cell survival, cell migration and proliferation, inflammation, angiogenesis and resistance to apoptotic cell death. Thus, in most contexts, S1P shows antagonizing effects to those of ceramide. S1P binds to G-coupled receptors (S1P receptors) on the cell surface regulating various intracellular signaling pathways. The control of cell fate by these two lipids (ceramide/S1P) has been called the SL rheostat or SL biostat (Bartke and Hannun 2009; Brocklyn and Williams 2012). Other members of the family of bioactive SLs include C1P, which has roles in inflammation and vesicular trafficking, and glucosylceramide, which is involved in post-Golgi trafficking and in drug resistance (Bartke and Hannun 2009).

It is worth mentioning that SM has been established as a membrane partner of cholesterol. SM regulates the capacity of membranes to absorb cholesterol and thereby controls sterol flux between the plasma membrane and regulatory pathways in the ER. This relationship exemplifies the importance of cholesterol/sphingolipid-rich domains in cholesterol homeostasis, as well as other aspects of cell signaling and transport (Ridgway 2000).

6.3. Ceramides and disease:

Ceramide has been linked to many complex diseases like alcoholism, obesity, atherosclerosis, pulmonary disease, neurodegenerative diseases and cancer.

Obesity and alcohol intake set the stage for increased ceramide generation. On one hand, increased circulation FFAs coming from the adipose tissue may induce ceramide *de novo* synthesis. On the other hand, both obesity and alcohol intake are characterized by inflammation and increased circulating levels of inflammatory cytokines, especially TNF-α, which in turn activates ASMase generating ceramide from SM hydrolysis.

Several groups have demonstrated that small changes in tissue ceramide are enough to antagonize insulin action, providing a link between abnormalities in SL metabolism and the mechanism of insulin resistance (Summers 2006). For instance, genetic ablation or

pharmacological inhibition of *de novo* ceramide synthesis in obese mouse models improves body weight, whole body insulin sensitivity and hepatic steatosis (Holland, Brozinick et al. 2007; Yang, Badeanlou et al. 2009). Furthermore, hepatic ceramide levels are increased in NAFLD (Deevska, Rozenova et al. 2009; Pagadala, Kasumov et al. 2012). In addition, chronic alcohol feeding in mice activates ceramide generation, contributing to hepatic steatosis (Deaciuc, Nikolova-Karakashian et al. 2000; Setshedi, Longato et al. 2011; Liangpunsakul, Rahmini et al. 2012).

Human data showed that the presence of hepatic steatosis compared to control subjects correlates with increased adipose tissue ceramide concentrations. In addition, weight loss decreases hepatic ceramide expression in obese patients with NAFLD and it correlates with lower serum ceramides. Furthermore, bariatric surgery decreases plasma ceramide levels and this decrease correlates with improved insulin sensitivity (Pagadala, Kasumov et al. 2012). Moreover, plasma ceramides are elevated in obese subjects with type 2 diabetes and correlate with the severity of insulin resistance (Haus, Kashyap et al. 2008).

All these data suggest that targeting ceramide production in metabolic diseases could improve the symptoms of several metabolic pathologies. Specifically, targeting the TNF-inducible SM hydrolysis into ceramide by ASMase might be of great importance since inflammation is a hallmark of almost all these diseases. Therefore, preventing ASMase activation might ameliorate or stop the progression of many pathologies.

6.4. Acid sphingomyelinase:

Acid sphingomyelinase (ASMase; EC 3.2.1.14) is a key SL metabolism enzyme that catalyzes the cleavage of the phosphocholine head group of SM to generate ceramide. The enzyme has an optimal pH of 5.0 and an optimal temperature of 37ºC. Importantly, ASMase retains 50% of its activity at a neutral pH of 7.0, which explains ASMase ability to work in other locations with higher pH (Zeidan and Hannun 2010).

Human ASMase is coded by SMPD1 gene located on the short arm of chromosome 11. There are no homologous or pseudogene sequences to SMPD1. It is a highly conserved gene among mammals and its human amino acid sequence shares 82% of homology with the mouse ASMase. ASMase undergoes extensive posttranslational modifications.

Glycosylation is an important determinant of glycoprotein sorting and folding. ASMase has six potential glycosylation sites that are required for its proper trafficking as well as to protect it from the proteolytic activity in the lysosomes (Zeidan and Hannun 2010).

The precursor of ASMase is a 75 KDa protein that is cleaved within the Golgi to a major 72 KDa form and a minor 57 KDa form. Within the Golgi, mannose 6 phosphate (M6P) residues are added to the enzyme for recognition by the M6P receptors in the trans-Golgi enabling ASMase to be transported via the endosomal system to the lysosomes. Within the lysosome, ASMase is further processed to a mature 70 KDa form (Figure I-32). The minor 57KDa form is targeted to the secretory pathway without alternative carbohydrate processing (Figure I-32). This is the secretory form of ASMase or sASMase (Zeidan and Hannun 2010). Another trafficking pathway involving the transmembrane Golgi protein sortilin has been also suggested as an alternative trafficking pathway for ASMase targeting the lysosomes (Zeidan and Hannun 2010) (Figure I-32).

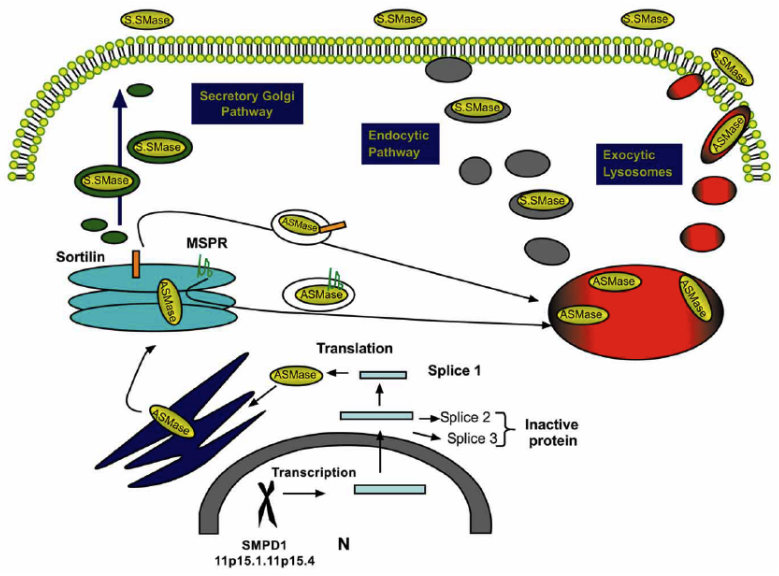

Figure I-32 . Cellular trafficking of ASMase (Zeidan and Hannun 2010).

To the date, three different ASMase pools have been described (Morales, Lee et al. 2007):

1. The acidic lysosomal/endosomal ASMase consistent with its strict acidic pH requirement.

2. The secretory ASMase, which has a key role in atherosclerosis, cell surface signaling and host inflammation.
3. The receptor-activated ASMase, which undergoes a translocation to the outer cell membrane in specific microdomains, where it converts SM into ceramide allowing receptor dimerization. Thus, it creates signaling platforms by the cell surface.

ASMase is activated by numerous receptors and non-receptor mediated cellular stimuli. Some of them are summarized below:

1. Death receptors (TNF-α, CD95 and TRAIL).
2. Radiation (UV-C and ionizing radiation).
3. Chemotherapeutic agents.
4. Viral, bacterial and parasitic infections.
5. Cytokines (IL-1β).
6. Oxidative stress (Induced by ischemia/Reperfusion or H_2O_2).

6.5. ASMase in hepatic injury and metabolic disorders:

To date, ASM inhibition using siRNA, pharmacologic inhibitors, or KO mice has been shown to render cells and animals resistant to the apoptotic effects of diverse stimuli, including but not limited to Fas, hepatic ischemia/reperfusion (Llacuna, Marí et al. 2006), radiation, chemotherapy, and TNF-α (García-Ruiz, Colell et al. 2003; Schuchman 2010). At a mechanistic level, previous work in our laboratory, showed that ASMase contributes to TNF/FAS or irradiation-induced apoptosis by targeting glycosphingolipids to the mitochondria and down-regulating of MAT1A, which leads to SAMe depletion, which sensitizes cells to other insults (García-Ruiz, Colell et al. 2003; Marí, Colell et al. 2004).

ASMase has been shown to promote several forms of liver injury. Some of them are described below:

- Hepatic Ischemia/Reperfusion (I/R): pharmacological inhibition of ASMase or ASMase knockdown by siRNA decreased ceramide generation during hepatic I/R, and attenuated serum ALT levels, hepatocellular necrosis, cytochrome c release,

and caspase 3 activation. The administration of TNF-α neutralizing agent, pentoxifylline blocked ASMase activation suggesting that TNF-α production is upstream of ASMase during I/R liver damage (Llacuna, Marí et al. 2006).

- Hepatic fibrosis: recent studies in our lab illustrated a role of ASMase in promoting hepatic stellate cell activation and liver fibrogenesis by regulating its downstream effectors cathepsin B/D (Moles, Tarrats et al. 2010). Interestingly, in a model of complete ASMase ablation, the lack of ASMase promotes liver fibrosis through a compensatory mechanism involving cathepsin B overexpression suggesting that the overexpression of cathepsin B may underlie the phenotype of Niemann Pick Disease (Moles, Tarrats et al. 2012).
- Liver cholestasis: ASMase has also been linked to bile-salt-induced liver injury. Primary rat hepatocytes treated with deoxycholic acid triggers ASMase activation and ceramide production that leads to JNK activation (Gupta, Natarajan et al. 2004). Bile salts activate ASMase by dropping the pH of ASMase-carrying lysosomes (Becker, Reinehr et al. 2007). Thus, ASMase is a key player in liver injury in cholestatic diseases as well.
- Wilson disease: Wilson disease is an autosomal recessive disorder resulting from a mutation in the copper transporter ATP7B. This condition leads to toxic accumulation of copper leading to chronic hepatitis, progressive liver failure and anemia. ASMase/ceramide pathway mediates liver cirrhosis and anemia in Wilson disease. Addition of copper to hepatocytes triggers ASMase activation and consequent apoptosis. Furthermore, blood samples of these patients show higher ASMase activity and ceramide levels (Lang, Schenck et al. 2007). Therefore, targeting ASMase might be useful for treatment of the clinical complications of Wilson disease.

Given the role of ASMase as an intermediate in stress responses and cell death regulation, ASMase is also involved in metabolic disorders:

- Obesity and insulin resistance: Early work on 3T3L1 adipocytes and rat hepatoma FAO cells showed that TNF-α inhibits insulin signaling via stimulation of TNFR1 and ASMase activation that results in negative phosphorylation of insulin receptor substrate (IRS) 1 and 2 which significantly reduces its ability to

interact with the insulin receptor (IR) (Kanety, Hemi et al. 1996; Peraldi, Hotamisligil et al. 1996). Later on, a group identified the death domain of TNFR1 responsible for the inhibitory effects of TNF-α on tyrosine phosphorylation of IRS-1, implicating ceramide generated by ASMase as a downstream mediator of the inhibition of IR signaling (Csehi, Mathieu et al. 2005). In addition, TNF-α via ASMase activation and ceramide production decreases mRNA levels of glucose transporter Glut4 in 3L3L1 adipocytes (Long and Pekala 1996). In a human setting, non-obese patients with type 2 diabetes have elevated Zn^{2+}-dependent ASMase activity in serum (Górska, Barańczuk et al. 2003). Moreover, adipose tissue from genetically obese ob/ob mice has increased expression of ASMase among other important enzymes of SL metabolism (Samad, Hester et al. 2006). Moreover, a recent study using ASMase deficiency in a genetic background of LDL receptor ablation (ALDLRDKO) showed that in a diet-induced obesity model ASMase deficiency increases insulin sensitivity, improves glucose tolerance and adiposity and protects from liver TG accumulation (Deevska, Rozenova et al. 2009). However, these animals demonstrate a paradoxical increase in hepatic ceramide content due to *de novo* ceramide synthesis induced by SPT activation. This study, suggested a mechanism by which ASMase regulates the partitioning of the major FA in the modified diet, palmitate, into two competitive and inversely related pools, TG and SLs, apparently via modulation of SPT (Deevska, Rozenova et al. 2009). Intriguingly, another study overexpressing ASMase in leptin receptor deficient db/db mice, reported glucose tolerance improvement with glycogen and lipid accumulation in the liver. In addition, this study showed that $ASMase^{-/-}$ mice were glucose intolerant due to Akt and AMPK regulation (Osawa, Seki et al. 2010). Thus, the role of ASMase in insulin resistance is still quite controversial.

- Fatty liver: A known dietary model of NASH is the methionine and choline deficient diet or MCD, which causes steatosis, mitochondrial dysfunction, hepatocellular injury, oxidative stress, inflammation, and fibrosis. Previous work in our lab examined the individual contributions of methionine and choline deficiency to MCD-induced liver injury and fibrosis showing that ASMase but not NSMase activity was induced upon two days of exposure to MCD or methionine deficient diet correlating with increased ceramide levels in the liver

(Caballero, Fernández et al. 2010). Importantly, increased ASMase gene expression has been reported in patients with NAFLD, which correlated with disease progression (Moles, Tarrats et al. 2010). Regarding alcoholic liver disease, recent studies focused on the role of ASMase in signs of liver injury. Ethanol treatment of hepatoma cells as well as feeding ethanol-containing Lieber-DeCarli diet to mice inhibited AMPK through increased hepatic ASMase activity and ceramide content. These effects were abrogated by imipramine, an ASMase inhibitor. This study suggested that the generation of ceramide via ASMase is stimulated by ethanol (Liangpunsakul, Sozio et al. 2010). Recent work from this group showed how imipramine reduces alcohol-induced hepatic steatosis by decreasing ASMase activity, hepatic ceramide content and recovering the alcohol-induced AMPK inhibition. Moreover, imipramine improved ethanol-impaired glucose tolerance and attenuated inflammatory pathways such as JNK and p38 (Liangpunsakul, Rahmini et al. 2012). Moreover, elevation of secretory ASMase activity has been reported in peripheral blood of active drinkers (Reichel, Beck et al. 2011).

Taken together, these findings support the idea that ASMase plays an important role in metabolic diseases, however the mechanisms underlying its activation and its downstream effectors command the actions that will make progress the disease remains unclear.

AIMS

ALD and NAFLD are two of the most prevalent metabolic liver diseases. Especially, NAFLD is of particular concern due to its association with obesity, insulin resistance and T2DM. Although etiology of both ALD and NAFLD are obviously different, they share common cellular and molecular mechanisms, which elicit similar histological and biochemical manifestations. Key events involved in either disease include hepatic steatosis, oxidative and ER stress, hepatocellular damage and a state of low grade chronic inflammation characterized by elevated circulating levels of TNF-α and FFAs. The latter two are of special interest since TNF-α and FFAs are key regulators of ceramide synthesis. Ceramide is a SL that mediates many cell responses including regulation of cell growth, differentiation, apoptosis and insulin signaling and it has been linked to many complex diseases including alcoholic liver disease, obesity and insulin resistance. Condensation of palmitic acid with serine is the rate-limiting step of *de novo* ceramide synthesis and hence increased palmitic acid availability increases ceramide synthesis. Moreover, TNF-α is a known activator of a second important pathway of ceramide generation, the hydrolysis of SM into ceramide by the action of ASMase. ASMase ceramide generation is quick and transient and generates ceramide in specific cellular localizations linked to the activation of apoptotic pathways. It has been demonstrated that ASMase gene expression and activity are increased both during ALD and NAFLD and ASMase ablation protects mice from different models of hepatic injury. Unfortunately despite intense investigation, molecular pathways underlying ALD and NAFLD are still poorly understood, limiting the efficacy of the current therapeutic armamentarium available for ALD and NAFLD. To contribute to fill this gap of knowledge the aims of this thesis were:

AIM 1:

- To study the role of ASMase in non-alcoholic steatohepatitis as potential regulator of systemic glucose homeostasis, hepatic steatosis and hepatic injury in a mouse model of high fat diet-induced obesity.

AIM 2:

- To determine the role of ASMase in alcoholic steatohepatitis as a potential regulator of hepatic steatosis and hepatic injury in a Lieber-DeCarli alcoholic mouse model and confirm the relevance of our findings in human samples of ASH.

MATERIALS AND METHODS

1. MOUSE MODELS:

All studies were performed in male mice to avoid hormonal fluctuations of female estrous cycle. Animals had free access to water and food with the exception of the Lieber-DeCarli liquid diet model where mice were pair-fed. All mice were raised under specific pathogen-free conditions with controlled temperature and humidity on a 12 h light–dark cycle in the animal care facility of the Medical School of Universitat de Barcelona.

1.1. ASMase knockout mice:

ASMase knockout mouse was created in 1995 in Dr. Schuchman's lab as a model of types A and B Niemann-Pick disease, as these types of NPD result from deficient ASMase activity (Horinouchi, Erlich et al. 1995). A PGK-neomycin expression cassette was inserted into the exon 2 of the ASMase murine genomic sequence, disrupting its coding sequence. As a result knockout mice have no detectable ASMase activity in their tissues. These mice are in a C57BL/6 genetic background. ASMase deficient mice follow a severe, neurodegenerative course that ends with a premature death between six and eight months of age. At the time of death, knockout mice weigh less than half of their wild type littermates. Cholesterol and SM levels are elevated in blood, liver and brain. These mice also show atrophy of the cerebellum and marked deficiency of Purkinje cells. Moreover, most tissues display presence of foam cells. Affected males can breed until 20 weeks of age and affected females until 10 weeks.

1.1.1. ASMase breeding:

ASMase knockout mice (C57BL/6 strain) were propagated using heterozygous breeding pairs (kindly provided by Dr. Gulbins and Dr. Kolesnick). ASMase$^{-/-}$ phenotype is inherited as an autosomal recessive trait so heterozygous breeding pairs yield 25% wild type (WT) mice and 25% ASMase$^{-/-}$ mice and 50% of heterozygous mice.

1.1.2. ASMase DNA extraction:

Mice deficient in ASMase were genotyped by PCR using ear-clipped DNA. Genomic DNA was extracted from ear clipped tissue at weaning time (21 days) with QuickExtract DNA kit (Epicentre, QE09050):

- Add 50µl of QuickExtract solution to each tube containing the tissue.
- Vortex the mix for 30 sec.
- Incubate 6 min at 65ºC.
- Vortex the mix for 30 sec.
- Incubate 2 min at 98ºC.
- Vortex the mix for 30 sec and place the tube on ice.
- Centrifuge the tube at 14.000 rpms for 2 min.
- Use 1µl of the extracted DNA (200ng of DNA approximately) for each PCR reaction.
- Store DNA at -20ºC.

1.1.3. ASMase genotyping:

Wild type primers were used to amplify a 269-base pair (bp) product that is specific for exon 2 of the wild type ASMase gene. To amplify the mutant gene, the same forward primer as wild type was used and a reverse neomycin gene-specific antisense primer was used to amplify a 523-bp product that was specific for the mutant gene containing part of the neo cassette and exon 2 of the ASMase gene (Table M1).

	Wild Type	**ASMase$^{-/-}$**
Forward	5'-AGCCGTGTCCTCTTCCTTAC-3'	
Reverse	5'-CGAGACTGTTGCCAGACATC-3'	5'-GGCTACCCGTGATATTGCTG-3'

Table M1. ASMase knockout genotyping primers.

PCR mix:

	[Stock]	**[Final]**	**x1 (µl)**
dH_2O		till 25 µl	18,875
dNTP	10mM	0,2mM	0,50
Taq Buffer (w/o Mg)	x10	1x	2,50
DMSO	100x	1%	0,25
Primer Fw	50µM	1µM	0,50
Primer Rev WT	50µM	0,5µM	0,25
Primer Rev KO	50µM	0,5µM	0,25
$MgCl_2$	50mM	1,5mM	0,75
EcoTaq (Ecogen, ETAQ-500)	5U/µl	0,625U	0,125
DNA	200ng/µl	200ng	1
		Final volume	25µl

Table M2. ASMase knockout genotyping PCR mix.

PCR protocol: Polymerase chain reaction amplification conditions consisted of

- Step1: 3 min at 93ºC.
- Step2: 39 cycles of [45 sec at 93°C, 45 sec at 58°C, and 45 sec at 72°C].
- Step 3: 3 min at 72ºC.
- Step 4: Forever at 10ºC.

Gel and development:

- Prepare a loading buffer mix with 1ml of loading buffer (AppliChem, A3144) and 1µl of the nucleic acid staining solution RedSafe (Chembio, #21141).
- Add 5µl of this mix to each PCR reaction.
- Prepare a 1,5% agarose gel with 100ml of 1x Tris Borate EDTA Buffer (TBE, Sigma, T4415) and 1,5g of Agarose (Sigma, A9539).
- Load the samples in the gel and run them in 1x TBE at 80v for 1h.
- Develop the gel in a Gel Doc™ XR+ System (Bio Rad) exciting the SafeRed component with UV light. One single band at 269bp indicates wild type, two bands at 269bp and 523bp indicates heterozygous and one single band at 523bp indicates ASMase$^{-/-}$.

1.2. TNFR1, TNFR2, TNFR1/R2 knockout mice:

Tumor Necrosis Factor Receptor 1 (TNFR1) knockout mice, Tumor Necrosis Factor Receptor 2 (TNFR2) knockout mice, and Tumor Necrosis Factor Receptor 1 and 2 (TNFR1/R2) mice (C57BL/6 strain) were a generous gift from Dr. Bluethmann (Discovery Technologies, Hoffmann-La Roche Ltd., Basel, Switzerland). These knockouts are viable and fertile. Homozygous breeding pairs were kept in the animal facility to obtain the three kinds of TNFR knockout.

1.3. Wild type mice:

All wild type mice (C57BL/6 strain) were purchased from Charles River, USA, with the exception of ASMase$^{-/-}$ studies where wild type littermates were used as controls. Prior to their use in a study, purchased mice rested for one week in order to get acquainted to the new environment.

2. *IN VIVO* EXPERIMENTAL MODELS:

All experimental protocols used in this thesis met the guidelines of the Animal Care Committee of Hospital Clinic-Universitat de Barcelona.

2.1. Diet models of steatohepatitis:

The diets used in this thesis are the high fat diet (HFD), the methionine and choline deficient diet (MCD), the hypercholesterolemic diet (HCD) and the ethanol-containing Lieber-DeCarli liquid diet (EtOH). HFD, MCD and HCD studies had as control diet the regular diet (RD) from the animal facility (Harlan, 2014). For alcohol studies, a control Lieber-DeCarli liquid diet was used (Ctrl) (Table M3).

	RD/HCD*	HFD	MCD	Ctrl	EtOH
Protein	20%	20%	14.8%	17.3%	17.3%
Fat	13%	60%	12.4%	35%	35%
Carbohydrates	67%	20%	72.8%	47.7%	47.7%**

Table M3. Diet percentage of macronutrients.
* HCD is a RD supplemented with 2% cholesterol and 0.5% sodium cholate.
** 36% of Kcal derived from ethanol.

2.1.1. Diet-induced obesity model:

Obesity is strongly associated with hepatic steatosis and insulin resistance in humans. When normal, lean C57BL/6 male mice are fed diets with high content in saturated or unsaturated fats, mice exhibit an increase in body weight due to a gradual accumulation of body fat (Hebbard and George 2011). This is a chronic dietary model (3-4 months) that courses with increased inflammation, oxidative and ER stress, insulin resistance and hepatic steatosis.

This model of diet-induced obesity (DIO) was used to induce insulin resistance and hepatic steatosis in the absence of ASMase. Mice were exposed from 4 weeks of age to a HFD (Research Diets, D12492) containing 60% of total Kcal content derived from fat. Mice were anesthetized using a lethal dose of sodium pentobarbital (0.1g/Kg) and sacrificed at 16 weeks of age (12 weeks on HFD) after a 6h fasting period (9h-15h). Blood, tissue lipids, protein and mRNA profiles were analyzed. For the amitriptilyne studies, C57BL/6 males were exposed to HFD since week 5 and were sacrificed at 21 weeks of age (16 weeks on HFD).

2.1.2. MCD diet-induced NASH model:

Feeding mice a MCD diet is a frequently used nutritional model of NASH that induces serum alanine transaminase (ALT) elevation and hepatic histological changes characterized by steatosis, focal inflammation, oxidative stress, hepatocyte necrosis, and fibrosis (Hebbard and George 2011). MCD diet is high in sucrose and fat (72.8% sucrose, 12.4% fat), but lacks methionine and choline, which are essential for hepatic β-oxidation and VLDL production. This results in accumulation of intrahepatic lipid and decreased VLDL synthesis. MCD-fed mice exhibit increased inflammation with activated macrophage infiltration into the liver. MCD diet activates NF-κB and increases levels of IL-6, transforming growth factor β (TGF-β) and TNF-α contributing to the liver injury. Histological changes occur rapidly (in 10 days, acute model of steatohepatitis) and are morphologically similar to those observed in human NASH. In contrast to the DIO, this dietary model does not cours with obesity or insulin resistance.

10 week-old male wild type and ASMase$^{-/-}$ mice were exposed to MCD diet (TestDiet, 578B) for two weeks. The diet was prepared every two days.

Diet preparation protocol:

- Mix 1,5g of Noble Agar (Sigma, A5431) in 100ml of tap water.
- Heat in the microwave until it boils and the noble agar melts completely.
- Allow to cool down.
- Add 60g of powdered MCD diet per each 100ml.
- Let it solidify.
- Cut in pieces to feed the mice.

2.1.3. Hypercholesterolemic diet-induced steatohepatitis model:

The HCD is a nutritional model of hepatic microvesicular steatosis characterized by FC accumulation in membranes. FC sensitizes hepatocytes to TNF-α -induced apoptosis and steatohepatitis development due to FC accumulation in mitochondria, which results in mGSH depletion (Marí, Caballero et al. 2006). HCD is a RD supplemented with 2% purified cholesterol and 0.5% sodium cholate (Dyets Inc.).

In results Aim 1, HCD was fed to 6-10 week-old wild type mice for 2 days in order to induce FC accumulation in lysosomal membranes and test whether FC accumulation would protect against lysosomal membrane permeabilization-induced apoptosis. In results Aim 2, HCD diet was fed to 6-10 week-old wild type mice for 3 days to induce FC accumulation, which down-regulates SREBP2 activation and its targeted genes. This strategy was used to dissociate StAR mRNA regulation from SREBP2 and link it to ER stress.

2.1.4. Alcohol-induced ASH model:

Ethanol feeding as part of a totally liquid diet (Ethanol containing Lieber-DeCarli liquid diet, EtOH diet) was developed in 1963 by Lieber CS and DeCarli LM in response to the need to develop an animal model in which alcohol consumption was clinically relevant while dietary control was maintained. Previously, ethanol had been administered to rats in drinking water, but due to a natural aversion to ethanol, the intake resulted in negligible blood ethanol levels. This model was insufficient to cause significant liver damage. However, the aversion to ethanol can be overcomed with the ethanol-containing liquid diet formula. This diet ensures a high daily consumption of 12-18g of ethanol/Kg and elevated blood ethanol levels (100-150mg/dl). EtOH diet causes significant liver lesions within 4 weeks inducing functional changes including impaired energy production, significant induction of microsomal ethanol oxidizing system (CYP2EI), generation of free radicals and alterations in defense mechanisms against this oxidative stress, which results in GSH depletion and lipid peroxidation. Thus, the Lieber-DeCarli liquid diet provides way to reproduce early stages of ALD and facilitates the study of the pathogenesis of ALD (de la M Hall, Lieber et al. 2001).

In this thesis, male ASMase$^{-/-}$ mice, TNFR1, TNFR2 or double TNFR1/R2 null mice and wild type mice (8-10 weeks of age) were pair fed with either Ctrl or EtOH diets (Test Diet, LD101 and LD101A, respectively) in which alcohol accounted for 36% of calories (Colell, García-Ruiz et al. 1998). Ethanol content of the diet was gradually increased over an 8-day period until they received 5% ethanol from day 8 for 4 weeks.

Diet preparation:

- Control Lieber-DeCarli liquid diet: to prepare 1 liter of diet mix 770ml of tap water and add 230g of control diet. Mix with a blender.
- Ethanol-containing Lieber-DeCarli liquid diet: to prepare 1 liter of diet mix 809ml of tap water, 140g of the test diet (LD101A) and 51ml of 96% ethanol. Mix with a blender.

Diets were prepared fresh daily and were administered in feeding tubes. Control and EtOH diet were pair fed taking in account that each animal eats approximately 20ml of liquid diet per day.

Alcohol diet adaptation protocol:

- Day 1: feed control Lieber-DeCarli liquid diet.
- Day 2-3: feed 2/3 of control diet and 1/3 of ethanol diet.
- Day 4-5: feed 1/2 of control diet and 1/2 of ethanol diet.
- Day 6-7: feed 1/3 of control diet and 2/3 of ethanol diet.
- Day 8-end of the study: feed ethanol containing Lieber-DeCarli liquid diet.

2.2. *In vivo* Treatment models:

2.2.1. ASMase inhibition models:

In order to explore potential therapeutic options to treat ASH and NASH we used a model of pharmacological inhibition of ASMase. For that purpose, mice were treated with amitriptilyne to functionally inhibit ASMase. Amitriptyline is a tricyclic antidepressant that also ease migraines, tension headaches, anxiety attacks and some schizophrenic symptoms. It has been reported that amitriptyline detaches ASMase from the lysosomal inner membrane inactivating the enzyme and exposing it to proteolytic degradation (Kornhuber, Tripal et al. 2010).

Advantages of this model are the good solubility in aqueous solutions so it can be administered to mice in drinking water. In addition, as a potential human treatment

for ASH and NASH, amitriptyline is a drug already approved to treat other affections.

2.2.1.1. Amitriptyline in drinking water:

To evaluate whether ASMase inhibition modulates NAFLD, 5 week-old wild type mice were exposed to RD or HFD for 16 weeks and treated with 1mM amitriptyline hydrochloride (Sigma, A8404) dissolved in the drinking water with a 1% saccharin sodium salt hydrate (Sigma, S1002) to avoid taste rejection. After a drinking test, we approximated a dosage per mouse and day of 20-25mg/Kg/day of amitriptyline.

2.2.1.2. Amitriptyline intra-peritoneal injection:

To evaluate whether ASMase inhibition modulates ALD, 8-10 week-old wild type mice were fed alcohol and from week two mice were treated with a daily intra-peritoneal (i.p.) injection of 2.5mg/Kg amitriptyline as previously described (Lang, Schenck et al. 2007). For the last two weeks of ethanol feeding amitriptyline dose was doubled to 5mg/Kg.

2.2.2. Acute liver damage models:

Accumulation of lipids in the cytoplasm of hepatocytes, mostly in the form of FFA and TG, is considered the first step in the development of steatohepatitis. Hepatic steatosis sensitizes the liver to secondary insults. In this thesis we used two models of acute liver damage: LPS and concanavalin A (Con A). Both models imply TNF-α release from the cells but LPS is believed to act mainly through soluble TNF-α binding to TNFR1 and Con A through cell-bound TNF-α that binds to TNFR2.

2.2.2.1. Lipopolysacharide:

LPS is a major constituent of the cell wall of most gram-negative bacteria. It is a highly immunogenic antigen with the ability to enhance immune responses. *In vivo*, it is known to cause hepatitis (Tsukamoto, Machida et al. 2009). In the HFD model, 8-10 week-old wild type and ASMase$^{-/-}$ mice were exposed to HFD for 6 weeks to develop some degree of liver steatosis and then were treated with 5mg/Kg LPS (Sigma, L4391) i.p. for 24h at the end

of the study. In the ethanol studies, at the end of the study after 4 weeks of ethanol feeding mice received an i.p. injection of LPS (5mg/Kg).

2.2.2.2. Concanavalin A:

Con A is a plant lectin with high affinity towards the hepatic sinus, which results in activation of T cells in the liver promoting the secretion of cytokines. When given intravenously to mice it leads to immune-mediated liver injury. Hepatotoxicity following Con A administration involves the systemic release of soluble TNF-α as well as cell-bound TNF-α, which acts through TNFR2. (Jaruga, Hong et al. 2004). In the ethanol model, at the end of the study after 4 weeks of ethanol feeding mice received an intra-venous (i.v.) injection of Con A (0.5mg/Kg) 24 hours before sacrifice.

2.2.3. ER stress-induction model:

In order to prove that ASMase$^{-/-}$ mice were capable to sense and respond to ER insults *in vivo*, wild type mice and ASMase$^{-/-}$ mice were treated with 1mg/Kg Tunicamycin (Tm) (Sigma, T7765) for 24 hours. Tm is an inhibitor of N-acetylglucosamine transferases; preventing formation of N-acetylglucosamine lipid intermediates and glycosylation of newly synthesized glycoproteins in the ER. Proteins that require glycosylation will remain in the ER and form protein aggregates causing ER stress and activating UPR.

2.3. Liver regeneration-Partial hepatectomy model:

Mice were anesthetized with 2% isoflourane with a 1,5-2L/min-oxygen flow for a 25g wild type mouse. Mice were subjected to midventral laparotomy with 70% liver resection (median lobe and left lateral lobe). Weight of the excised liver was determined. Sham surgery entailed midventral laparotomy. Survival was higher than 80% and all deaths were due to post-surgery complications during the first 24h post-PH. Hepatocyte proliferation was determined by detecting Proliferating cell nuclear antigen (PCNA) at different time points and liver regeneration index was calculated as the ratio of the liver remnant to body mass and ×100.

3. *IN VIVO* METABOLIC STUDIES:

3.1. Blood glucose levels:

Obesity and T2DM curse with hyperglycemia even in fasting periods. To assess glycemia in mice, blood glucose levels were measured every 4 weeks after a 6h period of fasting (9a.m. to 3p.m.). Blood glucose concentration was determined using 5µl of blood from the tail using Ascensia BREEZE blood glucose meter (Bayer).

3.2. Glucose tolerance test:

T2DM is characterized by glucose intolerance, which contributes to peripheral (muscle, fat, and liver) insulin resistance as well as islet β-cell dysfunction. The glucose tolerance test (GTT) is used in clinical practice and research to identify individuals with normal or impaired glucose tolerance. GTT is a tool to identify impaired glucose tolerance.

GTTs were performed with an i.p. glucose injection (2g/Kg) on conscious mice after an overnight (15h) fasting at 10 weeks of age. Mice were kept in individual cages during the experiment. Blood glucose clearance was measured at times 0, 15, 30, 60, 90 and 120 min after glucose injection using 5µl of blood from the tail using Ascensia BREEZE blood glucose meter. Statistical significance was assessed using the area under the curve of blood glucose levels of each animal during the experiment.

3.3. Insulin tolerance test:

Obesity and T2DM present a decrease in insulin action on insulin-responsive tissues such as liver, adipose tissues and muscle. This decrease in insulin function is called insulin resistance or intolerance. Insulin tolerance test (ITT) allows systemic assessment of insulin sensitivity by determining the fall in plasma glucose after injection of insulin.

ITTs were performed with an i.p. insulin injection (0.75IU/Kg, Actrapid, Novo nordisk) after a 6h fasting period (from 9a.m. to 3p.m.) at 14 weeks of age. Mice were kept in individual cages during the experiment. Blood glucose clearance was measured at times 0, 15, 30, 60, 90 and 120 min after insulin injection using 5µl of blood from the tail using Ascensia BREEZE blood glucose meter. Statistical significance was assessed using the area under the curve of blood glucose levels of each animal during the experiment.

3.4. Insulin portal vein infusion:

This technique is used to assess *in vivo* insulin sensitivity of tissues, especially liver, adipose tissue and muscle. After stimulation, insulin sensitivity can be assessed by checking insulin signaling events via WB.

Following 6 hours of food withdrawal, mice were anesthetized with an i.p. injection of tribromoethanol (250mg/Kg), and insulin (1IU/Kg, Actrapid-Novo Nordisk) or phosphate buffered saline (PBS, Sigma, P3813) in a 200µl final volume was injected through the portal vein. 30G bended needles were used to inject the vein. Three minutes after infusion, tissues were removed, frozen in liquid nitrogen and stored at -80°C until processing. Tissue insulin sensitivity was assessed by monitoring insulin receptor and Akt phosphorylation via WB.

4. SERUM ANALYSIS:

At the time of sacrifice, mice were anesthetized with a lethal dose of 100mg/Kg of sodium pentobarbital. Blood was harvested from the lower cava vein with heparinized 16G needles in order to avoid hemolysis. Blood was centrifuged for 15 min at 10.000 rpms at 4ºC and serum was collected from the top phase avoiding bottom phase contamination.

4.1. Total cholesterol, HDL and LDL:

Serum total cholesterol, HDL and LDL levels were measured with a biochemical analyzer at the Centre de Diagnòstic Mèdic of Hospital Clínic i Provençal de Barcelona.

4.2. Alanine transaminase:

ALT is found in serum and other tissues but is most commonly associated with liver. ALT is measured clinically to determine liver health. Its increased presence in serum indicates hepatocellular damage. We used ALT as indicator of liver injury. Serum ALT levels were measured with a biochemical analyzer at the Centre de Diagnòstic Mèdic of Hospital Clínic i Provençal de Barcelona.

5. HISTOLOGY:

5.1. Tissue harvesting and preservation:

Tissues were quickly harvested after blood collection and were either:

- Flash frozen in liquid nitrogen for cryostat sections, or if wanted, in a cassette with OCT and slowly freeze down on dry ice. OCT is an embedding medium for frozen specimens to ensure Optimal Cutting Temperature (Tissue-Tech #4583).
- Placed in histology cassettes, fixed in formalin (10% paraformaldehide) (Sigma, HT501128) for 48h and embedded in paraffin for microtome sections.

Flash frozen tissues were cut with a cryostat (Microm, HM550) at 14µm at an approximate temperature of -20ºC. Sections were placed in superfrost slides (MENZEL-GLÅSER, J18000AMNZ).

Formalin fixed tissues were included in paraffin in an automated paraffin inclusor (Citadel 1000, Shandon) following this protocol:

- 1h in H_2O two times.
- 1h in 70% ethanol two times.
- 1h in 90% ethanol two times.
- 1h in 100% ethanol two times.
- 1h in xylol two times.
- 2h in paraffin two times.

Once tissues were embedded in paraffin, paraffin blocks were made to improve the cutting process in the microtome (Leica, RM2155). Sections at 7µm were used for hematoxylin and eosin staining and cuts at 5µm were used for immunohistochemistry. Sections were placed in histogrip-treated slides.

5.2. Stainings:

5.2.1. Hematoxylin and Eosin staining (H&E):

H&E staining is the most widely used stain in histology. It has the ability to demonstrate a wide range of normal and abnormal cell and tissue components and it is a relatively simple stain to carry out on paraffin or frozen sections. Hematoxylin

has a basic pH and it has affinity for acid structures such as the nuclei, which are referred as basophilic structures. Eosin acts as an acid dye staining basic structures, which are referred as acidophilic structures. This staining was performed in 7µm liver and EWAT sections.

Protocol:

- Melt the paraffin in a stove at 100ºC.
- Wash out the paraffin 10 min in xylol.
- Sample hydration: Rehydrate the sample with dilution series of ethanol (100%- 90%- 70%- 30%) till distilled water. Hydrated sections will allow aqueous reagents to penetrate into the tissue.
- Hematoxylin staining: 4 min of Hematoxylin Solution, Harris Modified (Sigma, HHS32) for liver sections or 10 min for adipose tissue sections. Nuclei and acidic structures will appear reddish-purple stained.
- Wash out the extra hematoxylin with abundant running tap water.
- Differentiation: removes hematoxylin background staining and improves contrast. Rinse in alcoholic-HCl 96% (480ml absolute alcohol + 20ml HCl 12N) until a reddish stain appears.
- Rinse in ammoniacal water (distilled water with 3-4 drops of 25% ammoniac solution) until the staining turns blue again.
- Wash with running tap water for 2 min.
- Rinse with distilled water for 2 min.
- Eosin staining: rinse the sections in alcoholic eosin (Sigma, HT110132) for 1,5 min. This step will stain many non-nuclear elements in different shades of pink.
- Sample dehydration: rinse samples through alcohol to remove all traces of water (70%- 90%- 100% alcohol). Eosin staining washes out with water so the more we maintain the samples in 70% ethanol the less eosin staining will remain. Rinse in xylol for 5 min after that.
- Mount sections: use the DPX mounting media for histology (Fluka, 44581). Add a small drop of DPX to the specimen. Carefully place a cover slip onto the drop, avoiding air bubbles.
- Remove any excess of mount with a paper towel.

- Samples can be observed with transmitted light microscopy.

5.2.2. Oil-Red staining:

Oil-Red O is a fat-soluble dye used for staining of neutral lipids like TGs. It has the appearance of a red powder with maximum absorption at 518 nm. This staining was performed on liver frozen sections to determine liver macrosteatosis.

Solutions:

- Oil-Red Stock Solution: 0,5g Oil-Red O (Sigma, O0625) in 100ml of isopropanol. Stir the solution over night in a capped container to avoid isopropanol evaporation.
- Oil-Red Working Solution: 60ml of stock solution with 40ml of distilled water. Stir and let it sit for several days so oil red is completely dissolved. Always paper-filter before using it.

Protocol:

- Rinse in distilled water 5 min, three times.
- Dip in 60% isopropanol 10 sec.
- Rinse in Oil-Red working solution 30 min.
- Remove Oil-Red excess by rinsing in 60% isopropanol 5 min, two times.
- Wash with distilled water 5 min, 4 times.
- Counterstain with hematoxylin 5 min.
- Wash with distilled water 5 min, 3 times.
- Mount sections: use an aqueous mounting media (Aquatex, Merck, #108562) Carefully place a cover slip on the mounting media, avoiding air bubbles.
- Allow samples to dry.
- Samples can be observed with transmitted light microscopy.

5.2.3. Filipin staining:

Filipin is an antibiotic isolated by chemists in 1955 from a previously unknown actinomycete, *Streptomyces filipinensis*, which was discovered in a soil sample collected in the Philippine Islands, hence the name Filipin. Filipin has been widely used as a

probe for sterol location in biological membranes. Interaction with cholesterol alters filipin absorption and fluorescence spectra allowing visualization with a fluorescence microscope capable of excitation at 340-380 nm and emission at 385-470 nm. It is a tool for histochemical identification of unesterified cholesterol both *in vivo* and *in vitro*. This method of detecting cholesterol in cell membranes is used clinically in the study and diagnosis of Type C Niemann-Pick disease.

Protocol:

- Washes: in a 50ml container, wash the sections with PBS 2 times for 5 min.
- Fixation: fix sections 1h at room temperature (RT) with formalin 10%.
- Washes: wash with PBS 3 times for 5 min.
- Filipin staining: prepare 50ml of PBS containing 0.2mg/ml filipin (Sigma,F-9765) and incubate over night at 4°C protected from the light. (For a 50ml solution, weigh 10mg of filipin and dissolve it in 200µl of DMSO. Once dissolved, add it to the 50ml of PBS) note: reduce filipin concentration if the samples are known to have high levels FC like ASMase$^{-/-}$ liver sections.
- Washes: wash with PBS, 3 times for 5 min.
- Mounting: Use abundant fluorescent mounting medium (Dako #S3023) to mount the cover slips. Let dry for a few hours protected from the light.
- Microscope: use UV light to visualize the staining.

5.2.4. PCNA immuno staining:

Proliferating cell nuclear antigen, commonly known as PCNA, is a protein that acts as a cofactor of DNA polymerase delta and helps increase the processivity of leading strand synthesis during DNA replication. PCNA is strongly associated in the nuclear regions where DNA synthesis is occurring therefore it is used as a marker of proliferation and in this thesis, as a marker of liver regeneration after partial hepatectomy. PCNA staining was performed in paraffined liver sections from sham or partial hepatectomy operated mice using the Dako kit (K4006).

Reagents:

Make sure that all reagents are at RT before using them. All incubations will be at RT too.

- Washing buffer: PBS (20mM NaH_2PO_4; 150mM NaCl, pH7.0) Keep at 4ºC.
- Citrate buffer: 2% sodium citrate, pH 6.0.
- Primary antibody dilution buffer: 0.05M Tris-HCl, pH 7.2-7.6 and 1% BSA (Dako antibody diluent, S0809).
- Negative control: Sham animals will be used as negative control.
- Substrate-chromogen buffer: 1ml of this solution is enough to perform the immunohistochemistry in 10 slides. Calculate how many 1ml aliquots of this buffer (bottle 3a) will be needed and add 20µl of bottle 3b. Mix immediately and place it on top of the tissue with a Pasteur pipette. This buffer is stable 5 days at 4ºC. Always mix before using it.

Protocol:

- Deparaffinize and rehydrate tissue sections:
  - Rinse 6 min in xylol twice.
  - Rinse 4 min in 100% ethanol twice.
  - Rinse 4 min in 96% ethanol twice.
  - Dip 30 sec in distilled water.
  - Rinse 5 min in PBS.
- Demasking of antigen: this treatment will undo the bounds made by the action of formalin during the fixation.
  - Put the slides in a container compatible with the microwave.
  - Cover the slides with citrate buffer.
  - Heat 9 min in the microwave at 800W until it boils and then count 4 min.
  - Let it cool down for 20 min.
- Endogenous peroxidase blocking: endogenous peroxidase activity is any activity that results in the degradation of H_2O_2. Such activity is a property of catalases in the liver. Since this protocol has a horseradish peroxidase-based detection method it is necessary to block the endogenous peroxidase activity to reduce background staining.
  - Apply peroxidase-blocking solution on top of the liver sections for 10 min.
  - Wash 5 min with PBS three times.

- Primary antibody incubation: dilute the anti-PCNA antibody (Millipore, CBL407) 1/200 in primary antibody dilution buffer.
    - Apply 50μl of antibody to every sample.
    - Incubate 30-50 min at RT in a humidity chamber.
    - Wash 5 min in PBS three times.
- Peroxidase labeled polymer:
    - Tap off excess PBS and wipe slides.
    - Apply enough Labeled Polymer to cover specimen.
    - Incubate 30 min at RT in a humidity chamber.
    - Wash 5 min in PBS three times.
- Substrate-chromogen:
    - Wipe slides as before.
    - Apply enough of the prepared Liquid DAB + substrate-chromogen solution to cover specimen on a plastic tray (DAB is very toxic, be cautious.)
    - Incubate for 2-3 min until it develops.
    - Rinse gently with distilled water from a wash bottle (do not focus flow directly on tissue).
    - Collect substrate-chromogen waste in a hazardous materials container for proper disposal.
- Hematoxylin counterstain:
    - Apply a few drops of hematoxylin in excess on top of the samples with a plastic Pasteur pipette.
    - Incubate 30 sec to 2 min at RT.
    - Rinse gently in distilled water.
    - Dip slides 10 times into 0.037mol/L.
    - Rinse slides in distilled or deionized water for 2–5 min.
- Mounting:
    - Mount specimens and coverslip with the aqueous-based mounting medium Aquatex.

6. MITOCHONDRIAL ANALYSIS:

Cholesterol and GSH was determined in wild type and ASMase null mice liver isolated mitochondria.

6.1. Mitochondria isolation:

Buffers:

- Buffer A: 225mM Mannitol; 75mM Sucrose; 0,1mM EGTA; 1mg/ml FFA-BSA and 10mM Hepes-KOH, pH 7.4. Keep at 4ºC.
- Buffer B: 395mM Sucrose; 0,1mM EGTA and 10mM Hepes-KOH, pH 7.4. Keep at 4ºC. (Use this buffer to prepare percoll gradients.)

Protocol:

- For each gram of liver add 2ml Buffer A (Always maintain this 1:2 ratio).
- Cut the liver in pieces and add twice the volume of buffer A (V_{final}= 6ml).
- Use a pestle homogenizer at 1200 rpms to homogenate the sample (4 times up and down).
- Aliquot a sample of 700-800µl for Homogenate measurements.
- Centrifuge the rest of homogenate at 700 g, 15 min at 4˚C.
- Discard the pellet and collect the supernatant.
- Centrifuge the supernatant at 10.000 g, 15 min at 4˚C.
- Discard the supernatant and re-suspend the pellet containing the mitochondrias in 0,5ml of Buffer B (so the final volume will be approx 1ml).
- Per each gram of tissue, prepare 2 tubes with two gradients of 26% Percoll (Sigma, P1644) (7ml) and 60% Percoll (3ml) in Buffer B.
- Add the entire sample on top of the 26% Percoll top layer.
- Equilibrate the tubes to the same weight with Buffer B.
- Ultra centrifuge samples at 15.500 rpms, 35 min at 4˚C. In this step, mitochondria will pass through the 26% Percoll gradient and will stop at the beginning of the 60% Percoll.
- Discard with a plastic Pasteur pipette the layers above the mitochondria's band.
- Gently collect the mitochondria's band with a glass Pasteur pipette and put them in a new tube.

- Add a big volume of Buffer B to the mitochondria and centrifuge it at 10.000 g, 15 min at 4°C to wash them. Repeat this step twice.
- Discard the supernatant and resuspend the pellet containing the mitochondria with 350µl of Buffer A. (Approx. volume so the final volume of mitochondria is around 500µl due to the remaining volume of buffer B after discarding the supernatant)

6.2. Mitochondrial free cholesterol quantification:

In alcohol studies mitochondrial FC was measured from isolated mitochondria from wild type and ASMase null mice fed either control or ethanol diets.

Cholesterol measurements were performed with high performance liquid chromatography (HPLC). This protocol can measure both total and FC. Total cholesterol samples will undergo saponification to free all the sterified cholesterol. Thus, the reading of saponified samples will represent total cholesterol levels (the sum of free and sterified cholesterol).

Protocol:

- Cholesterol standards: prepare 1mg/ml cholesterol (Sigma, C8867) stock solution in isopropanol. Prepare 7 standard points 0-5-10-20-40-80-100µg. Prepare two sets, one for the FC and one for the total cholesterol samples. These standards will be carried along with the samples and will undergo the lipid extraction and saponification.
- Use 1mg of mitochondria in a final volume of 200µl (Adjust the volume with PBS). Use two tubes per sample for total and FC quantification.
- Add 200µl of ethanol- 33% KOH (100% ethanol and 1/10 33% KOH).
- Vortex 1 min.
- Saponification:
    - Total cholesterol: incubate 30 min at 60ºC (saponification process)
    - FC: incubate 30 min at RT.
- Let the samples cool down.
- Lipid extraction:
    - Add 200µl of miliQ H_2O.
    - Add 400µl of Hexane HPLC proof.

Always maintain the extraction relation of sample:ethanol-KOH:H_2O:Hexane (1:1:1:2).

- Vortex 1 min and wait 1 min three times.
- Spin down 2 min at 10.000 rpms at RT.
- Collect 200µl from the hexane top layer containing the cholesterol and transfer it into a new tube. (Lipid extraction efficiency: 200µl recovered/400µl hexane).
- Dry the hexane in a speed vac 45 min.

- Add 200µl of isopropanol.
- Vortex 3 min.
- Spin down 2 min at 10.000 rpms at RT.
- Transfer the extraction into HPLC tubes.
- HPLC detection:
  - Use a µBondapak C18 10µm 125Å column (WATERS, WAT027324) with an absorbance of 200 nm using the WATERS 717 plus Autosapler system.
  - Mobile phase composition:
    - Pump A: Acetonitrile.
    - Pump B: Isopropanol:Acetonitrile:miliQ H_2O (60:30:10)
  - Flow rate: 1ml/min
  - Reading time: 15 min per sample. Cholesterol peak will appear around the 7th min of reading.
- Quantification of the cholesterol peak is calculated according to a calibration line derived from commercial cholesterol with known concentrations.

6.3. Mitochondrial total GSH quantification:

GSH is a non-essential tripeptide that is synthesized in the body from the amino acids L-cysteine, L-glutamic acid, and glycine. It is an antioxidant that prevents damage to important cellular components caused by oxidative stress. Thus its abundance in the mitochondria protects this organelle and the cell from ROS-induced damage.

For total glutathione quantification (GSH and oxidized GSH (GSSG)) we used the enzymatic recycling method, using GSH reductase (GR) (Sigma, G3664).

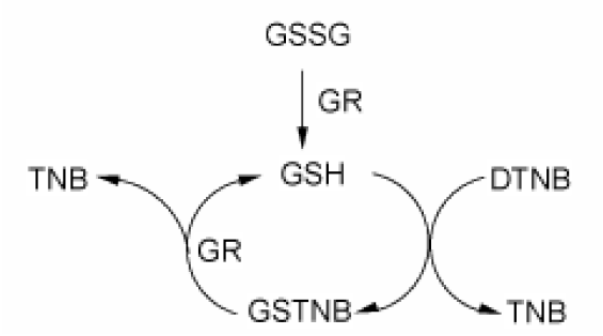

Figure M1. Recycling assay mechanism. GSSG, oxidized GSH; GR, GSH reducatase; DTNB, Ellman's reagent; TNB, 5-thionitrobenzoic acid; GSTNB, mixed disulfide GSH-TNB.

The sulfhydryl group of GSH reacts with DTNB (5,5'-dithio-bis-2-nitrobenzoic acid, Ellman's reagent. Sigma, D8130.) and produces a detectable yellow-colored TNB (5-thionitrobenzoic acid). The mixed disulfide, GSTNB (GSH linked to TNB) that is concomitantly produced, is reduced by GR to recycle the GSH and produce more TNB (Figure M1).

The rate of TNB production is directly proportional to this recycling reaction, which in turn is directly proportional to the concentration of GSH in the sample. Measurement of the absorbance of TNB at 412 nm provides an accurate estimation of total GSH in the sample.

ELLMAN ASSAY

Buffers:

- Ellman Buffer: 0,5M KH_2PO_4 (Fluka, 60220) at pH 8.0. Keep at 4ºC.
- Ellman Reagent: 10mM DTNB; 11,9mM $NaHCO_3$ (Sigma, S5761); 0,1M $Na_2HPO_4 \cdot 2H_2O$ (Fluka, 71643) at pH 7.4. Store it at -20ºC in 500µl aliquots.

Protocol:

- Prepare a 1mM GSH (Sigma, G6529) stock in PBS.
- Prepare a GSH standard curve in PBS: 0- 10- 20- 30- 40- 50 and 60 µM in a final volume of 4ml.
- Mix in a tube: 2ml of Ellman buffer, 1ml of standard and 30µl of Ellman Reagent. Perform the assay in duplicates.
- Mix thoroughly and wait 3 min before reading it.

- Read in a spectrophotometer (Beckman Coulter, DU800) at an absorbance of 412 nm.

The values obtained will be multiplied by 198 (coefficient of extinction of the spectrophotometer) and will represent the real concentration of the GSH standards prepared that we will use in the recycling assay as well. We will use these data to normalize the absorbance obtained in the recycling assay for the GSH standards.

RECYCLING ASSAY:

Buffers:

- 0.5M $NaPO_4$ at pH 7.4: prepare by mixing 95ml of $NaH_2PO_4 \cdot H_2O$ 1N, 405ml of $Na_2HPO_4 \cdot 2H_2O$ 1N and adjust with miliQ water up to 1L. Keep at RT.
- Recycling buffer: 1mM EDTA (Sigma, E5134); 0,1mM DTNB; 0,15mM NADPH (Sigma, N1630) and 50mM $NaPO_4$ at pH 7.4. Freshly prepared and protected from light.

Protocol:

- Prepare the recycling buffer, protect it from the light and warm it at 37ºC.
- Enzyme: prepare the GR at a concentration of 10U/ml in miliQ water. It will be stable a few weeks at 4 ºC.
- Mix in a tube: 2,5ml of recycling buffer at 37ºC, 100µl of sample/standard and 100µl of GR.
- Mix by inversion.
- Reed during 40sec in the spectrophotometer at an absorbance of 412 nm.
- GSH concentrations will be determined referring the samples to the standard curve normalized by the Ellman's assay and by protein concentration.

7. HEPATIC LIPID ANALYSIS:

7.1. Hepatic triglycerides, free fatty acid and total cholesterol content:

Liver TG, FFA and total cholesterol levels were measured at the Centre de Diagnòstic Mèdic of Hospital Clínic i Provençal de Barcelona from liver homogenates. Results were normalized by homogenate protein concentration.

7.2. Hepatic total ceramide and S1P quantification by HPLC:

Lipids were obtained and measured using HPLC to detect and quantify both SPH and S1P in one sample:

Protocol:

- First lipid extraction:
    - Use 2-5mg of protein from liver homogenates in a final volume of 250µl.
    - Add to 750µl of methanol:chloroform (1:2, v/v).
    - Vortex thoroughly and centrifuge at 5.000 rpm for 2 min.
    - Collect the chloroform phase extracts into a new tube. (Record the recovered volume to adjust the results by the extraction efficiency factor.)
    - Dry in a speed vac.
- Deacylation:
    - Resuspend samples in 250µl of 1M KOH-methanol. Use heat if necessary.
    - Incubate samples1h at 100ºC.
    - Allow samples to cool down.
- Second lipid extraction:
    - Add 500µl of chloroform and 250µl of PBS.
    - Thorough vortex and centrifuge at 5.000 rpm for 2 min.
    - Collect the chloroform phase containing the free long-chain bases into a new tube. (Record the recovered volume to adjust the results by the extraction efficiency factor.)
    - Dry in a speed vac.
- Derivatization:
    - Dissolve samples in 50µl of methanol.

  - Add 100µl of naphthalene-2,3-dicarboxaldehyde (NDA, Invitrogen, N1138) reagent, which is prepared fresh daily by mixing 50µl of 50mM boric acid in water (pH adjusted to 9 with KOH), 25µl of 5mM sodium cyanide in water and 25µl NDA 5mM in methanol.
  - Incubate 10 min at 50ºC in the dark.
  - Add 300µl of methanol.
- Centrifuge the samples and transfer them into HPLC tubes.
- HPLC detection:
  - Use a reverse phase C18 column (Teknokroma, TR-016343) using a Gilson fluorimetric detector (GILSON 322) with an excitation wavelength of 252 nm and an emission wavelength of 483 nm.
  - Mobile phase composition for the gradient system:
    - Pump A: 5mM potassium phosphate buffer (pH=6.5):methanol (85:15, v/v).
    - Pump B: acetonitrile:methanol (75:25, v/v).
  - Flow rate: 1ml/min.
  - Gradient program: 0-1 min 52.94 A, 47.06 B; 1-6 min 52.94-5.88 A, 47.06-94.11 B; 6-21 min 5.88 A, 94.11 B; 21-25 min 5.88-52.94 A, 94.11-47.06 B, 25-30 min 52.94 A, 47.06 B.
  - Reading time: 30 min per sample. S1P peak will appear around the 7th min for the reading and SPH(ceramide) at the 14th min approximately.
- Quantification of the ceramide and sphingosine-1-phosphate peaks is calculated according to a calibration curve (from 0,01mM to 0,1mM) derived from commercial, purified sphingosines (Sigma, S6879).

7.3. Hepatic total sphingomyelin:

SM is the substrate of ASMase. We analyzed hepatic SM levels in liver homogenates with a commercial colorimetric kit (Cayman, #10009928).

Protocol:

- Use 1-2mg of protein from liver homogenate and adjust to a final volume of 250µl with homo buffer (see section 10.1).
- Add 250µl of methanol and vortex.

- Add 500µl of chloroform.
- Vortex for 1 min and wait for 1 min three times.
- Spin down for 5 min at 5000 rpms at RT.
- Collect 400µl of chloroform (bottom layer).
- Dry for 1h at 45ºC in a speed vac.
- Resuspend in 100µl of detergent solution from the kit. (use 200µl in KO samples since they have much higher SM levels. Correct later the values obtained x2)
- Vortex for 10 min.
- Heat 10 min at 50ºC.
- Vortex until dissolved.
- Spin down.
- Load 10µl of sample per well using duplicates.
- Follow Cayman kit instruction for the assay protocol.
- Read at 585 nm in a plate reader (Bio Rad, xMark microplate spectrophotometer).

Note: Remember that the range of the kit is 5-50mg/dl. ASMase$^{-/-}$ samples tend to have high concentrations of SM. Take that in account to not exceed the kit detection range.

7.4. Hepatic lipidomic analysis of ceramide fatty acid chains:

Lipodomic analysis was carried out in Dr. Jesús Balsinde's Laboratory at the Institute of Molecular Biology and Genetics CSIC, Medical School of Universidad de Valladolid, CIBERDEM, Valladolid, Spain.

Protocol:

32nmol of internal standard [Cer(d18:1/17:0)] was added to every sample. Total lipids were extracted by chloroform:methanol as described before. Samples were evaporated until dryness, redissolved in chloroform/methanol (2:1) and spotted in HPTLC, separating ceramides from other lipids with chloroform/formic acid (85:15 v/v) as mobile phase. Silica portions containing ceramides were scraped from the plates and lipidic fractions were reextracted by chloroform:methanol. Samples were evaporated and resuspended in 200µl chloroform/methanol (1:2 v/v) 5mM ammonium acetate. Extracts were stored under N_2 at -80ºC until analysis.

Analyses were carried out in a Bruker esquire6000 ion-trap mass spectrometer, by direct infusion of the sample (400µl·h-1), 2 min acquisition.

Ceramide species were characterized by tandem MS in MRM and positive mode, detecting 266/284 for sphingosine (d18:0), 264/282 for sphinganine (d18:1) and 282/300 for phytosphingosine (t18:0).

8. HEPATIC ASMase ACTIVITY:

Hepatic ASMase activity was determined in liver homogenate samples using a fluorescence-based method. Fluorescent-labeled SM, (7-nitro-2-1,3-benzoxadiazol-4-yl) or NBD-SM, is cleaved hydrolytically by ASMase giving the fluorescent product NBD-ceramide. This product can be separated from the remaining substrate on thin layer chromatography (TLC) plates and can be quantified by detecting fluorescence intensity.

Buffers:

- Homogenization buffer: 1mM Hepes pH 7.4; 0,2% Triton X-100.
- ASMase buffer: 250mM NaAc ($CH_3COONa \cdot 3H_2O$. Sigma, S8625) pH 5.0; 0,1% Triton X-100.

Protocol:

- Use 75µg of protein per reaction.
- Adjust to a final volume of 250µl with the reaction buffer containing ASMase buffer and 10µM NBD-C6-Sphingomyelin (Molecular Probes, N3524).
- Reaction: incubate 1h at 37ºC in a thermomixer (Eppendorf, Thermomixer Confort) at 350 rpm.
- Stop the reaction by adding 750µl of a 2:1 mix of chloroform:methanol.
- Vortex 3 times for 1 min the samples. At this point, lipids will pass to the organic phase.
- Spin for 5 min at 5.000 rpm at RT to separate aqueous from organic phase.
- Extract 400µl of the organic phase avoiding methanol contamination.
- Dry the samples in a speed vac. (Approx. 1h 30 min).
- Resuspend the dried lipids in 50µl of a 1:1 mix of chloroform:methanol.
- Vortex well.

- Load 40µl of the sample on each TLC lane (Whatman, 4865-821) adding 20µl at a time. Wash the lipid pipettes with methanol between samples.
- Allow the loaded TLC to dry.
- Introduce the TLC in a gas chamber with 100ml of a 70:30:5 mix of chloroform:methanol:NH_4OH.
- Allow the samples to run through the TLC up to 3/4 of the plate.
- Dry the TLC.
- Read the results by exciting with UV light the TLC and capturing an image of the fluorescence (Bio-rad, Gel Doc XR). SM will be the lower band with a strong signal since we add it in excess in the reaction and the higher band will be the ceramide cleaved during the reaction.
- Results can be quantified with Image J by measuring density of pixels.

9. METHIONINE METABOLISM:

9.1. Serum homocystein quantification:

Serum homocysteine concentrations were measured per protocol in the clinical laboratory of the Hospital Clínic of Barcelona.

9.2. Hepatic SAM and SAH quantification:

Hepatic S-adenosylmethionine and S-adenosylhomocysteine were determined by HPLC as previously described (Song, Zhou et al. 2007).

Protocol:

- Deproteinize samples with 0,5M perchloric acid (v/v 1:1).
- Vortex and spin down for 10 min at 13.000 g at 4ºC.
- Collect the supernatant for HPLC quantification. (At this point samples can be frozen and kept at -80ºC until HPLC processing.)

HPLC detection:

- Use a reverse phase 5µm Hypersil C18 column (WATERS) with an absorbance of 254 nm using the WATERS 717 plus Autosapler system.

- The mobile phase composition for the isocratic flow:
    - Pump A: 40mM Amonium phosphate; 8mM 1-Heptanesulfonic acid sodium salt (Sigma, 221554); 6% Acetonitrile (Sigma, 270717) at pH 5.0 adjusted with 70% acid.
    - Pump B: miliQ water.
- Flow rate: 1ml/min.
- Reading time: 30 min per sample.
- Quantification of SAM and SAH peaks are calculated according to a calibration curve.

10. PROTEIN EXPRESSION ANALYSIS:

10.1. Homogenization and lysis:

Buffers:

- For liver homogenates: Homo buffer (70mM saccharose, 220mM mannitol, 2mM Tris-HCl pH 7.4, 0,1mM EDTA, 0,1% free-FA BSA) supplemented with protease and phosphatase inhibitors (Roche, #11 836 170 001 and 04906 837 001). This buffer was used to homogenize samples for further lipid analysis.
- For lysates: RIPA buffer (150mM NaCl, 1.0% IGEPAL, 0.5% sodium deoxycholate, 0.1% SDS, 50mM Tris, pH 8.0) (Sigma, R0278) supplemented with protease and phosphatase inhibitors. This buffer was used to obtain protein extracts for western blot analysis.

Protocol:

- Homogenize 100mg of liver with a pestle homogenizer in 1ml of homo buffer.
- Dilute 4 times liver homogenates with RIPA lysis buffer. (Note: For adipose protein extraction, 100mg of tissue were homogenized directly in 0,3ml of RIPA lysis buffer with protease and phosphatase inhibitors.)
- Incubate the samples 15 min at 4ºC vortexing them from time to time.
- Spin down 5 min at 10.000 rpms at 4ºC.
- Collect the supernatant avoiding contamination from pellet and upper lipidic phase.

10.2. Protein quantification:

Homogenates and lysates were quantified for protein concentration using Bradford protein assay. Bradford assay is a protein determination method that involves the binding of Coomassie Brilliant Blue G-250 dye to proteins that is detectable at an absorbance of 595 nm. There are certain chemical-protein or chemical-dye interactions that may interfere with the assay. In our case, it is important to always dilute the RIPA buffer at least 4 times to dilute the IGEPAL below 0.25%.

Protocol:

- Prepare bovine serum albumin (BSA) standard points to build a standard curve (E.g. 0- 0,1- 0,2- 0,3- 0,4 and 0,5 mg/ml) in PBS.
- Dilute samples in PBS to fit in the standard curve (Liver homogenates 1/75 dilution, liver lysates 1/20).
- Perform the assay in a 96 well plate in triplicates.
- Add 4µl of the diluted sample per well.
- Using a multichannel pipette add 200µl of Quick Start Bradford Protein Assay (Bio-rad, 500-0201).
- Incubate at RT for at least 5 min. Samples should not be incubated longer than 1h at RT.
- Set the spectrophotometer plate reader to 595 nm. Measure the absorbance of the standards, blanks, and unknown samples.
- Samples will be referred to the BSA standard curve and they will be assigned a protein concentration.

10.3. Sample preparation:

To be able to separate the proteins in a polyacrilamide gel, samples are mixed with a loading buffer to ensure protein stability and weight when loading them into the wells.

Protocol:

- Bring all samples to the same protein concentration so we can load 20-50µg of protein per well in a volume of 15-40µl. Adjust the volumes with RIPA buffer.
- Add 1/3 of the volume of loading buffer XT Sample Buffer 4x (Bio-Rad, 161-0791) with a 0,05% of β-mercaptoethanol.
- Pipette up and down.

- Boil the samples 5 min at 100ºC.
- Allow samples to cool down.
- Vortex and spin down.

As a protein standard marker for protein electrophoresis we used Novex Sharp Pre-stained Protein Standard (Invitrogen, LC5800).

10.4. Western blotting:

In this thesis we used SDS-PAGE, sodium dodecyl sulfate polyacrylamide gel electrophoresis to separate proteins from liver, hepatocytes and EWAT extracts. This technique allows separation of proteins according to their electrophoretic mobility, a function of the length of the polypeptide chain and its charge. SDS is an anionic detergent that linearizes proteins and confers them a negative charge. The binding of SDS to the polypeptide chain imparts an even distribution of charge per unit mass, thereby resulting in a fractionation by approximate size during electrophoresis. After the SDS-PAGE, separated proteins in the gel are electrotransfered into a nitrocellulose membrane and specifically detected on the surface of the membrane with antibodies.

Buffers:

- Running buffer: depending on the size of the protein to be detected we used
    - 20x XT MES Running Buffer (Bio-rad, 161-0789), to resolve low molecular weight proteins. Dilute in distilled water.
    - 20x XT MOPS Running Buffer (Bio-rad, 161-0788), to resolve high molecular weight proteins. Dilute in distilled water.
- Electrotransfer buffer: prepare the buffer and cool it down to 4ºC.
    - 10x T/G buffer: Tris/Glycine buffer (Bio-rad, 161-0771). For 1L: 100ml of T/G buffer, 200ml of methanol and 700ml of distilled water.
- TBST:
    - Tris Buffered Saline, with Tween 20 (TBST), pH 8.0 (Sigma, T9039). Contents of one pouch, when dissolved in one liter of distilled will yield 0.05M Tris buffered saline (NaCl - 0.138M; KCl - 0.0027M); TWEEN® 20 - 0.05%, pH 8.0, at 25 °C. We complement it with 5ml of 10% TWEEN 20 solution (Bio-rad, 161-0781) per liter to reach the 0.1%

tween. This buffer is used to wash, block and incubate the membranes with the antibodies.

Protocol:

- Electrophoresis:
    - Load 20-50µg of protein into the 4-12% SDS–polyacrylamide gel (Bio-rad, 345-0124).
    - Electrophoresis system: Criterion Cell (Bio-rad, 165-6001) vertical midi format electrophoresis cell and PowerPac Basic Power Supply (Bio-Rad, 165-6019).
    - Start the electrophoresis at 80v for 30 min and then increase the voltage up to 110v until the protein of interest is well resolved (check protein standard for an approximate molecular weight).
- Transfer:
    - Pre-wet materials in transfer buffer.
    - Stack in the following order forming a sandwich:
        - Case (black)
        - Sponge
        - Whatman paper (Whatman, 10426693)
        - Gel
        - Hybond ECL nitrocellulose membrane (Amersham, RPN303D)
        - Whatman paper
        - Sponge
        - Case (red).
    - Make sure that no bubbles remain in the sandwich, as they will interfere with the transfer.
    - Place the sandwich in the transfer apparatus with black side of the case facing black side of the apparatus.
    - Electrotransfer system: Criterion blotter (Bio-Rad, 170-4070) and PowerPac Basic Power Supply.
    - Electrotransfer 45 min at 50v on ice.

- Blocking: to avoid unspecific binding of antibodies, empty membrane areas were blocked for 1h with 5% BSA (Sigma, A4503) TBST at RT in a small container on an orbital shaker.

10.5. Immunodetection- Primary and secondary antibodies:

Membranes were incubated with primary antibodies in a 5% BSA-TBST solution overnight at 4ºC and shaking. For specific incubation conditions see table M4.

Antibody	Host	Dilution	Buffer	Brand	Catalog #
anti-Akt1/2/3	Rb	1:1000	5% BSA TBST	SCBT	sc-8312
anti-ATG7	Rb	1:500	TBST	Abgent	AP1813b
anti-αTubulin-HRP	Mo	1:5000	TBST	Abcam	ab40742
anti-βActin-HRP	Mo	1:25000	TBST	Sigma	A3854
anti-CHOP	Mo	1:1000	5% BSA TBST	SCBT	sc-7351
anti-CYP2E1	Rb	1:5000	TBST	Abcam	ab19140
anti-GRP78	Rb	1:1.000	TBST	Stressgen	SPA-826
anti-IR $^{[pTyr1162/1163]}$	Rb	1:1000	5% BSA TBST	Calbiochem	407707
anti-IRβ	Rb	1:1000	TBST	SCBT	sc-711
anti-IRE1α	Rb	1:1000	5% BSA TBST	Cell Signaling	3294
anti-LAMP2	Rat	1:500	5% BSA TBST	Abcam	ab13524
anti-LC3B	Rb	1:1000	5% BSA TBST	Cell Signaling	2775
anti-pAkt1/2/3$^{[Ser473]}$	Rb	1:1000	5% BSA TBST	SCBT	sc-7985-R
anti-p62	Rb	1:100	5% BSA TBST	Abgent	AP2183b
anti-PDI	Rb	1:1000	5% BSA TBST	Cell Signaling	2446
anti-pIRE1α$^{[pSer724]}$-HRP	Rb	1:1.000	5% BSA TBST	Novus Biologicals	NB100-2323H
anti-rabbit-HRP	G	1:20000	TBST	Sigma	A0545
anti-rat-HRP	G	1:15000	TBST	Invitrogen	819520
anti-mouse-HRP	Rb	1:20000	TBST	Sigma	A9044

Table M4. Primary and secondary antibodies used.
HRP, horseradish persoxidase conjugated. p, phospho. Rb, rabbit. Mo, mouse. G, goat.

After the overnight incubation:

- Wash at least 3 times for 10 min with TBST to wash out unspecific binding.
- Incubate membranes with the corresponding secondary antibodies at the indicated dilutions in TBST (Table M4).
- Wash at least 3 times for 10 min with TBST.

10.6. Development, image capturing and analysis:

Some primary and all secondary antibodies are conjugated with horseradish persoxidase. To develop the antibody protein detection we used a peroxidase substrate for enhanced chemiluminescence (ECL Western Blotting Substrate. Thermo Scientific, 32106).

Protocol:

- Warm to RT luminol and peroxide solutions.
- Mix in a tube, equal volumes of both solutions.
- Apply on top of the membrane and make sure it is evenly spread.
- Incubate 1 min at RT.
- Remove excess liquid.

To obtain the chemiluminescence signal, images were collected with image capturing instrument, LAS4000 (GE Healthcare) and analyzed with ImageJ software to quantify density of pixels.

11. GENE EXPRESSION ANALYSIS:

11.1. mRNA isolation and quantification:

To isolate mRNA we used a TRIzol-cholorform extraction (Invitrogen, 15596-018). TRIzol Reagent is a monophasic solution of phenol, guanidine isothiocyanate, and other proprietary components, which facilitate the isolation of a variety of RNA species of large or small molecular size. It maintains the integrity of the RNA due to highly effective inhibition of RNase activity while disrupting cells and dissolving cell components during sample homogenization. After homogenizing the sample with TRIzol, chloroform is added, and the homogenate is allowed to separate into a clear upper aqueous layer (containing RNA), an interphase, and a red lower organic layer (containing the DNA and proteins). RNA is precipitated from the aqueous layer with isopropanol.

RNA is very sensitive to nucleases. All material must be autoclaved and all the solutions and organic solvents need to be molecular biology graded, free of DNases and RNase.

Protocol:

- Homogenization:
    - From hepatocytes: add 0,5ml of TRIzol per every 500.000 hepatocytes. Lyse the cells by shaking the plates in an orbital shaker at 4ºC.
    - From liver: use 1ml of TRIzol per every 25-50mg of tissue and homogenate with a manual pestle.
- Phase separation:
    - Incubate the homogenized sample for 5 min at RT to allow complete dissociation of the nucleoprotein complex.
    - Add 0.2ml of chloroform per 1 ml of TRIzol used for homogenization. Cap the tube securely.
    - Shake tube vigorously by hand for 15 sec.
    - Incubate for 2–3 min at RT.
    - Centrifuge the sample at 12,000 × g for 15 min at 4°C. Note: The mixture separates into a lower red phenol-chloroform phase, an interphase, and a colorless upper aqueous phase. RNA remains exclusively in the aqueous phase. The upper aqueous phase is ~50% of the total volume.
    - Remove the aqueous phase of the sample by angling the tube at 45° and pipetting the solution out. Avoid drawing any of the interphase or organic layer into the pipette when removing the aqueous phase.
    - Place the aqueous phase into a new tube and proceed to the RNA Isolation Procedure.
- RNA precipitation:
    - Add 0.5ml of 100% isopropanol to the aqueous phase, per each 1ml of TRIzol used for homogenization and mix by inversion.
    - Incubate at RT for 10 min.
    - Centrifuge at 12,000 × g for 10 min at 4°C.
- RNA wash:
    - Remove supernatant from the tube, leaving only the RNA pellet.
    - Wash the pellet, with 1ml of 75% ethanol (in RNase free water) at -20ºC per each 1ml of TRIzol Reagent used in the initial homogenization. Note:

The RNA can be stored in 75% ethanol at least 1 year at –20°C, or at least 1 week at 4°C.

- Vortex the sample briefly, then centrifuge the tube at 7500 × g for 5 min at 4°C. Discard the wash.
- Air-dry the RNA pellet for 5–10 min. Note: Do not allow the RNA to dry completely, because the pellet can lose solubility. Partially dissolved RNA samples have an A260/280 ratio <1.6.

- RNA resuspension:
  - Resuspend the RNA pellet in RNase-free water by passing the solution up and down several times through a pipette tip.
  - Incubate at least 30 min at 4ºC to allow complete resuspension.
- RNA quantification:
  - Load 1µl of resuspended mRNA onto the NanoDrop spectrophotometer (Thermo Scientific, NanoDrop 1000).
  - Measure the sample absorbance at 260 nm and 280 nm to calculate nucleic acid concentration (260 nm) and the purity of the sample (260/280 ratio between 1,7-2,0).

11.2. cDNA synthesis:

The cDNA synthesis transforms the isolated mRNA into cDNA, which is a more stable product. This conversion is carried out by a reverse transcriptase (RT) and random primers that bind to non-specific pints along the RNA template. The resulting cDNA can be used as a template for a standard PCR.

Protocol:

- Prepare the cDNA synthesis reaction mix (Applied Biosystems, 4368814):

	x1
10x RT Buffer	2µl
25x dNTP mix (100mM)	0,8µl
10x RT Random Primers	2µl
Reverse Transcriptase, 50U/µL	1µl
RNA 0,25µg/µl (1µg)	4µl
RNase free H2Od	10,2µl
Vf	20µl

Table M5. cDNA synthesis reaction mix.

- Use 1µg of RNA template per reaction.
- Thermocycler (ECOGEN, G-Storm) protocol: 10 min at 25ºC; 120 min at 37ºC; 5 min at 85ºC and forever at 10ºC.

11.3. Real time PCR:

Real-time polymerase chain reaction (RT-PCR) technique is a refinement of the original PCR, which is used to amplify nucleic acids in a cyclic process to generate a large number of identical copies. In RT-PCR, the amount of product formed is monitored during the course of the reaction by recording the fluorescence of dyes or probes introduced into the reaction, which is proportional to the amount of product formed, and the number of amplification cycles required to obtain a particular amount of DNA molecules is registered. Assuming a certain amplification efficiency, which typically is close to a doubling of the number of molecules per amplification cycle, it is possible to calculate the number of DNA molecules of the amplified sequence that were initially present in the sample (Kubista, Andrade et al. 2006).

In this thesis, we used SYBR-green based RT-PCR as a method for analyzing hepatic gene expression changes. SYBR Green (Applied Biosystems, 4368702) is a fluorescent dye that binds to double-stranded DNA (i.e., amplicons) and fluoresces when is excited by a light source.

One important step in relative quantization is the selection of an endogenous control. Normalization to an endogenous control (or housekeeping gene) allows correcting results that can be skewed by differing amounts of input nucleic acid template. Any gene expressed at the same level in all study samples can potentially be used as an endogenous control. In this thesis we used β-actin and 18S as endogenous controls.

Results were analyzed using the relative quantification method ΔΔCt. Relative quantification relates the PCR signal of the target transcript in a treatment group to an untreated control. When using the comparative ΔΔCT method, is crucial that the target gene and endogenous control have similar or relatively equivalent PCR efficiencies.

The Cycle Threshold (Ct) is defined as the number of cycles required for the fluorescent signal to cross the threshold (e.g. exceeds background level). Ct levels are inversely proportional to the amount of target nucleic acid in the sample, so the lower the Ct level the greater the amount of target nucleic acid in the sample. The ΔΔCT Method uses arithmetic formulas to achieve the result for relative quantization. The amount of target, normalized to an endogenous control and relative to a calibrator (or control experimental grup), is given by:

$$\text{Gene expression} = 2^{-(\Delta\Delta Ct)}$$

Where ΔΔCt stands for: $\Delta\Delta Ct = \Delta Ct_{experiment} - \Delta Ct_{control}$

and ΔCt stands for: $\Delta Ct = Ct_{gene\ "X"} - Ct_{\beta Actin}$

Protocol:

- Dilute 1/20 in RNase free water the cDNA synthesis reaction.
- Prepare as many RT-PCR mixes as number of genes checked (Table M6).

	x1
RT Fw Primer 10µM	0,5µl
RT Rev Primer 10µM	0,5µl
RNase free H_2Od	7,5µl
SYBR green AB	12,5µl
cDNA	4µl
Vf	25µl

Table M6. RT-PCR mix.

- Samples followed the indicated PCR protocol in a MyiQ single color real-time PCR detection system (Bio-Rad) (Table M7).

	Time	**Temperature**	**Repetitions**
Step1	10 min	95ºC	-
Step2	15 sec	95ºC	x40 cycles
	30 sec	58ºC	
	30 sec	72ºC	
Step3	1 min	95ºC	-
Step4	10 sec	10ºC	x81

Table M7. RT-PCR protocol.

11.4. RT-PCR primers:

Gene	Accession #	Forward primer (5'-3')	Reverse primer (5'-3')
18S	X00686	AGTCCCTGCCCTTTGTACACA	CGATCCGAGGGCCTCACTA
Abca1	NM_013454	AAAACCGCAGACATCCTTCAG	CATACCGAAACTCGTTCACCC
ACDase	NM_019734	TGTTGGATATGTGGGCATGT	TTCCTTCCGAACATCCATTC
ASMase-h	NM_000543	CTGACTCTCGGGTTCTCTGG	AGGTTGATGGCGGTGAATAG
ASMase-m	NM_011421	TGGGACTCCTTTGGATGGG	CGGCGCTATGGCACTGAAT
Atf4	NM_009716	CCTTCGACCAGTCGGGTTTG	CTGTCCCGGAAAAGGCATCC
Atg7	NM_028835	GCCAGGTACTCCTGAGCTGT	ACTTGACCGGTCTTACCCTG
βactin	NM_007393	GACGGCCAGGTCATCACTAT	CGGATGTCAACGTCACACTT
Bhmt	NM_016668	ATTCCCCTTTGGATTGGAAC	TGTGCATGTCCAAACCACTT
Caveolin1	NM_007616	TGTACCGTGCATCAAGAGC	AAAGAGTGGATCGCAGAAGG
Cbs	NM_178224	CTTCAGGGACATCCCAGTGT	AGCTGCCAGGTACATCTGCT
Cd36	NM_007643	ATGGGCTGTGATCGGAACTG	GTCTTCCCAATAAGCATGTCTCC
CerS2	NM_029789	CCTCTGCTTCTCCTGGTTTG	TGAAGAGGTTGTTGCAGGTG
CerS4	NM_026058	AAGAATGAGGGCCAACTCTG	ACCAATGCACCCTCTGTTTC
CerS5	NM_028015	GATGGCCAATTATGCCAGAC	CCAGCTTTCAAAGAGGGTTG
Chop-m	NM_007837	CCACCACACCTGAAAGCAGAA	AGGTGAAAGGCAGGGACTCA
Chop-h	NM_001195053	GCGCATGAATTATAAATAAC	ACCATTCGGTCAATCCAGAGC
Dgat2	NM_026384	TGATCTTTGAGGAGGGTTCC	AGGGGGCGAAACCAATATAC
Edem	NM_138677	AAGCCCTCTGGA ACTTGCG	AACCCA ATGGCCTGTCTGG
Fabp1	NM_017399	ATGAACTTCTCCGGCAAGTACC	CTGACACCCCCTTGATGTCC
Fas	NM_007988	TGATTATGGCCCTCAGTTCC	CAGCATTGTGTCCATGAAGG
Fatp2	NM_011978	TCCTCCAAGATGTGCGGTACT	TAGGTGAGCGTCTCGTCTCG
Grp78-m	NM_022310	ACTTGGGGACCACCTATTCCT	ATCGCCAATCAGACGCTCC
Grp78-h	NM_005347	AATGACCAGAATCGCCTGAC	CGCTCCTTGAGGTTTTTGTC
Hmgcr	NM_008255	GGAACCGTGGGTGGTGGGAC	GCCTTCTTGGTGCATGTTCCC
Lc3b	NM_026160	AATCACTGGGATCTTGGTGG	AGTCAGATCGTCTGGCTCG
Ldlr	NM_010700	CTCCTGCATTCACGGTAGCC	CCCACTGTGACACTTGAACTTG
Mat1A	NM_133653	GACACCATCAAGCACATTGG	ATGCATTCCTCGGTCTCATC
Mln64	NM_021547	TGCCCATCATTTCATTCATCCTT	AAAAGCGGTTTCTCACTCTCC
Ms	NM_001081128	CATCCAAGAGTGTGGTGGTG	ATAAACGTGGGCTTCACTGG
p62	NM_011018	TCTGGGGTAGTGGGTGTCAG	AGAATGTGGGGGAGAGTGTG
Pdi	NM_011032	CAAGATCAAGCCCCACCTGAT	AGTTCGCCCCAACCAGTACTT
Ppara	NM_011144	AGAGCCCCATCTGTCCTCTC	ACTGGTAGTCTGCAAAACCAAA
Sms1	NM_001168525	ATGATCTCGGTCGTCCATGAA	AAAACGTGTCCGGTAGTGGAG
Sms2	NM_028943	CCACCAACACTTACACAAGCC	GCACCCTTTCGTAACCCGTT
Srebp1c	NM_011480	GGAGCCATGGATTGCACATT	GGCCCGGGAAGTCACTGT
Srebp2-m	NM_033218	CACCTGTGGAGCAGTCTCAA	TGGTAGGTCTCACCCAGGAG
Srebp2-h	NM_004599.2	CCCTTCAGTGCAACGGTCATTCAC	TGCCATTGGCCGTTTGTGTC
Star-m	NM_011485	AGATGTGGGCAAGGTGTTTC	ATGCGGTCCACAAGTTCTTC
Star-h	NM_000349	CTTGGGCATCCTTAGCAAC	ATCTTTTCCGATCTTCTGC

Table M8. RT-PCR primer sequences. h, stands for human. m, stands for mouse. When not indicated, primer sets are for mouse gene detection.

All primers were designed in PrimerBank, a public resource for primers designed for gene expression quantification (Table M8). The primer design algorithm of PrimerBank tests primers for specificity and efficiency and all experimental validation data is available online: http://pga.mgh.harvard.edu/primerbank/. All primers were ordered from Invitrogen.

12. CELL CULTURE:

12.1. Primary mouse hepatocytes:

12.1.1. Isolation:

Primary mouse hepatocytes from male mice (6–10 weeks old) were isolated with a liver collagenase perfusion followed by a differential centrifugation.

Buffers: prepare HANKS1x and KREBS buffers fresh.

- HANKS 10x: 1,4M NaCl; 53,6mM KCl; 8,1mM $MgSO_4 \cdot 7H_2O$; 6,7mM $Na_2HPO_4 \cdot 2H_2O$; 8,8mM KH_2HPO_4.
    - HANKS 1x: 10% HANKS 10x; 12,6mM Hepes; 25mM $NaHCO_3$.
        - HANKS I (Cleaning Buffer): HANKS1x, 0,5% BSA; 0,9mM EGTA.
        - HANKS II (Digestion Buffer): HANKS 1x; 160U/ml Collagenase (Sigma, C5138); 4mM $CaCl_2 \cdot 2H_2O$.
- KREBS: 0,95% Krebs-Henseleit (Sigma, K3753); 16,8mM Hepes; 24mM $NaHCO_3$; 2,7mM $CaCl_2 \cdot 2H_2O$, pH 7.4.

Protocol:

- Gas HANKS1x buffer and KREBS buffer (without the $CaCl_2$) with 95% CO_2 and 5% O_2 for 20 min to stabilize the pH.
- Add the rest of the components to complete HANKS I-II and KREBS buffers. EGTA is crucial in the cleaning buffer to avoid coagulation and calcium is necessary for the digestion buffer as a cofactor of the collagenase.
- Check the pH of Krebs buffer and adjust to 7.4 if needed with NaOH.
- Filter buffers through a 0.22µm filter.

- Allow buffers to reach 37ºC in a water bath.
- Clean the peristaltic pump tubes with 70% ethanol, distilled water and then fill the circuit with warm HANKS I buffer at a speed of 8-10ml/min.
- Anesthetize the mouse with a dose of 0,1g/Kg Sodium pentobarbital.
- Prepare two sutures (Lab. Aragó S.A., Seda trenada 2/0 #060), about 12cm long.
- Open the mouse with a laparotomy.
- Put two sutures under cava and portal vein.
- Insert the catheter (BD, 381212) into the portal vein and immobilize it with the suture around it. If the catheter does not fill with blood, fill it with warm HANKS I buffer avoiding bubble formation.
- Stop the peristaltic pump (Cole-Parmer, MasterFlex L/S #7553-79) and connect it to the catheter. Avoid bubble formation.
- Start the pump and cut the inferior cava vein so the blood can exit the system and clean the liver with HANKS I buffer. This will prepare the liver for digestion.
- Open the diaphragm and cut the superior cava vein. Then tie the suture that was previously placed around the inferior cava vein so liver circuits are cleaned in the other direction.
- Once the liver is clean, change to HANKS II buffer to start the digestion. It will take 2-3 min to digest. The liver will turn slightly white/brown while it starts swelling. It is crucial to reach an optimal digestion point. Too much or insufficient digestion will result in poor hepatocyte viability.
- Pour some KREBS buffer in a Petri dish and prepare a small Erlenmeyer with a funnel and a sterile maze to filter the non-digested parts of the liver.
- Take the liver out and with a pair of tweezers disaggregate the tissue in the Petri dish with KREBS buffer to liberate the hepatocytes from the digested liver.
- Filter hepatocytes through the maze and adjust to a final volume of 50ml with KREBS buffer.
- Centrifuge at 60 g for 4 min at 4ºC.

- Discard the supernatant containing KC, HSC and SEC and resuspend the pellet containing the hepatocytes with warm media (twice the volume of the pellet).
- Hepatocyte viability: After the isolation, check viability rate of hepatocytes in order to know the starting point of the cells before the experiments. Isolations with a viability rate below a 50% were discarded. To check viability we used the Trypan Blue staining which allows us to distinguish between living and dead cells (See method14.4).
    - Dissolve 50µl of the resuspended cells in 950µl of 0,2% Trypan Blue (Sigma, T8154).
    - Wait a minute and start to count for positive and negative cells using a Neubauer Chamber.
    - Multiply the number of cells by the Trypan Blue dilution factor (1/20) and by the volume of the Neubauer Chamber (10^4 cells/ml). The sum of alive and dead cells will give us the total number of cells that we will use to calculate the % of viability: negative cells/total number of cells x100.

12.1.2. Culture:

Primary mouse hepatocytes attach better in collagen-coated plates. For that reason, all plates were coated with rat-tail collagen.

Rat-tail collagen isolation protocol:

- Peal the rat-tail with a scalpel and visualize the four collagen fibers.
- Dissect the fibers avoiding contamination from the surrounding tissues.
- Incubate the fibers 24h at RT in 70% ethanol to clean them.
- Dry the fibers and weigh them.
- Prepare 300ml of 0,1% acetic acid per each gram of collagen isolated. Cut the fibers in pieces and incubate them 48h at 4ºC in 0,1% acetic acid agitating. After this incubation, collagen will be dissolved in the acetic acid.
- Centrifuge at 3000 rpms for 20 min at 4ºC to pull down the non-dissolved collagen fibers.

- Collect the supernatant in an autoclaved glass bottle and take it to irradiate in order to sterilize it (5 min at 1000 rads).

Collagen-coat plates:

- In the cell culture hood, dilute 1/3 the stock collagen in sterile water.
- Add 500µl of this dilution to each 6 well plate.
- Incubate 30 min at RT.
- Aspirate the collagen.
- Let it air dry in the hood for 30 min.
- Keep the plates at 4ºC until used.
- Before using the plates, wash them with PBS to remove any remaining acetic acid.

Media:

Two different medias were used for the primary hepatocyte culture. The supplemented media with fetal bovine serum (FBS) for the first hours post isolation and the basic media for the rest of the culture.

- Supplemented media: DMEM:F12 (Gibco, 21331-020) with 10% FBS (Gibco, 10-270-106), 10.000U/ml Penicillin-Streptomycin (Gibco, 15140-122), 200mM L-Glutamine (Gibco, 25030-024), 7,5mM D-Glucose (Sigma, G6152), 150mM Hepes pH 7.4 (Sigma,), 1mM Methionine (Sigma, M5308).
- Basic media: is the same media without the FBS.

Seeding:

- Hepatocytes have a tendency to precipitate at the bottom of the tube very quickly due to its size. Make sure to gently homogenize hepatocytes before seeding them by pipetting up and down.
- Seed $0,5x10^6$ cells per well of a 6 well collagen-coated plate for protein extracts and $0,25x10^6$ cells per well of a 12 well collagen-coated plate for mRNA isolation.

Culture:

- During the first four hours post isolation culture cells with Supplemented media. After the first 2h, change the media to remove all non-attached dead cells. This will improve the viability of attached cells.
- 4 hours post isolation, change to the basic media.
- Keep cells in an incubator at 37ºC with a 5% CO_2.
- Primary mouse hepatocytes keep their phenotype for 36-48h isolation, so treatments should be done during this time to avoid artifacts.

12.1.3. Treatments:

12.1.3.1. Insulin stimulation:

To examine insulin signaling pathway in primary mouse hepatocytes, cells were stimulated with 100nM insulin for 3 minutes. After that, plates were flash frozen in liquid nitrogen and their protein extracts were used to analyze phosphorylation events of insulin signaling pathway via WB.

12.1.3.2. ER stress induction:

To see whether ASMase$^{-/-}$ primary mouse hepatocytes were able to sense ER stress, cells were challenged with the bacterial AB5 subtilase cytotoxin (SubAB) or its mutant inactive form SubA_{A272}B (1 µg/ml). Active SubAB rapidly induces ER stress upon proteolytic cleavage of GRP78 (Paton, Beddoe et al. 2006). Cells were collected with TRIzol or RIPA buffer for mRNA and protein analysis.

12.1.3.3. Autophagic flux:

Autophagy is a highly dynamic process, which makes challenging to interpret results in a steady situation. For that reason, the study of autophagic flux requires the use of autophagy inducers and blockers that will help to interpret results.

Chloroquine (CHQ): is a lysosomotropic agent that prevents endosomal acidification. It accumulates inside the acidic parts of the cell, including endosomes and lysosomes. This accumulation leads to inhibition of lysosomal

enzymes that require an acidic pH, and prevents fusion of endosomes and lysosomes. CHQ inhibits autophagy as it raises the lysosomal pH, which leads to inhibition of both fusion of autophagosome with lysosome and lysosomal protein degradation. The inhibition of autophagy at this level allows us to study the basal autophagic flux when comparing it to a control. Primary mouse hepatocytes were treated for 3h with 50µM CHQ (Santa Cruz, sc-205629) in basic media.

Rapamycin: is an inhibitor of mTOR, which is a major negative regulatory axis of autophagy. Direct inhibitors of mTOR subsequently induce autophagy. This treatment allows us to study the cell ability to activate autophagy upon mTOR inhibition. Primary mouse hepatocytes were treated for 3h with 2µM rapamycin (Santa Cruz, sc-3504A) in basic media.

To study the autophagic flux, cells were processed for protein analysis via WB where lipidation of LC3BI to LC3BII and p62 degradation was monitored.

12.1.3.4. Lysosomal membrane permeabilization:

Lysosomotropic detergents, which selectively target lysosomal membranes, are compounds that remain predominantly unprotonated and inert in the cytosol, but they become protonated, accumulate, and acquire detergent properties in the acidic interior of lysosomes. Low concentrations of lysomotropic detergents cause translocation of lysosomal contents leading to apoptosis. Lysosomal membrane permeabilization and subsequent release of cathepsins is an early event during apoptosis induced by a number of stimuli, such as oxidative stress, death receptor ligation, and DNA-damaging drugs.

MSDH (O-methyl-serine dodecylamide hydrochloride) (Appelqvist, Nilsson et al. 2011) is lysomotropic detergent kindly gifted by Dr. Hanna Appelqvist (Linköping University, Linköping, Sweden). MSDH was used to induces cell death in WT and ASMase$^{-/-}$ primary mouse hepatocytes as well as hepatocytes derived from HCD exposed mice. Cells were treated for 24h

with 15-20-25µM MSDH. Cell viability was determined by MTT assay (See method 13.2).

12.1.3.5. TNF-α stimulation:

Primary mouse hepatocytes from control and alcoholic mice were incubated overnight with recombinant 280ng/ml of human TNF-α (Peprotech EC). Cell death was determined by Trypan Blue exclusion (0.2%) (see method 13.2).

12.2. Hep G2 cell line:

The Hep G2 cell line (ATCC # HB-8065) is a human hepatoma cell line originated from a hepatocellular carcinoma from a Caucasian 15 year old male. Hep G2 is an epithelial-like adherent cell line that often grows in clusters of multilayer of cells. It has been commonly used as a hepatocyte cell line for its good transfection properties. The cells express HMG-CoA reductase and hepatic triglyceride lipase activities but they do not express ADH.

12.2.1. Culture:

The base medium for this cell line is DMEM (Invitrogen, 41966-052) with 10% of fetal bovine serum and 10.000U/ml Penicillin-Streptomycin. The optimum growing are a temperature of 37.0°C in an atmosphere of 95% air and 5% CO_2.

Passaging protocol:

- Remove and discard culture medium.
- Wash with warm PBS to remove all traces of serum that could inhibit trypsin action.
- Add 2ml of Trypsin-EDTA (Invitrogen, 25200-056) to the flask and observe cells under an inverted microscope until cell layer is dispersed (usually within 5 to 15 min). Note: To avoid clumping do not agitate cells by hitting or shaking the flask while waiting for the cells to detach. Cells that are difficult to detach may be placed at 37°C to facilitate dispersal.
- Add 8ml of complete growth medium and collect cells by gently pipetting.

- Add appropriate aliquots of the cell suspension to new culture vessels. Suggested subcultivation ratio: 1:4 to 1:6 is recommended and a medium renewal should be done twice per week.

Preservation:

Aliquots of low passages should be frozen down in order to have always a source of cells in early passages.

- Prepare 5% DMSO growing media.
- Freeze down 5-10 million cells per cryotube and progressively freeze down by first placing the tube on dry ice for 1 hour, then to -80ºC for a week and then to liquid nitrogen for definitive storage.
- Thaw the cells quickly and seed them in a small flask.
- Switch the media after 4h when cells are attached in order to remove the toxic DMSO of the freezing media.

12.2.2. Treatments:

12.2.2.1. Exogenous sphingomyelinases:

Hep G2 cells were treated with a dose-response from 0 to 2U/ml of human placental ASMase (Sigma, S5283) and 2U/ml *Bacillus cereus* NSMase (Sigma, S9396) for 18h. Cells were processed for RNA isolation and analyzed for ER stress markers by gene expression. For Ca^{2+} ER release studies, cells were grown on coverslips and treated with 1U/ml human placental ASMase for 18h prior to Thapsigargin (Tg) (Sigma, T9033) stimulation (See section 14.4 for detailed protocol).

12.2.2.2. Thapsigargin-induced Ca^{2+} release:

In order to study Ca^{2+} release from the ER, cells were treated with 1µM Tg. Tg is a naturally occurring sesquiterpene lactone isolated from the umbelliferous plant *Thapsia garganica*. This tumor promoter releases Ca^{2+} from intracellular stores by specifically inhibiting the endoplasmic reticulum Ca^{2+}-ATPase, SERCA.

12.2.2.3. Tunicamycin-TUDCA treatment:

Hep G2 cells were challenged with 4µg/ml Tm for 4h in order to induce ER stress. TUDCA (Tauroursodeoxycholic acid) (Sigma, T0266) is a bile acid commonly used as a chemical chaperone to release ER stress. Hep G2 cells were pre-treated overnight with or without 500µg/ml TUDCA in order to prevent Tm-induced ER stress. Cells were processed for RNA isolation and gene expression analysis.

13. CELL DEATH:

13.1. MTT:

MTT assay measures the cell proliferation rate and conversely, when metabolic events lead to apoptosis or necrosis, the reduction in cell viability. The yellow tetrazolium MTT (3-(4, 5-dimethylthiazolyl-2)-2,5-diphenyltetrazolium bromide) is reduced by metabolically active cells, in part by the action of dehydrogenase enzymes, to generate reducing equivalents such as NADH and NADPH. The resulting intracellular purple formazan can be solubilized and quantified by spectrophotometric means.

Protocol:

- Seeding conditions: seed 250.000 hepatocytes per each 12 well.
- Perform the treatments.
- MTT reduction: during the last hour of treatment add 0,5mg/ml MTT to the medium. During this hour, MTT will be reduced to formazan by metabolically active cells.
- Aspirate the medium and allow plates to completely dry.
- Solubilize the generated purple formazan with 1ml of 1-propanol per well.
- Shake the plates until formazan is completely dissolved.
- In a plate reader spectrophotometer read at an absorbance of 570 nm corresponding to the formazan and 630 nm corresponding to the background.
- The final absorbance will be [Abs_{570}-Abs_{630}].
- To express the results in a percentage refer all samples to the controls to obtain a fold change.

13.2. Trypan blue:

Cell viability can be assessed by Trypan Blue exclusion. Trypan Blue (Sigma, T8154) is a vital stain that selectively stains dead cells. In a viable cell, Trypan Blue does not penetrate cell membranes, however, dying or already dead cells have compromised cell membranes that allow the entrance of Trypan Blue resulting blue in staining of these cells. 0.2% Trypan Blue in PBS was used for the staining and a Neubauer chamber was used to count positive and negative stained cells to create a percentage of viability within the sample.

14. CONFOCAL MICROSCOPY:

This technique allows visualizing specific components of cells or tissue sections by immunofluorescence, binding specific antibodies chemically conjugated with a fluorescent dye or by using fluorescent probes with specific targets.

The immunofluorescence direct method uses primary antibodies labeled with a fluorescent dye and the indirect method uses a secondary antibody labeled with a fluorescent dye that recognizes the primary antibody. This technique can be performed on cells fixed on slides and tissue sections. Samples can be examined under a fluorescence microscope or a confocal microscope for better resolution. On the other hand, the fluorescent probes allow us to specifically stain cellular compartments like mitochondria or lysosomes among others. These probes are added to the culture media of living cells during the treatments and are incorporated physiologically into the cell.

Confocal microscopy is an optical imaging technique that increases optical resolution and contrast of a sample by using point illumination and a spatial pinhole eliminating the out-of-focus light in specimens that are thicker than the focal plane.

14.1. Mitochondrial cholesterol:

In order to study whether FC was increased in mitochondrial membranes of ASMase deficient primary mouse hepatocytes we immunodetected cytochrome c as a mitochondrial marker and filipin, a fluorescent probe, as a FC marker.

Protocol:

- Seeding: 200.000 hepatocytes per 6 well plate containing collagen-coated coverslips.
- Fixation: fix hepatocytes 15 min with 4% paraformaldehyde (PFA) at RT.
- Washes: wash the cover slips with PBS twice.
- Blocking and permeabilization: block and permeabilize the cells for 15 min at RT using a blocking buffer (PBS +0.5% glycine + 1% FFA-BSA) with 0,025% saponinin.
- Primary antibody: incubate overnight with mouse anti-cytochrome c monoclonal antibody (clone 6H2.B4; Pharmingen, 556432) diluted 1:200 in 1x PBS with 1% FFA-BSA in a humidity chamber.
- Washes: wash the cover slips with PBS three times.
- Secondary antibody and filipin staining: incubate 1h at RT with a secondary anti-mouse IgG antibody, conjugated with Alexa Fluor 488 (1:1000, Molecular Probes, A10684) diluted 1:1000 in PBS + 0,1% FFA-BSA. Filipin was added during the secondary antibody incubation at a concentration of 250µg/ml.
- Washes: wash the cover slips with PBS three times.
- Mounting: mount the cover slips on glass slides with Dako fluorescent mounting medium.
- Allow mounting media to dry a few hours.
- Visualize the samples in the Leica SPE confocal laser-scanning microscope. (Filipin λ_{ex}340-380nm ; λ_{em}385-470nm. Alexa 488 λ_{ex}488nm ; λ_{em}495-519nm)

14.2. Lysosomal cholesterol:

In order to study whether FC was increased in lysosomes of ASMase deficient and hypercholesterolemic primary mouse hepatocytes we used the fluorescent probe Lysotracker (Invitrogen, 7528), which has high tropism towards acidic compartments like lysosomes. Filipin was used as a FC marker.

Protocol:

For these experiments we used 6-10 week old WT and ASMase$^{-/-}$ mice and 48h HCD exposed WT mice.

- Seeding conditions: 200.000 hepatocytes per 6 well plate containing collagen-coated coverslips.
- Lysotracker: 3h post-isolation switch to warm basic media containing 50nM Lysotracker. Incubate for 1h at 37ºC in the incubator.
- Washes: aspirate the media and wash three times with PBS.
- Fixation: fix cells with 4% PFA for 15 min at RT protecting from the light from now on.
- Washes: wash three times with PBS.
- Filipin staining: incubate for 15 min at RT with 250µg/ml of filipin in PBS.
- Washes: wash three times with PBS.
- Mounting: mount the cover slips on glass slides with 8µl of Dako fluorescent mounting medium.
- Allow mounting media to dry a few hours before visualizing with the microscope.
- Visualize the samples in the Leica SPE confocal laser-scanning microscope. (Filipin λ_{ex}340-380nm ; λ_{em}385-470nm. Lysotracker λ_{ex}577nm ; λ_{em}590nm)

14.3. Autophagosome formation:

In order to study autophagosome vacuoles in ASMase deficient primary mouse hepatocytes we used the fluorescent probe monodansylcadaverine or MDC (Santa Cruz, sc-214851) as autophagosome marker and Hoechst 33258 (Molecular Probes) staining as cell permeable nucleic acid counterstaining. MDC preferentially accumulates in autophagic vacuoles due to a combination of ion trapping and specific interactions with membrane lipids.

Protocol:

For these experiments we used 6-10 week old WT and ASMase$^{-/-}$ mice.

- Seeding conditions: 200.000 hepatocytes per 6 well plate containing collagen-coated coverslips.
- Autophagy induction: 2h post isolation treat cells with 2µM rapamycin for 1h in basic media.
- MDC staining: prepare a fresh stock of 17mg/ml MDC in methanol and perform a 1/1000 dilution in PBS. After rapamycin treatment, switch cells to warm PBS containing the MDC. Incubate for 10 min at 37ºC.

- Washes: aspirate the media and wash three times with PBS.
- Fixation: fix cells with 4% PFA for 15 min at RT protecting from the light from now on.
- Washes: wash three times with PBS.
- Hoechst staining: incubate for 15 min at RT with 2µg/ml Hoechst in PBS.
- Washes: wash three times with PBS.
- Mounting: mount the cover slips on glass slides with 8µl of Dako fluorescent mounting medium.
- Allow mounting media to dry a few hours before visualizing with the microscope.
- Visualize the samples in the Leica SPE confocal laser-scanning microscope. (MDC λ_{ex}335nm ; λ_{em}518nm. Hoechst λ_{ex}352nm ; λ_{em}461nm)

14.4. ER Ca^{2+} release:

To study the role of ASMase in ER Ca^{2+} stores, which regulate UPR, we used the calcium indicator Fluo-4 AM (Molecular Probes, F-14201) to determine ER Ca^{2+} homeostasis in Hep G2 cells in response to exogenous ASMase.

Protocol:

- Seeding conditions: seed 300.000 cells per 6 well plate containing glass coverslips.
- ASMase treatment: pre-treat cells with 1U/ml human placental ASMase for 18h.
- Calcium indicator: load cells with 4µM of the calcium indicator Fluo-4 AM and with 0.08% Pluronic F-127 to facilitate Fluo-4 AM solubilization (Molecular Probes, F-127) in DMEM at RT for 30 min.
- Washes: wash excess Fluo-4 from cells three times with DMEM.
- Stabilization: let the cells rest in calcium free DMEM for additional 15 min.
- Washes: wash three more times with calcium free DMEM.
- Mounting: mount the coverslip on the stage of an inverted confocal Leica TCS-SL microscope.
- Life image capturing: fluorescence images were collected every second over a 10 min period. 1µM Tg was added after two minutes of system stabilization. The ratio of basal to peak intensities of individual cells was calculated using Image J, and ratios for 10 individual cells were averaged per run.

15. HUMAN SAMPLES:

Human liver samples were obtained from patients with alcoholic hepatitis by transyugular biopsies (n=10) or from explanted livers from patients undergoing liver transplantation for alcoholic liver disease (n=7). Normal livers were obtained from cadaveric liver donors (n=3) or from resection for unrelated liver diseases (metastasis from distant organ cancer, n=8). All control donors had normal serum aminotransferase levels and normal liver histology.

Samples were immediately frozen in liquid nitrogen and stored at -80°C for mRNA analysis. Total RNA was extracted using Nucleospin®RNAII and one microgram of total RNA was retro transcribed using the High Capacity cDNA Reverse Transcriptase kit (Applied Biosystems) following manufacturer's recommendations. All patients gave written informed consent, and the protocol was approved by ethical committees from the Hospital Clínic i Provençal de Barcelona and Hospital Huriez, and followed ethical guidelines on humans and human samples. Clinical characteristics of patients are included in Table M9.

	Control (n=13)	Alcoholic Hepatitis (n=17)
Age (Years)	56 (40-73)	50.14 (38-56)
AST (U/L)	20.5 (20-22)	104.35 (3-222)
ALT (U/L)	23.25 (13-32)	38.5 (26-90)
Bilirrubin (mg/dL)	0.4 (0.3-0.6)	11.71 (4-21)
γGT (U/L)	101.6 (48-210)	337.75 (123-1100)

Table M9. Clinical and analytical characteristics of patients with acute alcoholic hepatitis. Numeric data is shown as median (interquartile range [IQR] 25-75) and categorical/nominal data in count. AST: Aspartate-aminotransferase; ALT: Alanine-aminotransferase; γGT: γ-glutamyltransferase.

16. STATISTICS:

Results are expressed as mean ±SEM unless otherwise indicated. Statistical significance of mean values was assed using Student t-test and one-way ANOVA followed by Bonferroni post-test. Statistics were performed using GraphPad Prism 5 software.

RESULTS

AIM 1. ROLE OF ACID SPHINGOMYELINASE IN NON-ALCOHOLIC STEATOHEPATITIS

1.1. Diet-induced body weight gain, glucose and insulin tolerance in ASMase null mice.

Since obesity and its associated co-morbidities such as insulin resistance and T2DM are known to contribute to NAFLD, we first examined the role of ASMase deficiency in body weight and systemic glucose homeostasis following HFD intake. On RD ASMase null mice were heavier than wild type mice (Figure 1.1). Moreover, while wild type mice gained body weight on HFD, as expected, this effect was significantly more pronounced in ASMase null mice.

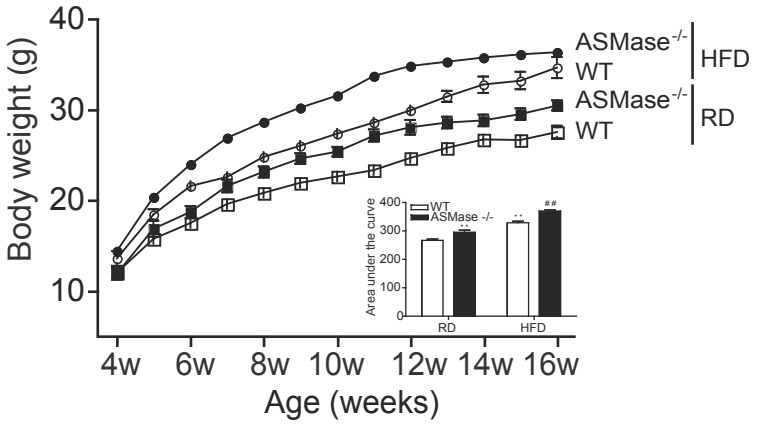

Figure 1.1 Body weight. WT and ASMase$^{-/-}$ mice body weight time course on RD and HFD (n>9). Inside figure represents area under the curve of each group. Results are expressed as mean ± SEM (**p<0.01 vs. RD-fed WT mice, ##p<0.01 vs. HFD-fed WT mice).

Considering that the primary function of adipose tissue is to store fat, we next examined whether enhanced adiposity could contribute to the body weight gain of ASMase knockout mice following HFD feeding. As expected, wild type mice exhibited increased adipose mass, in particular, epididymal (EWAT) and subcutaneous white adipose (SCWAT) stores upon HFD feeding (Figure 1.2). However, this effect was blunted in the absence of ASMase, as EWAT and SCWAT from ASMase null mice weighted significantly less than corresponding tissues from wild type mice (Figure 1.2).

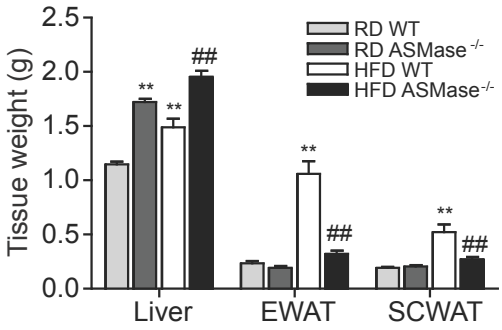

Figure 1.2. Tissue weight. Liver, epididymal (EWAT) and subcutaneous (SCWAT) white adipose tissue weight of WT and ASMase$^{-/-}$ mice fed either RD or HFD (n>9). Results are expressed as mean ± SEM (**p<0.01 vs. RD-fed WT, ##p<0.01 vs. HFD-fed WT).

Furthermore, on RD EWAT from ASMase null mice exhibited more crown-like structures than wild type mice, indicating mononuclear cell infiltration (Figure 1.3).

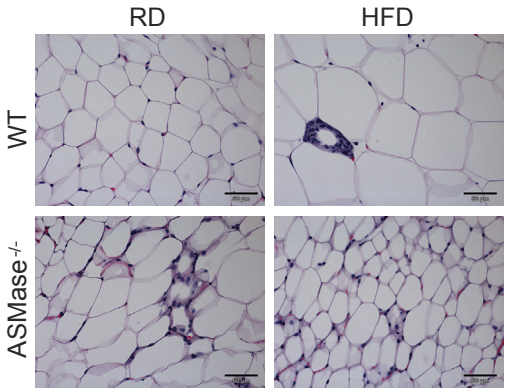

Figure 1.3. EWAT H&E staining. Epididymal white adipose tissue H&E staining from WT and ASMase$^{-/-}$ mice fed either RD or HFD.

Regarding systemic glucose homeostasis, ASMase null mice displayed higher fasting blood glucose levels than wild type mice on RD, and this effect worsened upon HFD feeding (Figure 1.4).

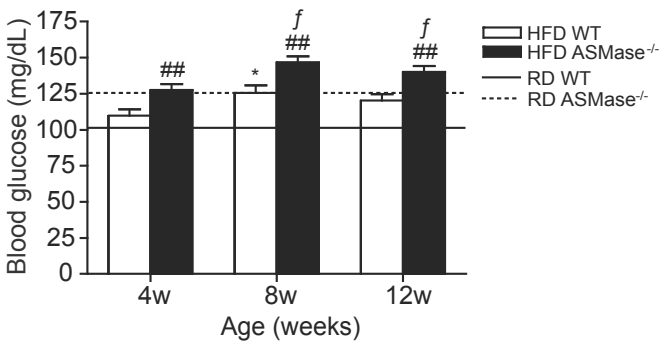

Figure 1.4. Blood glucose levels. 6h-fasted blood glucose levels of HFD-fed WT and ASMase$^{-/-}$ mice (n>12). Results are expressed as mean ± SEM (*p<0.05 vs. RD-fed WT mice, ##p<0.01 vs. HFD-fed WT and *f* p<0.05 vs. RD-fed ASMase$^{-/-}$ mice).

We next performed GTT and ITT to further investigate systemic glucose metabolism and insulin action. On RD, there were no major changes except for the moderate glucose tolerance of ASMase knockout mice with respect to wild type mice (Figure 1.5. A-C). However, upon HFD we observed lower glucose and insulin tolerance in ASMase null mice compared to wild type mice following GTT and ITT tests (Figure 1.5 D-F). Moreover, body weight gain, glucose homeostasis and tolerance in ASMase$^{+/-}$ mice fed HFD were similar to wild type mice (not shown). Since ASMase$^{+/-}$ mice exhibit 40-50% residual ASMase activity, these findings suggest that most of ASMase is dispensable in regulation of obesity and glucose homeostasis. These findings define a critical role for ASMase in the regulation of body weight and insulin sensitivity following HFD intake.

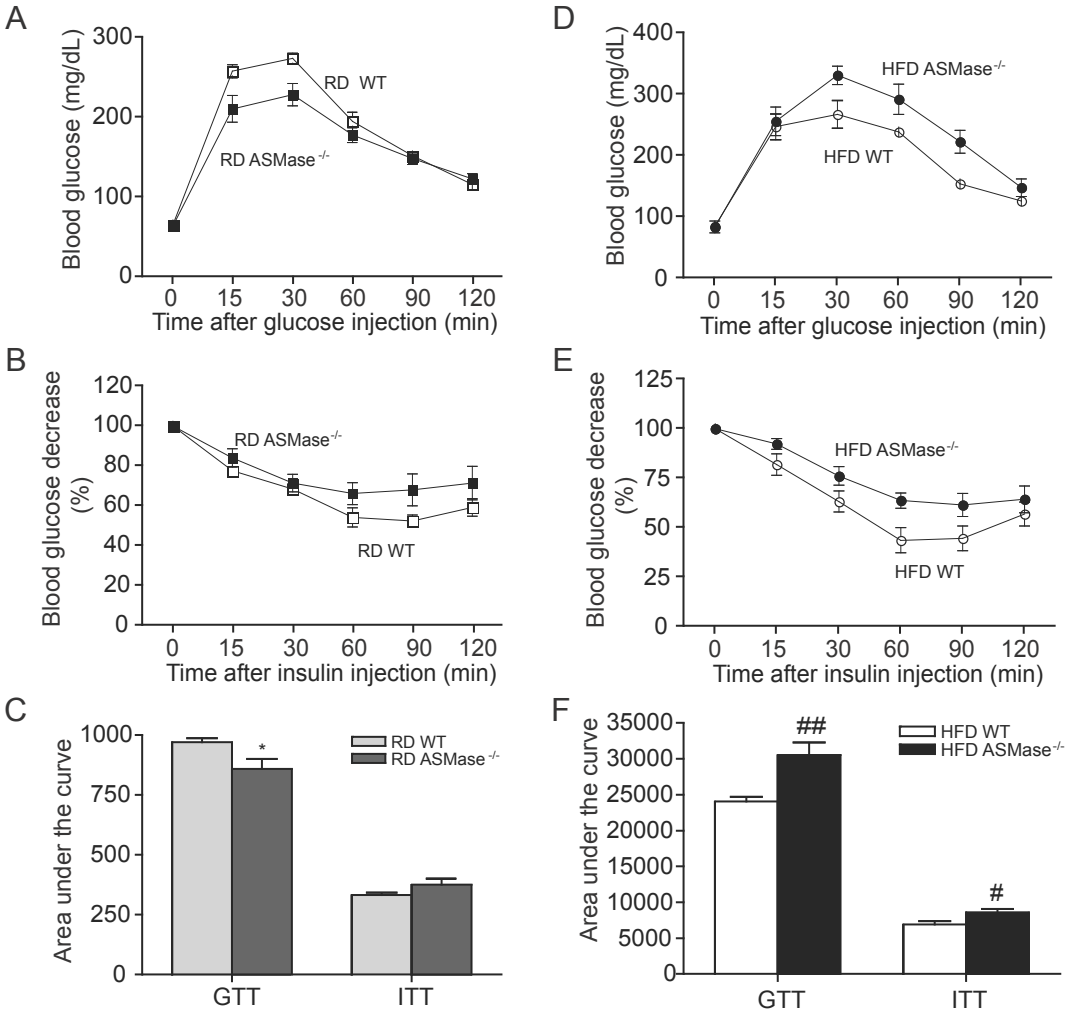

Figure 1.5. Analysis of systemic glucose homeostasis. Glucose tolerance tests of WT and ASMase$^{-/-}$ mice on (A) RD and (D) HFD. Insulin tolerance tests of WT and ASMase$^{-/-}$ mice on (B) RD and (E) HFD. Area under the curve of GTT and ITT on (C) RD and (F) HFD (n=6). Results are expressed as mean ± SEM (*p<0.05 vs. RD-fed WT mice, #p<0.05, ##p<0.01 vs. HFD-fed WT mice).

1.2. Hepatic insulin signaling in ASMase deficiency.

To specifically address whether hepatic insulin signaling was impaired in ASMase null mice, insulin was infused into the portal vein to examine early hepatic insulin signaling events. Liver extracts from wild type and ASMase null mice on RD exhibited similar phosphorylation of insulin receptor β (IRβ) subunit and Akt (Figure 1.6. A-C). Moreover, liver pattern of Akt phosphorylation in wild type and ASMase null mice did not change upon HFD feeding. HFD decreased IRβ phosphorylation in wild type mice, however, this effect was abrogated in ASMase$^{-/-}$ mice-fed HFD (Figure 1.6 A-C).

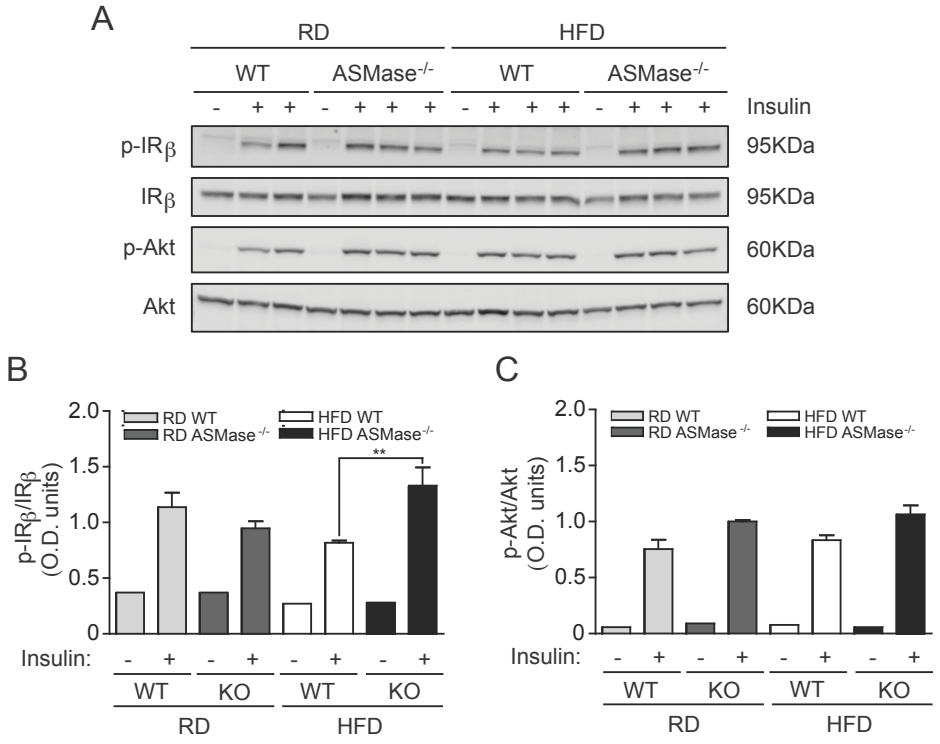

Figure 1.6. Hepatic insulin signaling in ASMase deficiency. (A) Liver insulin-stimulated phosphorylation of IRβ$^{[pT1162/1163]}$ and Akt$^{[pSer473]}$ after a 3 min portal vein infusion of 1U/Kg insulin or PBS. Each lane represents one animal. (B-C) Western blot quantification of panel A. Results are expressed as mean ± SEM (**p<0.01).

Furthermore, to ascertain specific contribution of parenchymal cells to these observations, we isolated and cultured primary hepatocytes from wild type and ASMase null mice. As observed, insulin induced a similar pattern of IRβ phosphorylation in hepatocytes from wild type and ASMase knockout mice (Figure 1.7 A-B), consistent with the observations in intact liver. Moreover, insulin stimulation of Akt phosphorylation in hepatocytes from ASMase$^{-/-}$ mice was increased respect to wild type hepatocytes. Overall, these findings indicate that the lack of ASMase does not impair early insulin signaling

events in the liver. These findings suggest that systemic effects observed in figure 1.4-5 likely reflect a role of ASMase in insulin resistance in extra-hepatic tissues.

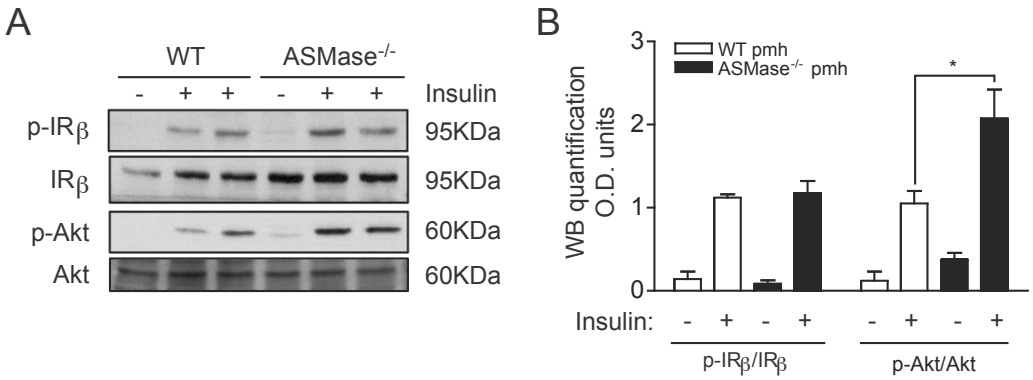

Figure 1.7. Primary mouse hepatocyte insulin signaling. WT and ASMase$^{-/-}$ primary mouse hepatocyte insulin stimulation. Representative image of a 3min 100nM insulin-stimulated phosphorylation of IRβ and Akt. Each lane represents one well. (B) Western blot quantification of three separate experiments of insulin-stimulated primary mouse hepatocytes (*p<0.05).

1.3. ASMase ablation prevents diet-induced liver steatosis and regulates lipid metabolism.

Another critical sign of NAFLD is the onset of hepatic macrovesicular steatosis, which is characterized by the accumulation of TG, FFA and cholesterol. ASMase null mice exhibited hepatomegaly on RD compared to wild type mice (Figure 1.2). Moreover, HFD feeding exacerbated this outcome in ASMase null mice. This effect, however, was not due to the onset of fatty liver as ASMase$^{-/-}$ mice were protected from HFD-induced accumulation of liver TG compared to wild type mice (Figure 1.8 A), which translated in lower macrovesicular steatosis, as confirmed by oil-red staining (Figure 1.8 B).

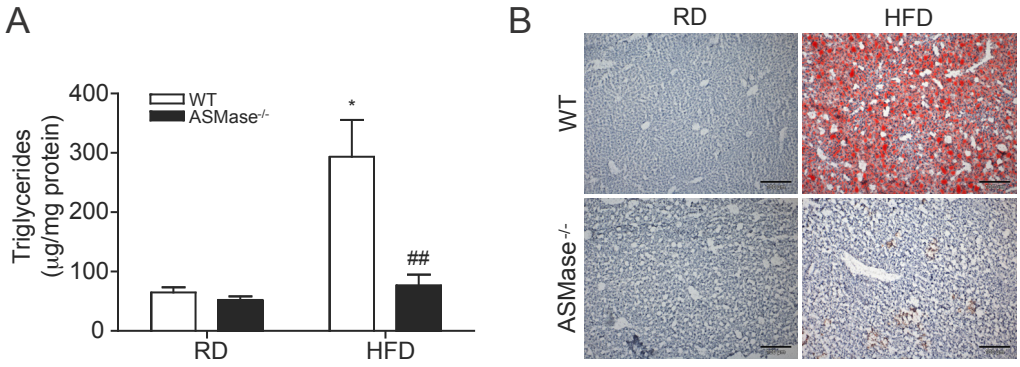

Figure 1.8. ASMase deficiency prevents diet-induced liver macrovesicular steatosis. Hepatic (A) triglycerides and (B) oil-red staining of RD and HFD-fed WT and ASMase$^{-/-}$ livers (n=5-7). Results are expressed as mean ± SEM (*p<0.05 vs. RD-fed WT mice, ##p<0.01 vs HFD-fed WT).

Parallel with these effects, HFD feeding increased levels of liver cholesterol in wild type mice (Figure 1.9 A), reflected mainly as free cholesterol accumulation, as indicated by filipin staining (Figure 1.9 B). However, ASMase null mice displayed endogenous liver free cholesterol accumulation, which further increased upon HFD feeding (Figure 1.9 A-B).

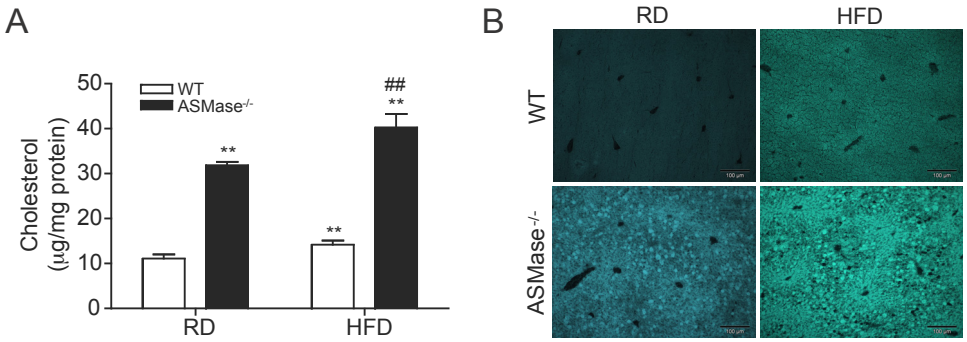

Figure 1.9. ASMase deficiency increases hepatic cholesterol deposition. Hepatic (A) total cholesterol and (B) filipin staining of RD and HFD-fed WT and ASMase$^{-/-}$ livers (n=5-7). Results are expressed as mean ± SEM (**p<0.01 vs. RD-fed WT mice, ##p<0.01 vs HFD-fed WT).

Moreover, FFAs slightly accumulated (although not significantly) in wild type mice fed HFD, but this trend was not observed in ASMase null mice following HFD intake (Figure 1.10).

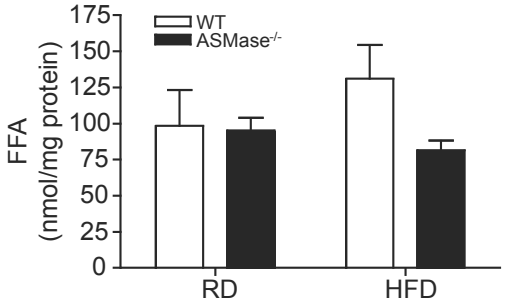

Figure 1.10. Hepatic free fatty acid content of regular and high fat diet-fed wild type and ASMase$^{-/-}$ mice. (n=5-7) Results are expressed as mean ± SEM.

Consistent with the observations in the HFD model, feeding a diet deficient in methionine and choline also resulted in liver macrovesicular steatosis and marked accumulation of TG in wild type mice (Figure 1.11 A-B). However, the increase in hepatic TG levels by MCD in ASMase null mice was significantly ameliorated resulting in decreased macrovesicular steatosis, indicating that the absence of ASMase prevents the induction of fatty liver independently of the nutritional approach used.

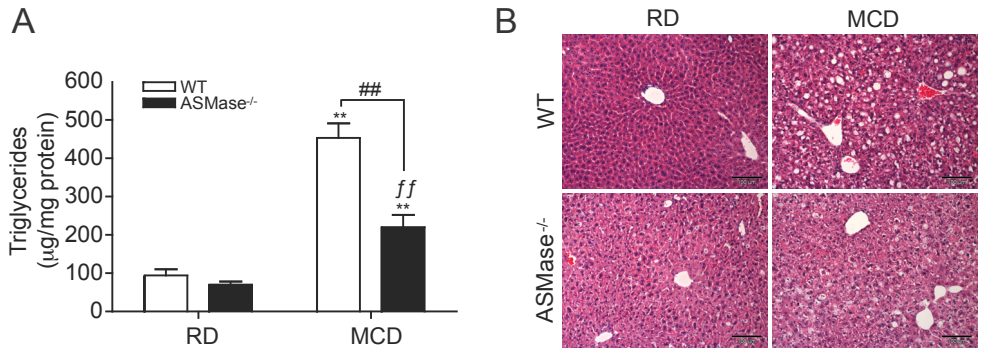

Figure 1.11. ASMase deficiency protects from of MCD-induced hepatic steatosis. Liver (A) triglycerides and (B) H&E staining of RD and MCD-fed WT and ASMase$^{-/-}$ mice (n=5-7). Results are expressed as mean ± SEM (**p<0.01 vs. RD-fed WT mice, ##p<0.01 vs MCD-fed WT and *ff* p<0.01 vs. RD-fed ASMase$^{-/-}$).

Analyses of serum cholesterol indicated increased total, HDL and LDL cholesterol levels in wild type fed HFD (Figure 1.12 A). ASMase null mice exhibited increased endogenous levels of serum cholesterol on RD, which further increased upon HFD feeding. Moreover, the effects on cholesterol homeostasis were accompanied by decreased gene expression of *Hmgcr*; the rate-limiting enzyme in cholesterol synthesis, suggesting that nutritional accumulation of cholesterol down regulates the *de novo* cholesterol synthetic pathway (Figure 1.12 B). In addition, ASMase null mice fed HFD exhibited decreased gene expression of *Ldl receptor (Ldlr)* and *ATP-binding cassette transporter (Abca1)* compared to wild type mice, suggesting a modulation of major hepatic cholesterol uptake and efflux pathways by ASMase (Figure 1.12 B).

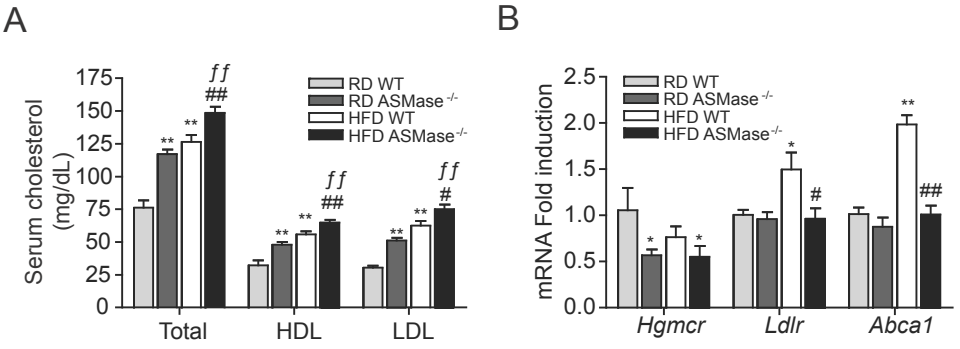

Figure 1.12. Serum cholesterol and hepatic cholesterol metabolism gene expression. (A) Total, HDL and LDL serum cholesterol levels in WT and ASMase$^{-/-}$ mice fed RD or HFD (n= 7-9). (B) Hepatic cholesterol metabolism gene expression (n=6). Results are expressed as mean ± SEM (*p<0.05, **p<0.01 vs. RD-fed WT mice, #p<0.05, ##p<0.01 vs HFD-fed WT mice and *ff* p<0.01 vs. RD-fed ASMase$^{-/-}$ mice).

Gene expression of enzymes involved in lipid metabolism indicated increased expression of *Srebp1c* and *Dgat2* in wild-type mice fed HFD. However, these effects were negated in ASMase$^{-/-}$ mice fed HFD (Figure 1.13), consistent with their resistance to HFD-mediated

liver steatosis. Moreover, wild type mice fed HFD increased the expression of fatty acid transporters *Cd36* and *Fatp2* but not *Fabp1* (Figure 1.13). However, ASMase$^{-/-}$ mice were refractory to diet induced expression of *Fatp2* and also showed a decreased expression of *Fabp1* on HFD (Figure 1.13). Quite intriguingly, *Cd36* expression was markedly increased in ASMase null mice both on RD and HFD (Figure 1.13). These findings underscore an important role for ASMase in fatty liver and indicate that the resistance of ASMase null mice to HFD-induced hepatic macrovesicular steatosis is largely due to impaired lipogenic pathways and decreased FA sterification.

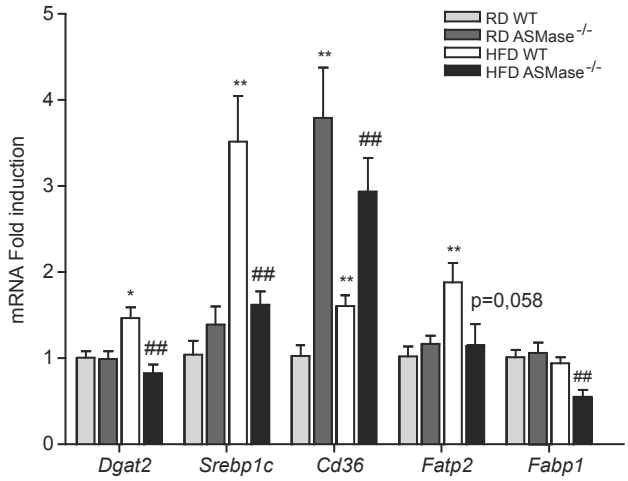

Figure 1.13. Hepatic lipogenic gene expression. Liver gene expression of RD and HFD-fed WT and ASMase$^{-/-}$ mice (n=5-6). Results are expressed as mean ± SEM (*p<0.05, **p<0.01 vs. RD-fed WT mice and #p<0.05, ##p<0.01 vs. HFD-fed WT mice).

1.4. HFD-mediated increase in hepatic ceramide levels requires ASMase.

Ceramide has been shown to regulate multiple cell pathways, including insulin resistance and metabolism (Holland, Brozinick et al. 2007; Bikman and Summers 2011). Given the above findings on the differential response of ASMase null mice to HFD-induced hepatic macrovesicular steatosis and glucose and insulin tolerance, we next explored potential alterations in ceramide metabolism. On RD, endogenous hepatic ceramide levels of ASMase null mice were lower compared to wild type mice (Figure 1.14 A). Moreover, in addition to the marked TG accumulation, HFD feeding increased hepatic total ceramide levels in wild type mice. However, this outcome was markedly defective in ASMase knockout mice (Figure 1.14 A), indicating that ASMase is essential for diet-induced liver ceramide accumulation. Consistent, with these results, wild-type mice displayed increased levels of ASMase mRNA upon HFD feeding (Figure 1.14 B).

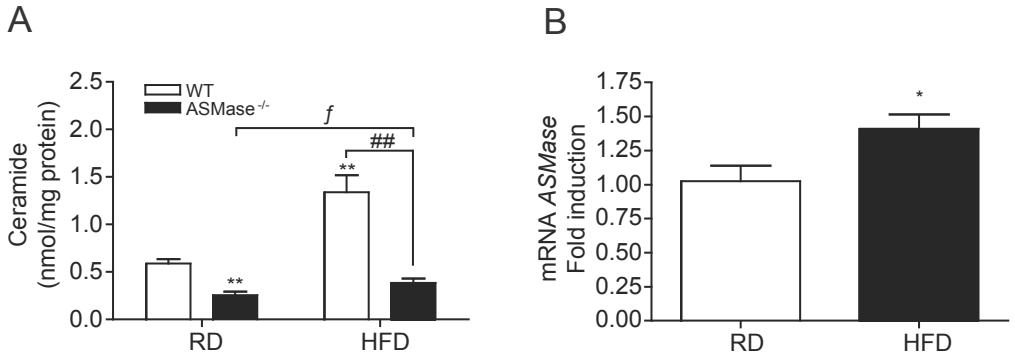

Figure 1.14. Hepatic total ceramide and *ASMase* gene expression. (A) Liver total ceramide content in RD and HFD-fed WT and ASMase null mice (n=9-10). (B) Liver *ASMase* gene expression in RD and HFD-fed WT mice (n=5-6). Results are expressed as mean ± SEM (*p<0.05, **p<0.01 vs. RD-fed WT mice, ##p<0.01 vs HFD-fed WT mice and *f* p<0.05 vs. RD-fed ASMase$^{-/-}$)

Furthermore, on RD ASMase knockout mice exhibited endogenous increased liver SM levels that further increased upon HFD feeding (Figure 1.15 A). However, unlike in wild type mice fed HFD, this outcome does not reflect increased expression of *Sphingomyelin synthase 1* and *2 (Sms1* and *Sms2)* (Figure 1.15 B), suggesting that ASMase plays an important role in hepatic SM turnover.

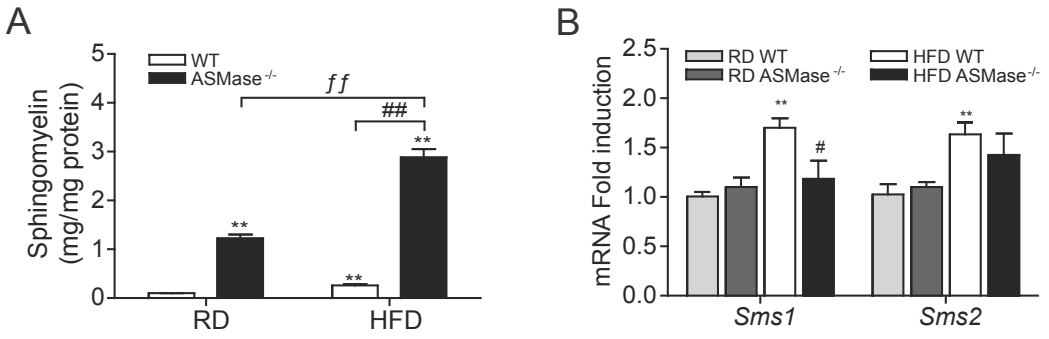

Figure 1.15. Hepatic sphingomyelin and *sphingomyelin synthases* gene expression. (A) Hepatic total sphingomyelin (n=5-7). Relative gene expression of (B) *Sms1* and *Sms2* in RD and HFD-fed WT and ASMase$^{-/-}$ livers (n=5-6). Results are expressed as mean ± SEM (**p<0.01 vs. RD-fed WT, #p<0.05, ##p<0.01 vs. HFD-fed WT and *ff* p<0.01 vs. RD-fed ASMase$^{-/-}$ mice)

In addition, HFD increased hepatic S1P in wild type mice. Surprisingly, ASMase knockout mice on RD already showed increased endogenous hepatic S1P compared to wild type mice and this effect further increased upon HFD intake (Figure 1.16 A). This outcome was accompanied by increased gene expression of *ACDase*, the lysosomal hydrolase that generates sphingosine from ceramide that can be later phosphorylated by sphingosine kinases to generate S1P (Figure 1.16 B).

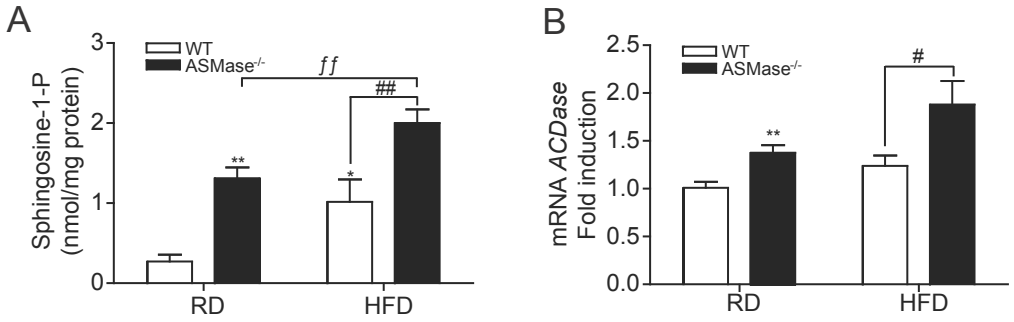

Figure 1.16. Hepatic S1P and *Acid ceramidase* gene expression. (A) Hepatic S1P (n=9-10) and relative gene expression of (B) *ACDase* in RD and HFD-fed WT and ASMase$^{-/-}$ livers (n=5-6). Results are expressed as mean ± SEM (*p<0.05, **p<0.01 vs. RD-fed WT, #p<0.05, ##p<0.01 vs HFD-fed WT and *ff* p<0.01 vs. RD-fed ASMase$^{-/-}$)

We next explored whether ASMase deficiency modulated gene expression of enzymes that regulate SL metabolism such as main hepatic ceramide synthases responsible for *de novo* ceramide synthesis. ASMase deficiency resulted in increased gene expression of *CerS5* that further increased upon HFD intake (Figure 1.17 A). Wild type mice fed HFD exhibited increased gene expression of *CerS2* and *CerS5*, while HFD feeding in ASMase null mice caused the repression of *CerS2* and *CerS4*. HFD feeding to ASMase knockout mice slightly increased liver ceramide levels compared to ASMase null mice fed RD (Figure 1.14 A), and this effect likely reflected the increase in the specific ceramide species C16:0 and C18:1 (palmitoyl and oleoyl ceramide respectively) (Figure 1.17 B). Overall, the above results indicate that ASMase is necessary for diet-induced hepatic ceramide accumulation and that ablation of ASMase modulates SL metabolism, resulting in SM and S1P accumulation.

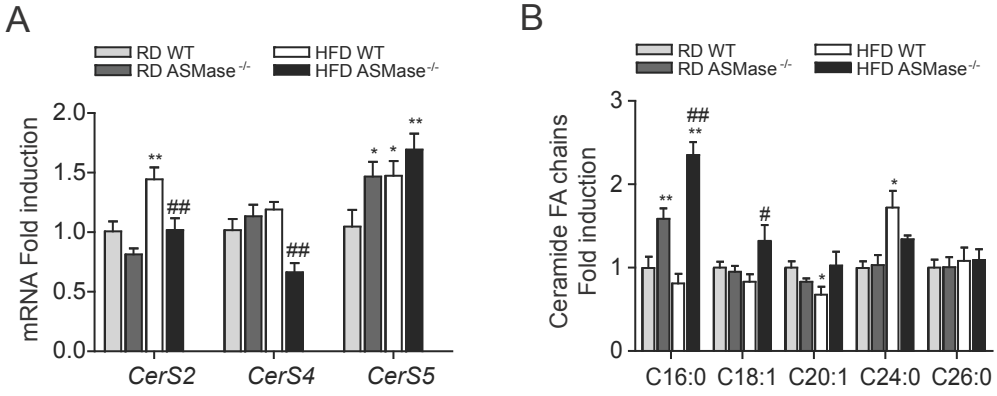

Figure 1.17. Hepatic ceramide synthases gene expression and ceramide fatty acid chains. (A) Gene expression of main hepatic ceramide synthases: *CerS2*, *CerS4* and *CerS5* of RD and HFD-fed WT and ASMase$^{-/-}$ mice (n=5-6). (B) Hepatic lipidomic analysis of ceramide fatty acid chains of RD and HFD-fed WT and ASMase$^{-/-}$ mice (n=4-5). Results are expressed as mean ± SEM (*p<0.05, **p<0.01 vs. RD-fed WT mice and #p<0.05, ##p<0.01 vs HFD-fed WT).

1.5. ASMase deficiency impact on autophagy.

Since autophagy regulates hepatic lipid metabolism (Singh, Kaushik et al. 2009), we analyzed whether stimulation of autophagy contributed to the resistance of ASMase null mice to diet-induced steatosis. Autophagy is a complex and dynamic process that comprises generation of autophagic double membranes, fusion of autophagosomes with lysosomes and degradation of cargo content. Autophagy can be monitored via expression of LC3BI, which during autophagy translocates from the cytosol to autophagosome membranes by lipidation of the cytosolic LC3BI form resulting in the membrane bound LC3BII form.

Analysis of hepatic extracts indicated increased LC3BII/I ratio in ASMase null mice compared to wild type mice, both on RD and HFD (Figure 1.18 A). Intriguingly, this outcome was accompanied by decreased endogenous expression of ATG7 (Figure 1.18 A). In order to exclude transcriptional regulation of these markers, their gene expression was analyzed by RT-PCR. HFD feeding increased the mRNA levels of *Atg7* and *Lc3b* in both wild type and ASMase null mice indicating that the regulation observed by WB was not due to changes in gene expression (Figure 1.18 B).

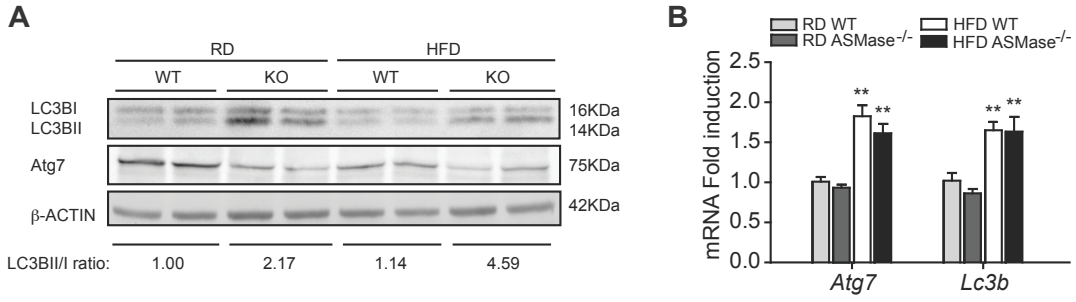

Figure 1.18. Hepatic autophagy in ASMase null mice. (A) Western blotting and immunodetection of autophagy-related markers in liver protein extracts and (B) gene expression of autophagy-related markers of RD and HFD-fed WT and ASMase null mice (n=5-6). Results are expressed as mean ± SEM (**p<0.01 vs. RD-fed WT mice).

Accumulation of LC3BII can result from autophagy induction or reflect a failure of autolysosomal degradation. To address autophagic flux, isolated primary mouse hepatocytes from wild type and ASMase$^{-/-}$ mice were exposed to chloroquine and/or rapamycin, an mTORC1 inhibitor, which promotes autophagy. Consistent with the findings in liver extracts, hepatocytes from ASMase null mice displayed increased

endogenous LC3BII/I ratio despite decreased ATG7 expression compared to wild type hepatocytes. Of interest, this outcome was paired with increased lysosomal proliferation as revealed by enhanced LAMP2 levels in ASMase deficient hepatocytes (Figure 1.19). However, despite increased basal autophagic flux (LC3BII/α-tubulin in CHQ-CTRL), rapamycin-mediated autophagic flux (LC3BII/α-tubulin in [C-R]-RAPA) was lower in ASMase null hepatocytes (Figure 1.19). This observation paralleled increased p62 levels in ASMase null hepatocytes, indicating decreased autophagic protein degradation upon rapamycin stimulation (Figure 1.19). The observation of increased levels of p62 despite increased basal autophagic flux in ASMase null hepatocytes is suggestive of impaired autophagosome-lysosome fusion or final cargo degradation.

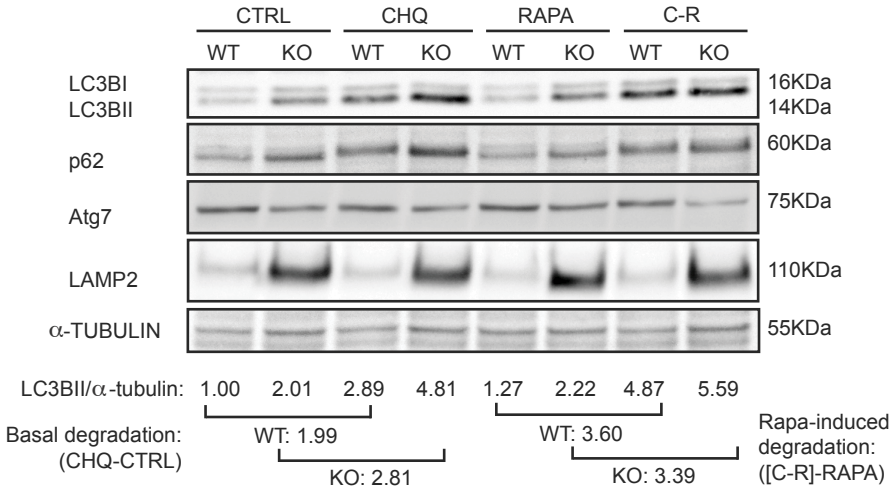

Figure 1.19. Autophagic flux in wild type and ASMase$^{-/-}$ primary mouse hepatocytes. Hepatocytes were treated for 3h with 2μM RAPA and 50μM CHQ. Basal and RAPA-induced degradation of LC3BII was calculated subtracting LC3BII levels in each condition from its respective CHQ treatment. Representative image of three individual experiments. CTRL, control. CHQ, chloroquine. RAPA, rapamycin.

To confirm these results, we next explored autophagic vacuole formation in primary mouse hepatocytes by confocal microscopy using monodansylcadaverine (MDC), a probe with high affinity for autophagic vacuoles. Rapamycin treatment increased MDC staining in wild type hepatocytes as expected (Figure 1.20). Similar to LC3BII levels, rapamycin treatment of ASMase null hepatocytes resulted in further accumulation of autophagic vacuoles compared to wild type hepatocytes (Figure 1.20). Taken together, these results demonstrate that in the absence of ASMase autophagy is impaired at a lysosomal level resulting in accumulation of autophagic vacuoles and delayed p62 degradation.

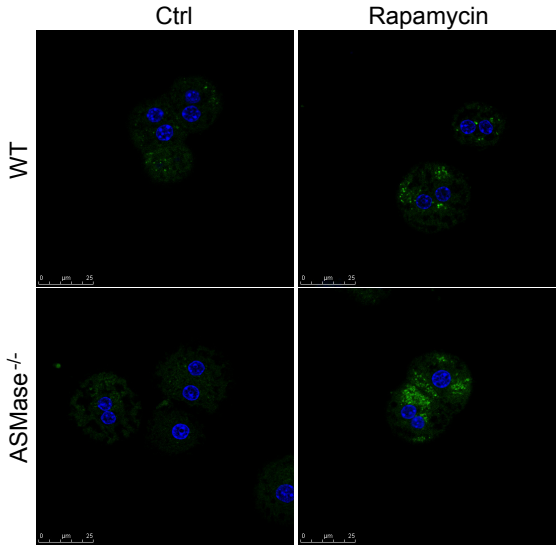

Figure 1.20. Autophagic vacuole formation in primary mouse hepatocytes. Representative image of wild type and ASMase$^{-/-}$ hepatocytes treated for 1h with 2μM rapamycin in order to induce autophagic vacuole formation. Green represents MDC staining or autophagic vacuoles. Blue represents Hoechst staining or nuclei.

1.6. ASMase deficiency increases lysosomal free cholesterol.

Since the above findings suggested an impairment of autophagy at a lysosomal level (Figure 1.9), we next assessed whether lysosomes accumulate cholesterol in ASMase null mice. In particular, FC loading in membranes is known to modulate the physical properties of membrane bilayers resulting in decreased membrane dynamics. Hence we hypothesized that ASMase deficiency results in lysosomal cholesterol accumulation, which in turn impairs autophagosome-lysosome fusion resulting in increased p62 levels. To test this hypothesis, we performed confocal imaging experiments in hepatocytes from wild type and ASMase null mice stained with filipin and lysotracker. As seen, ASMase$^{-/-}$ hepatocytes exhibited increased lysosomal proliferation revealed by increased lysotracker staining, consistent with enhanced LAMP2 levels in WB analysis and increased filipin staining compared to wild type hepatocytes (Figure 1.21 A). Moreover, lysotracker staining colocalized with filipin staining, indicating FC accumulation in lysosomes of ASMase null hepatocytes (Figure 1.21 A). Furthermore, ASMase$^{-/-}$ lysosomal phenotype can be reproduced in wild type mice fed a high cholesterol diet, as revealed by colocalization of lysotracker and filipin in isolated hepatocytes from mice fed HCD for two days (Figure 1.21 B). Although qualitatively similar, the degree of lysosomal cholesterol accumulation in ASMase$^{-/-}$ hepatocytes was markedly greater than HCD-exposed hepatocytes (Figure 1.21 A-B). These results indicate that lysosomal FC content

increases due to ASMase deficiency, which in turn may impair lysosomal membrane function.

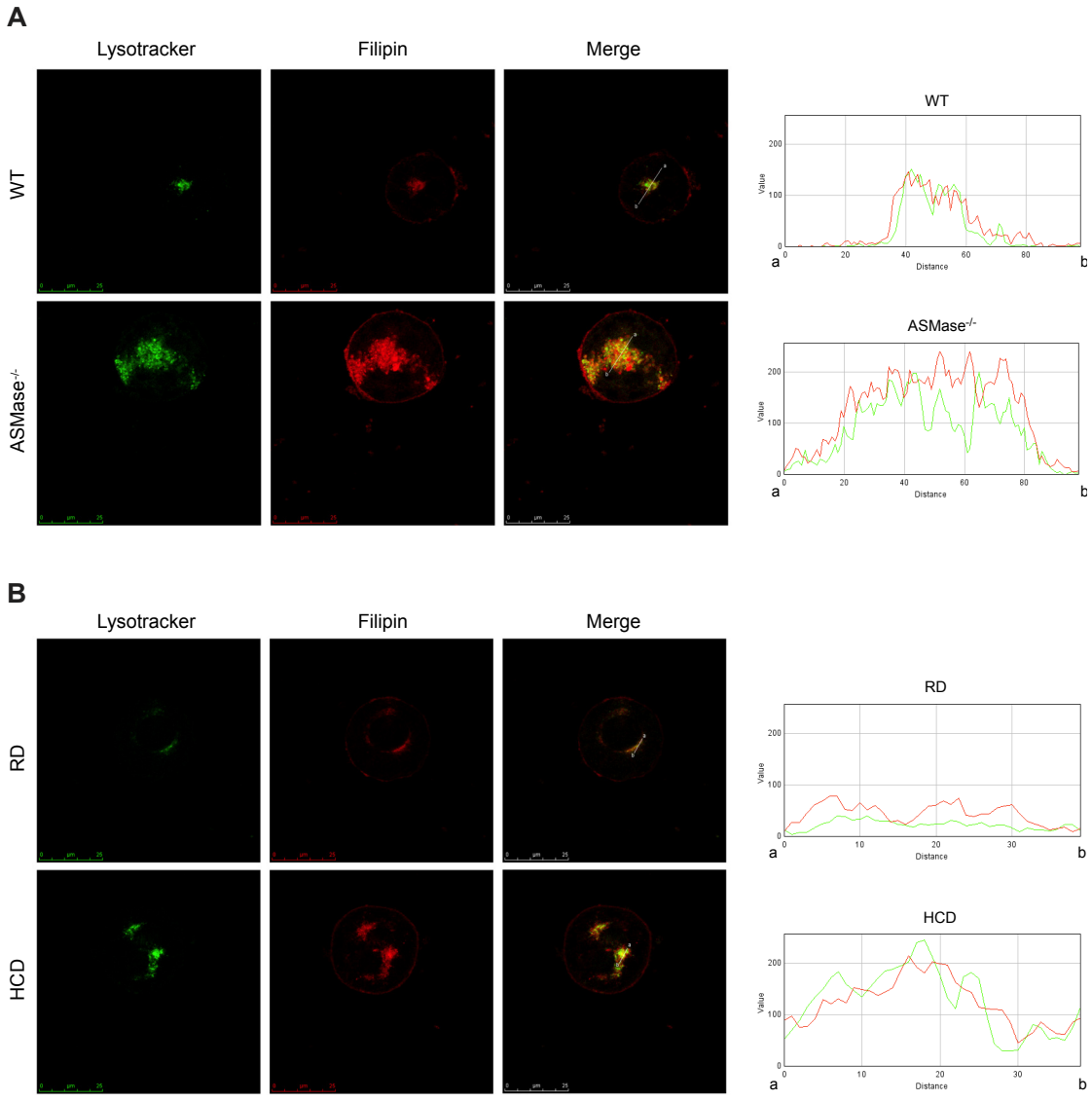

Figure 1.21. Lysosomal free cholesterol in ASMase$^{-/-}$ and HCD primary mouse hepatocytes. (A) Representative images and colocalization analysis of lysotracker (green) and filipin (red) staining and merge (yellow) of wild type and ASMase$^{-/-}$ primary mouse hepatocytes. (B) Representative images and colocalization analysis of lysotracker and filipin staining and merge of RD and HCD-exposed primary mouse hepatocytes. Representative images of three individual experiments.

1.7. ASMase deficiency protects hepatocytes from lysosomal membrane permeabilization-induced cell death.

Lysosomal permeabilization has been described as an important mechanism of cell death of relevance to NASH. For instance, saturated FA, such as palmitic acid, have been shown to induce hepatocellular apoptosis via lysosomal permeabilization-mediated

recruitment of mitochondria to activate apoptotic pathways (Li, Berk et al. 2008). Since cholesterol is known to regulate membrane physical properties and dynamics and given the preceding findings indicating increased lysosomal cholesterol accumulation (Figure 1.21), we examined the functional relevance in ASMase$^{-/-}$ hepatocytes. To this end, we used O-methyl-serinedodecylamide hydrochloride (MSDH, a gift of Dr. Hanna Appelqvist), a detergent that specifically permeabilizes lysosomes (Appelqvist, Nilsson et al. 2011). As seen, hepatocytes from ASMase null mice were resistant to MSDH-mediated cell death (Figure 1.22 A). Moreover, in parallel with lysosomal cholesterol accumulation induced by HCD-feeding, HCD-exposed hepatocytes were also resistant to MSDH-induced cell death (1.22B). These results indicate that increased lysosomal membrane FC in ASMase null hepatocytes protects from lysosomal permeabilization-induced cell death.

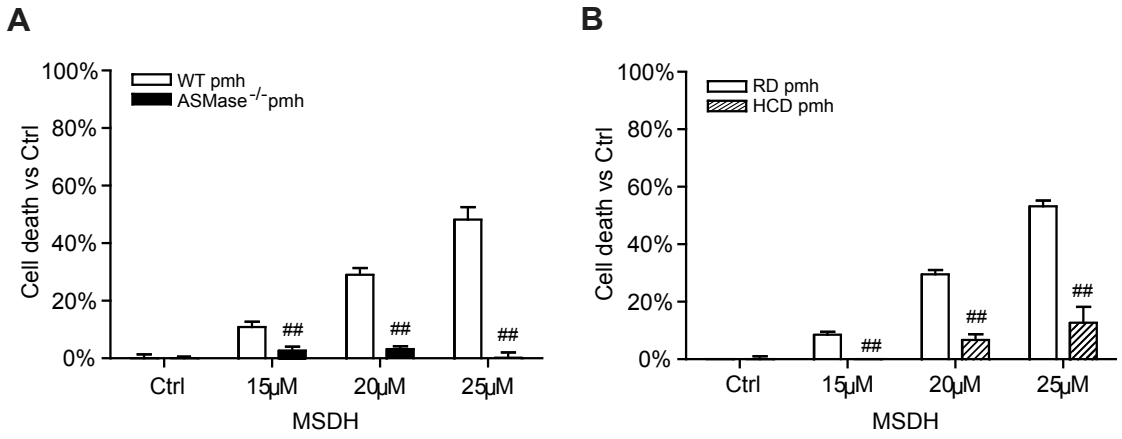

Figure 1.22. Lysosomal membrane permeabilization-induced cell death in primary mouse hepatocytes. (A) Wild type and ASMase$^{-/-}$ primary mouse hepatocytes cell death assessed by MTT. (B) RD and HCD-exposed primary mouse hepatocytes cell death assessed by MTT. Data are expressed as percentage vs. control and represent the mean of three individual experiments ± SD (##p<0.01 vs. same condition control group).

1.8. Hepatic ER stress in ASMase deficiency.

Since the preceding findings discard a role for autophagy in ASMase deficiency resistance to diet-induced liver steatosis, we next examined the sensitivity of ASMase null mice to HFD-induced hepatic ER stress, as this is a critical player in stimulation of lipogenic pathways and the onset of fatty liver (Ozcan, Cao et al. 2004; Fu, Yang et al. 2011). Liver extracts following HFD feeding were processed for analysis of ER stress markers. As seen, HFD induced gene expression of ER stress markers *Atf4, Pdi* and *Edem* as well as phosphorylation of IRE1α in wild type mice (Figure 1.23 A-D). However, ASMase null mice were protected from HFD-induced ER stress (Figure 1.23 A-D).

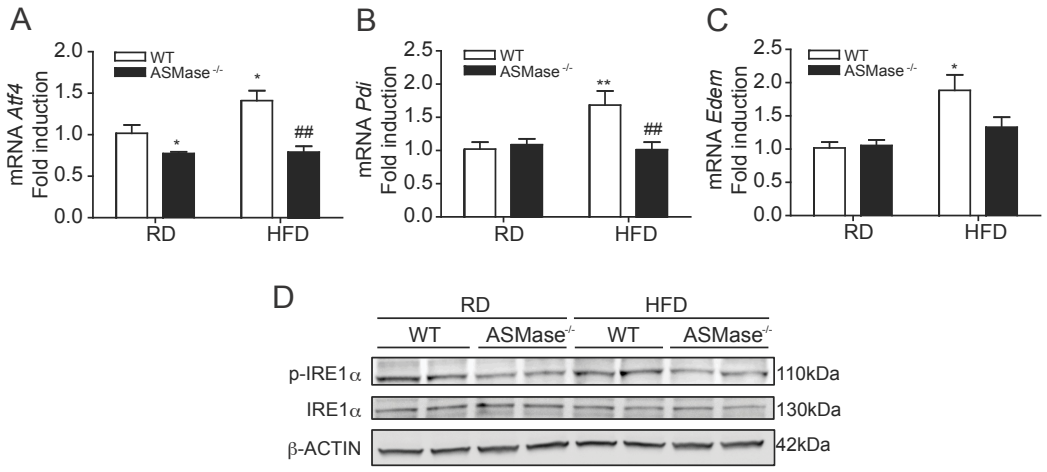

Figure 1.23. Hepatic ER stress in ASMase null mice. Relative gene expression of (A) *Atf4*, (B) *Pdi* and (C) *Edem* in RD and HFD-fed WT and ASMase$^{-/-}$ livers (n=5-6). (D) IRE1α phosphorylation in RD and HFD-fed WT and ASMase$^{-/-}$ liver protein extracts. Results are expressed as mean ± SEM (*p<0.05, **p<0.01 vs. RD-fed WT, ##p<0.01 vs. HFD-fed WT).

To address whether resistance of ASMase$^{-/-}$ mice to ER stress was specific to HFD feeding, we isolated primary mouse hepatocytes from wild type and ASMase null mice and challenged them with SubAB, a bacterial toxin that degrades the ER chaperone GRP78 that is essential for the proper glycosylation, folding and assembly of many membrane bound and secreted proteins. As expected, SubAB induced the cleavage of GRP78 both in wild type and ASMase null hepatocytes, whereas no cleavage was induced in the cells treated with the non-active mutant toxin SubA$_{[A727]}$B (Figure 1.24 A).

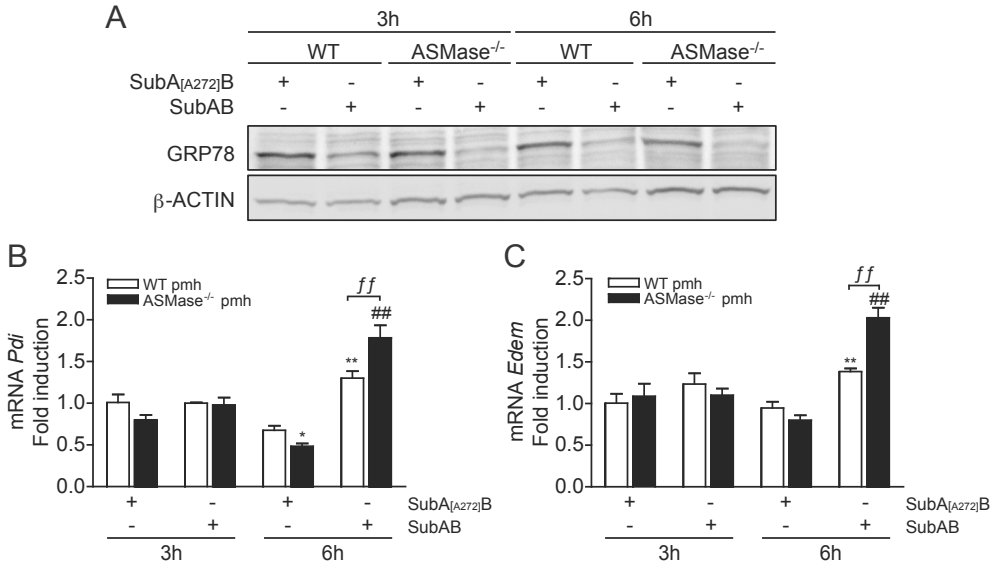

Figure 1.24. ASMase$^{-/-}$ primary mouse hepatocyte response to SubAB treatment. (A) GRP78 degradation in WT and ASMase$^{-/-}$ pmh after 3 and 6h treatment of 1μg/ml SubAB. Relative gene expression of (B) *Pdi* and (C) *Edem* after SubAB treatments in WT and ASMase$^{-/-}$ pmh (*p<0.05, **p<0.01 vs. SubA$_{[A272]}$B-treated WT pmh, ##p<0.01 vs. SubA$_{[A272]}$B-treated ASMase$^{-/-}$ pmh and *ff* p<0.01 vs. SubAB-treated WT pmh).

Moreover, in both genotypes, SubAB-mediated Grp78 degradation preceded expression of ER stress markers *Pdi* and *Edem* after 6h of treatment (Figure 1.24 B-C) compared to $SubA_{[A727]}B$ treated cells. These results indicate that the ER from ASMase null hepatocytes is capable of sensing ER stress and responding accordingly.

Furthermore, *in vivo* administration of glycosylation inhibitor tunicamycin (Tm) to ASMase$^{-/-}$ mice caused enhanced expression of ER stress markers *Atf4* and *Pdi* (Figure 1.25 A-B). In addition, Tm increased hepatic TG accumulation to a similar degree in wild type and ASMase$^{-/-}$ mice (Figure 1.25 C), indicating that the ER from ASMase$^{-/-}$ livers is able to sense Tm-induced stress and cause fat accumulation and hepatic steatosis. Although hepatic steatosis and ER stress are reciprocally regulated, these findings indicate that resistance of ASMase null mice to HFD-induced hepatic steatosis is likely due to defective ER stress response. Overall, these results indicate that the requirement of ASMase in nutritional ER stress, and that ER stress is sufficient to induce TG accumulation and hepatic steatosis in ASMase null mice.

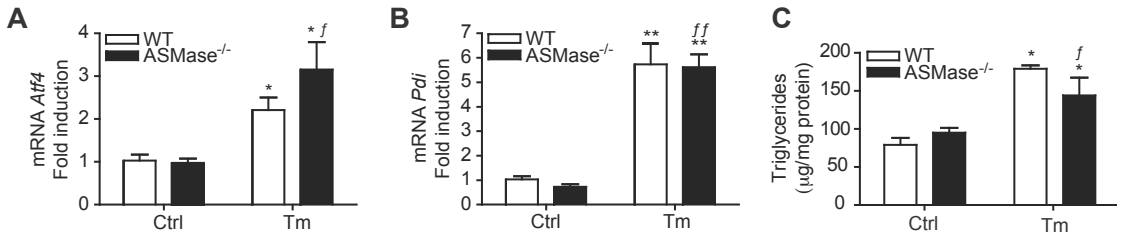

Figure 1.25. Tunicamycin-induced ER stress and lipogenesis in wild type and ASMase$^{-/-}$ mice. Hepatic gene expression of (A) *Atf4* and (B) *Pdi* and hepatic (C) triglyceride content in tunicamycin-treated WT and ASMase$^{-/-}$ mice (n=3-5). Results are expressed as mean ± SEM (*p< 0.05, **p<0.01 vs. WT Ctrl mice. *f* p<0.05, *ff* p<0.01 vs. ASMase$^{-/-}$ Ctrl mice).

1.9. ASMase antagonism protects against diet-induced liver injury and LPS sensitization.

As the onset of hepatic steatosis is considered the first hit in the two-hits hypothesis that sensitizes to subsequent factors leading to liver damage (Day and James 1998), we next examined the degree of hepatocellular injury in ASMase null mice following HFD. Wild type mice fed HFD exhibited increased serum ALT levels (Figure 1.26 A), indicating liver injury that was confirmed by histological analyses (Figure 1.26 B). Moreover, HFD-fed wild type mice displayed increased sensitivity to LPS-mediated liver damage (Figure 1.26 C-D). However, ASMase null mice were resistant to HFD-induced increased serum ALT

levels and liver damage (Figure 1.26 A-B), and more importantly, were refractive to HFD-mediated sensitization to LPS-induced liver injury (Figure 1.26 C-D).

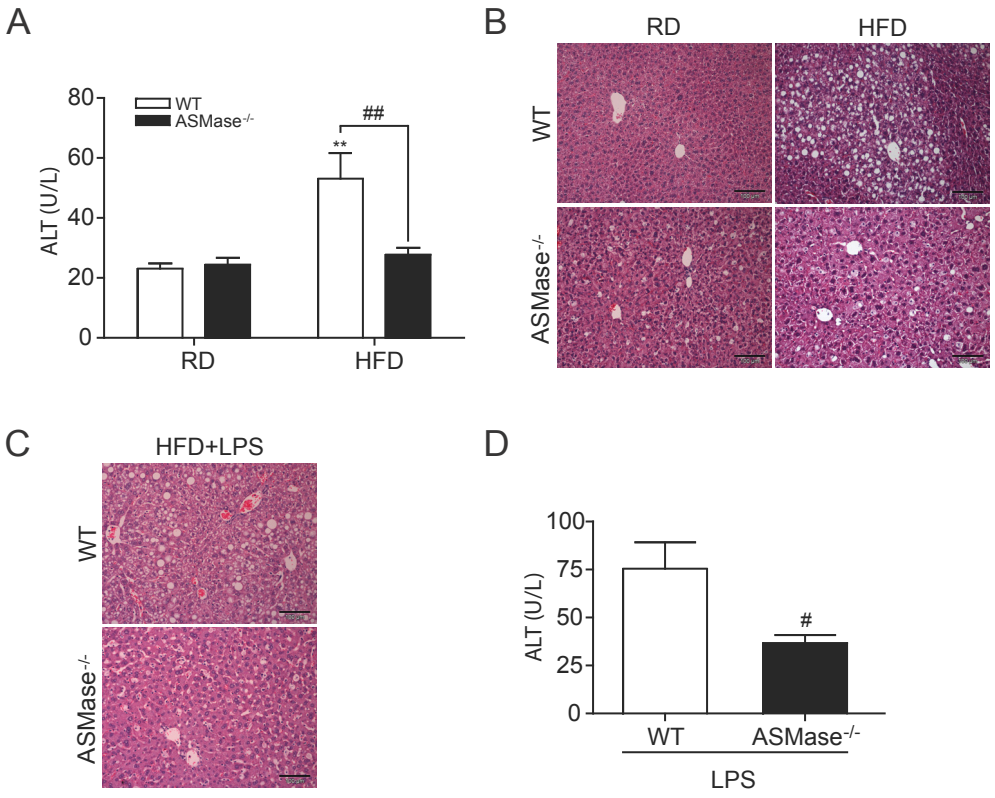

Figure 1.26. ASMase deficiency protects from diet-induced liver damage and LPS susceptibility. (A) Serum alanine transaminase levels (n>13) and (B) hepatic H&E staining of RD and HFD-fed WT and ASMase$^{-/-}$ mice. (C) Hepatic H&E staining and (E) serum alanine transaminase levels of HFD-fed WT and ASMase$^{-/-}$ mice challenged with 5mg/kg LPS for 24h (n=4-5). Results are expressed as mean ± SEM (**p<0.01 vs. RD-fed WT mice and #p<0.05, ##p<0.01 vs HFD-fed WT mice).

Furthermore, to address the potential relevance of the above findings, we next examined whether pharmacological inhibition of ASMase in wild type mice fed HFD would reproduce the effects observed in ASMase null mice. Wild type mice were fed HFD for 16 weeks with or without the tricyclic antidepressant amitriptyline in drinking water to functionally inhibit lysosomal ASMase processing and activation (Lang, Schenck et al. 2007). Amitriptyline treatment significantly inhibited hepatic ASMase activity by 25-30%, and this effect protected wild type mice against HFD-induced liver injury as seen by serum ALT release and histological analyses (Figure 1.27 A-B). However, unlike ASMase null mice, amitriptyline-treated wild type mice did not exhibit further insulin insensitivity and glucose intolerance after HFD intake (not shown). Thus, overall these findings indicate that ASMase plays a critical role not only in diet induced hepatic

macrovesicular steatosis but also in liver injury, and suggest that its pharmacological inhibition may be beneficial in diet-mediated NASH.

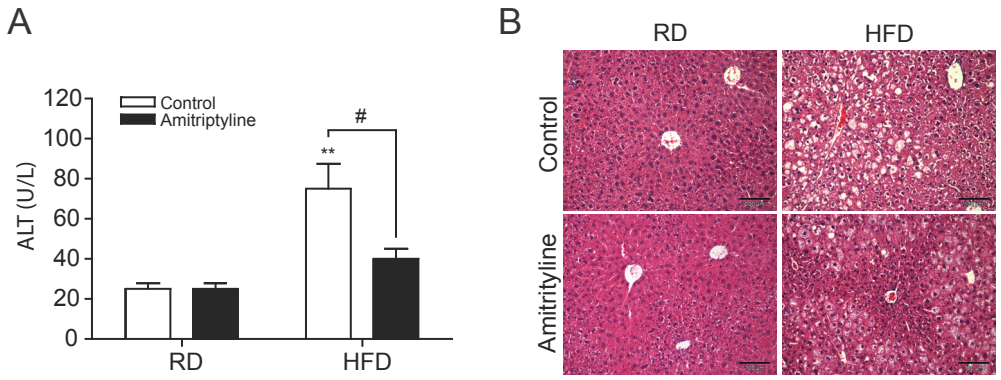

Figure 1.27. ASMase pharmacological inhibition protects from diet-induced liver damage. (A) Serum alanine transaminase levels (n=3) and (B) hepatic H&E staining of RD and HFD-fed control and 1mM amitriptyline in drinking water treated mice. Results are expressed as mean ± SEM (**p<0.01 vs. RD-fed WT mice and #p<0.05 vs. HFD-fed WT mice).

AIM 2. ROLE OF ACID SPHINGOMYELINASE IN ALCOHOLIC STEATOHEPATITIS

2.1. ASMase deficiency increases hepatic SM and cholesterol but prevents alcohol-induced TG, FFA accumulation and liver macrosteatosis.

Since fatty liver is one of the earliest symptoms of alcohol intake, we examined the hepatic lipid profile of wild type and ASMase knockout mice following chronic alcohol feeding. While alcohol administration increased hepatic TG and FFA levels in wild type mice, this response was blunted in ASMase knockout mice (Figure 2.1 A-B). In parallel with these changes, livers from wild type mice but not ASMase knockout mice exhibited macrovesicular steatosis as seen by oil-red staining (Figure 2.1 C).

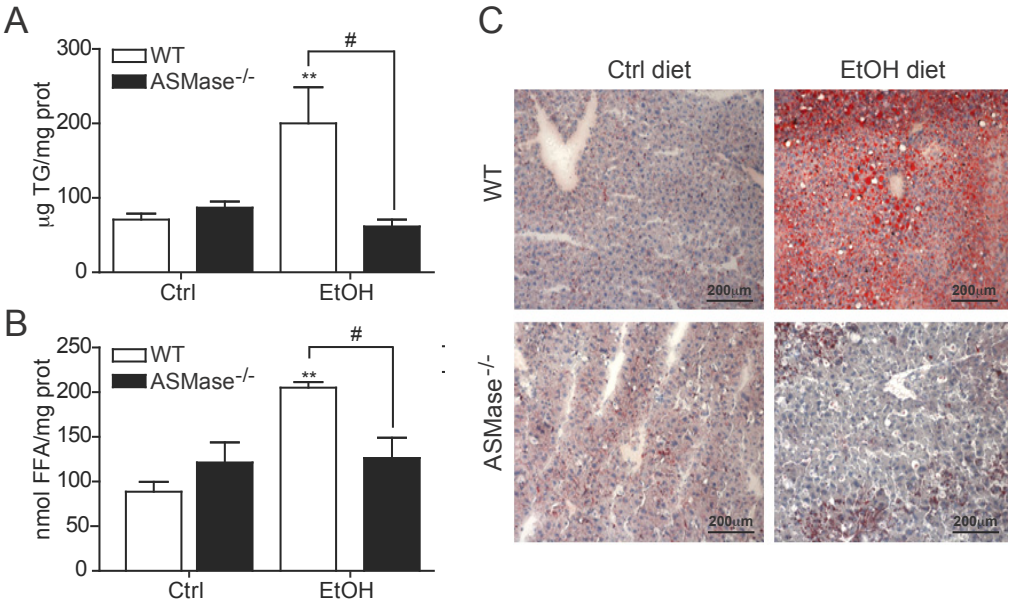

Figure 2.1. ASMase deficiency prevents alcohol-induced macrosteatosis. Hepatic (A) triglyceride and (B) free fatty acid content. (C) Oil-red staining in control and ethanol-fed WT and ASMase$^{-/-}$ livers. Results are expressed as mean ± SEM (**p<0.01 vs. control-fed WT mice, #p<0.05, vs. ethanol-fed WT mice).

Moreover, ethanol feeding also resulted in increased hepatic SM and cholesterol levels in wild type mice (Figure 2.2 A-B) with higher filipin staining (Figure 2.2 C), indicative of free cholesterol content. However, ASMase knockout mice fed control diet already exhibited increased hepatic SM and cholesterol content compared with wild type mice, consistent with recent observations (Prinetti, Prioni et al. 2011). Upon ethanol feeding, the hepatic SM and cholesterol levels further increased in ASMase knockout mice (Figure 2.2 A-C).

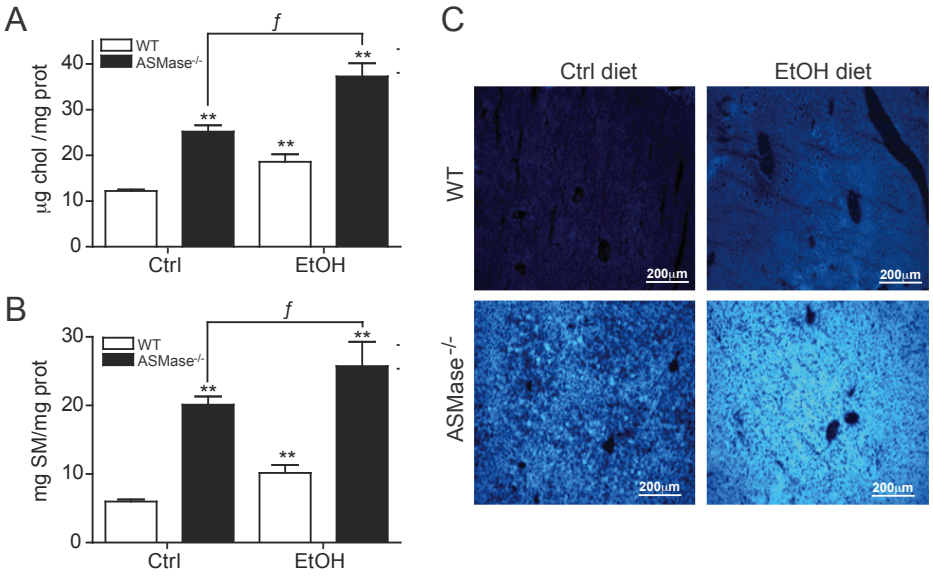

Figure 2.2. Hepatic cholesterol and sphingomyelin content. Hepatic (A) total cholesterol, and (B) sphingomyelin and (C) filipin staining in control and ethanol-fed WT and ASMase$^{-/-}$ livers. Results are expressed as mean ± SEM (**p<0.01 vs. control-fed WT mice, and *f* p<0.05 vs. control-fed ASMase$^{-/-}$ mice).

Consistent with these findings liver to weight ratio increased in ASMase null mice, although this increase in response to alcohol feeding was similar between wild type and ASMase knockout mice (Figure 2.3 A). Moreover, alcohol induced CYP2E1 up-regulation was similar in both wild type mice and ASMase null mice (Figure 2.3 B).

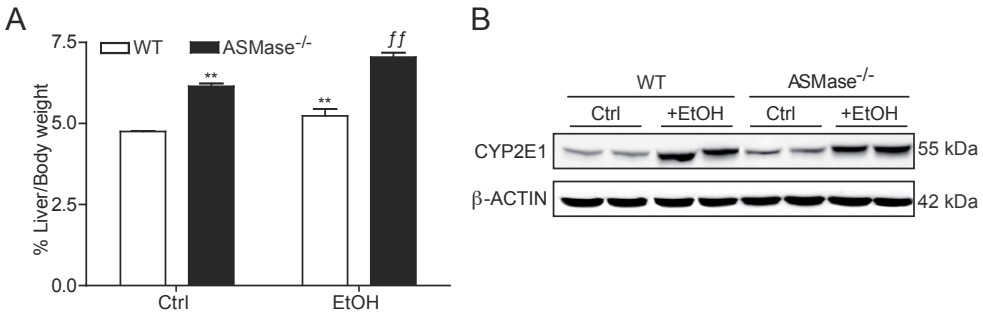

Figure 2.3. Liver to weight ratio and CYP2E1 expression after alcohol intake. (A) Liver vs. body weight ratio, and (B) CYP2E1 expression in control and ethanol fed WT and ASMase$^{-/-}$ livers. Results are expressed as mean ± SEM (**p<0.01 vs. control-fed WT mice and *ff* p< 0.01 vs. control-fed ASMase$^{-/-}$ mice)

Because ASMase is an intermediate in TNF signaling (García-Ruiz, Colell et al. 2003; Edelmann, Bertsch et al. 2011), we next examined the response of mice deficient in TNF receptors R1 and/or R2 to ethanol feeding. While TNFR1 or TNFR2 ablation exerted different effects in alcohol-induced hepatic lipid accumulation, both receptors were required for the accumulation of hepatic TG, FFA, SM and cholesterol in response to alcohol intake (Figure 2.4 A-D). Unlike ASMase, however, double TNFR1/R2 null mice

did not exhibit endogenous accumulation of SM or cholesterol. Thus, these findings indicate that the genetic elimination of ASMase prevents alcohol-induced macrosteatosis, but results in accumulation of SM and cholesterol.

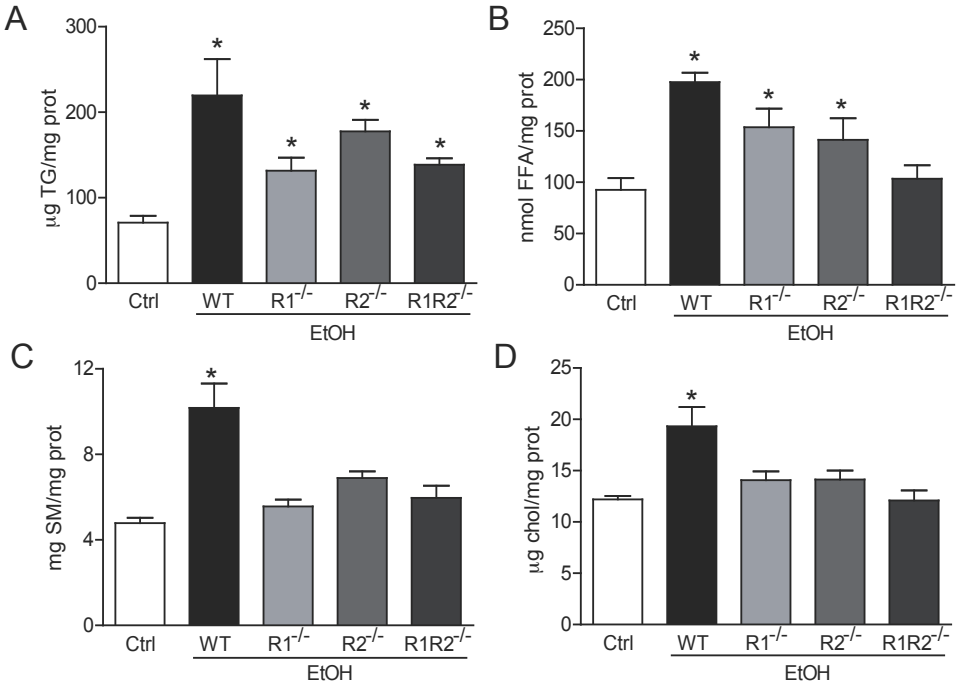

Figure 2.4. Alcohol-induced hepatic lipid accumulation in TNFR1, TNFR2 and TNFR1/2 null mice. Hepatic levels of (A) triglycerides, (B) free fatty acids, (C) sphingomyelin, and (D) cholesterol of WT, TNFR1, TNFR2 and TNFR1/R2 null mice after chronic ethanol intake. Results are expressed as mean ± SEM (*p<0.05 vs. control fed WT mice).

2.2. ASMase is required for alcohol-induced lipogenesis.

Since alcohol-induced lipogenesis contributes to hepatic steatosis, we next explored the effect of ASMase deficiency in the gene expression of lipogenic enzymes. As seen in figure 2.5, alcohol feeding to wild type mice increased the expression of the transcription factor *Srebp1c* and target enzymes including *Dgat2* and *Fas*, as well as *Srebp2*, which controls cholesterol homeostasis (Figure 2.5 A-D), consistent with previous findings (Wang, Yao et al. 2010). Interestingly, *Srebp1c*, *Dgat2* and *Fas* induction was blunted in ASMase$^{-/-}$ mice fed ethanol (Figure 2.5 A-C), consistent with the preceding findings in hepatic steatosis (Figure 2.1). However, ASMase null mice fed control diet exhibited increased expression of *Srebp2*, accounting for the intrinsic increase in hepatic cholesterol levels (Figure 2.5 D). Thus, these findings indicate that the absence of ASMase prevents the alcohol-induced expression of genes involved in lipogenesis, accounting for the observed protection from hepatic steatosis.

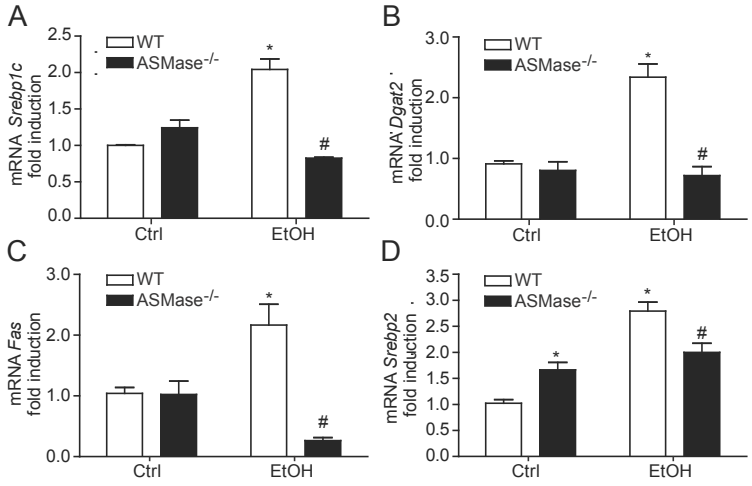

Figure 2.5. ASMase is required for alcohol-induced expression of lipogenic enzymes. Gene expression of (A) *Srebp1c*, (B) *Dgat2*, (C) *Fas*, and (D) *Srebp2* in control and ethanol-fed WT and ASMase$^{-/-}$ livers. Results are expressed as mean ± SEM (*p<0.05 vs. control-fed WT mice, #p<0.05 vs. ethanol-fed WT mice).

2.3. ASMase is required for alcohol-induced ER stress.

ER stress and UPR are critical adaptive mechanisms to metabolic alterations and stress in the liver, especially in the context of lipid metabolism. Alcohol intake has been shown to induce ER stress (Kaplowitz and Ji 2006), a mechanism that contributes to liver steatosis (Ozcan, Yilmaz et al. 2006).

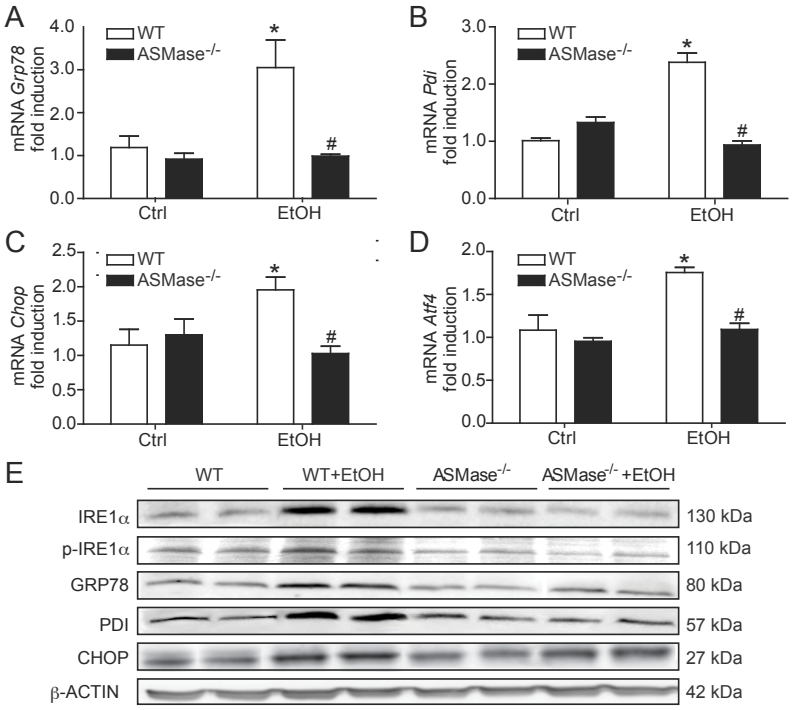

Figure 2.6. ASMase is required for alcohol-induced ER stress. Hepatic mRNA expression of (A) *Grp78*, (B) *Pdi*, (C) *Chop*, (D) *Atf4*, and (E) protein expression of IRE1α, phospho-IRE1α, GRP78, PDI and CHOP in control and ethanol-fed WT and ASMase$^{-/-}$ livers. Results are expressed as mean ± SEM (*p<0.05 vs. control-fed WT mice, #p<0.05 vs. ethanol-fed WT mice).

As expected, wild type mice exhibited increased up-regulation of ER stress markers, *Grp78*, *Pdi*, *Chop*, *Atf4* and IRE1α, both at the mRNA and protein level following ethanol feeding (Figure 2.6 A-E). However, these responses were prevented in ASMase$^{-/-}$ mice (Figure 2.6 A-E), suggesting a critical role for ASMase in alcohol-induced ER stress. Consistent with the resistance of double TNFR1/R2 knockout mice to alcohol-induced hepatic steatosis, mice deficient in TNFR1, R2 or double TNFR1/R2 knockout mice did not exhibit signs of alcohol-induced ER stress besides *Chop* in TNFR2$^{-/-}$ mice fed with ethanol diet (Figure 2.7 A-D).

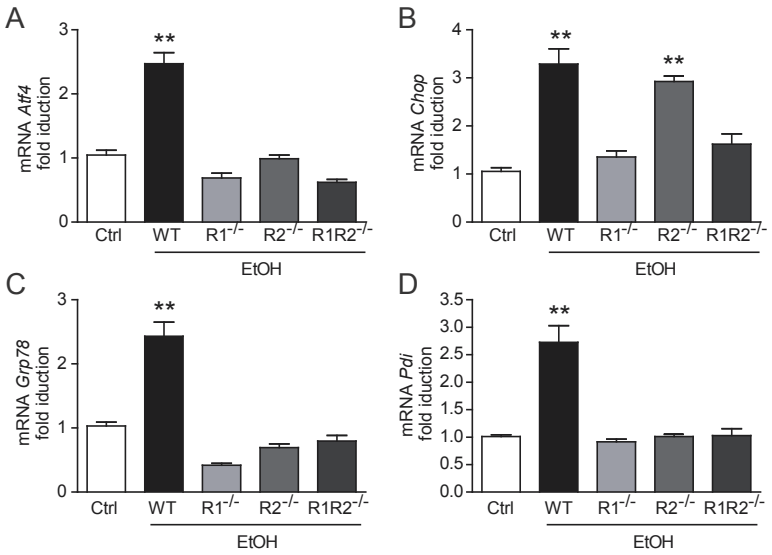

Figure 2.7. TNFR1, R2 or double TNFR1/R2 null mice do not exhibit alcohol-induced ER stress. Hepatic expression of (A) *Atf4*, (B) *Chop*, (C) *Grp78*, and (D) *Pdi* in WT, TNF-R1, TNF-R2 and TNFR1/R2 null mice after chronic ethanol intoxication. Results are expressed as mean ± SEM (*p<0.01 vs. control fed WT mice).

Moreover, in vivo treatment with tunicamycin induced liver ER stress and steatosis (Figure 2.8 A-B) both in wild type and ASMase knockout mice.

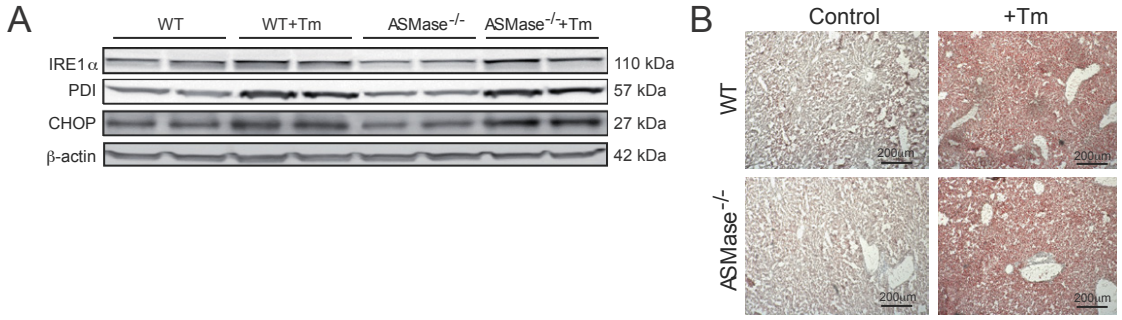

Figure 2.8. ASMase null liver responds to tunicamycin-induced ER stress and lipogenesis. (A) Expression of IRE1α, PDI and CHOP and (B) Oil-red staining of liver sections after tunicamycin challenge (Tm, 1 mg/kg, 24 hours) in WT and ASMase$^{-/-}$ mice.

Tm-induced steatosis increased by 2.5 the hepatic TG content in both wild type and ASMase deficient mice. These results suggest that resistance of ASMase$^{-/-}$ mice to alcohol-induced ER stress is not due to an inherent defect in ER stress response, and establish a cause-and-effect relationship between ER stress and steatosis. Thus, ASMase is critical for alcohol-induced ER stress.

2.4. Resistance of ASMase null mice to alcohol-induced ER stress is independent of hyperhomocysteinemia.

To explore putative mechanisms for the resistance of ASMase null mice to alcohol-induced ER stress, we analyzed metabolites of methionine cycle, in particular, homocysteine, which has been shown to contribute to alcohol-induced ER stress (Kaplowitz and Ji 2006). Plasma homocysteine concentration in wild type mice increased after ethanol feeding as expected and this increase was also observed in ASMase$^{-/-}$ mice (Figure 2.9 A). Moreover, while the hepatic SAM:SAH ratio was moderately lower (18%) in control-fed ASMase$^{-/-}$ mice, the decrease in SAM:SAH ratio induced by alcohol feeding was similar in wild type and ASMase$^{-/-}$ mice (Figure 2.9 B).

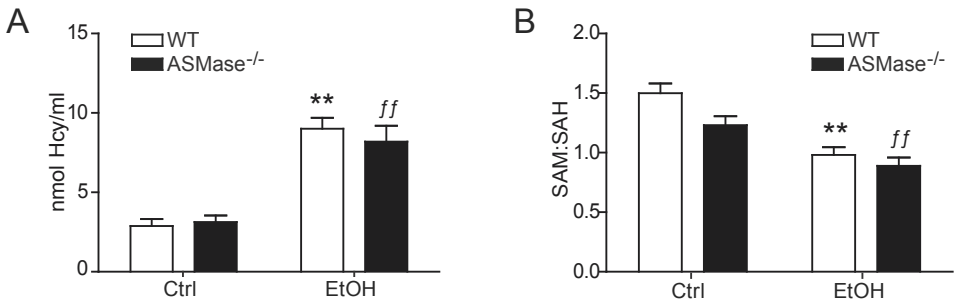

Figure 2.9. Methinonine metabolism is not altered in ASMase$^{-/-}$ mice. (A) Plasma homocysteine levels, and (B) hepatic SAM:SAH ratio in control and ethanol-fed WT and ASMase$^{-/-}$mice. Results are expressed as mean ± SEM (**p<0.01 vs. control-fed WT mice, *ff* p<0.01 vs. control-fed ASMase$^{-/-}$ mice).

Homocysteine levels are regulated by its remethylation to methionine via methionine synthase or betaine homocysteinemethyltransferase. Alcohol feeding decreased *Ms* mRNA levels in both wild type mice and ASMase null mice, but *Bhmt* expression remained unchanged in wild type and ASMase null mice regardless of alcohol feeding (Figure 2.10 A-B). In addition, expression of liver-specific *methionine adenosyltransferase 1A* (*Mat1A*) mRNA increased in wild type and ASMase null mice fed alcohol (Figure 2.10 C), and *cystathionine-β-synthase* (*Cbs*) expression increased in wild type but not in ASMase null

alcohol fed mice (Figure 2.10 D). The increase in homocysteine levels by alcohol intake was independent of TNFR1 or TNFR2 (Figure 2.10 E). Thus, these findings indicate that alcohol-mediated methionine metabolism disruption is independent of ASMase and that hyperhomocysteinemia does not contribute to ER stress induced by oral alcohol intake.

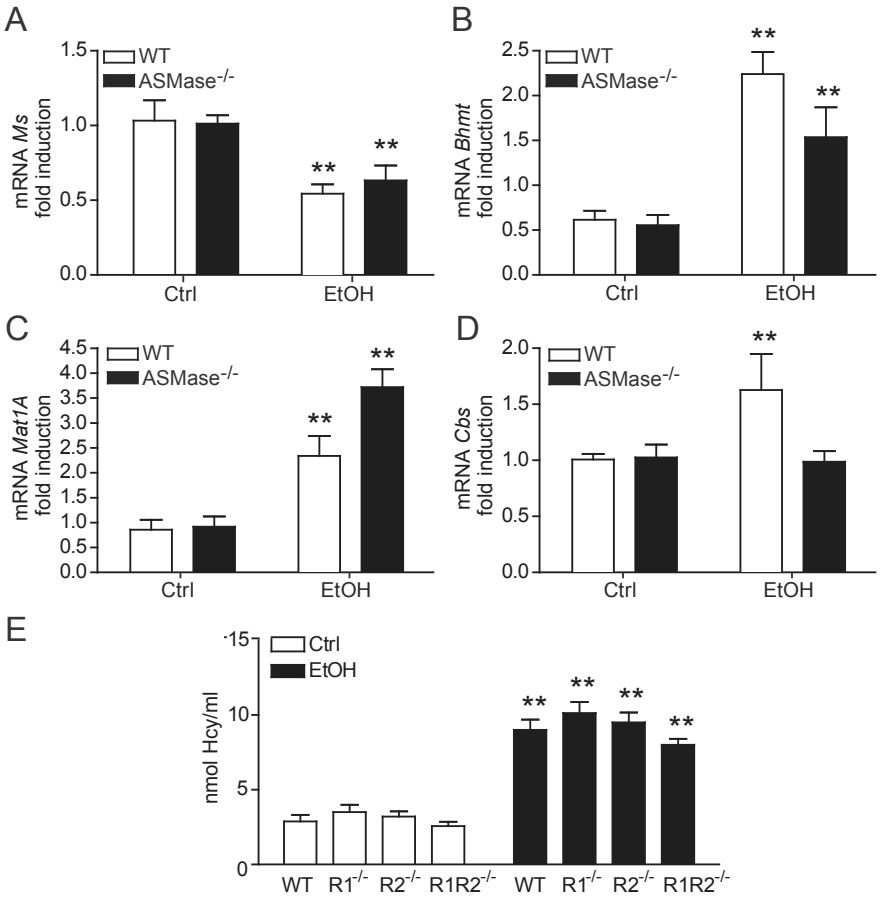

Figure 2.10. Effect of ethanol on the expression of enzymes of the methionine metabolism in wild type and ASMase$^{-/-}$ livers. Hepatic mRNA expression of (A) *methionine synthase* (*Ms*), (B) *betaine-homocysteine methyl-transferase* (*Bhmt*), (C) *methionine adenosyltransferase 1A* (*Mat1A*) and (C) *cystathionine-b-synthase* (*Cbs*) in control and ethanol-fed WT and ASMase$^{-/-}$ livers. (E) Plasma homocysteine levels in WT, TNF-R1, TNF-R2 and TNFR1/R2 null mice after chronic ethanol intoxication. Results are expressed as mean ± SEM (**p<0.01 vs. control-fed WT mice).

2.5. ASMase deficiency regulates ceramide metabolism.

Since ceramide metabolism has been linked to ER stress (Carracedo, Lorente et al. 2006; Spassieva, Mullen et al. 2009; Epstein, Kirkpatrick et al. 2012), we next examined whether ASMase deficiency was modifying ceramide metabolism. Alcohol feeding stimulated ASMase activity and increased total hepatic ceramide levels in wild type mice (Figure 2.11 A-B). However, ASMase null mice exhibited lower total ceramide levels

compared to wild type mice and were resistant to ceramide increase caused by alcohol intake (Figure 2.11 B), suggesting that ASMase is a critical source of alcohol-mediated ceramide generation.

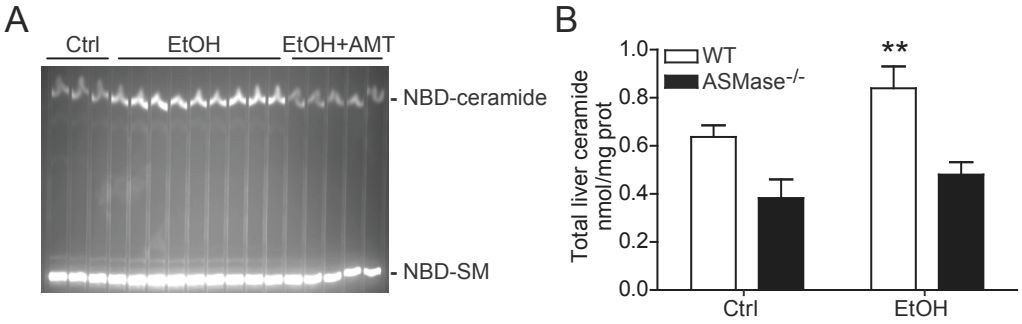

Figure 2.11. Hepatic ASMase activity and total ceramide levels. (A) Representative TLC of hepatic ASMase activity in WT ethanol-fed mice, and its inhibition after amitriptyline administration. (B) Total ceramide levels in the livers of control and ethanol-fed WT and ASMase$^{-/-}$ mice. Results are expressed as mean ± SEM (**p<0.01 vs. control-fed WT mice).

Moreover, transcriptional up-regulation of *Sms1* and *Sms2* by alcohol intake was similar in both wild type and ASMase null mice (Figure 2.12 A-B), accounting for the increase in SM by alcohol in wild type mice despite increased ceramide generation.

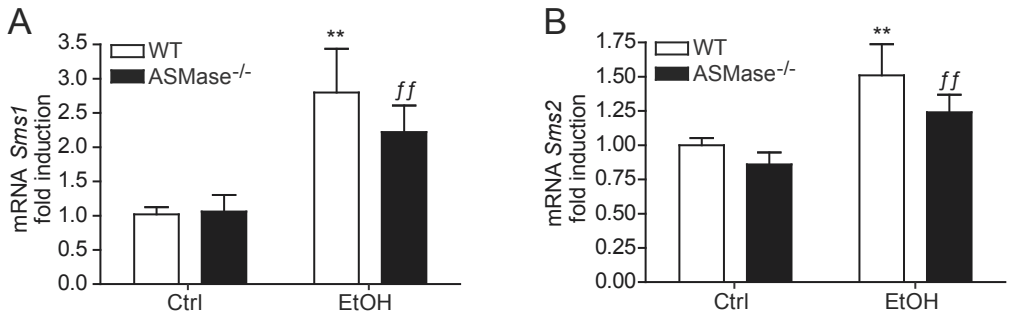

Figure 2.12. Hepatic sphingomyelin synthases gene expression. (A) *Sphingomyelin synthase-1* (*Sms1*), (B) *sphingomyelin synthase-2* (*Sms2*) gene expression in livers of control and ethanol-fed WT and ASMase$^{-/-}$ mice. Results are expressed as mean ± SEM (**p<0.01 vs. control-fed WT mice, *ff* p<0.01 vs. control-fed ASMase$^{-/-}$ mice).

Because ceramide can be metabolized into S1P, the antiapoptotic SL that promotes cell survival, after the consecutive action of ceramidases and sphingosine kinases, we determined the mRNA expression of *ACDase* as well as the S1P levels following alcohol feeding. *ACDase*, was unaffected by ethanol intake in wild type mice, and liver S1P concentration was not modified by alcohol consumption. However, ASMase null mice displayed increased expression of *ACDase* and S1P levels compared to wild type mice, and

these effects were unaffected following alcohol consumption (Figure 2.13 A-B). Thus, these findings indicate that ASMase is an important source of ceramide following alcohol intake and its absence modulates ceramide metabolism resulting in S1P generation.

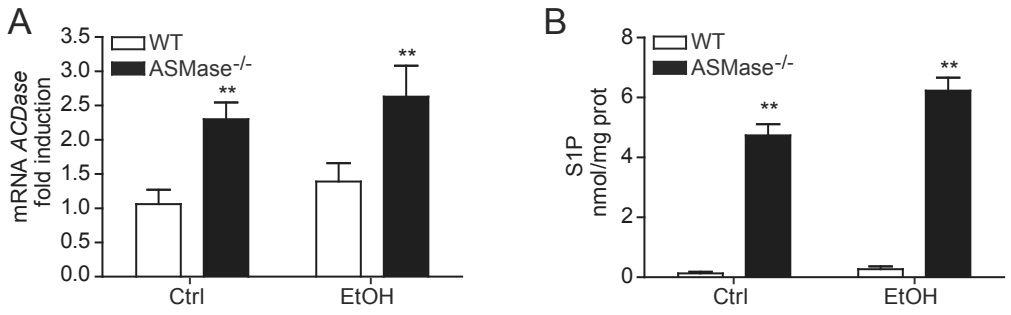

Figure 2.13. ASMase deficiency increases *Acid ceramidase* mRNA levels and S1P content in liver. (A) *ACDase* gene expression, and (B) S1P levels in the livers of control and ethanol-fed WT and ASMase$^{-/-}$ mice. Results are expressed as mean ± SEM (**p<0.01 vs. control-fed WT mice).

2.6. Exogenous ASMase induces ER stress and stimulates ER Ca^{2+} release.

To investigate the role of ASMase in alcohol-induced ER stress, we cultured human hepatocytes with exogenous human ASMase or NSMase from *Bacillus cereus* and determined expression of ER stress markers. Both ASMase and NSMase increase ceramide levels by 2 fold peaking by 60 minutes (García-Ruiz, Marí et al. 2000). Exposure of Hep G2 cells to human ASMase increased expression of *Chop* and *Grp78*, indicating the onset of ER stress (Figure 2.14 A-B). Moreover, the exposure of Hep G2 cells to NSMase from bacillus cereus failed to induce the expression of ER stress markers (Figure 2.14 A-B), indicating the specificity of SMases to cause ER stress, suggesting a link between endolysosomes and ER. Since ER Ca^{2+} stores regulate UPR and ER stress, we next determined ER Ca^{2+} homeostasis in Hep G2 cells in response to exogenous ASMase. Cells were loaded with the fluorescent calcium indicator Fluo-4 AM, switched to calcium-free medium and exposed to thapsigargin, a specific inhibitor of the ER calcium pump SERCA. Addition of thapsigargin to control hepatocytes resulted in release of ER Ca^{2+} stores towards the cytosol. However, exposure to exogenous ASMase decreased the thapsigargin-stimulated Ca^{2+} release, indicating lower ER Ca^{2+} storage (Figure 2.14 C-D). Thus, these findings suggest that alcohol-induced ASMase activation induces ER stress, at least in part, by disrupting ER Ca^{2+} homeostasis.

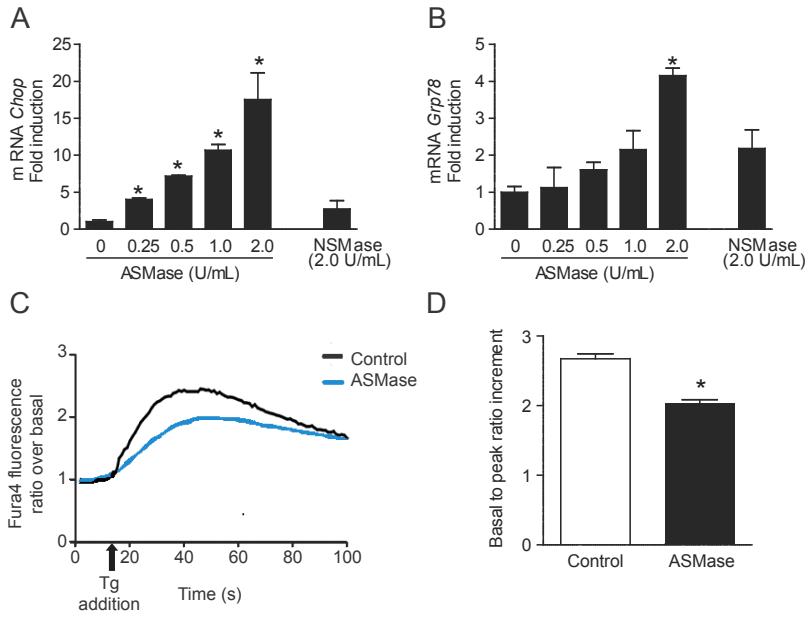

Figure 2.14. Exogenous ASMase induces ER stress. (A) *Chop* and (B) *Grp78* gene expression of Hep G2 cells treated for 18h with exogenous human ASMase or bacterial NSMase. (C) Representative fluorescence tracings of Fluo4-labeled Hep G2 cells exposed to ASMase (1U/ml) for 18 hours. Thapsigargin (Tg, 1μM) was added at the time indicated and fluorescence was recorded by confocal microscopy. (D) Quantification of basal to peak Fluo-4 fluorescence ratio after addition of Tg. Results are expressed as mean ± SD of n=4 individual experiments. *p<0.05 vs control cells.

2.7. ASMase knockout mice exhibit defective mitochondrial cholesterol trafficking.

Since wild type mice and ASMase null mice exhibited increased hepatic free cholesterol content upon alcohol feeding (Figure 2.2 A, C), we next examined its trafficking to mitochondria, as this process has been shown to regulate cell death and steatohepatitis (Marí, Caballero et al. 2006). Mitochondrial cholesterol trafficking was observed in cultured hepatocytes from alcohol-fed wild type mice as cholesterol (filipin staining in red) and mitochondria (cytochrome c staining in green) colocalized in confocal microscopy imaging (Figure 2.15 A); however, this process was defective in hepatocytes from ASMase$^{-/-}$ mice fed alcohol (Figure 2.15 B). To account for this unexpected finding, we analyzed expression of proteins known to regulate mitochondrial cholesterol homeostasis, including StAR and MLN64. While alcohol increased hepatic expression of *StAR* in wild type mice, this response was suppressed in ASMase$^{-/-}$ mice (Figure 2.16 A). *Mln64* expression was similar in both genotypes regardless of the type of diet (Figure 2.16 B). Moreover, we determined *caveolin-1* expression, as this protein has recently been uncovered for its ability to regulate mitochondrial cholesterol (Bosch, Marí et al. 2011).

Endogenous expression of *caveolin-1* was similar for wild type and ASMase$^{-/-}$ mice, however alcohol feeding increased mRNA levels of ASMase$^{-/-}$ mice (Figure 2.16 C).

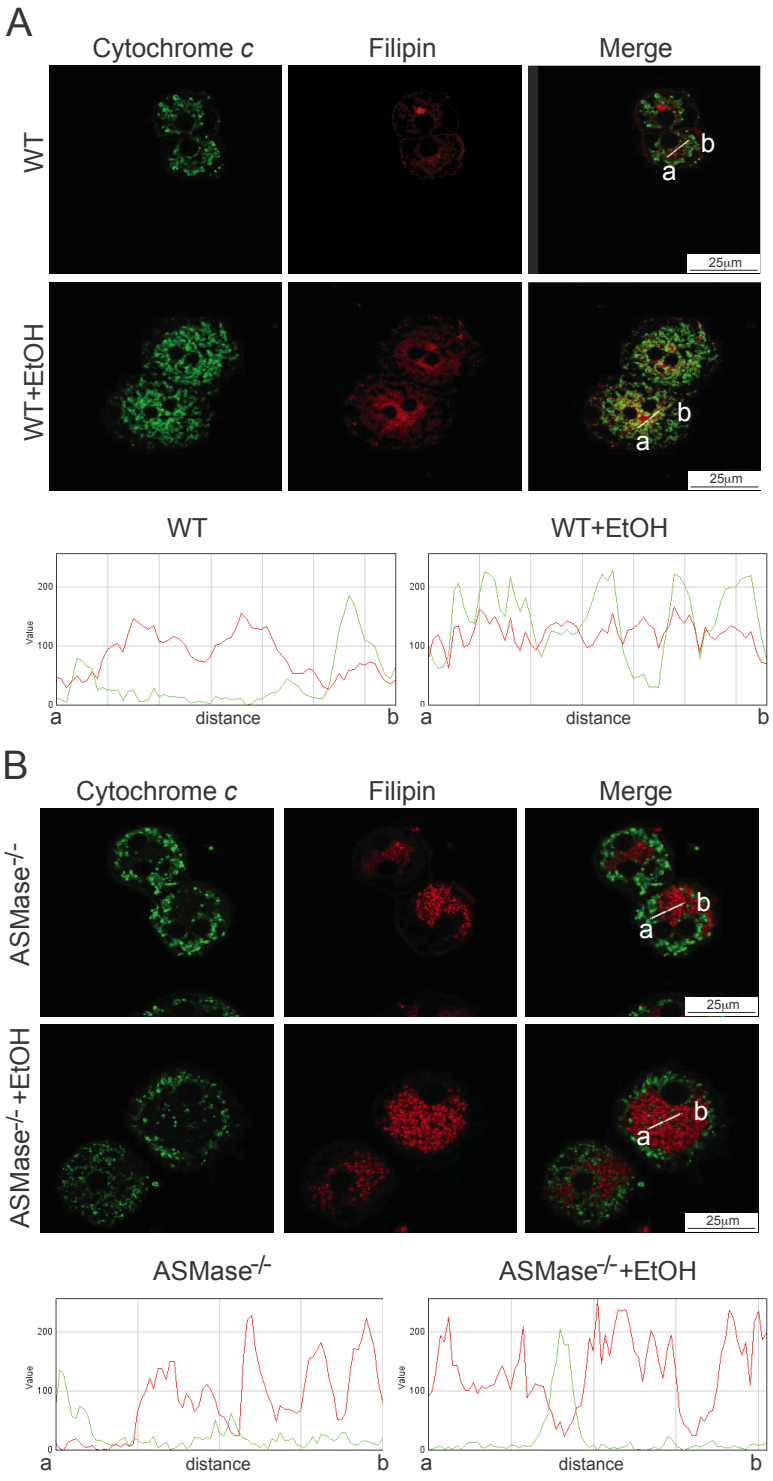

Figure 2.15. Ethanol-induced mitochondrial cholesterol loading is blunted in ASMase$^{-/-}$ primary mouse hepatocytes. Fluorescence immunocytochemistry of mitochondria (cytochrome c) and free cholesterol (filipin) in hepatocytes from control and ethanol-fed (A) WT, and (B) ASMase$^{-/-}$ mice.

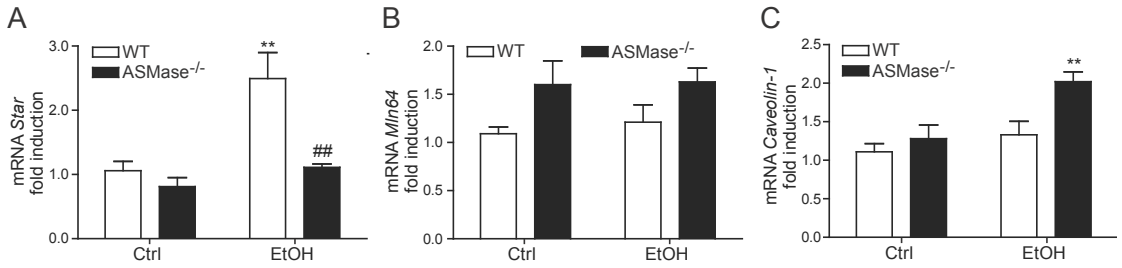

Figure 2.16. Gene expression of mitochondrial cholesterol homeostasis related proteins. mRNA expression of (A) *Star*, (B) *Mln64*, and (C) *Caveolin-1* in livers of control and ethanol-fed WT and ASMase$^{-/-}$ mice. Results are expressed as mean ± SEM (**p<0.01 vs. control-fed WT mice, ##p<0.01 vs. WT ethanol-fed mice).

Consistent with these findings, alcohol feeding increased cholesterol loading in mitochondria from wild type but not ASMase null mice, protecting ASMase$^{-/-}$ mice from the depletion of mitochondrial GSH pool (Figure 2.17 A-B). These results uncover a previously unrecognized role for ASMase in the regulation of mitochondrial cholesterol trafficking via StAR expression.

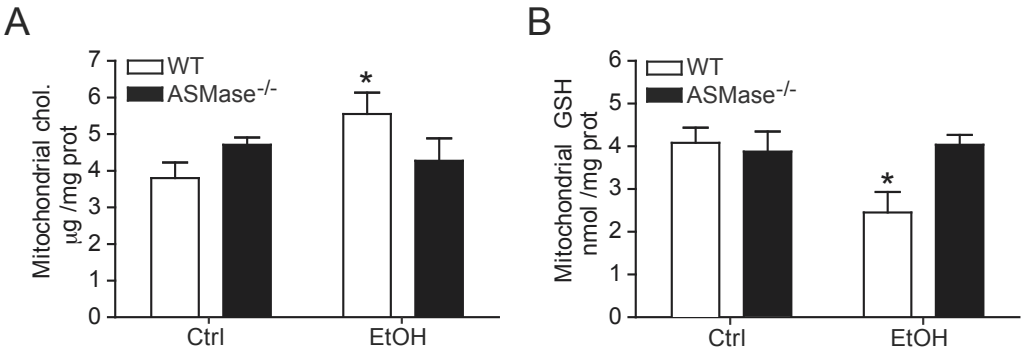

Figure 2.17. Alcohol-induced mitochondrial cholesterol loading and mGSH depletion does not occur in ASMase$^{-/-}$ livers. Hepatic (A) mitochondrial cholesterol and (B) mitochondrial glutathione in control and ethanol-fed WT and ASMase$^{-/-}$ mice. Results are expressed as mean ± SEM (*p<0.05 vs. control-fed WT mice).

To explore the relationship between ER stress and StAR, we examined the effect of Tm in StAR expression in Hep G2 cells. In addition to the induction of ER stress markers, Tm up-regulated evels of *Srebp2* and *StAR* (Figure 2.18 A-B). ER stress can be relieved by using chemical chaperones like Tauroursodeoxycholic acid (TUDCA) (Ozcan, Yilmaz et al. 2006). TUDCA pretreatment abrogated Tm-induced expression of both *Srebp2* and *StAR* in Hep G2 cells (Figure 2.18 A-B).

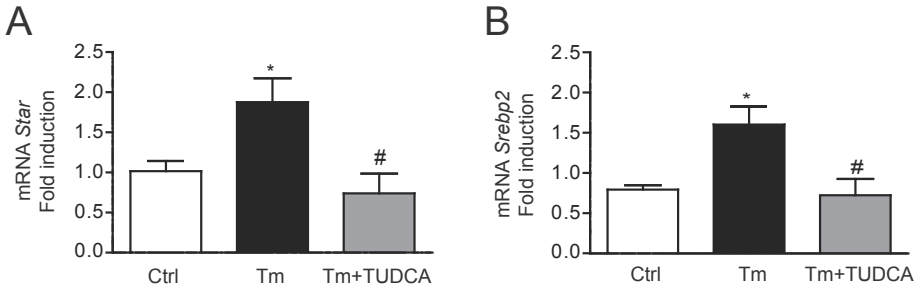

Figure 2.18. ER stress regulation of cholesterol synthesis and trafficking related genes in Hep G2 cells. (A) *Star* and (B) *Srebp2* gene expression of Hep G2 cells treated with tunicamycin (Tm) with or without TUDCA pre-treatment. Results are expressed as mean ± SD of 4 individual experiments. *p<0.01 vs. control , #p<0.01 vs. Tm-treated cells.

Genes involved in cholesterol metabolism are activated by SREBPs, particularly SREBP2. In order to confirm that StAR is an ER stress but not SREBP2 regulated gene, we fed mice a high cholesterol diet for three days. As expected, HCD feeding decreased gene expression of SREBP2 target gene *Hgmcr* as well as *Srebp2* itself but did not affect *Star* expression (Figure 2.19 A-C). Thus, these results uncover a previously unrecognized role for ASMase in the regulation of mitochondrial cholesterol trafficking via StAR expression.

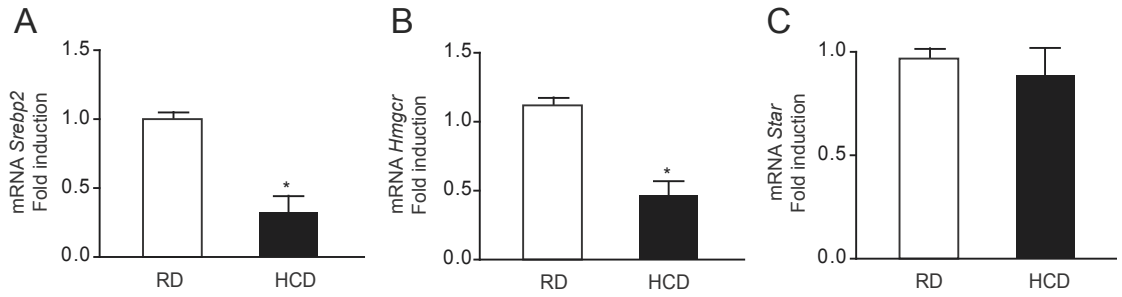

Figure 2.19. High cholesterol diet regulation of hepatic *Srebp2*, *Hmgcr* and *Star* gene expression. (A) *Srebp2*, (B) *Hmgcr* and (C) *Star* gene expression in livers from wild type mice exposed to either RD or HCD. Results are expressed as mean ± SD of 3 individual animals. *p<0.05 vs. WT mice fed RD.

2.8. ASMase ablation blunts alcohol-induced liver injury and susceptibility to LPS and ConA.

Alcohol-induced fatty liver is believed to sensitize to secondary hits, thereby accounting for the hepatocellular damage observed in ALD. To examine the contribution of ASMase to alcohol-induced liver injury and sensitization to circulating and cell-bound TNF, we examined liver damage in wild type and ASMase knockout mice following alcohol feeding with or without a low dose LPS or concanavalin-A. Endogenous liver damage to alcohol

intake was modest in wild type mice and reduced in ASMase$^{-/-}$ mice as revealed by lower ALT levels and histology analyses (Figure 2.20 A-C). However, alcohol feeding sensitized wild type mice to LPS and Con A-mediated liver damage, and this outcome was prevented in ASMase$^{-/-}$ mice (Figure 2.20 A-C).

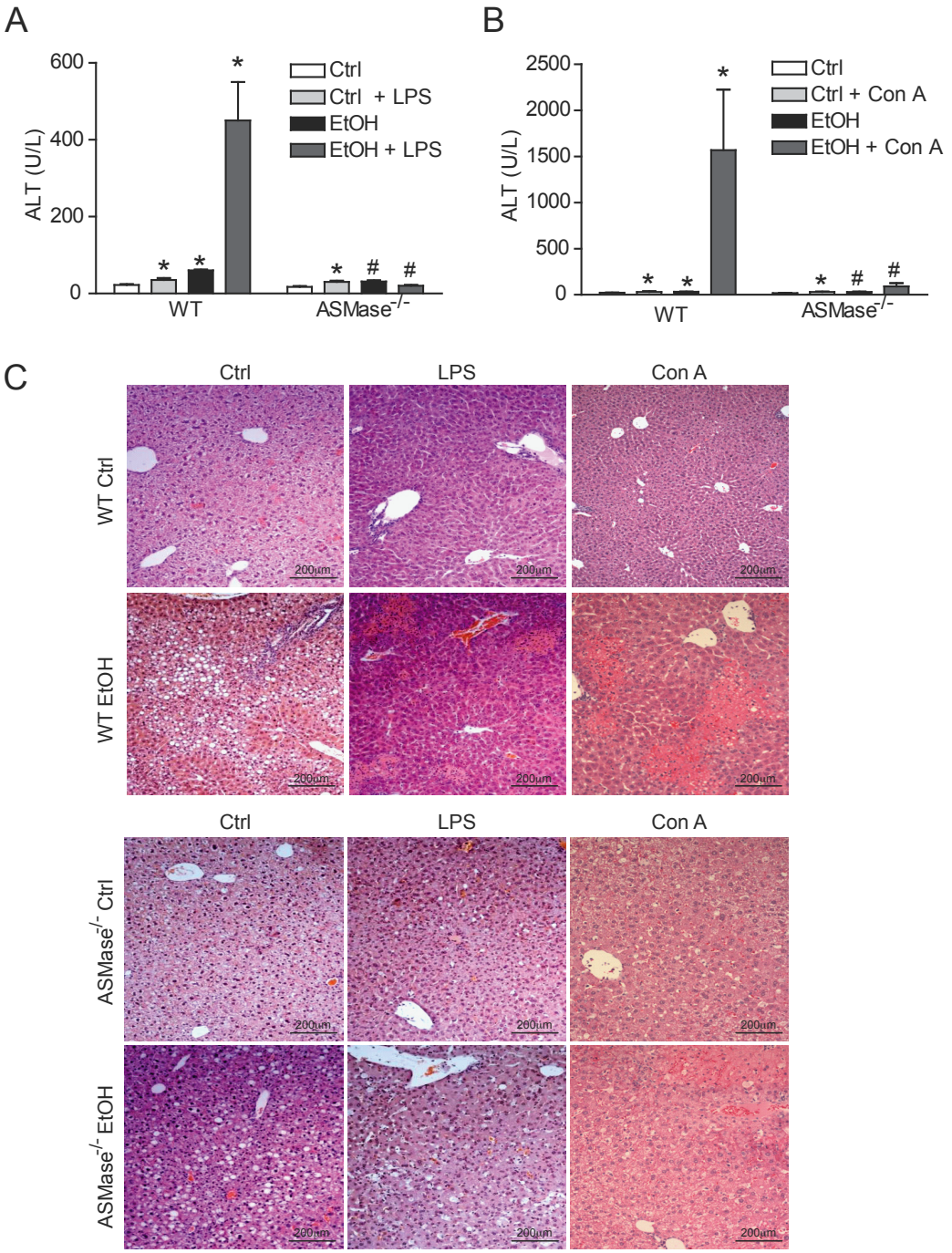

Figure 2.20. ASMase deficiency prevents alcohol-induced liver injury and susceptibility to LPS and Concanavalin A. Serum ATL in control and ethanol-fed WT and ASMase$^{-/-}$ mice challenged with (A) 5mg/Kg LPS i.p. or (B) 0.5mg/Kg ConA i.v. for 24h. (C) H&E staining of liver control and ethanol-fed WT and ASMase$^{-/-}$ mice challenged with LPS or Con A. Results are expressed as mean ± SEM (*p<0.05 vs. control-fed mice, #p<0.05 vs. same-treatment in WT mice).

Moreover, consistent with these findings cultured hepatocytes from wild type but not ASMase knockout mice fed alcohol exhibited enhanced susceptibility to TNF-induced cell death (Figure 2.21).

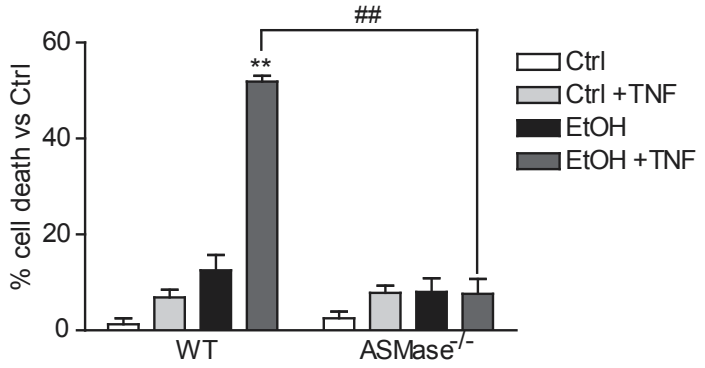

Figure 2.21. ASMase deficiency protects hepatocytes from alcohol-induced sensitization to TNF-induced cell death. Hepatocyte cell death determined by Trypan blue exclusion after TNF challenge (280ng/ml, 16h) in control and ethanol-fed WT and ASMase$^{-/-}$ mouse hepatocytes. Results are expressed as mean ± SEM (**p<0.01 vs. control-fed WT hepatocytes, ##p<0.01 vs. EtOH+TNF treated WT hepatocytes).

We next addressed the contribution of TNFR1 and TNFR2 to alcohol-induced susceptibility to LPS and ConA. In agreement with previous studies reporting the sensitization of galactosamine to ConA-induced liver injury (Maeda, Chang et al. 2003), TNFR1 knockout mice were resistant while TNFR2 deficiency ameliorated ConA-mediated liver damage following alcohol feeding, with similar findings observed for LPS (Figure 2.22 A-B). Thus, these findings indicate a critical role for ASMase in alcohol-induced liver damage and sensitization to circulating and cell-bound TNF.

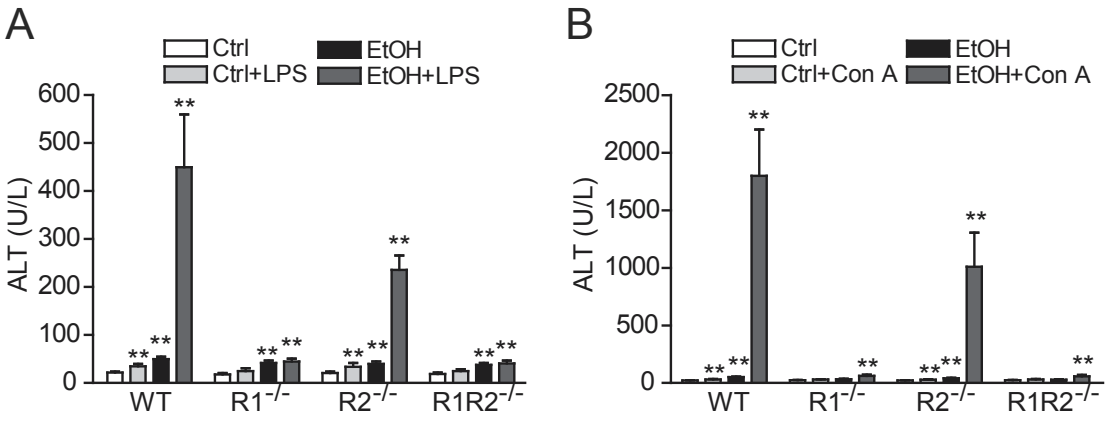

Figure 2.22. TNFR1-deficiency prevents alcohol-induced liver injury and susceptibility to LPS and Con A. Serum ALT in control and ethanol-fed WT, TNFR1, TNFR2, and TNFR1/R2 null mice challenged with (A) LPS (5mg/kg, 24h) or (B) Con A (0.5mg/kg, 24h). Results are expressed as mean ± SEM (**p<0.01 vs. control-fed mice).

2.9. Pharmacologic ASMase inhibition protects against alcohol-induced hepatic ER stress and TNF susceptibility.

To examine the potential relevance of these findings for ALD, we treated alcohol-fed mice with amitriptyline. Mice were fed alcohol for the first week and amitriptyline was administered daily i.p. for the last 3 weeks of alcohol intake. As seen, this approach significantly inhibited (>80%) the activation of ASMase by alcohol feeding (Figure 2.11 A). Importantly, compared to control alcohol-fed mice, amitriptyline treatment decreased alcohol-induced accumulation of TG as seen in the H&E staining decreased hepatic macrosteatosis (Figure 2.23 A). Moreover, amitriptyline ameliorated the alcohol-induced liver injury and the sensitization LPS (Figure 2.23 B).

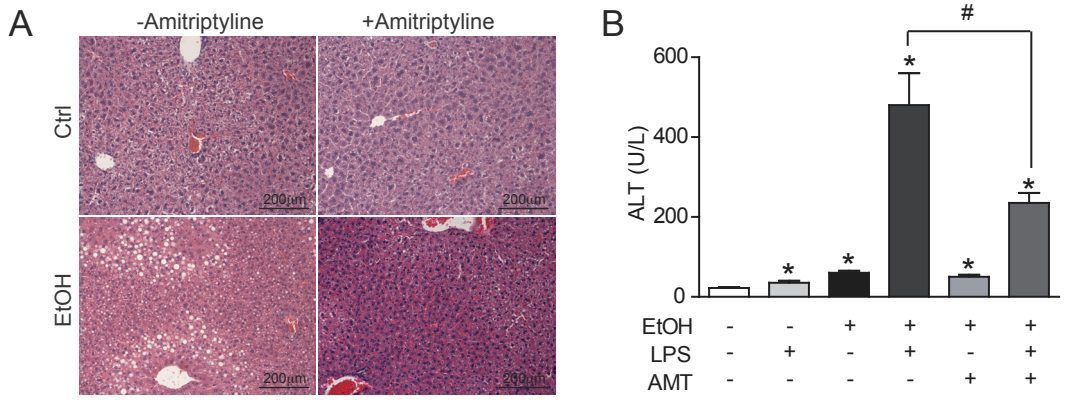

Figure 2.23. ASMase inhibition protects against alcohol-induced liver damage, steatosis and LPS susceptibility. (A) Hepatic H&E staining and (B) serum ALT after LPS challenge in control and amitriptyline-treated mice. Results are expressed as mean ± SEM (*p<0.05 vs. untreated mice, #p<0.01 vs ethanol-fed and LPS-treated mice).

Furthermore, amitriptyline also decreased alcohol-induced activation of ER stress markers (Figure 2.24). Thus, these findings indicate that the pharmacologic inhibition of ASMase reproduces the effects of genetic ablation of ASMase on symptoms of alcohol-induced liver injury.

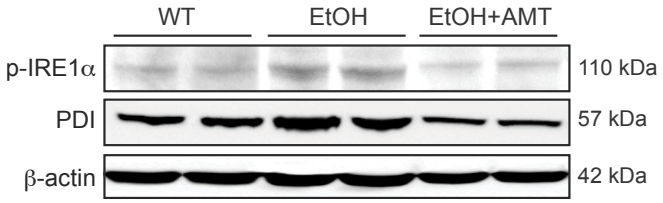

Figure 2.24. ASMase inhibition protects from alcohol-induced ER stress. Hepatic expression of phospho-IRE1α and PDI in control WT mice, ethanol-fed WT mice and amitriptyline treated alcohol-fed WT mice.

In addition, since liver regeneration can modulate ALD progression, we next asked whether the lack of ASMase affects the ability of the liver to regenerate following partial hepatectomy (PH). As seen, hepatocyte proliferation examined by PCNA staining and final liver mass 10 days after PH were similar between wild type mice and ASMase null nice (Figure 2.25 A-B). Thus, these findings show that ASMase deficiency does not compromise liver regeneration further supporting the potential relevance of targeting ASMase in human ALD.

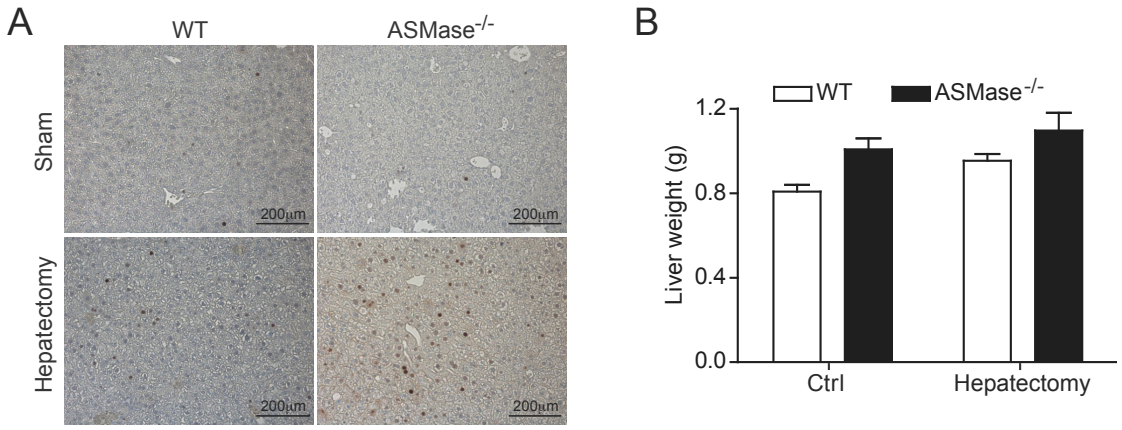

Figure 2.25. Liver regeneration in ASMase null mice. (A) PCNA immuno-staining and (B) liver weight of WT and ASMase$^{-/-}$ mice after partial hepatectomy.

2.10. Alcoholic hepatitis patients exhibit increased expression of ASMase, ER stress markers and StAR.

Given the above results, we next addressed the expression status of ASMase in ALD. For this purpose, we compared ASMase mRNA levels in liver biopsies from patients with acute alcoholic hepatitis (AH), whose characteristics are shown in Table 2.1.

	Control (n=13)	Alcoholic Hepatitis (n=17)
Age (Years)	56 (40-73)	50.14 (38-56)
AST (U/L)	20.5 (20-22)	104.35 (3-222)
ALT (U/L)	23.25 (13-32)	38.5 (26-90)
Bilirrubin (mg/dL)	0.4 (0.3-0.6)	11.71 (4-21)
γGT (U/L)	101.6 (48-210)	337.75 (123-1100)

Table 2.1. Clinical and analytical characteristics of patients with acute alcoholic hepatitis. Numeric data is shown as median (interquartile range [IQR] 25-75) and categorical/nominal data in count. AST: Aspartate-aminotransferase; ALT: Alanine-aminotransferase; γGT: γ-glutamyltransferase.

Compared to control subjects, patients with AH exhibited a 3-4-fold increase in the expression of ASMase as well as ER stress markers (Figure 2.26 A-C). Moreover, StAR mRNA levels increased 7 fold in liver biopsies from AH patients with respect to samples from control subjects (Figure 2.26 D). Thus, these findings support the potential relevance of ASMase in ALD.

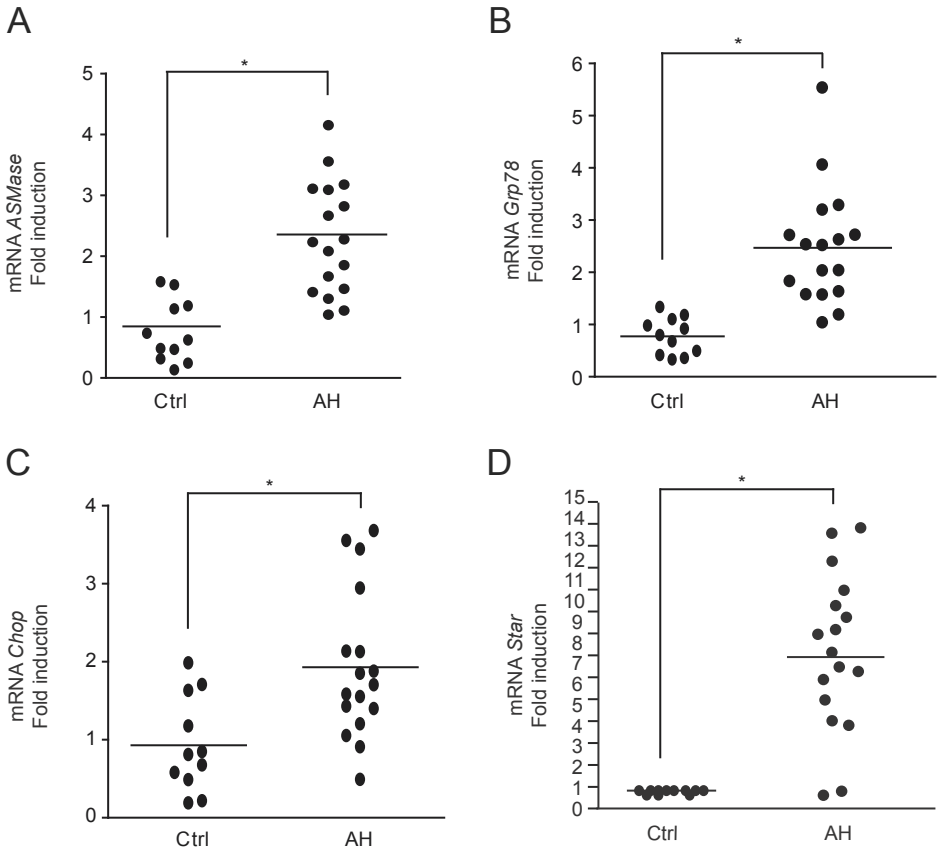

Figure 2.26. ASMase, ER stress markers and StAR expression in liver samples from patients with alcoholic hepatitis. Gene expression of (A) *ASMase*, (B) *Grp78*, (C) *Chop* and (D) *Star* by real time PCR analysis. Control group n=13 and AH group n=17 (*p<005 vs. control subjects).

DISCUSSION

Fatty liver disease is one of the most prevalent forms of liver disease worldwide, which encompasses both ALD and NAFLD. Although the etiology of both is different they share common mechanisms and biochemical features, including hyperglycemia, hyperinsulinemia, insulin resistance, hepatic steatosis and liver injury, which can progress to more advanced stages characterized by inflammation and fibrosis. The role of ASMase in NAFLD and ALD has been only examined in the context of glucose homeostasis and hepatic steatosis. The overall goal of the present thesis is to examine the relationship between ASMase and ER stress as this is a key mechanism in the regulation of insulin signaling and lipid metabolism resulting in activation of lipogenic pathways and hepatic steatosis.

1. Role of ASMase in NAFLD

Ceramide has been brought to the central stage of insulin resistance and T2DM (Chavez and Summers 2012). However, the role of ASMase in NAFLD has been less studied. To the best of our knowledge, only two studies focused on the role of ASMase in glucose homeostasis and hepatic steatosis (Deevska, Rozenova et al. 2009; Osawa, Seki et al. 2010). This thesis reports for the first time the role of ASMase in key aspects of diet-induced NAFLD, such as hepatic ER stress, autophagy, liver injury and LPS susceptibility.

An important feature of NAFLD is its association with insulin resistance and hepatic steatosis. Unlike the observations in ASMase/LDL receptor double knockout (ALDLRDKO) mice (Deevska, Rozenova et al. 2009), findings in this thesis indicate that HFD-fed ASMase$^{-/-}$ mice exhibit glucose intolerance and reduced insulin sensitivity upon GTT and ITT tests, in line with a recent study using adenoviral ASMase overexpression in db/db mice (Osawa, Seki et al. 2010). The impaired insulin sensitivity of ASMase$^{-/-}$ mice did not reflect defective hepatic parenchymal insulin signaling as insulin infusion into the portal vein phosphorylated IRβ subunit and Akt to a similar degree observed in wild type mice. Although, these findings suggest that ASMase is dispensable for hepatic insulin-mediated IRβ and Akt phosphorylation, they do not discard that ASMase may play a role in hepatic glucose transport specially knowing the potential

impact of FC and SM accumulation in ASMase$^{-/-}$ membranes that could affect its physic properties, specifically microdomains, and as a result influence membrane transporters translocation or activity (Liu, Leffler et al. 2004; Yuan, Hong et al. 2007; Sánchez-Wandelmer, Dávalos et al. 2009; Stancevic and Kolesnick 2010). Nonetheless, it is worth considering that ASMase ablation prevents HFD-induced fatty liver and TG accumulation, and hence it is conceivable that unimpaired hepatic insulin signaling may be due to decreased TG seen in ASMase$^{-/-}$ mice. This possibility suggests that glucose intolerance and insulin insensitivity of ASMase$^{-/-}$ mice may reflect defects in extra-hepatic tissues (e.g. adipose and muscle).

Another differential feature of our findings in ASMase$^{-/-}$ mice with respect to ALDLRDKO mice centers on ceramide homeostasis. While deletion of ASMase in the LDL receptor null background increased endogenous hepatic ceramide levels due to *de novo* synthesis in the ER by SPT activation (Deevska, Rozenova et al. 2009), ASMase deficiency *per se* results in decreased endogenous hepatic ceramide content, which is in agreement with previous findings (Osawa, Seki et al. 2010). Furthermore, we provide evidence that HFD increases liver ceramide via ASMase. Evidence in support for this relationship is dual. First, HFD induces gene expression of ASMase; and second, ASMase$^{-/-}$ mice are resistant to diet-mediated increase in hepatic ceramide levels. Moreover, results presented in this thesis indicate that ASMase is a key enzyme in ceramide metabolism since its deficiency affects gene expression of other enzymes of SL metabolism including ACDase and modulates hepatic SL profile reflected in accumulation of SM and S1P and decreased ceramide content. Cer/S1P ratio has been postulated as a biological rheostat, which controls cell fate (Brocklyn and Williams 2012). ASMase$^{-/-}$ livers display decreased Cer/S1P ratio, which according to Cer/S1P rheostat model would be expected to activate survival pathways resulting in protection against HFD-mediated liver injury.

The differential mode of ceramide generation between ALDLRDKO mice and our study is of relevance. *De novo* synthesized ceramide has been shown to play a critical role in glucocorticoids and diet-induced insulin resistance via inhibition of Akt activation (Holland, Brozinick et al. 2007). Moreover, hepatic ASMase-induced ceramide generation via adenoviral-mediated overexpression resulted in the activation of Akt and

glycogen synthase kinase-3β expression (Osawa, Seki et al. 2010). This outcome was accompanied by accumulation of S1P, which is known to activate Akt in hepatocytes (Osawa, Seki et al. 2010). Interestingly, we observed that ASMAse ablation also increased endogenous hepatic S1P levels, and this event is consistent with our data of enhanced insulin-mediated Akt phosphorylation in hepatocytes from ASMase$^{-/-}$ mice. Although HFD also increased S1P in wild type mice this response was less dramatic than that observed in ASMase$^{-/-}$ mice and suggests a threshold phenomenon for S1P to potentiate insulin-induced Akt phosphorylation. In parallel with enhanced hepatic S1P levels, ASMase$^{-/-}$ mice also displayed increased expression of ACDase, which is expected to provide sphingosine for its phosphorylation by sphingosine kinases, in particular Sphk2. Previous findings in C2C12 myotubes showed how ACDase overexpression prevented the inhibitory effects of FFAs on insulin signaling by decreasing ceramide content and increasing sphingosine levels (Chavez, Holland et al. 2005), thus supporting our findings in the liver. Finally, ACDase overexpression in ASMase absence also opens a door that invites to speculate about a potential regulation between these two lysosomal hydrolases in diet-induced obesity models of disease.

Due to resistance of ASMase null mice to diet-induced hepatic macrovesicular steatosis; independently of the nutritional approach used (e.g. HFD or MCD feeding), we investigated potential underlying mechanisms. While ER stress stimulates lipogenesis via activation of ER-based transcription factor SREBP1c, autophagy has emerged as an alternative mechanism regulating intracellular lipid stores (macrolipophagy). Consequently, impaired hepatic autophagy could contribute to intracellular lipid accumulation and hepatic steatosis (Singh, Kaushik et al. 2009).

Hepatic autophagy markers of ASMase null mice showed decreased levels of ATG7, suggesting that ASMase regulates proximal autophagic events. ATG7 is a critical gene in the organization of the autophagic process, including the conjugation of LC3B to PE at autophagosomal membranes (Ravikumar, Sarkar et al. 2010). However, decreased ATG7 levels were accompanied by a paradoxical increased lipidation of LC3BII. Whether increased basal LC3BII/LC3BI reflects an adaptive mechanism to decreased ATG7 expression remains to be further explored. Nevertheless, to establish if increased LC3BII levels in ASMase null mice reflect increased autophagic flux or decreased processing and

degradation at a lysosomal level, we incubated hepatocytes with autophagy inducer rapamycin and/or autophagy inhibitor chloroquine. Estimation of LC3BII levels in these conditions indicated that rapamycin-induced LC3BII degradation in the absence of ASMase reflects decreased lysosomal degradation and not increased autophagic flux. As a potential mechanism contributing to these observations, we examined lysosomal cholesterol content, and hypothesized that its accumulation may impair autophagosome/lysosome fusion and hence overall autophagy. Consistent with this possibility, we observed increased p62 levels in ASMase deficient hepatocytes compared to wild type hepatocytes. In line with this, confocal microscopy confirmed colocalization of FC with lysosomes in ASMase null hepatocytes, a key factor of autophagy impairment due to defective lysosome-autophagosome fusion, acidification and final proteolysis (Elrick, Yu et al. 2012). ASMase phenotype resembles Niemann Pick C fibroblasts phenotype, where unsterified cholesterol and SLs accumulate within lysosomes and regulate autophagy by increasing Beclin1 and LC3B II expression, thus promoting autophagosome maturation, while inhibiting autophagy at a lysosomal level due to impaired proteolysis (Lieberman, Puertollano et al. 2012). In addition, findings in a cell model of NPC induced by U18666A, which causes lysosomal cholesterol accumulation, results in increased LC3BII levels due to decreased autophagosome degradation (Appelqvist, Nilsson et al. 2011). All together, these results indicate that increased autophagy is not the mechanism responsible for ASMase deficiency protection from hepatic steatosis.

As an alternative mechanism involved in regulation of hepatic steatosis in ASMase null mice fed HFD, we next focused on hepatic ER stress. We observed that ASMase$^{-/-}$ mice are resistant to HFD-induced ER stress, accounting for the decreased expression of lipogenic pathways and transcription factor *Srebp1c*. Importantly, we also discarded that the defective ability of ASMase$^{-/-}$ mice to increase ER stress by HFD is mediated by an inherent defect of the ER, as ASMase$^{-/-}$ mice undergo the expected ER stress induced by tunicamycin or the bacterial AB5 subtilase cytotoxin (Paton, Beddoe et al. 2006). Thus, these results strongly suggest that ASMase is required for HFD-induced liver macrosteatosis by stimulating ER stress and subsequent activation of lipogenesis pathways (Figure D1). Since hepatic steatosis and ER stress are reciprocally regulated, it is conceivable that the reduced diet-induced ER stress in ASMase null mice may be a

consequence rather than a cause of decreased hepatic steatosis. However, exploiting the fact that ASMase null mice ER appear functional and able to sense stress, we treated ASMase null mice with Tm *in vivo*. As expected, Tm induced ER stress markers up-regulation as well as hepatic steatosis in ASMase$^{-/-}$ mice, arguing that resistance to diet-induced ER stress is the primary mechanism of decreased hepatic steatosis in ASMase null mice.

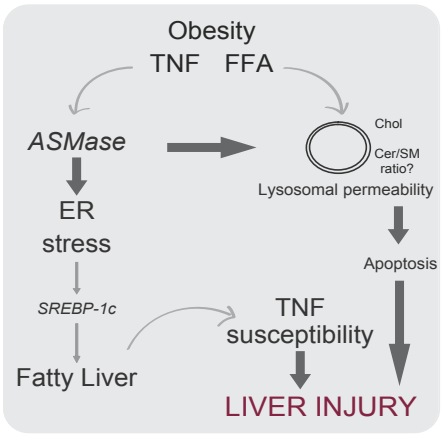

Figure D1. ASMase role in NAFLD model.

Finally, we focused on the role of ASMase in hepatocellular injury during HFD. Our data indicate a critical role for ASMase in this cardinal feature of NAFLD, as ASMase$^{-/-}$ mice exhibit less liver injury compared to wild-type mice, and become resistant to HFD-mediated sensitization to LPS-induced liver damage. These data are consistent with the role of ASMase as a critical intermediate in death receptor-induced cell death (García-Ruiz, Colell et al. 2003; Marí, Colell et al. 2004; Dumitru and Gulbins 2006), and suggest that targeting ASMase may be of relevance in NAFLD. Moreover, this thesis demonstrated that a good portion of increased FC of ASMase$^{-/-}$ hepatocytes resides within lysosomes. Recent data demonstrated that changes in lysosomal membrane FC confer lysosomal stability, thus protecting from lysosomal membrane permeabilization-induced cell death (Appelqvist, Nilsson et al. 2011). Results presented in this thesis show that ASMase deficient primary mouse hepatocytes are protected from lysomotropic agent, MSDH-induced apoptosis. This protection is of relevance since it has been described that saturated FFA lipotoxicity in hepatocytes act upon lysosomal membrane permeabilization-induced cell death (Li, Berk et al. 2008). Hence, in addition to the decreased Cer/S1P ratio, lysosomal permeabilization-mitochondrial axis is a second

mechanism of protection against liver injury in NAFLD regulated by ASMase (Figure D1).

Of interest, pharmacological ASMase inhibition is able to protect wild-type mice against HFD-mediated liver damage. Moreover, the correlation of ASMase expression and disease progression in NAFLD patients (Moles, Tarrats et al. 2010), lends further support for targeting ASMase in NAFLD. Thus, the findings suggest that targeting ASMase pharmacologically may be of benefit not only to prevent the action of major players in NAFLD, such as ER stress, but also to protect against diet-induced hepatocellular injury and liver dysfunction (Figure D1).

2. Role of ASMase in ALD:

To address the role of ASMase in ALD, this thesis characterized the response of ASMase knockout mice to *in vivo* alcohol intake. The observations in this thesis indicate that genetic ablation of ASMase prevents the adverse effects of chronic alcohol consumption including lipogenesis, fatty liver, ER stress, mitochondrial cholesterol trafficking, and hepatocellular susceptibility to cell-bound and circulating TNF.

Of significance, this thesis shows that ASMase null mice are refractory to alcohol-induced ER stress. The resistance is specific for alcohol-induced ER stress and not due to an inherent defect in ER stress response, as ASMase null mice exhibit signs of ER stress following tunicamycin challenging. Moreover, tunicamycin treatment in ASMase null mice resulted in increased TG levels and steatosis, thus establishing a cause-and-effect relationship between ER stress and fatty liver. Therefore, the mechanism whereby ASMase null mice are resistant to alcohol-induced steatosis is their insensitivity to alcohol-induced ER stress.

Interestingly, findings in this thesis indicate that the role of ASMase in alcohol-induced ER stress is independent of homocysteine, and that ASMase does not modulate alcohol-induced hyperhomocysteinemia. In contrast with Lieber-DeCarli oral administration of alcohol model, previous studies using intragastric alcohol infusion model in mice

indicated a role for homocysteine in hepatic ER stress. Compared to our observations of 3 fold higher plasma homocysteine in mice fed alcohol orally with respect to control mice, this effect was more pronounced (7-10 fold) in mice fed alcohol intragastrically (Ji and Kaplowitz 2003; Ji, Deng et al. 2004), suggesting a threshold phenomenon for homocysteine to mediate alcohol-induced hepatic ER stress. However, recent findings have reported that supplementing MCD diet with homocysteine attenuated MCD diet-induced hepatic ER stress and protected mice against MCD-induced steatohepatitis despite a 7-10 fold increase in homocysteine levels (Henkel, Elias et al. 2009). Moreover, mice fed a control diet supplemented with homocysteine had a 3-6-fold elevation in plasma homocysteine but demonstrated no pathophysiologic changes (Henkel, Elias et al. 2009). Thus, based on these findings it could be argued that alcohol-induced hepatic ER stress can be caused independently by increased homocysteine and ASMase activation, suggesting that the participation of the former might be determined by the severity of hyperhomocysteinemia (Figure D2).

Based on the link between ceramide and ER stress (Carracedo, Lorente et al. 2006; Spassieva, Mullen et al. 2009; Epstein, Kirkpatrick et al. 2012), we hypothesized that ASMase activation *per se* could induce ER stress, accounting for the resistance of ASMase null mice to both NAFLD and ALD. To test this hypothesis, we exposed Hep G2 cells to human placenta ASMase, previously characterized for its acid pH optimum to generate ceramide (García-Ruiz, Marí et al. 2000). While exogenous ASMase increased expression of ER stress markers, incubation of cells with NSMase from *Bacillus cereus* failed to induce these changes. These findings fit with the notion that the effects of ceramide may depend on the site of intracellular generation and imply that the activation of ASMase in acidic endolysosomal compartments is functionally linked to ER homeostasis. Previous findings in HeLa cells reported the ability of ceramide to release Ca^{2+} from the ER to the cytosol (Pinton, Ferrari et al. 2001). Consistent with the key role of Ca^{2+} to maintain ER homeostasis and that ER Ca^{2+} loss results in ER stress (Feng, Yao et al. 2003), we provide evidence that ASMase-induced ceramide leads to ER stress by stimulating ER Ca^{2+} release. Indeed, we observed that the stimulation of ER Ca^{2+} release by thapsigargin was decreased in cells exposed to exogenous ASMase. Of interest, stimulation of Ca^{2+} release from ER by exogenous ASMase preceded the expression of ER stress markers. Overall, our findings fit with the concept that aberrant lipid composition in the ER

regulates SERCA and hence ER Ca^{2+} homeostasis (Fu, Yang et al. 2011). Whether ASMase activation modulates SERCA activity in the ER by perturbing ER membrane physical properties remains to be examined. In support for endolysosomal/ER relationship, previous findings in NPC1 disease have shown that stimulation of ER Ca^{2+} release via SERCA by thapsigargin or curcumin to the cytosol overcomes reduced lysosomal Ca^{2+} in NPC1 null cells, correcting endocytic transport (Lloyd-Evans, Morgan et al. 2008). Further work remains to be done to fully understand the mechanism whereby ASMase-induced ceramide generation in endolysosomes stimulates ER Ca^{2+} release. Since NPC1 disease is characterized by increased accumulation of endolysosomal cholesterol and sphingolipids, it is conceivable that NPC1, whose physiological role is to transfer cholesterol from lysosomes to ER, may contribute to the transfer of ceramide from endolysosomes to ER.

The findings on cholesterol homeostasis in ASMase null mice deserve further consideration. In addition to the intrinsic liver phenotype characterized by increased SM levels, ASMase knockout mice exhibit high endogenous cholesterol content in liver. This finding is in agreement with recent reports relating cholesterol up-regulation in ASMase null mice with aging (Prinetti, Prioni et al. 2011). Although SM and cholesterol are functionally associated (Ridgway 2000), the mechanism whereby cholesterol accumulates secondary to the build up of SM in ASMase null mice has remained incompletely characterized. Results of this thesis showed increased expression of SREBP2 activation in the knockout mice, indicating that a potential source for the increase of cholesterol in the absence of ASMase derives from *de novo* cholesterol synthesis via the mevalonate pathway. Regardless of the source of hepatic cholesterol content we observed a defective trafficking of cholesterol to mitochondria in ASMase null mice that was associated with impaired expression of StAR, a mitochondrial cholesterol transporting polypeptide (Miller and Bose 2011). Given the increased basal cholesterol levels in ASMase null mice and the normal expression of StAR, it is conceivable that the trafficking of cholesterol to mitochondria may depend on stimulated up-regulation of StAR, which implies that the pre-existing StAR pool in basal ASMase null mice may be saturated with cholesterol.

Moreover, this thesis provides evidence that StAR is an ER stress target gene. First, tunicamycin induces the expression of StAR, which is blunted by the ER stress inhibitor

TUDCA (Ozcan, Yilmaz et al. 2006). Second, the outcome in mice fed a high cholesterol diet demonstrates repression of SREBP2 and its regulated gene HMG-CoA reductase but not StAR, indicating that StAR regulation is independent from SREBP2. Our findings are consistent with previous data in NIH-3T3 cells showing that ER stress stimulated expression of StARD5 but not of StARD4 or MLN64 (Soccio, Adams et al. 2005), implying a differential sensitivity of the individual members of the StART family of lipid transporting proteins to ER stress. Our findings, however, suggest a functional link between ER stress and mitochondrial cholesterol trafficking due to StAR up-regulation (Figure D2).

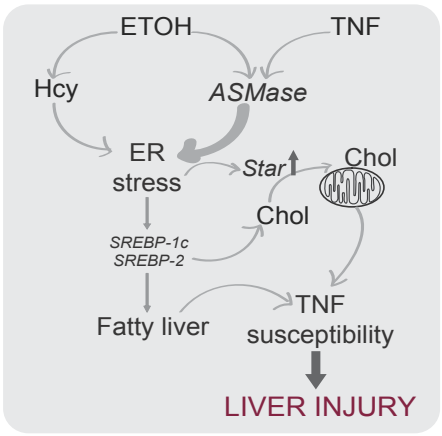

Figure D2. ASMase role in ALD model.

To address the potential relevance and applicability of the findings with the genetic ablation of ASMase, we addressed the effects of alcohol feeding in wild type mice treated *in vivo* with a pharmacological ASMase inhibitor. Although recent studies reported that ASMase inhibition by imipramine ameliorated alcohol-induced hepatic steatosis and insulin resistance (Liangpunsakul, Rahmini et al. 2012), the role of imipramine on alcohol-induced hepatic ER stress, lipogenesis, liver injury and TNF susceptibility was not investigated. Here, we show that amitriptyline treatment reduced alcohol-induced ER stress markers, fatty liver and protected against the sensitization to LPS-induced liver injury. Consistent with the functional relationship between TNF and ASMase, the resistance of ASMase null mice to the deleterious effects of alcohol was reproduced in mice deficient in TNFR1/R2. However, unlike TNF, which is critical for liver regeneration (Yamada, Webber et al. 1998; Tarrats, Moles et al. 2011), the deficiency of ASMase did not impair the recovery of the liver mass after partial hepatectomy. This feature is of significant clinical relevance as defects in liver regeneration is a serious

concern that can contribute to the fatal outcome in patients with acute alcoholic hepatitis. Moreover, consistent with the observations in the experimental model, our data indicate enhanced expression of ASMase, StAR and ER stress markers in liver biopsies from patients with alcoholic hepatitis. StAR up-regulation suggests increased mitochondrial cholesterol trafficking, however confirmation at this level in patients would require larger size samples to determine cholesterol content in isolated mitochondria.

Overall, our study defines a previously unrecognized role of ASMase in ALD by inducing ER stress and suggests that targeting ASMase may be a novel and therapeutic option for the treatment of ALD without compromising liver regeneration.

CONCLUSIONS

The conclusions from this thesis are:

1. ASMase is necessary for alcohol and diet-induced hepatic ceramide generation and its ablation results in a shift of hepatic SL content resulting in SM and S1P accumulation.

2. ASMase counteracts diet-induced body weight gain and is required for diet-mediated lipid storage in adipose tissue.

3. ASMase contributes to maintenance of whole body glucose homeostasis but it is dispensable for early hepatic insulin signaling events.

4. ASMase is essential for both nutritional and alcohol-induced hepatic steatosis.

5. Although ASMase is important for appropriate hepatic autophagic flux, its impairment in the absence of ASMase plays a minimal role in resistance to diet-induced hepatic steatosis.

6. ASMase-mediated autophagy regulation likely resides at the lysosomal level by modulating lysosomal cholesterol homeostasis.

7. ASMase-induced ceramide generation promotes ER stress. This role accounts for the resistance of ASMase null mice to both diet and alcohol-induced ER stress.

8. ASMase is dispensable for alcohol-induced hyperhomocysteinemia.

9. ASMase-mediated ER stress causes cholesterol trafficking to mitochondria contributing to alcohol-induced mitochondrial GSH depletion.

10. The regulation of lysosomal and mitochondrial cholesterol by ASMase are important mechanisms involved in nutritional and alcohol-mediated liver injury and sensitization to circulating and cell-bound TNF.

11. ASMase targeting does not impair liver regeneration.

12. Pharmacological ASMase inhibitors emerge as novel and promising agents in the treatment of both NAFLD and ALD.

BIBLIOGRAPHY

Adams, D. H. and B. Eksteen (2006). "Aberrant homing of mucosal T cells and extra-intestinal manifestations of inflammatory bowel disease." Nat Rev Immunol **6**(3): 244-51.

Ahima, R. S. (2011). "Digging deeper into obesity." J. Clin. Invest. **121**(6): 2076-2079.

Altamirano, J. and R. Bataller (2011). "Alcoholic liver disease: pathogenesis and new targets for therapy." Nat Rev Gastroenterol Hepatol **8**(9): 491-501.

Anstee, Q. M. and C. P. Day (2012). "S-adenosylmethionine (SAMe) therapy in liver disease: A review of current evidence and clinical utility." Journal of Hepatology **57**(5): 1097-109.

Appelqvist, H., C. Nilsson, et al. (2011). "Attenuation of the lysosomal death pathway by lysosomal cholesterol accumulation." The American Journal of Pathology **178**(2): 629-39.

Bartke, N. and Y. A. Hannun (2009). "Bioactive sphingolipids: metabolism and function." The Journal of Lipid Research **50 Suppl**: S91-6.

Basseri, S. and R. C. Austin (2012). "Endoplasmic reticulum stress and lipid metabolism: mechanisms and therapeutic potential." Biochemistry Research International **2012**: 841362.

Becker, S., R. Reinehr, et al. (2007). "Hydrophobic bile salts trigger ceramide formation through endosomal acidification." Biological Chemistry **388**(2): 185-96.

Bikman, B. T. and S. A. Summers (2011). "Ceramides as modulators of cellular and whole-body metabolism." J. Clin. Invest. **121**(11): 4222-4230.

Bosch, M., M. Marí, et al. (2011). "Caveolin-1 deficiency causes cholesterol-dependent mitochondrial dysfunction and apoptotic susceptibility." Curr Biol **21**(8): 681-6.

Brocklyn, J. R. V. and J. B. Williams (2012). "The control of the balance between ceramide and sphingosine-1-phosphate by sphingosine kinase: Oxidative stress and the seesaw of cell survival and death." Comparative Biochemistry and Physiology, Part B **163**(1): 26-36.

C. Guyton, A. and J. E. Hall (2000). "Medical Physiology." 1064.

Caballero, F., A. Fernández, et al. (2010). "Specific contribution of methionine and choline in nutritional nonalcoholic steatohepatitis: impact on mitochondrial S-adenosyl-L-methionine and glutathione." J Biol Chem **285**(24): 18528-36.

Carracedo, A., M. Lorente, et al. (2006). "The stress-regulated protein p8 mediates cannabinoid-induced apoptosis of tumor cells." Cancer Cell **9**(4): 301-12.

Colell, A., C. García-Ruiz, et al. (1998). "Selective glutathione depletion of mitochondria by ethanol sensitizes hepatocytes to tumor necrosis factor." Gastroenterology **115**(6): 1541-51.

Colombini, M. (2010). "Ceramide channels and their role in mitochondria-mediated apoptosis." Biochim Biophys Acta **1797**(6-7): 1239-44.

Csehi, S.-B., S. Mathieu, et al. (2005). "Tumor necrosis factor (TNF) interferes with insulin signaling through the p55 TNF receptor death domain." Biochemical and Biophysical Research Communications **329**(1): 397-405.

Cusi, K. (2012). "Role of obesity and lipotoxicity in the development of nonalcoholic steatohepatitis: pathophysiology and clinical implications." Gastroenterology **142**(4): 711-725.e6.

Czaja, M. J. (2010). "Autophagy in health and disease. 2. Regulation of lipid metabolism and storage by autophagy: pathophysiological implications." Am J Physiol, Cell Physiol **298**(5): C973-8.

Chavez, J. A., W. L. Holland, et al. (2005). "Acid ceramidase overexpression prevents the inhibitory effects of saturated fatty acids on insulin signaling." J Biol Chem **280**(20): 20148-53.

Chavez, J. A. and S. A. Summers (2010). "Lipid oversupply, selective insulin resistance, and lipotoxicity: molecular mechanisms." Biochim Biophys Acta **1801**(3): 252-65.

Chavez, J. A. and S. A. Summers (2012). "A ceramide-centric view of insulin resistance." Cell Metabolism **15**(5): 585-94.

Dara, L., C. Ji, et al. (2011). "The contribution of endoplasmic reticulum stress to liver diseases." Hepatology **53**(5): 1752-63.

Day, C. P. and O. F. James (1998). "Steatohepatitis: a tale of two "hits"?" Gastroenterology **114**(4): 842-5.

de la M Hall, P., C. S. Lieber, et al. (2001). "Models of alcoholic liver disease in rodents: a critical evaluation." Alcoholism: Clinical & Experimental Research **25**(5 Suppl ISBRA): 254S-261S.

Deaciuc, I. V., M. Nikolova-Karakashian, et al. (2000). "Apoptosis and dysregulated ceramide metabolism in a murine model of alcohol-enhanced lipopolysaccharide hepatotoxicity." Alcoholism: Clinical & Experimental Research **24**(10): 1557-65.

Deevska, G. M., K. A. Rozenova, et al. (2009). "Acid Sphingomyelinase Deficiency Prevents Diet-induced Hepatic Triacylglycerol Accumulation and Hyperglycemia in Mice." J Biol Chem **284**(13): 8359-68.

Ding, W.-X., S. Manley, et al. (2011). "The emerging role of autophagy in alcoholic liver disease." Experimental Biology and Medicine **236**(5): 546-56.

Dong, H. and M. J. Czaja (2011). "Regulation of lipid droplets by autophagy." Trends Endocrinol Metab **22**(6): 234-40.

Dumitru, C. A. and E. Gulbins (2006). "TRAIL activates acid sphingomyelinase via a redox mechanism and releases ceramide to trigger apoptosis." Oncogene **25**(41): 5612-25.

Edelmann, B., U. Bertsch, et al. (2011). "Caspase-8 and caspase-7 sequentially mediate proteolytic activation of acid sphingomyelinase in TNF-R1 receptosomes." EMBO J **30**(2): 379-94.

Elrick, M. J., T. Yu, et al. (2012). "Impaired proteolysis underlies autophagic dysfunction in Niemann-Pick type C disease." Human Molecular Genetics.

Epstein, S., C. L. Kirkpatrick, et al. (2012). "Activation of the unfolded protein response pathway causes ceramide accumulation in yeast and INS-1E insulinoma cells." Journal of lipid research **53**(3): 412-20.

Feng, B., P. M. Yao, et al. (2003). "The endoplasmic reticulum is the site of cholesterol-induced cytotoxicity in macrophages." Nat Cell Biol **5**(9): 781-92.

Fernández, A., A. Colell, et al. (2008). "Cholesterol and sphingolipids in alcohol-induced liver injury." J Gastroenterol Hepatol **23 Suppl 1**: S9-15.

Fernandez-Checa, J. C., A. Colell, et al. (2005). "Ceramide, tumor necrosis factor and alcohol-induced liver disease." Alcohol Clin Exp Res **29**(11 Suppl): 151S-157S.

Flamment, M., E. Hajduch, et al. (2012). "New insights into ER stress-induced insulin resistance." Trends Endocrinol Metab **23**(8): 381-90.

Friedman, S. L. (2000). "Molecular regulation of hepatic fibrosis, an integrated cellular response to tissue injury." J Biol Chem **275**(4): 2247-50.

Fu, S., L. Yang, et al. (2011). "Aberrant lipid metabolism disrupts calcium homeostasis causing liver endoplasmic reticulum stress in obesity." Nature **473**(7348): 528-31.

Furuhashi, M. and G. S. Hotamisligil (2008). "Fatty acid-binding proteins: role in metabolic diseases and potential as drug targets." Nat Rev Drug Discov **7**(6): 489-503.

Gao, B. and R. Bataller (2011). "Alcoholic liver disease: pathogenesis and new therapeutic targets." Gastroenterology **141**(5): 1572-85.

García-Ruiz, C., A. Colell, et al. (2003). "Defective TNF-alpha-mediated hepatocellular apoptosis and liver damage in acidic sphingomyelinase knockout mice." J. Clin. Invest. **111**(2): 197-208.

Garcia-Ruiz, C., M. Marí, et al. (2011). "Metabolic therapy: lessons from liver diseases." Curr Pharm Des **17**(35): 3933-44.

García-Ruiz, C., M. Marí, et al. (2000). "Human placenta sphingomyelinase, an exogenous acidic pH-optimum sphingomyelinase, induces oxidative stress, glutathione depletion, and apoptosis in rat hepatocytes." Hepatology **32**(1): 56-65.

Gault, C. R., L. M. Obeid, et al. (2010). "An overview of sphingolipid metabolism: from synthesis to breakdown." Adv Exp Med Biol **688**: 1-23.

Gentile, C. L., M. A. Frye, et al. (2011). "Fatty acids and the endoplasmic reticulum in nonalcoholic fatty liver disease." BioFactors **37**(1): 8-16.

Gordon, H. (2001). "Detection of alcoholic liver disease." World J Gastroenterol **7**(3): 297-302.

Górska, M., E. Barańczuk, et al. (2003). "Secretory Zn2+-dependent sphingomyelinase activity in the serum of patients with type 2 diabetes is elevated." Horm Metab Res **35**(8): 506-7.

Grassmé, H., J. Riethmüller, et al. (2007). "Biological aspects of ceramide-enriched membrane domains." Progress in Lipid Research **46**(3-4): 161-70.

Gupta, S., R. Natarajan, et al. (2004). "Deoxycholic acid activates the c-Jun N-terminal kinase pathway via FAS receptor activation in primary hepatocytes. Role of acidic sphingomyelinase-mediated ceramide generation in FAS receptor activation." J Biol Chem **279**(7): 5821-8.

Hannun, Y. A. and C. Luberto (2000). "Ceramide in the eukaryotic stress response." Trends Cell Biol **10**(2): 73-80.

Hannun, Y. A. and L. M. Obeid (2011). "Many ceramides." J Biol Chem **286**(32): 27855-62.

Haus, J., S. Kashyap, et al. (2008). "Plasma Ceramides Are Elevated in Obese Subjects with Type 2 Diabetes and Correlate with the Severity of Insulin Resistance." Diabetes.

Hebbard, L. and J. George (2011). "Animal models of nonalcoholic fatty liver disease." Nat Rev Gastroenterol Hepatol **8**(1): 35-44.

Henkel, A. S., M. S. Elias, et al. (2009). "Homocysteine supplementation attenuates the unfolded protein response in a murine nutritional model of steatohepatitis." J Biol Chem **284**(46): 31807-16.

Holland, W. L., J. T. Brozinick, et al. (2007). "Inhibition of ceramide synthesis ameliorates glucocorticoid-, saturated-fat-, and obesity-induced insulin resistance." Cell Metabolism **5**(3): 167-79.

Horinouchi, K., S. Erlich, et al. (1995). "Acid sphingomyelinase deficient mice: a model of types A and B Niemann-Pick disease." Nat Genet **10**(3): 288-93.

J. Tortora, G. and B. H. Derrickson (2009). "Principles of Anatomy and Physiology 12th Edition Atlas and Registration ...": 732.

Jaruga, B., F. Hong, et al. (2004). "Chronic alcohol consumption accelerates liver injury in T cell-mediated hepatitis: alcohol disregulation of NF-kappaB and STAT3 signaling pathways." Am J Physiol Gastrointest Liver Physiol **287**(2): G471-9.

Ji, C. (2008). "Dissection of endoplasmic reticulum stress signaling in alcoholic and non-alcoholic liver injury." J Gastroenterol Hepatol **23 Suppl 1**: S16-24.

Ji, C., Q. Deng, et al. (2004). "Role of TNF-alpha in ethanol-induced hyperhomocysteinemia and murine alcoholic liver injury." Hepatology **40**(2): 442-51.

Ji, C. and N. Kaplowitz (2003). "Betaine decreases hyperhomocysteinemia, endoplasmic reticulum stress, and liver injury in alcohol-fed mice." Gastroenterology **124**(5): 1488-99.

Ji, C. and N. Kaplowitz (2004). "Hyperhomocysteinemia, endoplasmic reticulum stress, and alcoholic liver injury." World J Gastroenterol **10**(12): 1699-708.

Kahn, S. E., R. L. Hull, et al. (2006). "Mechanisms linking obesity to insulin resistance and type 2 diabetes." Nature **444**(7121): 840-6.

Kanety, H., R. Hemi, et al. (1996). "Sphingomyelinase and ceramide suppress insulin-induced tyrosine phosphorylation of the insulin receptor substrate-1." J Biol Chem **271**(17): 9895-7.

Kaplowitz, N. and C. Ji (2006). "Unfolding new mechanisms of alcoholic liver disease in the endoplasmic reticulum." J Gastroenterol Hepatol **21**(s3): S7-S9.

Kmieć, Z. (2001). "Cooperation of liver cells in health and disease." Adv Anat Embryol Cell Biol **161**: III-XIII, 1-151.

Kornhuber, J., P. Tripal, et al. (2010). "Functional Inhibitors of Acid Sphingomyelinase (FIASMAs): a novel pharmacological group of drugs with broad clinical applications." Cell Physiol Biochem **26**(1): 9-20.

Kotronen, A., T. Seppänen-Laakso, et al. (2010). "Comparison of lipid and fatty acid composition of the liver, subcutaneous and intra-abdominal adipose tissue, and serum." Obesity **18**(5): 937-44.

Kubista, M., J. M. Andrade, et al. (2006). "The real-time polymerase chain reaction." Mol Aspects Med **27**(2-3): 95-125.

Lang, P. A., M. Schenck, et al. (2007). "Liver cell death and anemia in Wilson disease involve acid sphingomyelinase and ceramide." Nat Med **13**(2): 164-70.

Li, Z., M. Berk, et al. (2008). "The lysosomal-mitochondrial axis in free fatty acid-induced hepatic lipotoxicity." Hepatology **47**(5): 1495-503.

Liangpunsakul, S., Y. Rahmini, et al. (2012). "Imipramine blocks ethanol-induced ASMase activation, ceramide generation, and PP2A activation, and ameliorates hepatic steatosis in ethanol-fed mice." Am J Physiol Gastrointest Liver Physiol **302**(5): G515-23.

Liangpunsakul, S., M. S. Sozio, et al. (2010). "Inhibitory effect of ethanol on AMPK phosphorylation is mediated in part through elevated ceramide levels." AJP: Gastrointestinal and Liver Physiology **298**(6): G1004-12.

Lieberman, A. P., R. Puertollano, et al. (2012). "Autophagy in lysosomal storage disorders." Autophagy **8**(5): 719-30.

Liu, P., B. J. Leffler, et al. (2004). "Sphingomyelinase activates GLUT4 translocation via a cholesterol-dependent mechanism." Am J Physiol, Cell Physiol **286**(2): C317-29.

Long, S. D. and P. H. Pekala (1996). "Lipid mediators of insulin resistance: ceramide signalling down-regulates GLUT4 gene transcription in 3T3-L1 adipocytes." Biochem J **319 (Pt 1)**: 179-84.

Llacuna, L., M. Marí, et al. (2006). "Critical role of acidic sphingomyelinase in murine hepatic ischemia-reperfusion injury." Hepatology **44**(3): 561-572.

Lloyd-Evans, E., A. J. Morgan, et al. (2008). "Niemann-Pick disease type C1 is a sphingosine storage disease that causes deregulation of lysosomal calcium." Nat Med **14**(11): 1247-55.

Maeda, S., L. Chang, et al. (2003). "IKKbeta is required for prevention of apoptosis mediated by cell-bound but not by circulating TNFalpha." Immunity **19**(5): 725-37.

Malhi, H. and R. J. Kaufman (2011). "Endoplasmic reticulum stress in liver disease." Journal of Hepatology **54**(4): 795-809.

Marí, M., F. Caballero, et al. (2006). "Mitochondrial free cholesterol loading sensitizes to TNF- and Fas-mediated steatohepatitis." Cell Metabolism **4**(3): 185-98.

Marí, M., A. Colell, et al. (2004). "Acidic sphingomyelinase downregulates the liver-specific methionine adenosyltransferase 1A, contributing to tumor necrosis factor-induced lethal hepatitis." J Clin Invest **113**(6): 895-904.

Mari, M., S. A. Tooze, et al. (2011). "The puzzling origin of the autophagosomal membrane." F1000 Biol Rep **3**: 25.

Miller, W. L. and H. S. Bose (2011). "Early steps in steroidogenesis: intracellular cholesterol trafficking." Journal of lipid research **52**(12): 2111-35.

Moles, A., N. Tarrats, et al. (2012). "Cathepsin B overexpression due to acid sphingomyelinase ablation promotes liver fibrosis in Niemann-Pick disease." J Biol Chem **287**(2): 1178-88.

Moles, A., N. Tarrats, et al. (2010). "Acidic sphingomyelinase controls hepatic stellate cell activation and in vivo liver fibrogenesis." The American Journal of Pathology **177**(3): 1214-24.

Morales, A., H. Lee, et al. (2007). "Sphingolipids and cell death." Apoptosis **12**(5): 923-39.

Musso, G., R. Gambino, et al. (2009). "Recent insights into hepatic lipid metabolism in non-alcoholic fatty liver disease (NAFLD)." Progress in Lipid Research **48**(1): 1-26.

Neuschwander-Tetri, B. A. (2010). "Hepatic lipotoxicity and the pathogenesis of nonalcoholic steatohepatitis: the central role of nontriglyceride fatty acid metabolites." Hepatology **52**(2): 774-88.

Ogretmen, B. and Y. A. Hannun (2004). "Biologically active sphingolipids in cancer pathogenesis and treatment." Nat Rev Cancer **4**(8): 604-16.

Osawa, Y., E. Seki, et al. (2010). "Acid sphingomyelinase regulates glucose and lipid metabolism in hepatocytes through AKT activation and AMP-activated protein kinase suppression." FASEB J.

Ouchi, N., J. L. Parker, et al. (2011). "Adipokines in inflammation and metabolic disease." Nat Rev Immunol **11**(2): 85-97.

Ozcan, U., Q. Cao, et al. (2004). "Endoplasmic reticulum stress links obesity, insulin action, and type 2 diabetes." Science **306**(5695): 457-61.

Ozcan, U., E. Yilmaz, et al. (2006). "Chemical chaperones reduce ER stress and restore glucose homeostasis in a mouse model of type 2 diabetes." Science **313**(5790): 1137-40.

Pacheco, C. D. and A. P. Lieberman (2007). "Lipid trafficking defects increase Beclin-1 and activate autophagy in Niemann-Pick type C disease." Autophagy **3**(5): 487-9.

Pagadala, M., T. Kasumov, et al. (2012). "Role of ceramides in nonalcoholic fatty liver disease." Trends Endocrinol Metab **23**(8): 365-71.

Paton, A. W., T. Beddoe, et al. (2006). "AB5 subtilase cytotoxin inactivates the endoplasmic reticulum chaperone BiP." Nature **443**(7111): 548-52.

Peraldi, P., G. S. Hotamisligil, et al. (1996). "Tumor necrosis factor (TNF)-alpha inhibits insulin signaling through stimulation of the p55 TNF receptor and activation of sphingomyelinase." J Biol Chem **271**(22): 13018-22.

Pinton, P., D. Ferrari, et al. (2001). "The Ca2+ concentration of the endoplasmic reticulum is a key determinant of ceramide-induced apoptosis: significance for the molecular mechanism of Bcl-2 action." EMBO J **20**(11): 2690-701.

Prinetti, A., S. Prioni, et al. (2011). "Secondary alterations of sphingolipid metabolism in lysosomal storage diseases." Neurochem Res **36**(9): 1654-68.

Rautou, P.-E., A. Mansouri, et al. (2010). "Autophagy in liver diseases." Journal of Hepatology **53**(6): 1123-34.

Ravikumar, B., S. Sarkar, et al. (2010). "Regulation of mammalian autophagy in physiology and pathophysiology." Physiological Reviews **90**(4): 1383-435.

Reichel, M., J. Beck, et al. (2011). "Activity of secretory sphingomyelinase is increased in plasma of alcohol-dependent patients." Alcohol Clin Exp Res **35**(10): 1852-9.

Ridgway, N. D. (2000). "Interactions between metabolism and intracellular distribution of cholesterol and sphingomyelin." Biochim Biophys Acta **1484**(2-3): 129-41.

Samad, F., K. D. Hester, et al. (2006). "Altered adipose and plasma sphingolipid metabolism in obesity: a potential mechanism for cardiovascular and metabolic risk." Diabetes **55**(9): 2579-87.

Sánchez-Wandelmer, J., A. Dávalos, et al. (2009). "Inhibition of cholesterol biosynthesis disrupts lipid raft/caveolae and affects insulin receptor activation in 3T3-L1 preadipocytes." Biochim Biophys Acta **1788**(9): 1731-9.

Schuchman, E. H. (2010). "Acid sphingomyelinase, cell membranes and human disease: lessons from Niemann-Pick disease." FEBS Lett **584**(9): 1895-900.

Setshedi, M., L. Longato, et al. (2011). "Limited therapeutic effect of N-acetylcysteine on hepatic insulin resistance in an experimental model of alcohol-induced steatohepatitis." Alcohol Clin Exp Res **35**(12): 2139-51.

Singh, R., S. Kaushik, et al. (2009). "Autophagy regulates lipid metabolism." Nature **458**(7242): 1131-5.

Smith, B. W. and L. A. Adams (2011). "Nonalcoholic fatty liver disease and diabetes mellitus: pathogenesis and treatment." Nature Reviews Endocrinology **7**(8): 456-65.

Soccio, R. E., R. M. Adams, et al. (2005). "Differential gene regulation of StarD4 and StarD5 cholesterol transfer proteins. Activation of StarD4 by sterol regulatory element-binding protein-2 and StarD5 by endoplasmic reticulum stress." J Biol Chem **280**(19): 19410-8.

Song, Z., Z. Zhou, et al. (2007). "Alcohol-induced S-adenosylhomocysteine accumulation in the liver sensitizes to TNF hepatotoxicity: possible involvement of mitochondrial S-adenosylmethionine transport." Biochemical Pharmacology **74**(3): 521-31.

Spassieva, S. D., T. D. Mullen, et al. (2009). "Disruption of ceramide synthesis by CerS2 down-regulation leads to autophagy and the unfolded protein response." Biochem J **424**(2): 273-83.

Stancevic, B. and R. Kolesnick (2010). "Ceramide-rich platforms in transmembrane signaling." FEBS Lett.

Stewart, S. F. and C. P. Day (2011). "Chapter 28 - Alcoholic Liver Disease." Zakim and Boyer's Hepatology: 493-528.e8.

Summers, S. A. (2006). "Ceramides in insulin resistance and lipotoxicity." Progress in Lipid Research **45**(1): 42-72.

Sun, B. and M. Karin (2012). "Obesity, inflammation, and liver cancer." Journal of Hepatology **56**(3): 704-13.

Sun, K., C. M. Kusminski, et al. (2011). "Adipose tissue remodeling and obesity." J. Clin. Invest. **121**(6): 2094-2101.

Tait, S. W. G. and D. R. Green (2010). "Mitochondria and cell death: outer membrane permeabilization and beyond." Nat Rev Mol Cell Biol **11**(9): 621-32.

Talley, N. J., K. D. Lindor, et al. (2010). "Practical Gastroenterology and Hepatology: Liver and Biliary Disease."

Tarrats, N., A. Moles, et al. (2011). "Critical role of tumor necrosis factor receptor 1, but not 2, in hepatic stellate cell proliferation, extracellular matrix remodeling, and liver fibrogenesis." Hepatology **54**(1): 319-27.

Trauner, M., M. Arrese, et al. (2010). "Fatty liver and lipotoxicity." Biochim Biophys Acta **1801**(3): 299-310.

Tsukamoto, H., K. Machida, et al. (2009). ""Second hit" models of alcoholic liver disease." Semin Liver Dis **29**(2): 178-87.

Van Gaal, L. F., I. L. Mertens, et al. (2006). "Mechanisms linking obesity with cardiovascular disease." Nature **444**(7121): 875-80.

Wang, Z., T. Yao, et al. (2010). "Chronic alcohol consumption disrupted cholesterol homeostasis in rats: down-regulation of low-density lipoprotein receptor and enhancement of cholesterol biosynthesis pathway in the liver." Alcohol Clin Exp Res **34**(3): 471-8.

Wellen, K. E. and G. S. Hotamisligil (2005). "Inflammation, stress, and diabetes." J. Clin. Invest. **115**(5): 1111-9.

Yamada, Y., E. M. Webber, et al. (1998). "Analysis of liver regeneration in mice lacking type 1 or type 2 tumor necrosis factor receptor: requirement for type 1 but not type 2 receptor." Hepatology **28**(4): 959-70.

Yang, G., L. Badeanlou, et al. (2009). "Central role of ceramide biosynthesis in body weight regulation, energy metabolism, and the metabolic syndrome." Am J Physiol Endocrinol Metab **297**(1): E211-24.

Yang, L., P. Li, et al. (2010). "Defective hepatic autophagy in obesity promotes ER stress and causes insulin resistance." Cell Metabolism **11**(6): 467-78.

Yuan, T., S. Hong, et al. (2007). "Glut-4 is translocated to both caveolae and non-caveolar lipid rafts, but is partially internalized through caveolae in insulin-stimulated adipocytes." Cell Res **17**(9): 772-82.

Zeidan, Y. H. and Y. A. Hannun (2010). "The acid sphingomyelinase/ceramide pathway: biomedical significance and mechanisms of regulation." Curr Mol Med **10**(5): 454-66.

Zhang, K. and R. J. Kaufman (2008). "From endoplasmic-reticulum stress to the inflammatory response." Nature **454**(7203): 455-62.